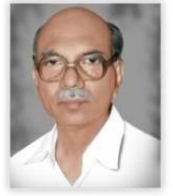




**P.B.R. VISVODAYA INSTITUTE OF TECHNOLOGY & SCIENCE**

*(Affiliated to J.N.T.U.A, Approved by AICTE and Accredited by NAAC)*

**KAVALI – 524201, S.P.S.R Nellore Dist., A.P. India. Ph: 08626-243930**



### **3.3.2.**

**Number of papers published per teacher in the Journals notified on UGC website during the year**

PBR VISVODAYA INSTITUTE OF TECHNOLOGY AND SCIENCE, KAVALI  
(AUTONOMOUS)

**3.3.2 Number of research papers per teachers in the Journals notified on UGC website during the year**

S.No.	Title of paper	Name of the author/s	Department of the teacher	Name of journal	Year of publication	ISSN number	Link to the recognition in UGC enlistment of the Journal
1	Design of Wideband Elliptical Ring Monopole Antenna Using Characteristic Mode Analysis	Dr.A.Maheswara Rao	ECE	Journal of Electromagnetic Engineering and Science	2021	671-7263	<a href="http://jees.kr/upload/pdf/jees-2021-4-r-37.pdf">http://jees.kr/upload/pdf/jees-2021-4-r-37.pdf</a>
2	Artificial Neural Network Based SIW Bandpass Filter Design Using Complementary Split Ring Resonators	Mr R Ranjith Kumar	ECE	Progress In Electromagnetics Research C	2021	1937-8718	<a href="https://www.jpier.org/PIERC/pierc115/20.21072305.pdf">https://www.jpier.org/PIERC/pierc115/20.21072305.pdf</a>
3	Tumor Detection In Skin Using Electromagnetic Band Gap Structure Antenna	Dr V Prakasam	ECE	International Research Journal of Engineering and Technology (IRJET)	2021	2395-0072	<a href="https://www.irjet.net/volume8-issue8">https://www.irjet.net/volume8-issue8</a>
4	Intelligent High Tech Street Lightning Pole for Smart City	Dr M Venkatesan	ECE	Annals of the Romanian Society for Cell Biology	2021	1583-6258	<a href="https://www.annalsofrscb.ro/index.php/journal">https://www.annalsofrscb.ro/index.php/journal</a>
5	Performance Analysis and Development of printed circuit Microstrip Patch Antenna with proximity coupled feed at 4.3 GHz (C-band) with linear polarization for Altimeter Application	Dr V Prakasam	ECE	International Journal of Computing and Digital Systems (IJCDS)	2021	2210-142X	<a href="https://journal.uob.edu.bh/handle/123456789/4205">https://journal.uob.edu.bh/handle/123456789/4205</a>
6	Plant Leaf Detection Using Convolutional Neural Networks	Mr K Penchalaiah	ECE	International Journal of Analytical And Experimental Modal Analysis	2021	0886-9367	<a href="http://www.ijaema.com/VOLUME-XIII-ISSUE-XII-DECEMBER-2021/">http://www.ijaema.com/VOLUME-XIII-ISSUE-XII-DECEMBER-2021/</a>
7	Segmentation Based Image Steganography	Mr K Penchalaiah	ECE	Asian Journal of Current Research	2021	2456-804X	<a href="https://ikprress.org/index.php/AJOCR/article/view/7559">https://ikprress.org/index.php/AJOCR/article/view/7559</a>
8	FPGA based CHOS based bitwise dynamical PRNG using seed generation	Mr. V.Narayana Reddy	ECE	Journal of Information and Computational Science	2021	1548-7741	<a href="https://drive.google.com/file/d/1dXUbfQCDAq2K7TFeVBiH15Kbc8EFBLh/view">https://drive.google.com/file/d/1dXUbfQCDAq2K7TFeVBiH15Kbc8EFBLh/view</a>
9	Class Oriented Common Object Mapping In Digital Images	Mr K Penchalaiah	ECE	Journal of Information and Computational Science	2021	1548-7741	<a href="http://www.joics.org/VOL-11-ISSUE-10-2021/">http://www.joics.org/VOL-11-ISSUE-10-2021/</a>

S.No.	Title of paper	Name of the author/s	Department of the teacher	Name of journal	Year of publication	ISSN number	Link to the recognition in UGC enlistment of the Journal
10	A Novel Approach For Under Water Image Enhancement Using CFA And Robust Retinex Model	Mr K Penchalaiah	ECE	Journal of Information and Computational Science	2021	1548-7741	<a href="http://www.joics.org/VOL-11-ISSUE-10-2021/">http://www.joics.org/VOL-11-ISSUE-10-2021/</a>
11	Different Feeding Techniques of Elliptical Patch Antenna at X Band for Radar Applications	Dr V Prakasam	ECE	International Journal of Computing and Digital Systems	2022	2210-142X	<a href="https://journal.uob.edu.bh/handle/123456789/4210">https://journal.uob.edu.bh/handle/123456789/4210</a>
12	Analyzing the Effect of Uncertainty in Low Power SRAM Cells using Artificial Intelligence Technique	Dr M Venkatesan	ECE	Journal of Uncertain Systems	2022	1752 8909	<a href="https://www.worldscientific.com/doi/10.1142/S1752890922420016">https://www.worldscientific.com/doi/10.1142/S1752890922420016</a>
13	Analyzing the Effect of Uncertainty in Low Power SRAM Cells using Artificial Intelligence Technique	Dr N Satheesh Kumar	ECE	Journal of Uncertain Systems	2022	1752 8909	<a href="https://www.worldscientific.com/doi/10.1142/S1752890922420016">https://www.worldscientific.com/doi/10.1142/S1752890922420016</a>
14	Analysis of a Compact 4-shaped Annular Ring Ultra Wideband Antenna Using Characteristic Modes	Dr.A.Maheswara Rao	ECE	Intl Journal of Electronics and Telecommunications	2022	2081-8491	<a href="https://yadda.icm.edu.pl/baztech/element/bwmeta1.element.baztech-77e87446-cc1c-4989-b8b7-9d9b5f5b6f33/c/229_Analysis_of_a_Compact_3399-11428-1-PB.pdf">https://yadda.icm.edu.pl/baztech/element/bwmeta1.element.baztech-77e87446-cc1c-4989-b8b7-9d9b5f5b6f33/c/229_Analysis_of_a_Compact_3399-11428-1-PB.pdf</a>
15	Hexagon Shape SIW Bandpass Filter with CSRRs Using Artificial Neural Networks Optimization	Mr R Ranjith Kumar	ECE	Progress In Electromagnetics Research C	2022	1937-8719	<a href="https://www.jpier.org/PIERL/pier.php?paper=22031901">https://www.jpier.org/PIERL/pier.php?paper=22031901</a>
16	New IOT Ecosystem frontier-A Survey	Dr G Vijay Kumar	CSE	International Academy of Science, Engineering, and Technology	2021	2278-9960	<a href="https://www.iaset.us/download/archives/28-04-2021-1619594112-6-%20IJCE-4-%20IJCE%20-https://www.iaset.us/download/archives/21-09-2021-163222352-6-%20IJCE-abstract-2-Abc-%20IJCE%20">https://www.iaset.us/download/archives/28-04-2021-1619594112-6-%20IJCE-4-%20IJCE%20-https://www.iaset.us/download/archives/21-09-2021-163222352-6-%20IJCE-abstract-2-Abc-%20IJCE%20</a>
17	A Study of Bandwidth Consumption Gains for Improving Smart Grid Qos	Dr G Vijay Kumar	CSE	International Journal of CSE	2021	2278-9960	<a href="https://www.iaset.us/download/archives/21-09-2021-163222352-6-%20IJCE-abstract-2-Abc-%20IJCE%20">https://www.iaset.us/download/archives/21-09-2021-163222352-6-%20IJCE-abstract-2-Abc-%20IJCE%20</a>
18	An efficient method to prevent should side attacks using machine learning techniques	B Murali Krishna	CSE	Journal of InterDisciplinary cycle of research	2021		
19	An efficient analysis of crop yeild prediction using deep learning	B Muralikrishna	CSE	The journal of Analytical and experimental model analysis	2021		
20	IOT based application case-study for transmission of sleep apnea patients video with Sound	Dr G Vijay Kumar	CSE	PARIPEX-Indian Journal of Research	2021	2250 - 1991	<a href="https://www.worldwidejournals.com/paripex/fileview/iot-based-application-casestudy-for-transmission-of-sleep-apnea-">https://www.worldwidejournals.com/paripex/fileview/iot-based-application-casestudy-for-transmission-of-sleep-apnea-</a>

S.No.	Title of paper	Name of the author/s	Department of the teacher	Name of journal	Year of publication	ISSN number	Link to the recognition in UGC enlistment of the Journal
21	Implementation of Real Time Recommender System Using Product Quantization	PVN Rajeswari	CSE	Design Engineering	2021		<a href="https://drive.google.com/open?id=1t81soAknSkyJ0MMFkKy1huRWSJsVaXct">https://drive.google.com/open?id=1t81soAknSkyJ0MMFkKy1huRWSJsVaXct</a>
22	Implementation of Real Time Recommender System Using Product Quantization	PVN Rajeswari	CSE	Design Engineering	2021		<a href="https://drive.google.com/open?id=1EfLAFfiqSXlalcKRBZlq8H_-8-6VuRQ5">https://drive.google.com/open?id=1EfLAFfiqSXlalcKRBZlq8H_-8-6VuRQ5</a>
23	Detection of Spam in Iot Devices Using Machine Learning	PVN Rajeswari	CSE	Design Engineering	2021		<a href="https://drive.google.com/open?id=1xAB2J11RyBVIT-BaS752N4xsXivpcowC">https://drive.google.com/open?id=1xAB2J11RyBVIT-BaS752N4xsXivpcowC</a>
24	An Android Based Mobile Application for Women Security	PVN Rajeswari	CSE	The International journal of analytical and experimental modal analysis	2022		<a href="https://drive.google.com/open?id=14IuBpIQDLujcrRN5d6267qozcvKd372z">https://drive.google.com/open?id=14IuBpIQDLujcrRN5d6267qozcvKd372z</a>
25	Effective intrusion detection system using concept drifting data stream and support vector machine	PVN Rajeswari	CSE	Concurrency and Computation-practice and experience (Wiley and sons)	2022		<a href="https://drive.google.com/open?id=1a-3Fv-XGS0HiHhvRJubJKU8cWqea8cgt">https://drive.google.com/open?id=1a-3Fv-XGS0HiHhvRJubJKU8cWqea8cgt</a>
26	Intelligent Financial Fraud Detection Using Node2VEC and Machine Learning Models	PVN Rajeswari	CSE	Advanced Engineering Sciences	2022		<a href="https://drive.google.com/open?id=1ozfqvWR7G032sSyQ7Wb5ckzfrsW3kviX">https://drive.google.com/open?id=1ozfqvWR7G032sSyQ7Wb5ckzfrsW3kviX</a>
27	A Fraud Detection Model for Online Product Reviews Using Machine Learning	PVN Rajeswari	CSE	Advanced Engineering Sciences	2022		<a href="https://drive.google.com/open?id=1jBAvuArkSu3U14xyCI0ZRWHZovjF6NdK">https://drive.google.com/open?id=1jBAvuArkSu3U14xyCI0ZRWHZovjF6NdK</a>
28	Comparative Analysis of Deep Learning Models in Depression Detection Using EEG Data	PVN Rajeswari	CSE	Advanced Engineering Sciences	2022		<a href="https://drive.google.com/open?id=1ZHVtTqObXZCN5GJxoc-g6tlFw-MgvpAV">https://drive.google.com/open?id=1ZHVtTqObXZCN5GJxoc-g6tlFw-MgvpAV</a>
29	A Fraud Detection Model for Online Product Reviews Using Machine Learning	J Murali	CSE	Advanced Engineering Sciences	2022		<a href="https://drive.google.com/open?id=1DquJ82yU5W19SGyeEW-3fUDei5HBAylR">https://drive.google.com/open?id=1DquJ82yU5W19SGyeEW-3fUDei5HBAylR</a>
30	Comparative Analysis of Deep Learning Models in Depression Detection Using EEG Data	J Murali	CSE	Advanced Engineering Sciences	2022		<a href="https://drive.google.com/open?id=1bnjk7vliZBadPQY2FkWzLRLau5a_-ETv">https://drive.google.com/open?id=1bnjk7vliZBadPQY2FkWzLRLau5a_-ETv</a>
31	Intelligent Financial Fraud Detection Using Node2VEC and Machine Learning Models	J Murali	CSE	Advanced Engineering Sciences	2022		<a href="https://drive.google.com/open?id=1g0V0IdjrWUsipmXva44xM1TBpWcz_Peu">https://drive.google.com/open?id=1g0V0IdjrWUsipmXva44xM1TBpWcz_Peu</a>
32	Comparative Analysis of Deep Learning Models in Depression Detection Using EEG Data	Ch Venkateswarlu	CSE	Advanced Engineering Science	2022		<a href="https://drive.google.com/open?id=1EZcT5stD9ROllgK87uQCHKOCL1OOXXFU">https://drive.google.com/open?id=1EZcT5stD9ROllgK87uQCHKOCL1OOXXFU</a>

S.No.	Title of paper	Name of the author/s	Department of the teacher	Name of journal	Year of publication	ISSN number	Link to the recognition in UGC enlistment of the Journal
33	Intelligent Financial Fraud Detection Using Node2VEC and Machine Learning Models	Ch Venkateswarlu	CSE	Advanced Engineering Science	2022		<a href="https://drive.google.com/open?id=1UizlmYeSeHI6pLLQzPq_iVMWGeG3E5q">https://drive.google.com/open?id=1UizlmYeSeHI6pLLQzPq_iVMWGeG3E5q</a>
34	A Fraud Detection Model for Online Product Reviews Using Machine Learning	Ch Venkateswarlu	CSE	Advanced Engineering Science	2022		<a href="https://drive.google.com/open?id=1tVMkk00zZqa2hpg1sXqm_vGPdpG3E5q">https://drive.google.com/open?id=1tVMkk00zZqa2hpg1sXqm_vGPdpG3E5q</a>
35	Intelligent Financial Fraud Detection Using Node2 VEC and Machine Learning Models	Ch Venkateswarlu	CSE	Advanced Engineering Science	2022		<a href="https://drive.google.com/open?id=136W4x9VnZemTmtvYOcxliwJljz_kFR8R">https://drive.google.com/open?id=136W4x9VnZemTmtvYOcxliwJljz_kFR8R</a>
36	IOT Based Prepaid Energy Meter With Data Acquisition Using GSM And Node MCU	Dr V Madhusudana Reddy	EEE	International Journal of Advanced Research in Science and Technology	2021	2581 – 4575	<a href="https://www.ijarst.in/public/uploads/paper/146751634137463.pdf">https://www.ijarst.in/public/uploads/paper/146751634137463.pdf</a>
37	An Advanced Filter Topology and Effects for compensating common Mode Voltage in Vehicular Induction Motor Drives	A.Bakthavachala	EEE	Journal of Emerging Technologies and Innovative Research	2022	2349-5162	<a href="https://www.jetir.org/papers/JETIR2206264.pdf">https://www.jetir.org/papers/JETIR2206264.pdf</a>
38	Implementation of LMMN-Based Adaptive Filtering Method For Control Of Single-Phase Solar Power Generation System With Universal Active Power Filter	A.Bakthavachala	EEE	Journal of Information and Computational Science	2022	1548-7741	<a href="https://drive.google.com/file/d/1Z5kD6h6K-gCPjoc2IdZ1BiZxzErGdyo9/view">https://drive.google.com/file/d/1Z5kD6h6K-gCPjoc2IdZ1BiZxzErGdyo9/view</a>
39	Implementation Of A Novel Controller For Wind-PV-Diesel Based Standalone Microgrid	Dr V Madhusudana Reddy	EEE	Journal of Information and Computational Science	2022	1548-7741	<a href="https://drive.google.com/file/d/1C-95Yj-hVKgRINgwcYTShS8yO7-kbwr8/view">https://drive.google.com/file/d/1C-95Yj-hVKgRINgwcYTShS8yO7-kbwr8/view</a>
40	Design, Development & Analysis of Aircraft Droop Nose Ribs by Using Optimization Technique	K. Manikantesh	ME	International Journal of Engineering Sciences & Research Technology	2021	2277-9655	<a href="https://doi.org/10.29121/ijesrt.v10.i5.2021.4">https://doi.org/10.29121/ijesrt.v10.i5.2021.4</a>
41	Engineering College Websites in Andhra Pradesh: An Evaluation Study	O. Sessaiah	H&S	Journal of Advancements in Library Sciences	2021	349-4352	<a href="http://sciencejournals.stmjournals.in/index.php/JoALS/index">http://sciencejournals.stmjournals.in/index.php/JoALS/index</a>
42	Common Coupled Fixed Points of Generalized Contraction Maps in b-Metric Spaces	N.Siva Prasad	H&S	Electronic Journal of Mathematical Analysis and Applications	2021	2090-729X	<a href="http://math-frac.org/Journals/EJMAA/Vol9(1)_Jan_2021/Vol9(1)_Papers/12)%20Vol.%209(1)%20Jan.%202021,%20pp">http://math-frac.org/Journals/EJMAA/Vol9(1)_Jan_2021/Vol9(1)_Papers/12)%20Vol.%209(1)%20Jan.%202021,%20pp</a>
43	Coupled fixed points of generalized rational type Z-contraction maps in b-metric spaces	N.Siva Prasad	H&S	International Journal of Nonlinear Analysis and Applications (IJNAA )	2022	2008-6822	<a href="http://dx.doi.org/10.22075/ijnaa.2020.20566.2172">http://dx.doi.org/10.22075/ijnaa.2020.20566.2172</a>

# Design of Wideband Elliptical Ring Monopole Antenna Using Characteristic Mode Analysis

Bhaskara Rao Perli<sup>1,\*</sup> · Maheswara Rao Avula<sup>2</sup>

## Abstract

This paper presents the systematic design of an elliptical ring monopole wideband antenna using characteristic mode analysis. The modal analysis is used to analyze the bandwidth and the radiation performance of the radiating patch. The resonance frequencies of three characteristic modes are close to each other with similar modal current distributions and characteristic fields. These three characteristic modes are simultaneously excited by an effective feeding technique. The proposed model achieves wideband characteristics. The proposed model is printed on an inexpensive FR4 substrate with a size of 20 mm × 18 mm × 1.6 mm and has a wide impedance bandwidth of 124.4% in the range of 3.6–15.46 GHz. The prototype has been fabricated and the measured results show good agreement with simulated results. The antenna will cover WLAN, WiMAX, Wi-Fi, and X-band applications.

**Key Words:** Characteristic Modes, Elliptical Ring Patch, Surface Currents, Tapered Feed, Wideband Antenna.

## I. INTRODUCTION

Recently, microstrip patch antennas (MSAs) have become more popular and attractive in mobile communication, global positioning system, satellites, military applications, and modern wireless systems due to their exciting attributes they are lightweight, have low production costs, are low profile, have conformal configuration, and are ease to integrate and fabricate [1]. Designing antennas with wideband characteristics is an important aspect to ensuring high data rates. However, microstrip antennas intrinsically have narrow bandwidth and low gain. However, practical applications currently require wider impedance bandwidth and small antennas. Many approaches have been tried to improve the bandwidth of various microstrip antennas [2–4]. These antenna designs have been performed through simulation and experimental studies. The initial design

procedure was based on engineering experience and parametric research but was not carried out systematically.

The Theory of Characteristic Modes (TCM) was initiated by Garbacz [5] in 1965 and subsequently revised by Harrington and Mautz [6, 7] in the 1970s. TCM can provide physical insights into the potential radiation properties of a conductive object. A conductive object naturally consists of characteristic modes (CMs), which are calculated numerically before using the source. Each CM consists of a characteristic angle or an eigenvalue that provides information about the mode resonance and resonant behavior. CMs depend only on the shape and size of the radiation element to govern the performance of the antenna design. TCM has been involved in the design of antennas for wireless applications [8].

The potential of TCM has been successfully extended to enhance the bandwidth of antennas including the bowtie antenna

Manuscript received November 24, 2020 ; Revised March 10, 2021 ; Accepted March 29, 2021. (ID No. 20201124-184J)

<sup>1</sup>Department of Electronics and Communication Engineering, Jawaharlal Nehru Technological University, Anantapur, Andhra Pradesh, India.

<sup>2</sup>Department of Electronics and Communication Engineering, PBR Visvodaya Institute of Technology & Science, Kavali, Andhra Pradesh, India.

\*Corresponding Author: Bhaskara Rao Perli (e-mail: mail2bhaskarp@gmail.com)

This is an Open-Access article distributed under the terms of the Creative Commons Attribution Non-Commercial License (<http://creativecommons.org/licenses/by-nc/4.0>) which permits unrestricted non-commercial use, distribution, and reproduction in any medium, provided the original work is properly cited.

© Copyright The Korean Institute of Electromagnetic Engineering and Science.

[9], an antenna with circular aperture [10], a dodecagonal-shaped antenna [11], a circular ring antenna [12], and an H-shaped slot antenna [13]. TCM was used to design a metallic loop wideband antenna with a size of  $36 \text{ mm} \times 36 \text{ mm} \times 0.8 \text{ mm}$ , in which two CMs were combined to improve the impedance bandwidth by 51.6% [14]. A combination of a dipole and a loop antenna with a size of  $80 \text{ mm} \times 40 \text{ mm} \times 0.8 \text{ mm}$  was proposed, in which a wide impedance bandwidth reached up to 44.2% by simultaneous excitation of the first two modes [15]. TCM was used to analyze the resonance behavior of the rectangular U-slot patch antenna with the various feed techniques, exciting the modes that contribute to the total radiation [16]. The size of the proposed model was  $140.17 \text{ mm} \times 134.54 \text{ mm} \times 7.62 \text{ mm}$ , which aimed to achieve a wide impedance bandwidth of 96% by exciting three CMs such as 1, 3, and 4. These antennas have a complex feed structure to excite the desired modes and improve the antenna impedance bandwidth. The present paper aims to improve the bandwidth of a simple and small antenna structure by simultaneously exciting the first two modes with higher order modes using a simple microstrip feed technique.

## II. CHARACTERISTIC MODE ANALYSIS

CM analysis is a process of solving an eigenvalue problem. The eigenvalues describe the radiation behavior of a radiating structure. Two important parameters involved in CMA for evaluating each CM of a given object are presented as per Chen and Wang [17].

Modal significance (MS) is represented as

$$MS = \frac{1}{|1+j\lambda_n|}, \text{ a real quantity.} \quad (1)$$

In this case,  $\lambda_n$  is real eigenvector and  $n$  is the index of the order of each mode. MS is an inherent characteristic of each mode, specifying the ability to connect each mode to external sources. It measures each mode's contribution to the total electromagnetic response regarding a particular source. In some cases, it is easier to use the MS in addition to eigenvalues to examine the resonance of a structure. Regions of the frequency spectrum with  $MS > 0.7$  are considered significant modes that are suitable for radiation. Ideally, the perfect radiating mode should be  $MS = 1$  for  $\lambda_n = 0$ .

Characteristic angle (CA) is defined as

$$CA = 180^\circ - \tan^{-1}(\lambda_n). \quad (2)$$

CA can provide information about the behavior of the mode near the resonance. For  $CA = 180^\circ$ , the mode will be resonant. CA values are between  $90^\circ$  and  $180^\circ$  or  $180^\circ$  and  $270^\circ$ ; the modes are inductive or capacitive, respectively. For a good radiator, the  $CA = 180^\circ$  for  $\lambda_n = 0$ .

## III. CMA OF THE ANTENNA STRUCTURE

The CMA of antenna structures was analyzed using a multi-layer solver of the full-wave simulator. In the case of a multilayer solver, the radiating elements and ground plane were set as perfect electric conductors with a zero thickness, and the substrate component was set at loss-free with a thickness of 1.6 mm. CMA was applied to the antenna structure without a feed port. The basic structure of antenna-1 used for CMA is shown in Fig. 1 with the x-radius and the y-radius of the ellipse set to 5 mm and 6 mm, respectively. The geometry of the antenna-1 consisted of an ellipse-shaped patch and the partial ground plane, which were arranged on the top and bottom of the FR4 substrate.

The MS of the first six CMs is shown in Fig. 2. In this, modes 1, 2, 5, and 6 have large MS values at frequencies of 4.9, 8, 14.6, and 12 GHz; these modes are good radiators. Modes 3 and 4 have small MS values, so these modes are not good radiators. Here, surface currents are only considered for the radiating patch.

According to Fig. 3, the surface currents of the first six modes of antenna-1 are described as follows:

- Mode 1 consists of medium current density at the bottom of the ellipse contour.
- Modes 2 and 5 have more current density on the left and

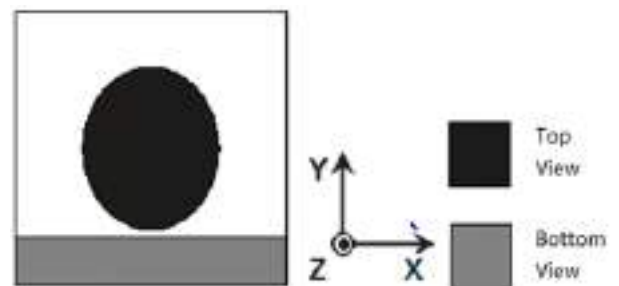


Fig. 1. Geometry of basic antenna-1.

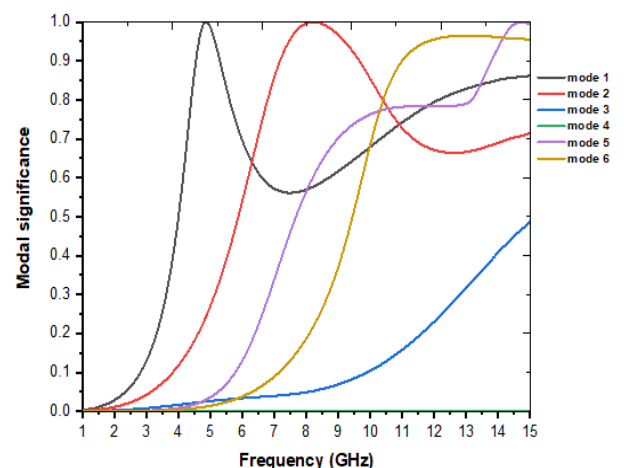


Fig. 2. Modal significance of the first six CMs of basic antenna-1.

# Artificial Neural Network Based SIW Bandpass Filter Design Using Complementary Split Ring Resonators

Ranjit Kumar Rayala\* and Raghavan Singaravelu

**Abstract**—A novel Artificial Neural Network (ANN) based two Substrate integrated waveguide (SIW) bandpass filters comprising Complementary Split Ring Resonators (CSRRs) are proposed in this paper. These CSRRs are modelled on the upper layer of the SIW cavity. A feed forward multilayer perceptron (FF-MLP) neural network is used to optimize the physical dimensions of the proposed filters. To validate the analytical results, physical prototypes of the proposed filters are fabricated, and a measurement is carried out with a Combinational Network Analyzer (Anritsu-MS2037C), and the obtained experimental results agree well with the estimated results using full wave analysis. Within the passband from 8.22 to 8.95 GHz,  $S_{12}$  of the first filter shows better than  $-0.5$  dB insertion loss (IL) and a fractional bandwidth of 8.5%, and within the passband from 8.21 to 8.73 GHz, the second filter shows IL about  $-0.8$  dB and a fractional bandwidth of 6.1%.

## 1. INTRODUCTION

Substrate Integrated Waveguide (SIW) filters have recently attracted a lot of attention because of their high efficiency, easy fabrication process with simple printed circuit board (PCB) technology, small size, low insertion loss, high selectivity, and ease of integration with microwave and millimetre wave circuits [1, 2]. In modern communication systems, one of the important requirements is miniaturization. SIW bandpass filter has been designed and investigated using slow wave method [3, 4]. SIW structures are typically composed of conducting vias which are placed in a dielectric substrate that connects two parallel metal plates, enabling the use of traditional rectangular waveguide components in planar form. The conventional PCB technique can be used in SIW based passive, active devices, microwave components, and antennas. The latest developments in SIW technology in terms of its modelling, design, and technological implementation of SIW structures and components have been reported [5–8]. To acquire compact size and modular geometry, a new type of quasi-elliptic pass-band filters based on mushroom-shaped metallic resonators in SIW technology has been proposed [9]. SIW bandpass filter with a cross-shaped cavity that realizes six symmetrically simulated modes out of first eight higher order resonant modes has been proposed [10]. An SIW band-pass filter having wide and sharp stop band, which differs from filters with a direct coupling between input and output has been proposed [11]. An SIW bandpass filter, modelled on a double layer dielectric substrate consisting of metallic via holes in order to realize the classical H-plane filter has been proposed [12]. Two cascaded mushroom resonators have been modelled on the SIW cavity that works as a dual band bandpass filter has been presented [13]. On the waveguide top metal layer, a number of cross-slot patterns have been modelled to act as dual mode SIW filters [14].

The performance of SIW filters can be improved by using some special types of electromagnetic topologies like split ring resonator (SRR) and complementary split ring resonator (CSRR) and have been

---

*Received 23 July 2021, Accepted 19 September 2021, Scheduled 9 October 2021*

\* Corresponding author: Ranjit Kumar Rayala (ranjit.rayala@gmail.com).

The authors are with the Department of Electronics and Communication Engineering, National Institute of Technology Tiruchirappalli, Trichy 620015, India.



adapted into SIW technology [15]. A novel diamond-shaped CSRR has been proposed and investigated based on an SIW bandpass filter [16]. An extended doublet bandpass filter that uses an SIW cavity with CSRRs on the top layer has been proposed, and a single layer bandpass filter with two transmission zeros (TZ) was analyzed [17]. An SIW filter with square CSRRs has been proposed, and the characteristics of passband have been observed by varying the directions of the CSRRs [18]. CSRR has been modelled on the top surface of the SIW that provides a passband below the initial cutoff frequency of the waveguide  $TE_{10}$  mode [19]. By loading CSRRs onto the SIW cavity, the SIW bandpass filters have been achieved in compact size and high selectivity [20]. A double sided CSRR half mode SIW filter that provides lower resonant frequency than the conventional model because of the coupling effect between CSRRs of the upper and lower plates has been proposed [21]. Based on evanescent-mode propagation, a compact SIW bandpass filter using broad side coupled CSRR [22] and fractal open complementary split-ring resonators (FOCSRRs) unit-cell has been presented [23]. Complementary open-ring resonators (CORRs) loaded half mode substrate integrated waveguide (HMSIW), with many transmission zeros and wide stopband, have been proposed [24]. Novel dual mode SIW filters that can provide multiple transmission zeros have been proposed [25].

One of the issues with designing SIW components and RF circuits in the above literature is that the simulation actually needs a lot of calculations, so optimization of the parameters takes a very long time. ANN has been chosen as an alternative method to design microwave circuits and devices, hence ANNs have been used to design circular and rectangular resonators modelled in SIW technology [26, 27]. A back-propagation neural network-based approach for modelling the SIW power dividers has been proposed [28]. In order to model and optimize the microwave components and devices, an efficient hybrid sampling method has been proposed to get optimum design parameters by using the ANN model [29].

The main contribution of the proposed research work is a feed forward multilayer perceptron (FF-MLP) neural network that has been used to optimize the proposed filter parameters. In this work, two networks with  $2 \times 12 \times 1$  and  $1 \times 8 \times 1$  have been used. The trainlm function in MATLAB has been used to efficiently train the FF-MLP neural networks. The  $S_{11}$  parameter has been calculated to evaluate the proposed networks, and the results obtained are in good agreement with the simulated results. Instead of a single CSRR, two CSRRs have been employed to enhance the proposed band pass filter's roll-off rate.

This paper is organized as follows. Section 2 explains how the basic topology of the proposed SIW filter is designed. Section 3 explains how the filter parameters are optimized using neural networks. Section 4 shows how the filter was simulated and the simulation results. Section 5 provides the fabrication process, measurement setup, and the measured results plotted against the simulated ones.

## 2. DESIGN OF CROSS SHAPED SIW CAVITY WITH CSRR

The proposed cross shaped SIW cavity topology is depicted in Figure 1. The basic SIW topology consists of three layers. The perfect electric conductor (PEC) is used as bottom layer and top layer, and the middle layer is dielectric material. The dielectric material used is Rogers RO4003C with dielectric constant  $\epsilon_r = 3.55$  and height of the substrate  $h = 0.81$  mm. The optimized design dimensions of this SIW cavity are as follows. The length of the SIW cavity is  $L = 40.8$  mm; the length of the dielectric substrate used is  $L_{sub} = 60$  mm; the feeding slot length  $L_{slot} = 5.4$  mm; the feeding slot width  $W_{gap} = 1.4$  mm; the width of the microstrip line is  $W_{mst} = 2$  mm; the diameter of the metallic post or via-hole is  $d = 1.2$  mm. These metallic posts are placed with two different allowable separation distances or pitches (via-to-via distance) of the vias  $p = 1.7$  mm and  $p_1 = 2$  mm. The geometries of this cross shaped SIW cavity in horizontal and vertical directions are the same.

### 2.1. Design of CSRR

The square shape CSRR is used in the filter design process, and the physical appearance of this CSRR is as depicted in Figure 2. The CSRR acts as an electric dipole, and this CSRR structure is etched on the upper PEC of the SIW cavity. The excited mode of the CSRR is the same as the dominant mode  $TE_{10}$  of the SIW cavity.

# TUMOR DETECTION IN SKIN USING ELECTROMAGNETIC BAND GAP STRUCTURE ANTENNA

Dr. V.PRAKASAM\*<sup>1</sup>, R.MEGHANA#<sup>2</sup>, A.SRAVANI#<sup>3</sup>, SK.KARISHMA#<sup>4</sup>, B.DIVYA#<sup>5</sup>, N.CHANDU#<sup>6</sup>

\*Professor, ECE Department, Visvodaya Engineering College, Kavali, Nellore (Dt.) Andhra Pradesh.

#UG Student, ECE Department, Visvodaya Engineering College, Kavali, Nellore (Dt.) Andhra Pradesh.

\*\*\*

**Abstract** - Tumor in skin could lead to death if not taken proper attention. Sometimes it may lead to most serious situations like skin cancer, which is Glioblastoma. The death rate is about 0.7 in last 2 years due to delay in the diagnosis. This distributed nature of the cancer also made this challenge in the treatment and diagnosis of the tumor or cancer in the skin muscles. Imaging techniques are traditionally used in detection of tumor in skin. Another approach is by using RF reflection approach, in which detect of tumor in skin done by analyzing variations in received signals from the skin model with and without tumor. So, in this work a EBG based monopole patch of circular shape with rectangular slot antenna is proposed that can detect the cancer related tumors in skin. The patch is pasted in the economical dielectric substrate Polymide. The design has its dimensions of  $35 \times 35 \times 1.5 \text{ mm}^3$  and that can radiate with a maximum gain of 1.12 at ISM 2.4GHz with 0.3519 GHz bandwidth from 2.2987 to 2.6506 GHz. The radiating efficiency of antenna is 65.3%.

**Keywords:** Monopole Antenna, Skin Tumor, Monostatic Radar and radiation efficiency.

## 1. INTRODUCTION

In nature there are many health issues that cause human death, in which cancer is one which causes significantly high death rates. This is happened due to late identification and also lack of self confidence [1-2]. There is high possibility of increasing patient life time, and sometimes cured if it identified in early stages like first and second stage. The many imaging techniques such as PET-CT (Positron Emission Tomography scan, Computed Tomography), Magnetic Resonance Imaging (MRI), Electro Encephalography (EEG), Magneto Encephalography (MEG), Magnetic Induction Tomography (MIT), and Electrical Impedance Tomography Technique (EIT) etc., are used in the detection of suspected tumors. But these methods require pre medical preparation of patient and need of experience doctor's observation. The process is time taking and costly. And also the results are not obtained instantly. So latest investigations in RF engineering is made to support the bio medical application such as in detection of tumor cells in human body with less time and low cost.

In this sensor antenna plays a vital role. An impressive flexible antenna that used to detect various glands based on Electromagnetic Impedance Tomography

technique using microwave frequency to detect tumor [3-4]. There are various works made by changing substrate properties like GIGML1032, FR4, Taconic (TLY-5) substrate etc., and obtained satisfactory results detection of breast cancer in [5-8]. But the sizes are not comfort to patient to fit over breast. In [7] smart antenna using PCA and LDA classification algorithms also applied to differentiate cancer tumors from normal glands. Some works used the Inverse Fast Fourier Transform (IFFT) for spectral analysis to filter out the noise for accurate results. An antenna array is proposed in [10] to detect tumor, that is fabricated on PET substrate. A polyester based antenna array and skin wearable array antenna for skin tumor detection is proposed by Alqadami et.al, it has multilayer and large size. [11-12]. The detection is done by imaging system. Compact conformal antennas are also used based on EMIT technique to detect tumors.

From above literature, a pentagon slotted disc monopole antenna is proposed in this work. The proposed design is patched on 1.6 mm FR4 substrate with dielectric constant of 4.4. The article is organized to four sections. Section I includes introduction along with literature, the patch antenna design geometry is discussed in section II, Human skin modeling using CST values covered in Section III, results and discussion are in Section IV, and finally Section V concludes the work. The design made to radiate at ISM 2.4 GHz band. Design and simulation is done using CST studio software and results are recorded.

The proposed circular patch micro strip antenna is constructed by three layers; they are ground layer, substrate and patch. Here the shape of patch is considered as circular. The substrate material is Polymide dielectric material and the properties of this material are noted as: height is 1.5 mm, dielectric constant of 3.5 and 0.0025 loss tangent. The micro strip line method is used to provide the excitation. The dimensions of substrate is  $35 \times 35 \times 1.5 \text{ mm}^3$  and this is the size of proposed antenna. length of the feed line 17.134 mm, and width of the feed line 4.4 mm.

A rectangular shape of slot is introduced in a circular patch. In this the ground is removed till the feed line that allows radiation in the desired ISM band frequency. The finalized design shown in Figure 1 is obtained by number of approximation using the software and the final design metrics of proposed antenna are listed in Table 1.

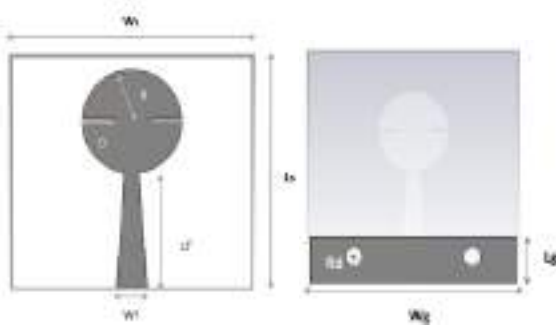


Figure 1: Design Model of the proposed antenna

Table 1: Design parameters of the proposed antenna

Variable Name	Symbol	Unit (mm)
Width of substrate	$W_s$	35
Length of substrate	$L_s$	36
Width of the feeding line	$W_f$	4.4
Thickness of substrate	$T$	1.5
Length of feeding line	$L_f$	17.134
Radius of circular disc	$R$	6
Length of one side ground plane	$L_g$	5.9
Width of one side ground plane	$W_g$	35
Radius of EBG unit cell	$R_d$	1.5
Length of one side slot in patch	$D$	4.4
Width of one side slot in patch	$D_1$	0.5

### 3. MODELING OF HUMAN SKIN

The proposed antenna is designed for detecting the stroke in human skin. The human skin models of three layers were created in CST MW Studio with the help of dielectric properties. The three layers of human skin model are skin, fat and bone. The dielectrical properties are dielectric constant and conductivity depending upon the size and thickness of layers. The Figure 2 shows the placement of antenna in front of human skin model. Then the antenna exhibits parameters like electric field, magnetic field, surface current and current density. These values are analyzed and then tumor of size 3 mm is placed on human skin model.

The same antenna parameters are analyzed and compared with previous parameters of antenna. The figure 3 shows the human skin mode with tumor model.

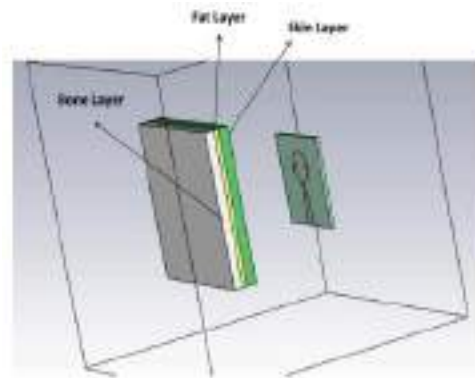


Figure 2: The positioning of proposed antenna in front human skin model in CST MWS

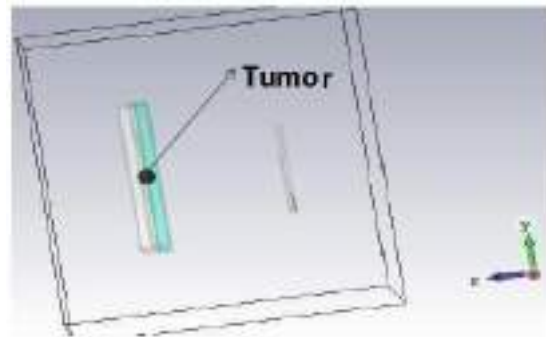


Figure 3: The spherical shape of tumor is introduced in human skin in CST MWS

Table 2: Human skin and tumor model

Skin model	Depth of layer (mm)	$\epsilon_r$	$\sigma$ (S/m <sup>2</sup> )
Skin (Dry)	2	38	1.5
Fat	2	5.3	0.1
Muscle	4	53.5	1.8

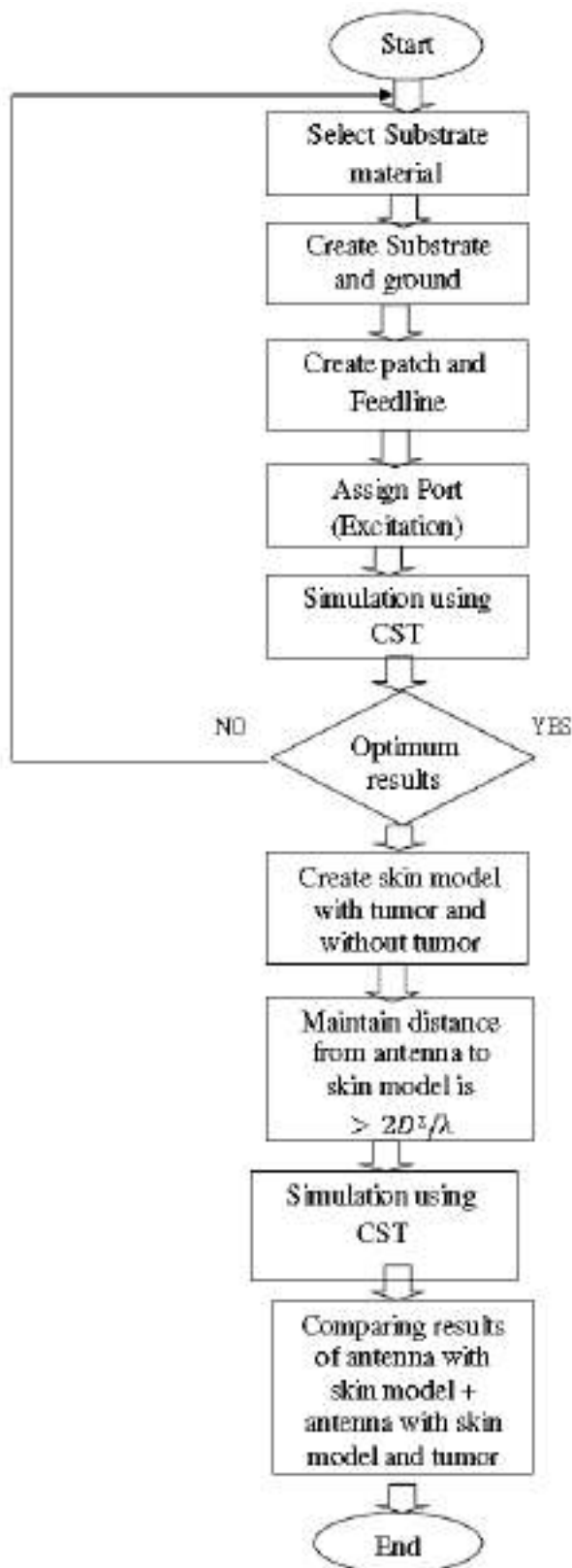


Figure 4: Flow chart of proposed design

#### 4. RESULTS AND DISCUSSION

The simulation results of proposed micro strip patch antenna shown in figure 4. By observing the S-parameter graph(return loss Vs Frequency), the proposed antenna operate at 2.45 GHz frequency and it provide band width 351.9 MHz at -10 db return loss and reflection coefficient is -15.265. An efficiency of 63.5% and gain is 1.12 dB in a normal position for proposed circular patch antenna which is being simulated in free space.

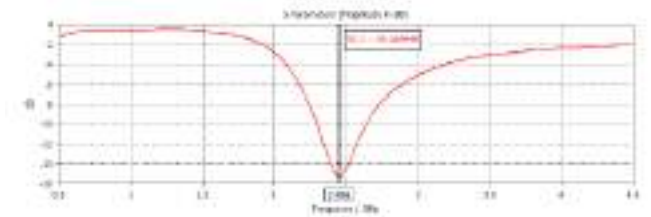


Figure 5: S-parameter plot for the proposed micro strip patch antenna

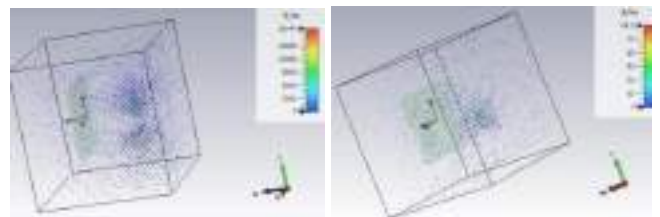


Figure 6: Electric and Magnetic Field values of the proposed antenna with skin model in CST MWS

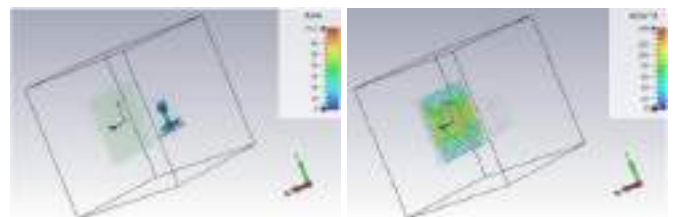


Figure 7: Surface current and current density values of the proposed antenna with skin model in CST MWS

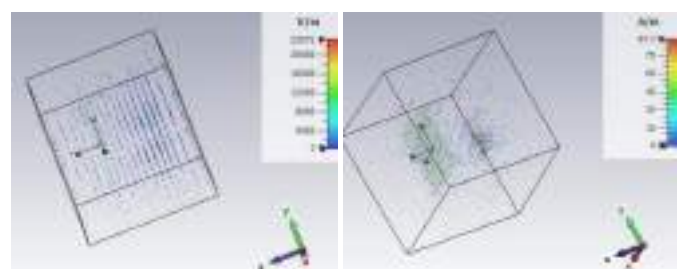
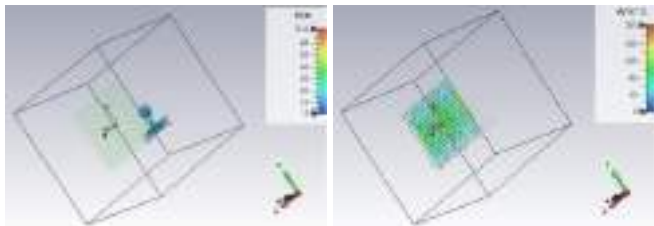


Figure 8: Electric and Magnetic Field values of the proposed antenna with skin model and tumor in CST MWS



**Figure 9:** Surface current and current density values of the proposed antenna with skin model and tumor in CST MWS

**Table 3:** The result comparison among the proposed antenna without tumor and with tumor

	Electric Field (V/m)	Magnetic Field (A/m)	Surface current (A/m)	current density (A/m <sup>2</sup> )
For proposed antenna with skin model without tumor	18744	89.5	73.1	148
For proposed antenna with skin model and tumor	23072	87.7	71.6	203

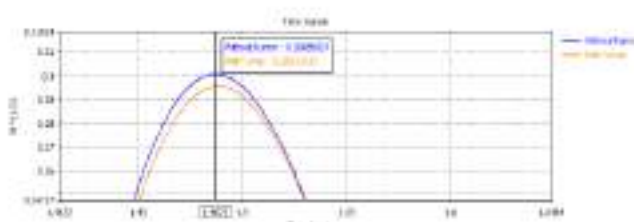


**Figure 10:** Amplitude Variation between Reflected signals with and without tumor model

Table 3 shows the comparison of antenna parameters among the proposed antenna without tumor and with tumor. From the above table, electric field, magnetic field, surface current and current density values for without tumor and with tumor are varied, with help these threshold values and also using the variation in Reflected signals with and without tumor model (shown in figure 9), the proposed circular patch antenna able to detect tumor in skin.

### 5. CONCLUSION AND FUTURE SCOPE

In this article a rectangular slotted and circular shaped microstrip patch is proposed for tumor tissue detection in skin that can radiate 2.4 GHz. It has significant

radiation band from 2.2987 to 2.6506 GHz) allows S and applications along with ISM 2.4GHz band. Removal of complete ground gives the radiation similar to monopole. The slot provided in the patch makes the patch radiate at low frequencies, so one can treat it as electrically small antenna. The size  $35 \times 35 \times 1.5 \text{ mm}^3$  shows compactness and easy to use with patient. More accuracy can be obtained by using a group of such pact antennas by forming a curved shape to suit the skin structure.

### ACKNOWLEDGEMENT

We would like to thank all who have helped us in completing this project. We would like to thank our Guide and H.O.D of Electronics and Communication Department, Visvodaya Engineering College for providing us an opportunity to work on project “TUMOR DETECTION IN SKIN USING ELECTROMAGNETIC BAND GAP STRUCTURE ANTENNA”.

### REFERENCES

[1] Lozano, R., et al., “Global and regional mortality from 235 causes of death for 20 age groups in1990 and 2010: A systematic analysis for the Global Burden of Disease Study 2010,” The Lancet, Vol. 380, No. 9859, 2095–2128, 2012.

[2] Murray, C. J., et al., “Disability-adjusted life years (DALYs) for 291 diseases and injuries in 21 regions, 1990–2010: A systematic analysis for the Global Burden of Disease Study 2010,” The Lancet, Vol. 380, No. 9859, 2197–2223, 2012.

[3] Munawar Qureshi, A., Z. Mustansar, and A. Maqsood, “Analysis of microwave scattering from a realistic human skin model for skin stroke detection using electromagnetic impedance tomography,” Progress In Electromagnetics Research M, Vol. 52, 45–56, 2016.

[4] Ch. Amarnatha Sarma1, et al., “Effect of Ground Etching, Inset Feed and Substrate Height on Elliptically Shaped Patch Antenna”, International Journal of Emerging Trends in Engineering Research, Volume 8. No. 7, July 2020.

[5] Mobashsher, A. T., K. Bialkowski, A. Abbosh, and S. Crozier, “Design and experimental evaluation of a non-invasive microwave skin imaging system for intracranial haemorrhage detection,” PlosOne, Vol. 11, No. 4, e0152351, 2016.

[6] Prakasam, V. and Sandeep, P., Design and Analysis of 2×2 Circular Micro-Strip Patch Antenna Array for 2.4 GHZ Wireless Communication Application (November 22, 2018). International Journal for Innovative Engineering & Management Research, Vol. 7, No. 12, Nov. 2018. Available at SSRN: <https://ssrn.com/abstract=3288983>

[7] V. Prakasam, P. Sandeep "Mode Patterns in Rectangular Waveguide" Published in International Journal of Trend in Research and Development (IJTRD), ISSN: 2394-9333, Special Issue | RIET-17, December 2017, URL: <http://www.ijtrd.com/papers/IJTRD13587.pdf>

[8] Prakasam V., Sandeep P., AnudeepLaxmiKanth K.R. (2021) Design and Analysis of Rectangular Microstrip Patch Antenna for 2.4 GHz Wireless Communication Applications Using CST Microwave Studio. In: Smys S., Palanisamy R., Rocha Á., Beligiannis G.N. (eds) Computer Networks and Inventive Communication Technologies. Lecture Notes on Data Engineering and Communications Technologies, vol 58. Springer, Singapore. [https://doi.org/10.1007/978-981-15-9647-6\\_89](https://doi.org/10.1007/978-981-15-9647-6_89)

[9] Prakasam, V., & Sandeep, P. (2019). Series-fed 3×3 square patch array for wireless communication applications using CSTMWS. International Journal of Engineering and Advanced Technology, 9(1), 5424–5429.

[10] V. Prakasam and N. Reddy, "Hexagonal Shaped Micro-strip Patch Antenna Design for 2.45 GHz WLAN System," 2021 6th International Conference on Inventive Computation Technologies (ICICT), Coimbatore, India, 2021, pp. 13-18, doi: 10.1109/ICICT50816.2021.9358687.

[11] V. Prakasam and N. Reddy, "Matlab And CST MWS Based Rectangular Micro-strip Patch Antenna Design for WLAN Applications," 2020 International Conference on Recent Trends on Electronics, Information, Communication & Technology (RTEICT), Bangalore, India, 2020, pp. 304-309, doi: 10.1109/RTEICT49044.2020.9315554.

[12] V. Prakasam, P. Sandeep and K. R. A. LaxmiKanth, "Rectangular Micro Strip Patch Array Antenna With Corporate Feed Network For Wireless Communication Applications," 2020 5th International Conference on Communication and Electronics Systems (ICCES), COIMBATORE, India, 2020, pp. 311-316, doi: 10.1109/ICCES48766.2020.9138028.

[13] V. Prakasam and N. Reddy, "Design and Simulation of Elliptical Micro strip Patch Antenna with Coaxial Probe Feeding for Satellites Applications Using Matlab," 2020 Fourth International Conference on I-SMAC (IoT in Social, Mobile, Analytics and Cloud) (I-SMAC), Palladam, India, 2020, pp. 228-234, doi: 10.1109/I-SMAC49090.2020.9243472.

## BIOGRAPHIES



**Dr. V. Prakasam** received B.Tech degree from JNTUA, M.Tech degree in VLSISD from JNTUK and completed p.h.d from SSSUTMS. He is currently an Associate Professor in the department of Electronics and Communication Engineering at VEC, Kavali. His research interests Signal Processing, Image Processing, Microwave Engineering and RF Engineering. He has more than 28 publications in various journals and conferences at national and International level including SCOPUS, IEEE, Springer, Elsevier and UGC.



**R. Meghana**, as B.Tech student in the department of ECE at Visvodaya Engineering College, Kavali. She has completed B.Tech from JNTUA University. Her areas of interests are Communication Systems, Embedded Systems, Java and Python.



**A. Sravani**, as B.Tech student in the department of ECE at Visvodaya Engineering College, Kavali. She has completed B.Tech from JNTUA University. Her areas of interests are Embedded Systems, Networks, Communication Systems and Object Oriented Programming Language.



**Sk. Karishma**, as B.Tech student in the department of ECE at Visvodaya Engineering College, Kavali. She has completed B.Tech from JNTUA University. Her areas of interests are Communication Systems, Electronics, Java.



**B. Divya**, as B.Tech student in the department of ECE at Visvodaya Engineering College, Kavali. She has completed B.Tech from JNTUA University. Her areas of interests are Communication Systems, Networks.



**N. Chandu**, as B.Tech student in the department of ECE at Visvodaya Engineering College, Kavali. She has completed B.Tech from JNTUA University. Her areas of interests are Embedded Systems, Communication Systems, Networks.

## Intelligent High Tech Street Lightning Pole for Smart City

**Dr.D.Vijendra Babu<sup>1\*</sup>,Dr.A.SahayaAnselin Nisha<sup>2</sup>,D.Bharathi  
Dhasan<sup>3</sup>,Dr.M.Venkatesan<sup>4</sup>,Dr.C.Karthikeyan<sup>5</sup>**

<sup>1</sup>Aarupadai VeeduInstitute of Technology, Vinayaka Mission's Research Foundation, Tamil Nadu, India

<sup>2</sup>Sathyabama Institute of Science and Technology, Chennai, Tamil Nadu, India

<sup>3</sup>R.M.D. Engineering College, Chennai, Tamil Nadu, India

<sup>4</sup>Visvodaya Engineering College, Kavali, Andhra Pradesh, India

<sup>5</sup>Koneru Lakshmaiah Education Foundation, Vaddeswaram, Guntur, Andhra Pradesh, India

<sup>1\*</sup>drdvijendrababu@gmail.com

### ABSTRACT

The alarming increase in energy price and maintenance cost results in significant increase in lighting budgets. With Smart Street lights, cities can save energy and minimize CO<sub>2</sub> emissions, limit light pollution & minimizes maintenance cost. Street light is the basic infrastructure of a city. Utilization of Sensors for data collection in Street light becomes the basic design of a Smart City. Smart Street light provide secure traffic situations and secure pedestrian environment resulting in better infrastructural improvement to Smart cities. The article elaborates on the design of Intelligent Street lightning pole towards energy efficient lightning management services and other emergency handling facilities. The features of the design covers to way finding, business advertisement, weather station, rain and flood monitoring and so on.

### Keywords

Smart city;Secure solution;Intelligent street light; Light pole;Energy saving;Light pollution;EV charging;Embedded

### Introduction

Street Light [1] plays a major role in current smart cities. Street light is the primary source of light on road and located in the intersections of roads. In majority of locations, traditional street lights are used, which uses heavy materials & more power. In current scenario of cost hike in materials & various social responsiveness to issues in environment leads to identifying the alternative technologies to save power and cost. LED Street lightning answers the issue towards environment friendly & reduction in cost. With the utilization of Embedded Sensors & Digital Networks, they gather and transfer data which help to monitor cities and respond to any situations. Intelligent Street lightning system can detect bottleneck in traffic and detects the vacant parking slots. Also, the networks can minimize the energy consumption by controlling the LED lights remotely to turn off and on, flash and dim. Smart lightning system results in saving energy, minimizing cost, reduction in maintenance and CO<sub>2</sub> emissions. The intelligent Street lightning [3-5] can be made as Smart Poles also, which caters combined smart services & amplify the business potentials. The Smart pole can cater as infrastructure for 5G, Wi-Fi hotspots, Surveillance cameras, Environmental sensors and Electric vehicle charging points.

The 3 significant force in developing the smart street lightning are regulatory policies, Internet of Things (IoT) convergence and LED prices drop [1].Figure 1 shows the key market drivers of smart street lightning. Across Globe, 320 million street lightning poles are present with Asia possessing 25%, North America and Europe 20% and South America for 10%. Figure 2 displays the top 10 cities implementing connected streetlights. Street lightning infrastructure has three potential parameters towards smart cities implementation comprising capillarity, electrification and connectivity. Smart Cities [6] uses various sensors, information technologies aligning with IoT to collect and supply from city infrastructure [2].Smart city results in more accessible, cleaner, healthier, safer and pleasant for its residents. Figure 3 displays the smart city components comprising home, transportation & mobility, farming, mobile payments and various other services.



**Figure 1.** Key Market drivers of Smart Street Lighting

Rank	City	Connected streetlights	Country
1	Miami	100,000	United States
2	Paris	750,000	France
3	Madrid	275,000	Spain
4	Los Angeles	185,000	United States
5	Jakarta	140,000	Indonesia
6	Montreal	133,000	Canada
7	Birmingham	130,000	United Kingdom
8	Dongguan	120,000	China
9	Buenos Aires	105,000	Argentina
10	Milan	101,000	Italy

**Figure 2.** Key Market drivers of Smart Street Lighting



**Figure 3.** Smart City Components



## Literature Review

B.C.Mishra [7], et al described that using Zigbee based Wireless devices optimization done in efficiency of street lighting systems. Using Embedded Internet Technology, a monitoring system design done for Street light. The results proves that the proposed system solves various essential applications such as street light management, real time access and so on pertaining to Embedded Internet applications. Eungha Kim[8], et al described a methodology where people can control certain devices utilizing Internet services in Smart Home. It proposes an integrated community service platform system architecture which provides solution for Smart city/home using a single integrated and intelligent community services. M.K.Sheu [9], et al, describes about Smart Street light which results in road safety and energy saving. Embedded System monitors the status of road and output control instruction. Low color temperature light is generated by embedded system when fog or rain is detected. Proposed LED Street light results in better ambience of intelligent city by improving the road safety for pedestrian and driver. E.Kougianos[10], et al, described that the Image or Video exchanges over the IoT is a requirement in various applications such as smart structures, intelligent health care and smart city planning.

A.Murtuza [11], et al, proposed a system which detects presence of vehicle for a certain distance and the light gets switched on during the vehicle passing the defined radius. Also, a prototype is incorporated to intimate the defect in street light if any identified. The proposed system results in consumption of power and also uses solar energy during day period. Also, the system elaborates on the minimum utilization of manpower for detecting the faulty street lights and intimation to the substation. S.Arslan [12], et al, discusses about significant application of IoT in designing a smart city for street lightning system. The designed system operates on the principle Light Dependent Resistor (LDR) which operates the bulb depending on the light intensity. Also, the discussed system is designed at economical prize with inclusion of various sensors to measure the atmospheric parameters with the aid of Android [20] operating system for effective utilization. N.Ouerhani [13], et al, elaborates on real time solution for street light control and utilization of IoT system. The design results in energy saving with respect to traditional street light control system.

M.S.A.Muthanna [14], et al, elucidates on the implementation concept of Smart City using a Wireless technology which caters long range and consumes low about power named LoRa. The system discusses with smart street lightning including the overall network organization with logical implementation. D.VijendraBabu [15], et al, discusses remote street light monitoring and controlled system. It results in conservation of power with the use of PIC Microcontroller.

Y.Yang [16], et al, proposes about efficient system for street light and utilization of sensors included to obtain the interface of data collection. The system details about Edge Computing services with high commercial value. RishikeshLohote [17], et al, exposes the conventional usage of Street lightning which results in wastage of electricity between 20 to 40% & proposed usage of Smart street light lamps which results in energy efficiency and assists in displaying various significant parameters such as weather forecast, water level sensor alerts & emergency notifications overcoming the drawbacks of conventional street light system.

Yoo S Song [18], et al, elaborates on smart lamppost composing of intelligent edge unit, camera, short range communication device, digital signage, etc. One of the main functions in the smart lamppost is to forward the safety information to the gateway node by an I2I communication system. The article analyses on the latency and throughput at each node during multi-hop data transmission to the gateway node. GunjanBhartiya [19], et al, elaborates on intelligent lightning control and energy management system. It describes about designing an efficient energy saving mechanism using microcontroller and sensors which turn on/off street lights automatically which results in energy consumption with the utilization of sensors. M.Suresh [20], et al, elaborates on utilization of reliable smart management proposal for minimizing the wastage of power in street light with the utilization of Wi-Fi module, Light Dependent Resistor (LDR), accelerometer and ultrasonic sensors are employed. Intelligent lightning control and energy management system. A Predictive model based on Improved Bayesian Neural Network (IBNN) model is applied which eliminates the power wastage during night time if there is no vehicle or trespassers passing.

## System Design

The purpose is to design an Intelligent High Tech Street lighting pole which runs an embedded web server for Smart Web based services in addition to the energy efficient lighting management services and other emergency handling



Camera, LED Lights and connected to server. The unique features of the design are as follows

- Business advertising
- Weather station
- Rain and flood Monitoring
- Way Finding
- RGB LED light
- Festival lighting
- IP Surveillance Camera



**Figure 6.** Features of Intelligent Street Pole



**Figure 7.** Snapshot of Hardware Module

Fig.5 displays the proposed Lightning pole consisting of Wireless dual band mesh Transceiver, Smart grid lightning, Image sensors, Digital street sign & Signage, Concealed placement speaker, Dynamic lightning, Environmental sensors & emergency call station. Fig.6 displays features of Intelligent Street Light Pole which consists of Sensors, Video monitoring, RFID, Wireless network, Intelligent lightning, Information display & charging pile. The snapshot of Hardware module is displayed in Fig. 7.

## Results & Discussions

IP Surveillance camera helps in monitoring the street continuously, which helps in assisting the theft/robbery incidents if happens. The Way finding is used to determine the correct path. Weather parameters such as Pressure and Temperature are measured continuously and uploads to the Internet. Using Festival lightning mode, the color of the Street light can be varied to fit with the festival conditions. Emergency speaker provides mass notification services during an emergency situations. Using Photocell control, the Street light is automatically turned on and turned off depending upon the circumstances. The Street lightning pole can also be used for business advertising resulting in revenue generation for authorities. Fig.8 displays the snapshot of result which displays the various modules/features listed in intelligent street lightning system.

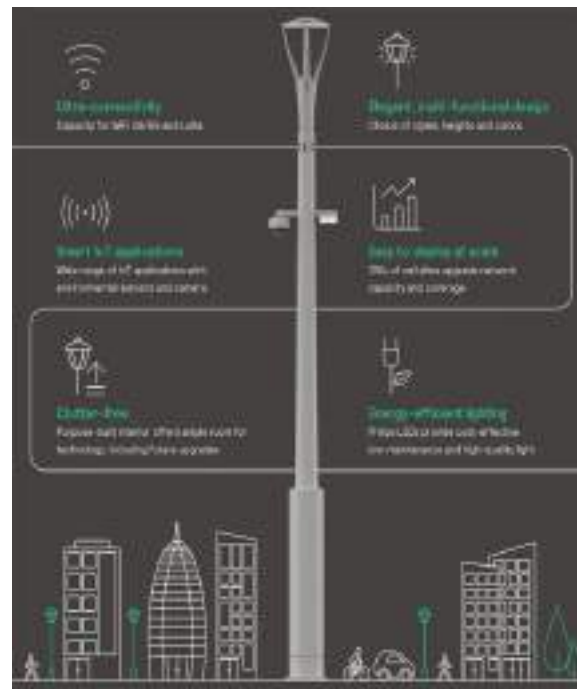


**Figure 8.** Intelligent Street Light

## Conclusion

The article describes the concepts of an Intelligent High Tech Street Lighting Pole which caters the additional services along with essential services which runs on an Embedded Web Server This smart lighting system can be implemented in smart cities, parks, schools, educational institutions and common venues. It provides opportunity for revenue generation too & helps in emergency situations. Smart City journey starts with Smart Street lights which connects over 300-410 million streetlights worldwide with access with 24/7. The future ready systems becomes an open architecture with interconnected applications such as Traffic systems, Security systems, Environmental sensors, Weather systems, Emergency response, EV charging, etc. The overall result in implementing Intelligent Street Lightning results in Adequate Light always, Optimization of Operation & Maintenance, Increased Public Safety, Minimization of Environmental impact, Secure Data connection & Globally compatible.

## References

- [1] <https://www.adlittle.com/en/evolution-street-lighting-market>
- [2] <https://futurecity.glasgow.gov.uk/intelligent-street-lighting/>
- [3] <https://inteliglight.eu/intelligent-street-lighting-control/>
- [4] <https://www.internetofthingsagenda.techtarget.com>
- [5] <https://smartbhopal.city/smart-pole-and-intelligent-street-light-project>
- [6] <https://www.silverspringnet.com/solutions/smart-cities/smart-cities-street-lights/>
- [7] <https://www.manufacturer.lighting/info/232/>
- [8] B.C.Mishra,A.S.Panda,N.K.Rout,S.K.Mohapatra(2015).A Novel Efficient Design of Intelligent Street Lighting Monitoring System Using Zigbee Network of Devices and Sensors on Embedded Internet Technology.*International Conference on Information Technology*,200-205.
- [9] Eungha Kim ,ChangsupKeum(2016).Integrated community service platform system linked to smart home and smart city.*Eighth International Conference on Ubiquitous and Future Networks*,380-382.
- [10] M.H.Sheu,L.H.Chang,S.C.Hsia,C.Sun(2016).Intelligent system design for variable Color temperature LED street light.*IEEE International Conference on Consumer Electronics*,1-2.
- [11] L. Sathish Kumar & A. Padmapriya (2019) Information Extraction and Prediction Using Partial Keyword Combination and Blends Measure, *IETE Journal of Research*, 65:2, 164-171, DOI: 10.1080/03772063.2017.1409666.
- [12] A.Murtuza,M.Fatima,S.Kumar,R.Anand(2017).Design and implementation of solar based smart street lightning system.*International Conference On Smart Technologies For Smart Nation*, 283-287.
- [13] S.Arslan,O.Dagdeviren,G.Kardas(2019).An IoT LDR Bulb Application with Android Things Operating System for Smart Cities.*Innovations in Intelligent Systems and Applications Conference* ,1-5.
- [14] L. Sathish Kumar and A. Padmapriya, "Evidence based subsequent disease extraction from EMR Health Record by Grade Measure," 2016 Online International Conference on Green Engineering and Technologies (IC-GET), Coimbatore, 2016, pp. 1-5, doi: 10.1109/GET.2016.7916771.
- [15] M.S.A.Muthanna,M.M.A.Muthanna,A.Khakimov,A.Muthanna(2020).Development of Intelligent Street lighting services model based on LoRatechnology.*IEEE Conference of Russian Young Researchers in Electrical and Electronic Engineering*, 90-93.
- [16] D.VijendraBabu,AdharshNair,NikhilSreenivas,ShammasNasar(2020).Intelligent Street lightning using Traffic & ambient lightning.AIP Conference Proceedings,Vol. 2271,1-5.
- [17] R. Lohote, T. Bhogle, V. Patel,V. Shelke(2018).Smart Street Light Lamps.International Conference on Smart City and Emerging Technology,1-5.
- [18] Y. S. Song, S. K. Lee,K. W. Min(2020).Analysis of Smart Street Lighting Mesh Network Using I2I Communication Technology.International Conference on Information and Communication Technology Convergence, Korea (South),981-983.
- [19] G.Bhartiya,P.Pathak(2020).Intelligent Lighting Control and Energy Management System. International Conference on Power Electronics & IoT Applications in Renewable Energy and its Control, India, 86-89.
- [20] M. Suresh, A. M.S., P. V. and M. H. A (2020).An Intelligent Smart Street Light System with Predictive model.International Conference on System, Computation, Automation and Networking, India, 1-4.
- [21] Y.Yang,S.Lee,G.Chen,C.Yang,Y.Huang,T.Hou(2016).An Implementation of High Efficient Smart Street

Light Management System for Smart City.*IEEEAccess*,Vol. 4, 38568-38585.

[22] D.VijendraBabu,D.C.Jennifer,R.Karthikeyan(2020).Line follower Robot & Obstacle detection using PID controller.*AIP Conference Proceedings*, Vol. 2271, pp.1-7.



# Performance Analysis and Development Of Printed Circuit Microstrip Patch Antenna with Proximity Coupled Feed at 4.3 GHz (C-band) with Linear Polarization for Altimeter Application

P. Upender<sup>1</sup>, Dr. P. A. Harsha Vardhini<sup>2</sup> and V. Prakasam<sup>3</sup>

<sup>1,3</sup>Department of Electronics and Communication, Vignan Institute of Technology and Science, Hyderabad, India

<sup>33</sup>Department of Electronics and Communication, VEC, Kavali, Nellore, India

Received 7 May 2020, Revised 4 Mar. 2021, Accepted 30 Jul. 2021, Published 25 Nov. 2021

**Abstract:** This paper aims at design, develop, optimize and realize a printed circuit Microstrip patch antenna at 4.3 GHz (C-band) with Linear polarization for Altimeter Application with proximity coupled feed method. Antenna is a device which acts as a transducer converting electrical signal to electromagnetic wave and vice-versa during transmission and reception respectively. Development, optimization and testing of high performance Microstrip antenna working in C-band are carried out for Altimeter applications. Various types of antennas are available to meet these requirements. Among these, the printed circuit Microstrip antennas have gained great prominence. With modern wireless method of contact the basic antenna requirements are Gain, Bandwidth, polarization, Size must be low, weight must be low, ease of fabrication. All the requirements mentioned above could be done with the help of printed circuit antennas. Patch antenna is resonant style radiator having narrow bandwidth. Because of its narrow bandwidth this antenna tends to be more efficient and also it tends to be smaller in size which allows the use of this element in antenna arrays and helps in good control of radiation performance. In this project, first we design patch antenna with some design equations and model it in HFSS software.. The simulated results obtained from software are compared with tested fabricated results.

**Keywords:** Antenna, Gain, Microstrip Patch Antenna, Return Loss , VSWR, Return loss.

## 1. INTRODUCTION

Webster's dictionary defines an antenna as a "normally metallic structure" designed to radiate or absorb radio waves as a rod or cord. An antenna is a device that provides radio wave propagation or receives radio waves. The transformation from a directed wave to a transmit line wave called "Free Space" provides a different term [1]. It is an information instrument that converts EM photons into circuit current and can convert energy into photons which are radiated in space. For Radar Altimeter (RA) applications, Microstrip Antenna (MSA) operating in a C-band is performed [2]. In the previous forty years, the information paces of optical correspondence frameworks have encountered a bewildering increment from 100 Mbit/s per fiber during the 1970s to 10 Tbit/s in current business frameworks [3]. As of now, more than 95% of advanced information traffic is continued optical fiber

organizations, which structure a significant piece of the public and worldwide correspondence framework [4]. To meet these requirements there are numerous types of antennas available. The MSA printed circuit has gained considerable popularity among these. Gain, bandwidth, polarization, size must be medium, weight must be medium, ease of fabrication are the basic antenna specifications of modern wireless method of communication. Most of them, however, are not workable or impractical. Compact MSA has been developed for RA applications at operating frequencies from 3.98 to 4.47 GHz. But antenna production was not examined [5]. MSA with I slot was designed and simulated at 4.5GHz. The results shown are not very promising and can hardly be feasible [6]. Antenna is designed to work within 4.3 GHz. Designed antenna is unfeasible and have not been analyzed for practical applications [7]. An array MSA with 2x2 configurations has been simulated and measured for RA which makes the design complex because of array



of antennas [8]. The practical results are not embedded and will not be useful for communication applications [9]. Double L-probe fed for RA applications is developed in [10] at 4.3 GHz and a gain of about 5.95 dB is observed.

Radar Altimeter (RA) is a device that is used to measure a low altitude or elevation from an aircraft or a satellite to land or sea level. With the theory of radar, a vertical distance in an aircraft from the terrain just below it can be determined with an altimeter. Radio altimeter is a member of the radar [5-10]. With the support of printed circuit antennas any of the above requirements could be done. The fundamental theory of radar is that radio waves are transmitted to land or sea level and receive an echo signal for a long time.

Fig 1. depicts the schematic of MSA. It consists of ground plane at the bottom, a dielectric substrate of height  $h$  and a patch built on the substrate. Dimensions of ground plane are greater than substrate and patch [11].

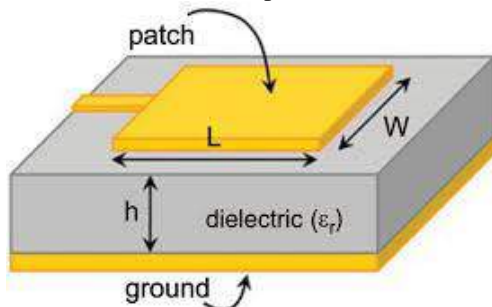


Figure 1. Microstrip Patch design

For the design of antenna, finding the parameters are essential. Important parameters are described below.

#### A. Radiation Pattern and HPBW

An antenna radiation is defined as "a graphic representation of the antenna's radiation properties as function of the space coordinates. The reflection coefficient is measured in the field region for certain instances and is perceived as a feature of the directional coordinates. It provides information on the antenna beam diameter, antenna side lobes. The most functional antenna designs include a main lobe and many secondary lobes which are called side lobes. The width of half the Power Beam "HPBW" is the same division in which the scale of the geometry of the radiation reduces by half (or -3 dB) from the peak of the main beam [12, 13].

#### B. Voltage Standing Wave Ratio (VSWR)

When reflection occurs in an incorrectly terminated line, voltage and power vary in magnitude along its length. When the transmission line is not terminated correctly, at the termination, the electromagnetic wave traveling from the generator at end of the line reflected in whole or in part. The standing wave ratio may be defined

as the ratio of maximum to minimum current or voltage on a line having Voltage Standing Waves and this Ratio is abbreviated (VSWR) [14, 15].

Thus,

$$VSWR = \left| \frac{V_{\max}}{V_{\min}} \right| \quad (1)$$

Relation between VSWR (S) and Reflection coefficient ( $\Gamma$ ):

$$VSWR = \left| \frac{V_{\max}}{V_{\min}} \right| = \frac{1 + \rho}{1 - \rho} \quad (2)$$

#### C. Return Loss

This is the best and most convenient method for estimating the sources of signal input and output. If the other end is not balanced the power returned is Return Loss [16]. In dB it is given as

$$RL = -20 \log |\Gamma| \text{ dB} \quad (3)$$

$$\Gamma = \frac{V_o^+}{V_o^-} = \frac{Z_L - Z_o}{Z_L + Z_o} \quad (4)$$

Where,

$\Gamma$  = Reflection coefficient.

$V_o^+$  = Incident voltage.

$V_o^-$  = Reflected voltage.

$Z_L$  and  $Z_o$  are the load and characteristic impedance.

#### D. Gain

Gain of antenna is the capacity of antenna to focus emanated power in proper direction [17].

## 2. METHODOLOGY

A patch antenna (PA) consists of a conductive layer of one side of the dielectric substratum and the opposite leg, covered by certain planar arrangement ground line [18]. A variety of benefits including lightweight, low volume, low cost, planar configuration, integrated circuit performance, etc. Less profile antennas are needed for high-performance space craft, missile applications are restricted in size, weight, expense, strength, installation ease & aerodynamic profile. A feed line is used for arousing over or indirect interaction with the radiation. There are several different feeding methods, and four most common methods are the line Microstrip feed, Coaxial probing, Aperture coupling, Coupling of proximity [19, 20].

#### A. Coaxial Feeding

Coaxial feeding is a method of feeding during which the coaxial inner conductor is bound to the antenna's radiation field where as the external conductor is linked to basement as described in Fig. 2 [22, 23].



# Plant Leaf Detection Using Convolutional Neural Networks

Mohammed Tanvi Basha<sup>1</sup>, Mr.K.Penchalaiah<sup>2</sup>

#1PG Scholar, Dept. OF E.C.E, PBR Visvodaya Institute of Technology and Science [PBR VITS], Nellore

#2Assistant Professor, Dept. OF E.C.E,PBR Visvodaya Institute of Technology and Science [PBR VITS], Nellore

## Abstract

A country's economic progress is heavily influenced by its agriculture output rate. Despite that, plant diseases are the most serious stumbling block to food supply and quality. For global health and well-being, early detection of plant diseases is critical. A pathologist assesses an individual plant visually during on-site inspections in the traditional diagnosis process. However, due of the lower accuracy and limited availability of human resources, manual agricultural disease examination is limited. To address these difficulties, recently several automated methods have been studied for identifying and categorizing a wide range of plant diseases. Precise identification and classification of plant diseases is a difficult task due to the presence of low-intensity information in the image background and foreground, the large color resemblance in the healthy and diseased plant areas, the presence of noise in the samples, and changes in the position,

chrominance, structure, and size of plant leaves. To address the above-mentioned issues we introduced an automated plant disease classification system using convolutional neural networks (CNN). To conduct the performance analysis, we have used the PlantVillage Kaggle database, which is the standard dataset for plant diseases and challenges in terms of intensity variations, color changes, and differences found in the shapes and sizes of leaves.

**Keywords:** Plant leaf, convolutional neural networks.

## 1.Introduction

The issue of effective plant disease prevention is intertwined with the issues of sustainable agriculture and climate change [1]. According to research findings, climate change can alter the stages and rates of pathogen growth; it can also impact host resistance, resulting in physiological alterations in host-pathogen interactions [2, 3]. The predicament is exacerbated by the

fact that diseases are now more easily transmitted globally than ever before. New infections can emerge in previously recognized locations and, inherently, in areas with no local ability to combat them [4–6]. Pesticide use by inexperienced users can lead to microorganisms developing long-term resistance, severely limiting their ability to fight back. One of the pillars of precision agriculture [7] is timely and precise plant disease identification. By tackling the long-term pathogen resistance development problem and minimizing the negative consequences of climate change, it is critical to avoid excessive waste of financial and other resources, thus attaining healthier output.

In today's changing environment, accurate and fast disease identification, as well as early disease prevention, has never been more crucial. Plant diseases can be detected in a variety of methods. Some diseases have no obvious symptoms, or the damage becomes apparent too late to respond, in which case a detailed investigation is required. However, because most illnesses produce some type of visible manifestation, the naked eye examination of a skilled specialist is the primary technique used in practice for plant disease detection. A plant pathologist should have good

observation skills in order to recognize distinctive signs in order to accomplish accurate plant disease diagnoses [8]. Variations in symptoms displayed by diseased plants may result in an incorrect diagnosis since amateur gardeners and hobbyists may have more difficulty determining it than a professional plant pathologist. An automated system developed to aid in the identification of plant illnesses based on the look and visual symptoms of the plant could be of great assistance to both amateur gardeners and skilled professionals as a verification system in disease diagnostics.

Advances in computer vision provide an opportunity to broaden and improve the practice of precise plant protection while also expanding the market for computer vision applications in precision agriculture. The detection and classification of plant diseases was accomplished by employing basic digital image processing techniques such as color analysis and thresholding [9]. Artificial neural networks (ANNs) [10] and Support Vector Machines (SVMs) [11] are two of the most common technologies for detecting plant diseases now in use. In order to improve feature extraction, they are paired with various picture preprocessing approaches.

The method discussed in this research is a new strategy to identifying plant diseases that use a deep convolutional neural network that has been trained and fine-tuned to fit accurately to a database of a plant's leaves gathered independently for various plant diseases. The developed model's advancement and innovation stem from its simplicity; healthy leaves and backdrop images are consistent with other classes, allowing the model to distinguish between damaged and healthy leaves or from the surroundings using deep CNN.

## 2.Related Work

Many state-of-the-art DL models/architectures evolved after the introduction of AlexNet [12] (as shown in Figure 2.1) for image detection, segmentation, and classification. This section presents the researches done by using famous DL architectures for the identification and classification of plants' diseases. Moreover, there are some related works in which new visualization techniques and modified/improved versions of DL architectures were introduced to achieve better results. Among all of them, the PlantVillage dataset has been used widely as it contains 450 images of 14 different crops having 15 plant diseases [13]. Moreover,

they used several performance metrics to evaluate the selected DL models, which are described as below.

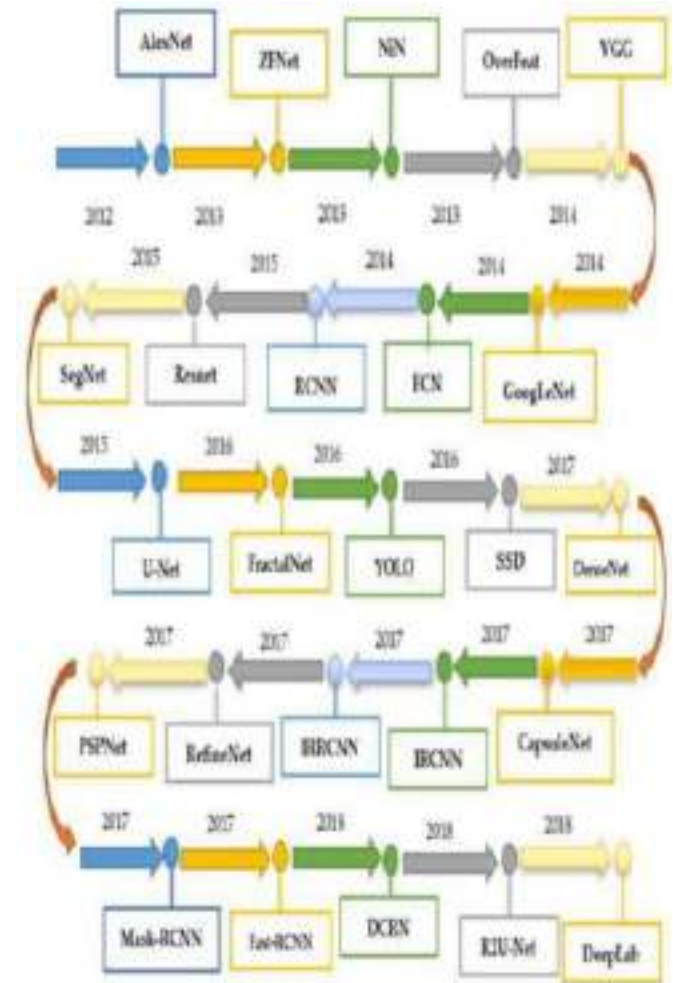


Figure 2.1: evolution of deep learning models.

In [14], CNN was used for the classification of diseases in maize plants and histogram techniques to show the significance of the model. In [15], basic CNN architectures like AlexNet, GoogLeNet and ResNet were implemented for identifying the tomato leaf diseases.

Training/validation accuracy were plotted to show the performance of the model; ResNet was considered as the best among all the CNN architectures. In order to detect the diseases in banana leaf, LeNet architecture was implemented and CA, F1-score were used for the evaluation of the model in Color and Gray Scale modes [16]. Five CNN architectures were used in [17], namely, AlexNet, AlexNetOWTbn, GoogLeNet, Overfeat, and VGG architectures in which VGG outclassed all the other models.

In [18], eight different plant diseases were recognized by three classifiers, Support Vector Machines (SVM), Extreme Learning Machine (ELM), and K-Nearest Neighbor (KNN), used with the state-of-the-art DL models like GoogLeNet, ResNet-50, ResNet-101, Inception-v3, InceptionResNetv2, and SqueezeNet. A comparison was made between those models, and ResNet-50 with SVM classifier got the best results in terms of performance metrics like sensitivity, specificity, and F1-score. According to [19], a new DL model—Inception-v3—was used for the detection of cassava disease. In [20], plant diseases in cucumber were classified by the two basic versions of CNN and got the highest accuracy, equal to 0.823. The traditional plant disease recognition and classification method was replaced by

Super-Resolution Convolutional Neural Network (SRCNN) in [21].

For the classification of tomato plant disease, AlexNet and SqueezeNet v1.1 models were used in which AlexNet was found to be the better DL model in terms of accuracy [22]. A comparative analysis was presented in [23] to select the best DL architecture for detection of plant diseases. Moreover in [24], six tomato plant diseases were classified by using AlexNet and VGG-16DL architectures, and a detailed comparison was provided with the help of classification accuracy. In the above approaches, no visualization technique was applied to spot the symptoms of diseases in the plants.

### **3. Convolutional Neural Networks (CNN)**

Deep learning is a sub-branch of the machine learning field, inspired by the structure of the brain. Deep learning (DL) models attempt to learn high-level features automatically from the input images through the hierarchical architecture. Among all DL methods, CNN has been achieved great success for analyzing medical images. CNN consists of several layers including convolutional layer, pooling layer, activation layer, Batch normalization layer and fully

connected layer, dropout layer and softmax layer to perform these operations effectively. The feature extraction process takes place in both convolutional and pooling layers. On the other hand, the classification process occurs in fully connected layer and softmax layer.

**3.1 Convolution Layer:** A convolution layer transforms the input image in order to extract features from it. In this transformation, the image is convolved with a kernel (or filter). A kernel is a small matrix, with its height and width smaller than the image to be convolved. It is also known as a convolution matrix or convolution mask. This kernel slides across the height and width of the image input and dot product of the kernel and the image are computed at every spatial position. The length by which the kernel slides is known as the stride length. In the image below, the input image is of size 5X5, the kernel is of size 3X3 and the stride length is 1. The output image is also referred to as the convolved feature.

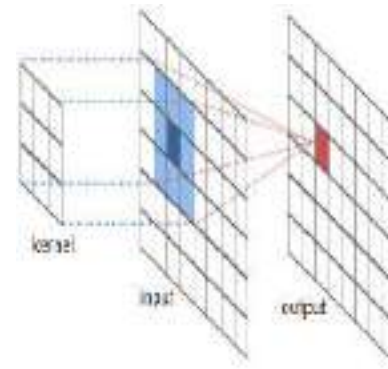


Fig1: Convolution operation on image

When we want to extract more than one feature from an image using convolution, we can use multiple kernels instead of using just one. In such a case, the size of all the kernels must be the same. The convolved features of the input image the output are stacked one after the other to create an output so that the number of channels is equal to the number of filters used. (Ref: Figure 2)

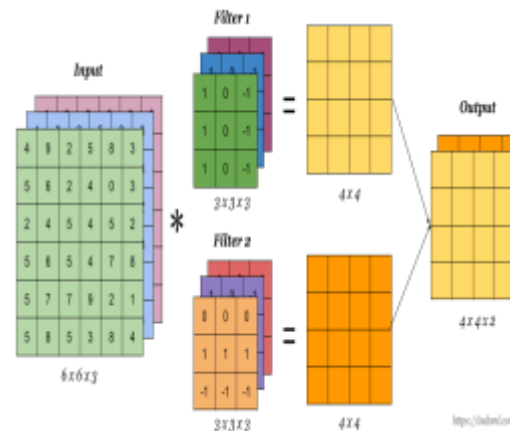


Fig 2: Convolution operation on RGB image

**3.2. Activation Layer:**

An activation function is the last component of the convolutional layer to increase the non-linearity in the output. This decides which information of the model should fire in the forward direction and which ones should not at the end of the network. Generally, ReLU function or Tanh function is used as an activation function in a convolution layer. The above operation is described in Figure 3. Here is an image of a simple convolution layer, where a 6X6X3 input image is convolved with two kernels of size 4X4X3 to get a convolved feature of size 3X3X2, to which activation function is applied to get the output, which is also referred to as feature map.

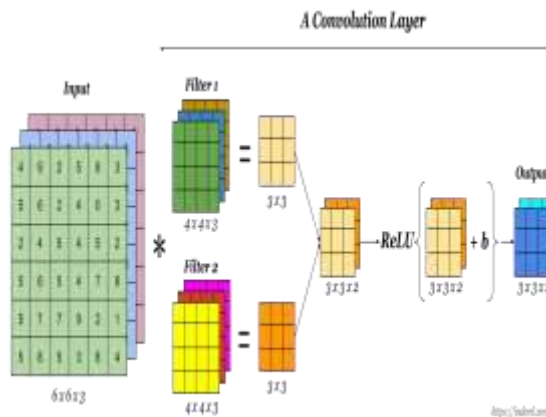


Fig3: Activation function

**3. 3. Batch normalization:**

It mainly used to

1. To improve the network speed

2. To enhances the network performance by smoothing the image.
3. It reduces the over fitting problems.

**3. 4. Pooling Layer**

Pooling layer is used to reduce the size of the input image. In a convolutional neural network, a convolutional layer is usually followed by a pooling layer. Pooling layer is usually added to speed up computation and to make some of the detected features more robust. Pooling operation uses kernel and stride as well. In the Figure 4, 2X2 filter is used for pooling the 4X4 input image of size, with a stride of 2.

There are different types of pooling.

1. Max pooling and
2. Average pooling is the most commonly used pooling method a convolutional neural network.

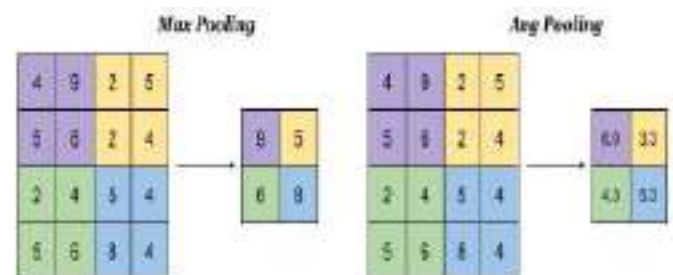


Fig4: Pooling operation on image

In max pooling, from each patch of a feature map, the maximum value is selected

to create a reduced map, where as in average pooling, from each patch of a feature map, the average value is selected to create a reduced map.

**3.5 Fully Connected Layer**

A fully connected layer is at the end of a convolutional neural network. The features map produced by the earlier layer is flattened to a vector. Then this vector is fed to a fully connected layer so that it captures complex relationships between high-level features. The out of this layer is a one-dimensional feature vector. In this work, we utilized three fully connected layers.

**3.6. Dropout layer:** It reduces the over fitting by dropping some feature maps.

**3.7. Softmax layer:** It classifies the given plant leaf images.

**4. Proposed System**

The suggested CNN architecture includes five blocks and they are represented in Figure 5. The first three blocks are quite similar to each other and they include convolutional, batch norm, ReLU, and max pooling layers in sequence. Fourth block consists of convolution layer followed by a ReLU activation layer. Similarly, in the fifth block having convolution, non-linear activation (ReLU) and max pooling. Finally, the last three blocks are unlike the other

blocks since it holds two dense layers followed by a softmax layer. The size of the convolutional filter kernel in the first four blocks is 3x3 and the corresponding numbers of filter channels are 32, 64, 128, 192, and 256. Besides that, in blocks 1, 2, 3, and 5 we employed 3x3max pooling with stride 2.

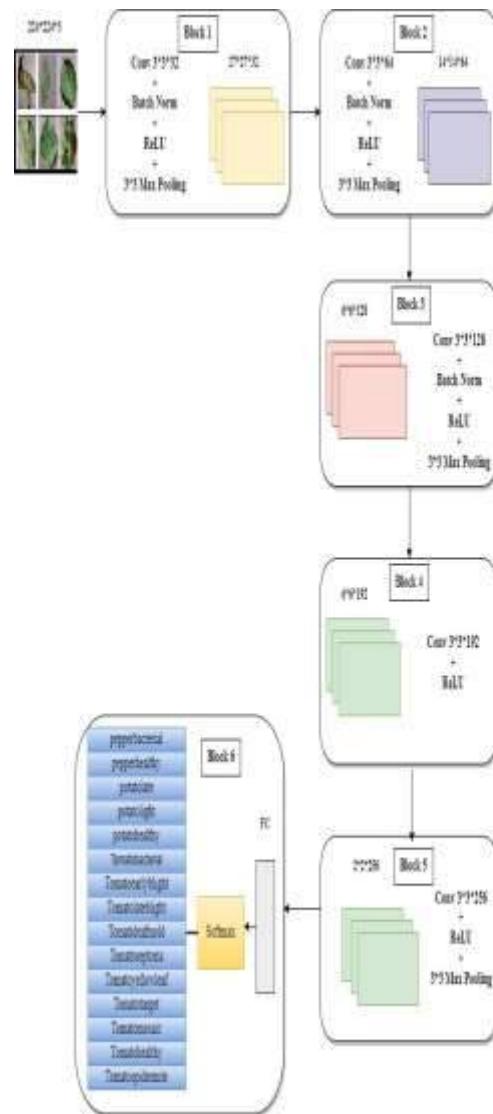


Fig 5: Block diagram of the proposed approach.

#### 4.1. Performance Measures

To assess the performance of the proposed approach, we consider the following metrics.

$$\text{Accuracy} = \frac{TP + TN}{TP + TN + FP + FN}$$

$$\text{Sensitivity or Recall} = \frac{TP}{TP + FN}$$

$$\text{Precision or Positive Predictive Value (PPV)} = \frac{TP}{TP + FP}$$

$$\text{F-Score} = 2 \left( \frac{\text{Precision} \times \text{Recall}}{\text{Precision} + \text{Recall}} \right)$$

$TP$  = True Positive,  $FN$  = False Negative,  $FP$  = False Positive and  $TN$  = True Negative.

### 1. Dataset

We analyze 450 images of plant leaves, which have a spread of 15 class labels assigned to them. Each class label is a crop-disease pair, and we make an attempt to predict the crop-disease pair given just the image of the plant leaf. Figure 1 shows one example each from every crop-disease pair from the PlantVillage dataset. In all the approaches described in this paper, we resize the images to  $224 \times 224$  pixels, and

we perform both the model optimization and predictions on these downscaled images.

Across all our experiments, we use three different versions of the whole PlantVillage dataset. We start with the PlantVillage dataset as it is, in color; then we experiment with a gray-scaled version of the PlantVillage dataset, and finally we run all the experiments on a version of the PlantVillage dataset where the leaves were segmented, hence removing all the extra background information which might have the potential to introduce some inherent bias in the dataset due to the regularized process of data collection in case of PlantVillage dataset. Segmentation was automated by the means of a script tuned to perform well on our particular dataset. We chose a technique based on a set of masks generated by analysis of the color, lightness and saturation components of different parts of the images in several color spaces (Lab and HSB). One of the steps of that processing also allowed us to easily fix color casts, which happened to be very strong in some of the subsets of the dataset, thus removing another potential bias. This set of experiments was designed to understand if the neural network actually learns the “notion” of plant diseases, or if it is just learning the inherent biases in the dataset.



Figure 6 represents the sample plant leaf diseases.

precision, 75.72% recall, and 74.51% F-score.

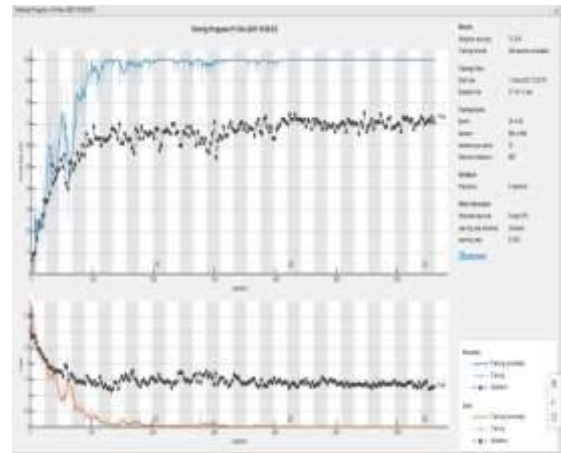


Fig 7: Training progress of the proposed model.

Figure 6: Samples from our Imagery Dataset that Show Different Types of Healthy and Diseased Plant Leaves

**5.Results**

To evaluate the performance of the proposed model, the entire dataset split into 80% training and 20% testing. Figure 7 and 8 represents the training progress as well confusion matrix of the suggested framework. By the proposed approach, we obtained 73.33% accuracy, 73.33%

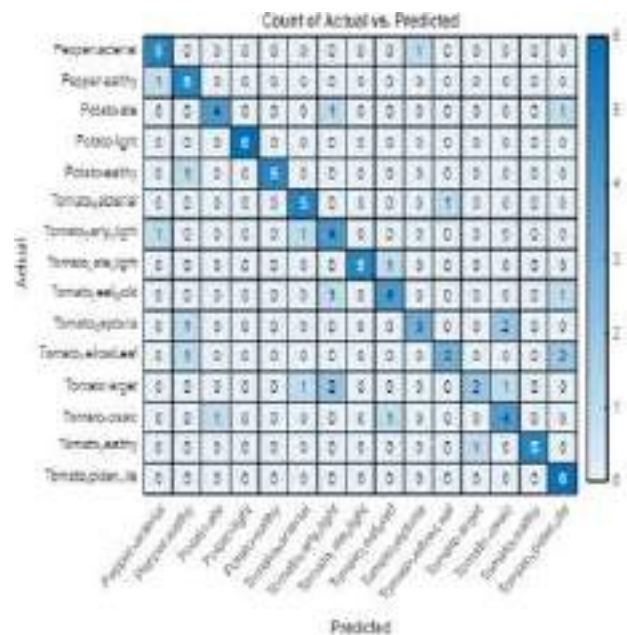


Fig 8: Confusion matrix of the proposed model.

## 6. Conclusion and Future scope

Disease detection in plants at the early stages is a hard and challenging task. Many researchers have used different Machine Learning and Deep Learning techniques for automatic plant disease detection. However, most of these techniques either use millions of training parameters or have a low classification accuracy. In this work, a special deep learning model has been developed based on convolutional neural networks to detect plant diseases through images of healthy or diseased plant leaves. In future, for better accuracy a hybrid model was proposed for automatic plant disease detection.

## References

1. K. A. Garrett, S. P. Dendy, E. E. Frank, M. N. Rouse, and S. E. Travers, "Climate change effects on plant disease: genomes to ecosystems," *Annual Review of Phytopathology*, vol. 44, pp. 489–509, 2006.
2. S. M. Coakley, H. Scherm, and S. Chakraborty, "Climate change and plant disease management," *Annual Review of Phytopathology*, vol. 37, no. 1, pp. 399–426, 1999.
3. S. Chakraborty, A. V. Tiedemann, and P. S. Teng, "Climate change: potential impact on plant diseases," *Environmental Pollution*, vol. 108, no. 3, pp. 317–326, 2000.
4. A. J. Tatem, D. J. Rogers, and S. I. Hay, "Global transport networks and infectious disease spread," *Advances in Parasitology*, vol. 62, pp. 293–343, 2006.
5. J. R. Rohr, T. R. Raffel, J. M. Romansic, H. McCallum, and P. J. Hudson, "Evaluating the links between climate, disease spread, and amphibian declines," *Proceedings of the National Academy of Sciences of the United States of America*, vol. 105, no. 45, pp. 17436–17441, 2008.
6. T. Van der Zwet, "Present worldwide distribution of fire blight," in *Proceedings of the 9th International Workshop on Fire Blight*, vol. 590, Napier, New Zealand, October 2001.
7. S. A. Miller, F. D. Beed, and C. L. Harmon, "Plant disease diagnostic capabilities and networks," *Annual Review of Phytopathology*, vol. 47, pp. 15–38, 2009.
8. M. B. Riley, M. R. Williamson, and O. Maloy, "Plant disease diagnosis. The Plant Health Instructor," 2002.
9. J. G. Arnal Barbedo, "Digital image processing techniques for detecting,

- quantifying and classifying plant diseases,” *SpringerPlus*, vol. 2, article 660, pp. 1–12, 2013.
10. H. Cartwright, Ed., *Artificial Neural Networks*, Humana Press, 2015.
  11. I. Steinwart and A. Christmann, *Support Vector Machines*, Springer Science & Business Media, New York, NY, USA, 2008.
  12. Krizhevsky, A., Sutskever, I., and Hinton, G. E. (2012). “Imagenet classification with deep convolutional neural networks,” in *Advances in Neural Information Processing Systems*, eds F. Pereira, C. J. C. Burges, L. Bottou, and K. Q. Weinberger (Curran Associates, Inc.), 1097–1105.
  13. Hughes, D. P., and Salathé, M. (2015). An open access repository of images on plant health to enable the development of mobile disease diagnostics. arXiv:1511.08060
  14. Brahim, M.; Arsenovic, M.; Laraba, S.; Sladojevic, S.; Boukhalfa, K.; Moussaoui, A. Deep learning for plant diseases: Detection and saliency map visualisation. In *Human and Machine Learning*; Springer: Berlin, Germany, 2018; pp. 93–117.
  15. Sibiya, M.; Sumbwanyambe, M. A Computational Procedure for the Recognition and Classification of Maize Leaf Diseases Out of Healthy Leaves Using Convolutional Neural Networks. *AgriEngineering* **2019**, 1, 119–131.
  16. Amara, J.; Bouaziz, B.; Algergawy, A. A Deep Learning-based Approach for Banana Leaf Diseases Classification. In *Proceedings of the BTW (Workshops)*, Stuttgart, Germany, 6–10 March 2017; pp. 79–88.
  17. Zhang, K.; Wu, Q.; Liu, A.; Meng, X. Can Deep Learning Identify Tomato Leaf Disease? *Adv. Multimed.* 2018, 2018, 10.
  18. TÜRKÖGLÜ, M.; Hanbay, D. Plant disease and pest detection using deep learning-based features. *Turk. J. Electr. Eng. Comput. Sci.* 2019, 27, 1636–1651.
  19. Ferentinos, K.P. Deep learning models for plant disease detection and diagnosis. *Comput. Electron. Agric.* 2018, 145, 311–318.
  20. Ramcharan, A.; Baranowski, K.; McCloskey, P.; Ahmed, B.; Legg, J.; Hughes, D.P. Deep learning for image-based cassava disease detection. *Front. Plant Sci.* 2017, 8, 1852.
  21. Fujita, E.; Kawasaki, Y.; Uga, H.; Kagiwada, S.; Iyatomi, H. Basic investigation on a robust and practical plant diagnostic system. In *Proceedings of the 2016 15th IEEE International Conference on*

- Machine Learning and Applications (ICMLA), Anaheim, CA, USA, 18–20 December 2016; pp. 989–992.
22. Yamamoto, K.; Togami, T.; Yamaguchi, N. Super-resolution of plant disease images for the acceleration of image-based phenotyping and vigor diagnosis in agriculture. *Sensors* 2017, 17, 2557.
23. Durmuş, H.; Güneş, E.O.; Kırıcı, M. Disease detection on the leaves of the tomato plants by using deep learning. In *Proceedings of the 2017 6th International Conference on Agro-Geoinformatics*, Fairfax, VA, USA, 7–10 August 2017; pp. 1–5.
24. Too, E.C.; Yujian, L.; Njuki, S.; Yingchun, L. A comparative study of fine-tuning deep learning models for plant disease identification. *Comput. Electron. Agric.* 2019, 161, 272–279.



## SEGMENTATION BASED IMAGE STEGANOGRAPHY

A. SIVA SAI KUMAR<sup>1\*</sup>, J. SUNIL KUMAR<sup>1</sup> AND K. PENCHALAI AH<sup>1</sup>

<sup>1</sup>Department of ECE, Narayana Engineering College (JNTUA), Nellore, A.P, India.

### AUTHORS' CONTRIBUTIONS

This work was carried out in collaboration among all authors. All authors read and approved the final manuscript.

Received: 20 March 2020

Accepted: 25 May 2020

Published: 28 December 2021

Original Research Article

### ABSTRACT

In recent years, the advancements in digital communications and information technology has become important for secured information transmission. For providing secured communication, steganography plays an important role. Different algorithms are utilized in steganography to conceal secret information in digital images. Imperceptibility is one of the major concerns in steganography. In the proposed method, segmentation and improved LSB algorithm has been used for embedding secret information in digital images. In order to maintain high imperceptibility in the proposed algorithm, the cover image is splitted after which the secret data is embedded into any one of the segment of cover image by using a secret key. The test results demonstrate that the stego image quality has been improved contrasted with other existing algorithms of data hiding. Various parameters like NCC, MSE and PSNR are determined to check the robustness of this method. Higher estimations of NCC and PSNR are obtained compared to existing methods.

**Keywords:** Digital image; imperceptibility; LSB algorithm; MSE; NCC; PSNR; steganography.

### 1. INTRODUCTION

In the present days Communication plays a vital role. Wireless and wired communications are the available types of communications. With the rapid advancements in the internet, transfer of information became easier and faster, but fails to protect the information being transmitted. Now a day's all the communication technologies transmits the information in digital form. The data is protected from unauthorized access and corruption by using data security. In latest communication trends, a wide scope of advancements are essential to identify and overcome the security threats. The information security systems are ordered into various classifications as shown Fig. 1.

The major techniques used for secured transmission are Data hiding and cryptography. In cryptography, the secret information is converted to cipher text (unreadable form) using an encryption algorithm. In cryptography, the intruder can sense about the transmission of information.

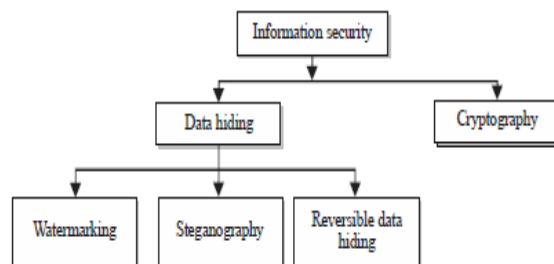


Fig. 1. Categories of information security systems

\*Corresponding author: Email: sivasai.kumar6@gmail.com;

## 1.1 Data Hiding

In data hiding, the data was concealed in a cover medium and the obtained stego file is transmitted over the communication network. Compared to cryptography, data hiding conceals the presence of secret information and it can't be distinguished by the natural eye. Imperceptibility, security, payload, robustness and embedding complexity are the important factors that are to be considered in designing an ideal data concealing framework.

Watermarking technique is widely used for copyright protection. Watermarking inserts sequence of bits in digital cover file that acknowledges the file copyright data [1]. Steganography is totally devoted for secret communication. As the transmission of data is invisible, the secret information cannot be identified easily. In steganography after extracting the secret information, cover medium does not hold any significance, where as in reversible data hiding, the cover medium also hold the secret data after extraction. In reversible data concealing [2], it is possible to hide more number of information bits into cover image and also we can reconstruct the original image from the stego medium. This technique is best suitable for applications where one can store the secret data in cover image, and recover actual cover image without any degradation, after extracting the data [3]. The cover medium might be an image, audio file or a video file and the secret data might be in the form a text file or an image. Watermarking schemes are used to protect digital media like audio, images, videos, official reports, etc in the form of images or logos or text in the file or they can be invisible. Steganography can be utilized in intelligence agencies, medical, military organizations etc., to achieve covert data exchange.

## 1.3 Steganography

Steganography is an efficient technique that provides security to the data during communication [4]. In steganography the secret data is transmitted through the images, video or audio files so that no one can extract the secret data except the intended receiver. Steganalysis is the process of finding the concealed data from cover file. Steganalysis methods are grouped as blind processes [5].

Steganography [4] means covered writing. Steganography is a greek word derived from steganos and graphein. Steganos implies covered or hidden and graphein intends to write. Markus Kahn characterized steganography as the art of communication that conceals the existence of the transfer of information” [6].

The basic steganographic system is shown in Fig. 2.

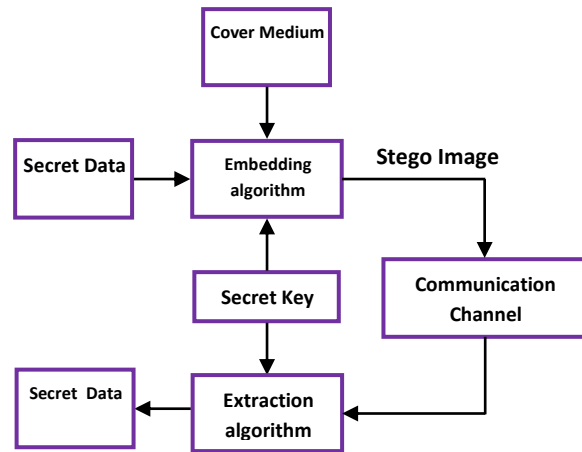


**Fig. 2. Basic steganography system**

In any steganography system, the secret data to be transferred is concealed in cover medium utilizing an embedding algorithm and secret key. The resultant image is called stego image, which is looks like cover image but it contains secret data. The stego image is transmitted to recipient over communication medium. At the recipient, by utilizing a similar secret key and extraction algorithm the secret data is retrieved from stego image.

The diverse steganography conventions are

- Pure Steganography
- Public Key Steganography
- Secret Key Steganography

In pure steganography, secret key utilized in embedding process is not shared with intended receiver. Pure steganography provides less security.

In public key steganography, the transmitter hides the secret data in cover image by utilizing a secret key. The resultant image is transmitted to the intended receiver. By utilizing another key, the receiver retrieves secret data from stego image. This system provides more security compared to pure steganography.

In secret key steganography, the key utilized by transmitter in embedding process was sent along with stego image to the receiver. By utilizing the key received by the receiver, secret data is retrieved from stego image. This system provides greater security compared with other steganographic conventions.

## 1.4 Segmentation

Image segmentation decomposes the digital image into different segments which altogether covers the entire image. The key objective behind image segmentation is to analyze the digital image easily and to detect objects and boundaries in images. It is used in various fields like object detection, face recognition, video surveillance, finger print and iris recognition, medical imaging, machine vision etc. The basic method in image segmentation is threshold segmentation. In threshold segmentation, threshold value is utilized to transform the gray scale image to binary image [7].

Image segmentation is used to detect the edges of an object. The discontinuous local features of the image are used to detect the edges. The various parts of the image changes occurs in texture changes, color mutation, change in gray values and so on [8].

Clustering is the basic concept used in image segmentation. Clustering refers to the grouping of similar elements. In clustering, the widely used algorithm is k-means algorithm. This algorithm assembles the samples into non-indistinguishable groups according to the distance [9].

## 2. REVIEW OF LITERATURE

Various algorithms have been proposed for image steganographic systems. The various advancements in image steganographic system attempts to conceal secret information effectively and to provide greater security.

Lossless image steganographic scheme was proposed by Chih-Chiang Lee et al. In this scheme secret data bits are embedded in fixed size blocks of cover image. Number of bits inserted in each block is based on the complexity of cover image. This technique is an improvement over Alattar's scheme [10]. This technique hides more bits, thus increasing hiding capacity.

The basic image steganographic algorithm is Least Significant Bit (LSB) algorithm. Here secret information and every pixel of the cover image are converted into bits. Then the least significant bit of each pixel of the cover image is overwritten by secret information bit as depicted in Fig. 3.

By utilizing encryption and LSB algorithm, Data concealing technique was proposed by Fahim Irfan Alam, Fateha Khanam Bappee, Farid Uddin Ahmed Khondker. In this technique, the secret information to be transferred is encoded utilizing an encryption

algorithm and by utilizing LSB algorithm, encrypted data is hidden into cover image [11].

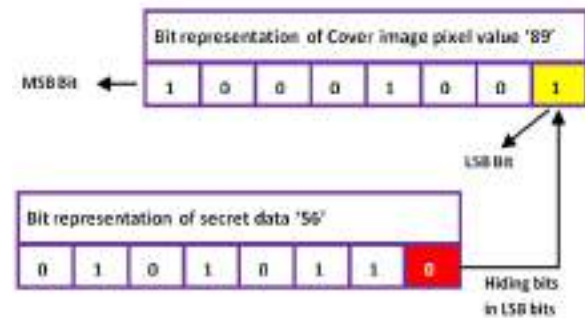


**Fig. 3. LSB algorithm**

By utilizing wavelet transform and OPA algorithm, S. Jayasudha proposed a steganographic technique. This technique uses integer wavelet transform to increase hiding capacity and OPA algorithm to improve the quality of image [12].

An effective steganography algorithm was proposed by Souvik Bhattacharyya et al., [13] that utilizes DWT difference modulation. In this algorithm the secret data bits are concealed in nearby DWT coefficient differences. Various image attacks can be avoided by using this technique and suitable for compressed and uncompressed domains.

DWT based data hiding technique was proposed by Barnali Gupta Banik et al. [14] for image steganography. This steganography method maintains high secrecy.

Based on singular value decomposition(SVD), Yambem Jina Chanu, Kh. Manglem Singh and Themrichon Tuithung [15] proposed a data hiding technique. In SVD technique the cover image is partitioned into number of blocks and the secret data bits are embedded in the singular values of the blocks of cover image. This technique is effective against the various intruder threats during communication.

## 3. PROPOSED FRAMEWORK

In the proposed framework, improved LSB technique and segmentation process are utilized. The embedding process is depicted Fig. 4.

The various steps involved in embedding process are as follows:

*Step 1:* Select cover image.

*Step 2:* Partition the selected image into four segments.

*Step 3:* The secret data is in text format. Convert the text into corresponding bits.

*Step 4:* Select any one of the four segments of cover image. Every pixel value of the selected segment is converted into corresponding bits.

*Step 5:* By using secret key, the LSB of each pixel of selected segments was inserted by the corresponding bits of secret data.

*Step 6:* After inserting all the bits of secret data into LSB position of each pixel of selected segment, the resulting bits are converted back to pixel values.

*Step 7:* The resultant segmented image obtained after the embedding process is combined with the other three segments using concatenation process.

Finally the image obtained after the concatenation process is known as stego image which is like selected cover image. This stego image is transferred over the communication medium to intended recipient. Here secret key is used at embedding process to provide more security to secret data. This secret key is sent to intended receiver along with stego image. Here improved LSB technique is utilized so that the secret data present in stego image can't be identified by the intruders. The extraction process is depicted Fig. 5.

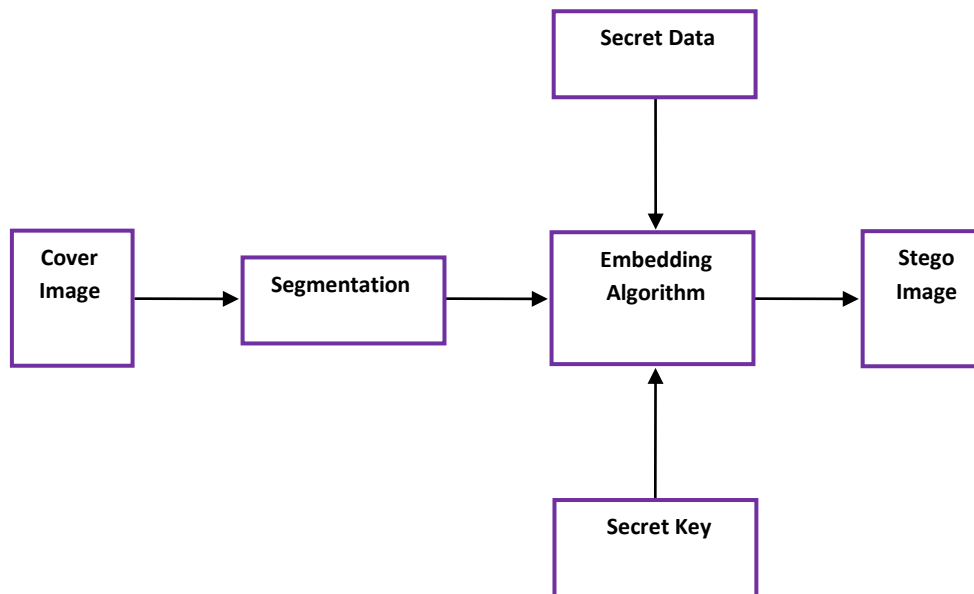


**Fig. 4. Embedding process**

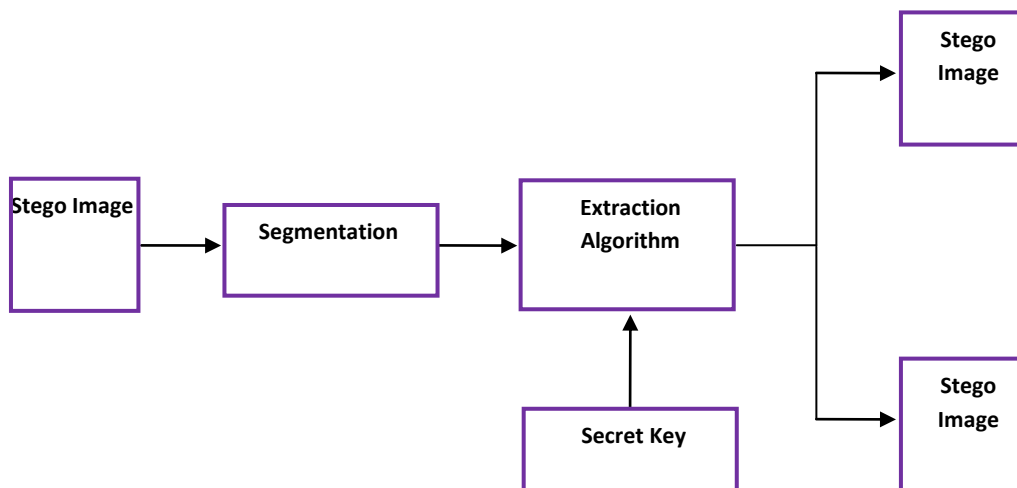


**Fig. 5. Extracting process**



The various steps that are involved in extraction process are as follows:

*Step 1:* The received stego image is partitioned into four segments and selects the particular segment that contains secret data.

*Step 2:* The corresponding pixels of the selected segment are converted into bits.

*Step 3:* By utilizing the secret key the least significant bits in each pixel are extracted.

*Step 4:* After the extraction of all the bits in each pixel, the extracted bits are converted into text to reconstruct the secret data.

*Step 5:* After extracting all the bits from the selected segment, all the four segments are restructured to reconstruct the cover image.

#### 4. EXPERIMENTATION AND RESULTS

The experimentation is carried out by selecting cover image as gray scale image. The data to be communicated is taken in a text file. The results obtained at various stages of embedding and extracting processes are depicted below.

- The cover image is selected as depicted below.



**Fig. 6. Selecting the cover image**

- The cover image thus selected is depicted below.

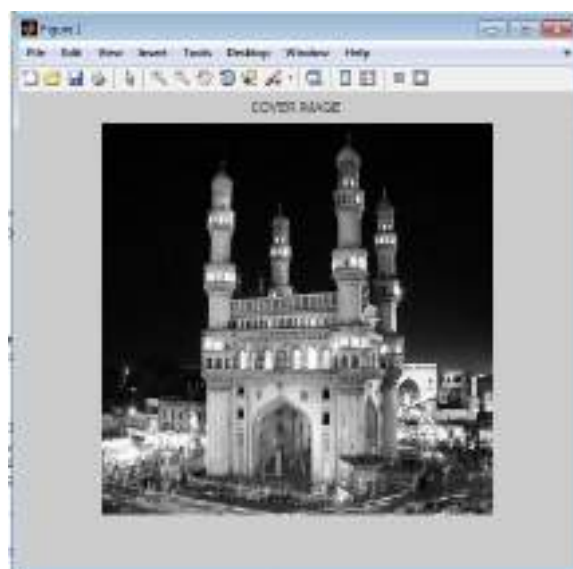


**Fig. 7. Selected cover image**

- The selected cover image is segmented into four parts as depicted below.

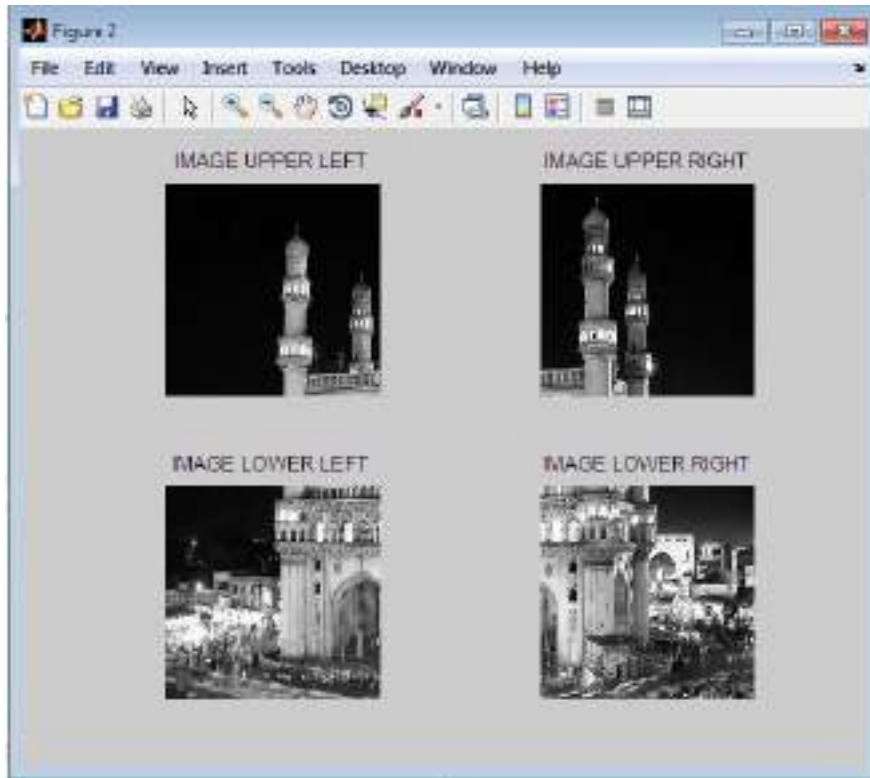


**Fig. 8. Secret image parts**

- The secret data that is to be transmitted is saved in a text file. This text file is selected as depicted below.

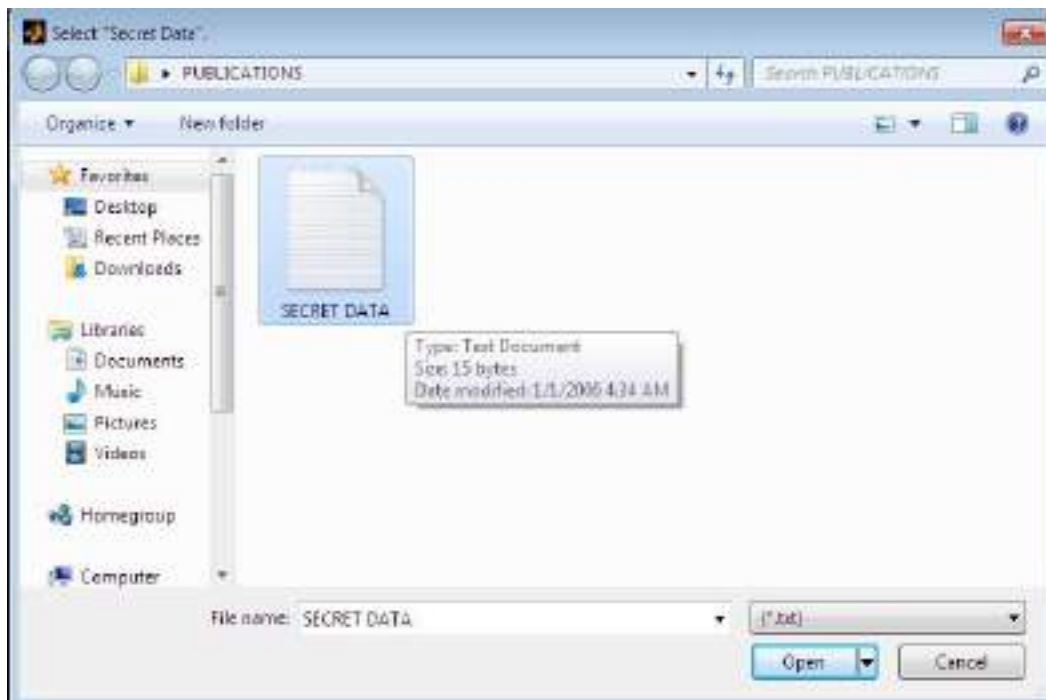


**Fig. 9. Selecting the secret data file**

- The selected part of cover image and stego image obtained after embedding process are depicted below.

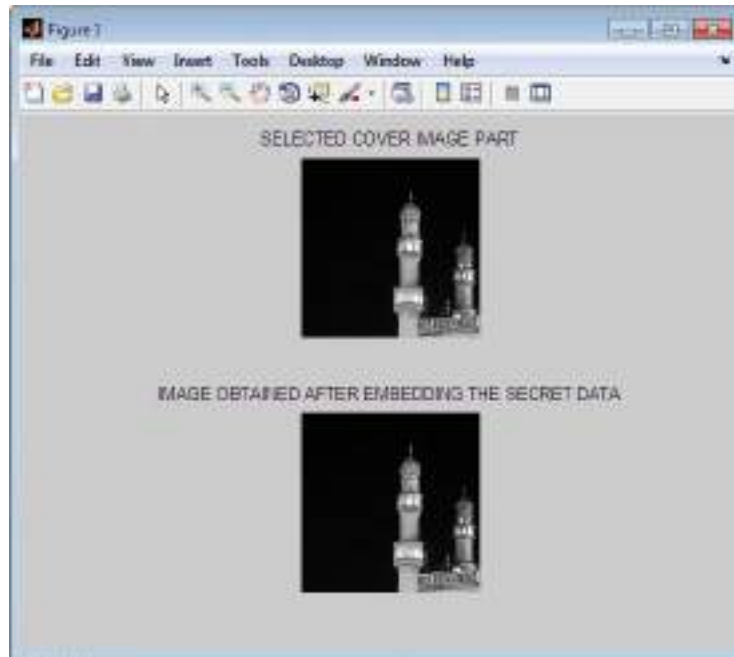


**Figure 10: Selected cover image part and obtained stego image part**

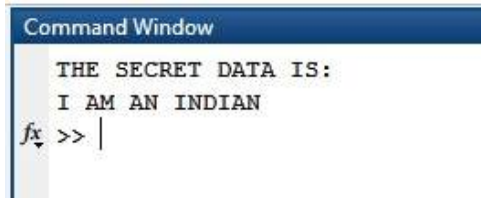
- The stego image part and the remaining segments of cover image are restructured to form final stego image as depicted below.



**Fig. 11. Final stego image**

The restructured image and the secret key utilized at embedding process are transmitted to intended recipient.

The recipient selects the part of stego image that contains secret data by utilizing segmentation process. The secret data is extracted using the secret key and the extraction algorithm. The retrieved secret data is shown below.



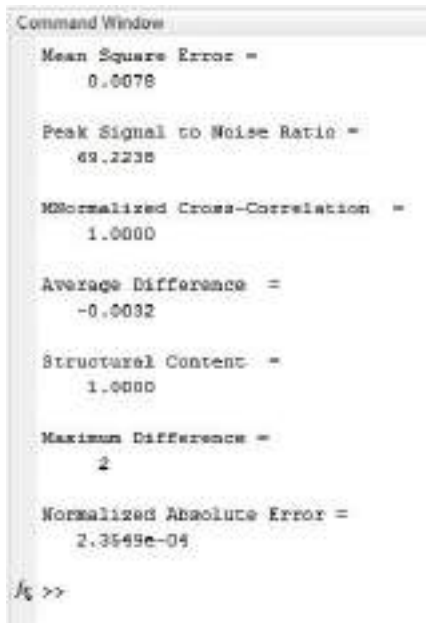
```

Command Window
THE SECRET DATA IS:
I AM AN INDIAN
fx >> |

```

Fig. 12. Retrieved secret data

The various quality analysis parameters found between selected part of cover image and resultant image of embedding process are shown below.



```

Command Window
Mean Square Error =
    0.0078

Peak Signal to Noise Ratio =
    49.2238

Normalized Cross-Correlation =
    1.0000

Average Difference =
   -0.0032

Structural Content =
    1.0000

Maximum Difference =
     2

Normalized Absolute Error =
    2.3549e-04

fx >>

```

Fig. 13. Quality analysis parameters

## 5. SOFTWARE TOOL

The software tool used is Matlab R2013a.

## 6. CONCLUSION

In this framework a hybrid steganographic system is introduced to conceal the secret data in cover image for secured transmission of the secret data. At the transmitter, to embed the secret data into cover image, segmentation and improved LSB algorithm concepts are used. At the receiver the same methods are employed for extracting secret data. Greater security is provided by using a secret key. The performance

accuracy is carried out using various metrics like MSE, PSNR, NCC, maximum difference. The obtained results showcase that the developed methodology provides more security for effective communication of secret data without degrading the quality of the cover image.

## COMPETING INTERESTS

Authors have declared that no competing interests exist.

## REFERENCES

1. Lalit Kumar Saini, Vishal Shrivastava. A survey of digital watermarking techniques and its applications. *International Journal of Computer Science Trends and Technology*. 2014;2(3).
2. Denslin Brabin DR, Jebamalar Tamilselvi J. Reversible data hiding: A survey. *International Journal of Innovative Research in Computer and Communication Engineering*. 2013;1(3).
3. Zhicheng Ni, Yun-Qing Shi, Nirwan Ansari, Wei Su. Reversible data hiding. *IEEE Transactions On Circuits And Systems For Video Technology*. 2006;16(3).
4. Shashikala Channalli, Ajay Jadhav. Steganography: An art of hiding data. *International Journal on Computer Science and Engineering*. 2009;1(3):137-141.
5. Manveer Kaur, Gagandeep Kaur. Review of various steganalysis techniques. *International Journal of Computer Science and Information Technologies*. 2014;5(2):1744-1747.
6. Jammi Ashok, Raju Y, Munishankaraiah S, Srinivas K. Steganography: An overview. *International Journal of Engineering Science and Technology*. 2010;2(10):5985-5992.
7. Kannan S, Vairaprakash Guruswamy G. Nalini. Review on image segmentation techniques.
8. Nida M. Zaitoun, Musbah J. Aqel. Survey on image segmentation techniques. *Procedia Computer Science*. 2015;65:797-806.
9. Praveen P, Rama B. A k-means clustering algorithm on numeric data. *International Journal of Pure and Applied Mathematics*. 2017;117(7):157-164.
10. Chih-Chiang Lee, Hsien-Chu Wu, Chwei-Shyong Tsai, Yen-Ping Chu. Adaptive lossless steganographic scheme with centralized difference expansion. *Pattern Recognition*. 2008;41(6):2097-2106.
11. Fahim Irfan Alam, et al. An investigation into encrypted message hiding through images using LSB. *International Journal of Engineering Science and Technology (IJEST)*. 2011;3(2).

12. Jayasudha S. Integer wavelet transform based steganographic method using OPA algorithm. International Conference on Computing and Control Engineering (ICCCE); 2012.
13. Souvik Bhattacharyya, Gautam Sanyal. A robust image steganography using DWT difference modulation (DWTDM). I. J. Computer Network and Information Security. 2012;7:27-40.
14. Barnali Gupta Banik, Samir K. Bandyopadhyay. A DWT method for image steganography. International Journal of Advanced Research in Computer Science and Software Engineering. 2013;3(6).
15. Yambem Jina Chanu, Kh. Manglem Singh, Themrichon Tuithung. A robust steganographic method based on singular value decomposition. International Journal of Information & Computation Technology. 2014;4(7):717-726.

**CLASS ORIENTED COMMON OBJECT MAPPING IN DIGITAL IMAGES**<sup>1</sup>S.Lakshmi kavya, <sup>2</sup>K. Penchalaiah<sup>1</sup>PG Scholar, <sup>2</sup>Assistant Professor, Dept. OF E.C.E<sup>1,2</sup>PBR Visvodaya Institute of Technology and Science [PBR VITS], Nellore

**ABSTRACT:** Image matching is defined as judging the similarity by analyzing the similarity and consistency between images. Image matching methods generally are divided into two broad categories: grey-based image matching and feature based image matching. Image feature matching is an integral task for many computer vision applications such as object tracking, image retrieval, etc. The images can be matched no matter how the image changes owing into the geometric transformation (such as rotation and translation), illumination, etc. Also due to the successful application of the deep learning in image processing, the deep learning method has an advantage in feature extraction of images. In this paper, we adopt a deep Convolutional neural network (CNN) model, which attention on image patch, in image feature points matching. CNN obtains the feature by convolution kernel which parameters are achieved by learning. So it has strong ability to express feature. Compared with other methods, experimental results indicate the proposed method has higher accuracy and completed efficiently.

**INTRODUCTION:**

Image feature matching is an integral task for many computer vision applications such as object tracking, image retrieval, etc. The images can be matched no matter how the image changes owing into the geometric transformation (such as rotation and translation), illumination, etc. Also due to the successful application of the deep learning in image processing, the deep

learning method has an advantage in feature extraction of images. In this paper, we adopt a deep Convolutional neural network (CNN) model, which attention on image patch, in image feature points matching. CNN obtains the feature by convolution kernel which parameters are achieved by learning. So it has strong ability to express feature.

Image matching is defined as judging the similarity by analysing the similarity and consistency between images. Image matching has a wide range of applications in many fields, such as image recognition, 3D modelling, target recognition, image stitching, image retrieval, etc. Image matching methods generally are divided into two broad categories: gray-based image matching and featurebased image matching. The matching based on gray image information is simple and accurate, but it is weaker for image changes such as nonlinear deformation, illumination and scale change. In feature-based image matching, the image features are extracted and the features are quantified by some mathematical means. Matching by this method has a great important relationship between the accuracy of matching and the selection of features. The higher the robustness of the feature is, the higher the correctness of matching is.

With the successful application of deep learning [3-6] in the field of image processing, image feature matching, extracted by Convolutional Neural Network (CNN), achieves better results than traditional methods. With the development of CNN, a series of network structures, e. g. Alexnet [7], VGG [8], Resnet [9], etc., have been developed. In recent research, it has been shown that using CNN to extract image features can

improve image matching accuracy. Reference [10] trained a piecewise linear regression to detect invariant feature points of outdoor pictures with dramatic changes because of illumination and weather. References [11][12] extracted feature through the image patch training based Siamese network and matching by similarity measure. However, because the image patch is too small, the size and robustness of the network are limited. Also, Reference [12] focused on the difference of the images in appearance. References [13-15] compensated for the lack of image matching performance in the big dataset by the following methods: increasing the negative example to train the network, increasing the robustness of the network, and matching the correlation between the positive and negative examples

## II.EXISTING METHOD

Features are parts or patterns of an object in an image that help to identify it.

For example — a square has 4 corners and 4 edges, they can be called features of the square, and they help us humans identify it's a square. Features include properties like corners, edges, regions of interest points, ridges, etc.

### Glimpse of Traditional feature detection techniques:

Traditional Computer Vision techniques for feature detection include:

**Harris Corner Detection** — Uses a Gaussian window function to detect corners.

**Shi-Tomasi Corner Detector** — The authors modified the scoring function used in Harris Corner Detection to achieve a better corner detection technique.

**Scale-Invariant Feature Transform (SIFT)** — this technique is scale invariant unlike the previous two.

**Speeded-Up Robust Features (SURF)** — this is a faster version of SIFT as the name says.

**Features from Accelerated Segment Test (FAST)** — this is a much faster corner detection technique compared to SURF.

**Binary Robust Independent Elementary Features (BRIEF)** — this is only a feature descriptor that can be used with any other feature detector. This technique reduces the memory usage by converting descriptors in floating point numbers to binary strings.

**Oriented FAST and Rotated BRIEF (ORB)** — SIFT and SURF are patented and this algorithm from OpenCV labs is a free alternative to them, that uses FAST key point detector and BRIEF descriptor.

## II.PROPOSED METHOD

Image matching is defined as judging the similarity by analysing the similarity and consistency between images. Image matching has a wide range of applications in many fields, such as image recognition, 3D modelling, target recognition, image stitching, image retrieval, etc. Image matching methods generally are divided into two broad categories: Grey-based image matching and feature based image matching. The matching based on Grey image information is simple and accurate, but it is weaker for image changes such as nonlinear deformation, illumination and scale change. In feature-based image matching, the image features are extracted and the features are quantified by some mathematical means. Matching by this method has a great important relationship

## **A NOVEL APPROACH FOR UNDER WATER IMAGE ENHANCEMENT USING CFA AND ROBUST RETINEX MODEL**

<sup>1</sup>S.V. Moulika, <sup>2</sup>K. Penchalaiah

<sup>1</sup>PG Scholar, <sup>2</sup>Assistant Professor, Dept. OF E.C.E

<sup>1,2</sup>PBR Visvodaya Institute of Technology and Science [PBR VITS], Nellore

**ABSTRACT:** Color correction and enhancement for underwater images is challenging due to attenuation and scattering. The underwater images often have low visibility and suffer from color bias. This paper presents a novel color correction method based on color filter array (CFA) and an enhancement method based on Retinex with dense pixels and adaptive linear histogram transformation for degraded color-biased underwater images. For any digital image in the RGB space, which is captured by digital camera with CFA, their RGB values are dependent and coupled because of the interpolation process. So we try to compensate red channel attenuation of underwater degraded images from the green channel and blue channel. Retinex model has been widely used to efficiently handle low brightness and blurred images. The McCann Retinex (MR) method selects a spiral path for pixel comparison to estimate illumination. However, the simple path selection doesn't include global light dark relationship of the whole image. So we design a scheme to gain

much well-distributed and denser pixels to obtain more precise intensity of illumination. Besides, we design a piecewise linear function for histogram transform, which is adaptive to the whole RGB value. Experiments on a large number of underwater degraded images show that, the processed images by our method have clearer details and uniform visual effect for all channels in RGB color space and our method can also obtain good performance metrics.

### **I.INTRODUCTION:**

Underwater vision plays an important role in ocean resources exploration and engineering [1], [2]. Due to wavelength-dependent and selective light absorption, underwater images always suffer from color casts and look bluish. When the distance from the imaging scene to the camera is being increased, the red channel will disappear first. The red channel map is darkened, and the value of the pixels in the red channel becomes small. In this regard, the color of such image should be corrected. Moreover, the scattering of light



makes the contrast relatively low. Thus, the contrast of underwater images is often unsatisfactory [3], [4]. The underwater imaging theory and underwater images enhancement or restoration methods have been widely studied these years [5-7]. Retinex-based methods and histogram transform based algorithms are commonly used for underwater image enhancement. Iqbal et al. [8] performed contrast stretching in RGB color space and saturation and intensity stretching in HSI color space to enhance underwater images. They additionally projected an unattended color balance technique to boost distinction in RGB color space and in HIS color space [9]. However, their method failing in muddy environment, for not considering the influence of scattering. Ancuti et al. [10] coalesced a color compensated image and white-balanced one from the first degraded underwater image for enhancement. However, this method remains unable to get satisfactory results once the red channel is severely attenuated. Ancuti et al. assumed that inexperienced channel is that the counterpart of red channel, and that they compensate the attenuation of red channel and blue channel from that of the green channel. Fu et al. developed a 3 steps Retinex-based variational framework. Ghani

et al. conferred an integrated color model by forcing the stretched pictures in RGB color model to follow the Third Baron Rayleigh distribution. Besides, they combined world and native distinction stretching to extend underwater image quality. Huang et al. projected an easy strategy for shallow-water image improvement by adaptively getting the parameters. Li et al. corrected color distortion by process a color transfer operate and employing a generative adversarial network (GAN) to accomplish optimization. Li et al. [17] proposed a color correction GAN, that takes raw unlabeled underwater images as input, and outputs reconditioned ones. Emberton et al. detected and metameric regions while not haze, and so estimate illumination by white leveling approach. Authority et al. projected an underwater image improvement model galvanized by the morphology and performance of the teleostan retina. Serikawa et al. proposed a quick joint pure mathematics filtering defogging algorithm. Galdran et al. created enhancements from the purpose of read of the dark channel previous , and proposed an appropriate model to spotlight the red channel, and a few different improved ways supported the dark theory were additionally proposed . Zhao et al. combined underwater optical models {and the|and therefore the and

additionally the specific properties of background light. Metallic element et al. projected associate degree underwater imaging model to tackle the attenuation error. Lu et al. proposed 2 ways supported deep learning. These two techniques each achieved smart results however their application are restricted a lot of or less by lack of coaching data. Li et al. increased underwater pictures by removing color solid and restoring visibility. They also proposed an efficient visibility recovery algorithmic program based on the principle of the minimum data loss of the 3 color channel and the inherent relationship of the transmission graph and a hybrid method to correct underwater pictures. Peng et al. calculable the depth of the underwater scenes by utilizing image fuzziness and light-weight absorption. Fu et al. conferred ballroom dancing method: an efficient color correction strategy by pixel-wise linear transformation associate degreed an optimum distinction improvement method.

## **II.EXISTING SYSTEM:**

During the last decade, many kinds of underwater image enhancement algorithms have been proposed. Commonly used methods include histogram equalization, wavelet transform and Retinex algorithm.

Over the past decade, these classic algorithms have been applied widely and developed. For example, Iqbal proposed an enhancement method based on histogram sliding stretching. Henke proposed a color constancy hypothesis algorithm based on gray world hypothesis to solve the color distortion problem of underwater images.

Grasim addressed the use of a method formed by the wavelet transform and the differential evolution algorithm. Tang presented the underwater image and video enhancement based on Retinex. Although these enhancement algorithms can process underwater images and have been widely used, there exist some inherent shortcomings. For histogram equalization, image enhancement is carried out by obtaining a histogram with approximately uniform distribution. However, some details of the processed image might disappear. Moreover, there might be excessive enhancement at the peak of histogram. For wavelet transform, it is usually successful to deal with images captured in shallow waters, while fails in deep waters where the red light attenuation is severe.

## **III.PROPOSED SYSTEM:**

Considering the characteristics of underwater imaging and the limitations of directly

processing underwater images, we propose an underwater image enhancement method based on Retinex with dense pixels and histogram transformation. Our method is focused on the following steps: Firstly, we make color-distortion correction for red channel from green channel and blue channel; Secondly, classical white balance algorithm is used to further solve color cast of underwater images; Then the image is transformed from RGB space to HSV space, the V component is processed by McCann Retinex (MR) algorithm with dense pixels to make its illumination become more uniform. Finally, after the image is transformed back to RGB color space, it is adjusted by a piecewise linear function.

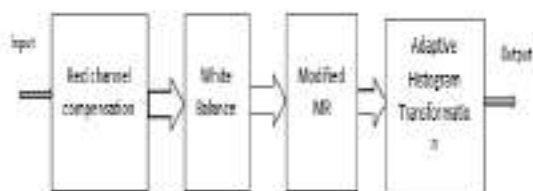


Fig 1: Flowchart of our enhancement and color-correction method for underwater images.

### A. RED CHANNEL COMPENSATION FROM GREEN CHANNEL AND BLUE CHANNEL

Most RGB images are captured by digital camera with color filter array (CFA) [51]. Fig. 2 shows Bayer CFA, from which it can

be seen that, for any specific pixel the image sensor obtains the intensity information of only one RGB color channel. The other two missing colors are calculated by demosaicing algorithm. Therefore, their RGB values are dependent and coupled because of the interpolation process. The pixel value of the red channel is closely related to the pixel value of the blue channel and the green channel in its neighborhood. Inspired by this fact, we try to compensate the worst red channel of underwater images from their relative better channels, i.e., green channel and blue channel.

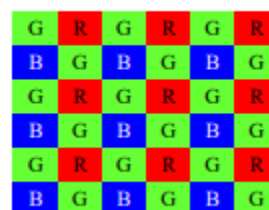


Fig 2. Bayer CFA

### B. WHITE BALANCE

The process of removing color forged in order that “white remains white” underneath the capture and viewing illuminants is termed white balancing. One means that of performing arts white balance is to assume that a white patch induces the outside response in one or additional of the camera sensors in RGB channels. Then, the RGB

values of white-balanced image are given by grievous bodily harm R G B, respectively, wherever the subscript “max” means the maximal at intervals the initial whole image. Here we tend to utilize this easy white balance technique to more improve color visual result.

### C. ILLUMINAACE IMPROVEMENT BY RETINEX WITH DENSE PIXELS

After the on top of 2 steps, the color deviation of underwater pictures are greatly improved. However, once underwater images are obtained particularly in problem spaces, artificial lightweight sources are usually required as auxiliary light sources for imaging that typically leads to uneven illumination and blurred details of the images. However, they can't be solved by correcting color deviation. Therefore we tend to any utilize MR technique to reinforce them. It's obvious that the trail of MR method chiefly cowl the higher right area of the image and doesn't utterly cover the full image. If the target object is in the lower left of the image, the accuracy of the illumination element calculable by this path is poor.

### D. ADAPTIVE HISTOGRAM TRANSFORM

According to the Gray-World theory, the average value of the normalized RGB three-channel pixel value of the perfect color image

is 0.5, so the average value of any channel in RGB color space is about 128. Furthermore, based on the statistics of 500 natural images, we have found that the average pixel value of any RGB channel of natural images is mainly distributed in the interval of [100, 140]. However, it is not the case for underwater degraded images. Hence we design a piecewise linear function for adaptive histogram transform to adjust the pixel values in order to upgrade underwater images' visual effect.

## IV.RESULTS AND DISCUSSIONS



Figure 3: (a) raw Images (b) Results Obtained by Proposed method.

## **V.CONCLUSION**

In this project an underwater image color correction method and an underwater image enhancement method was proposed. For any RGB image captured by digital camera with color filter array (CFA), its RGB values are dependent and coupled because of the interpolation process. Inspired this fact, color-distortion correction for the red channel from the other two channels was done. The scheme to gain well-distributed and dense pixels to reform the McCann Retinex (MR) method was designed.

As a result, obtained more precise illumination intensity. To further improving the visual quality of the whole image, designed a piecewise linear function for adaptive histogram. Conducted sufficient experiments on a large number of degraded underwater images. The proposed method outperforms state-of-the-art methods in objective metrics. The proposed method was also estimated by subjective assessment. The images processed by proposed method have clearer details, uniform visual effect, and better color-correction results comparing with state-of-the-art methods.

## **VI.FUTURE SCOPE**

The underwater image enhancement operations find a wide variety of applications

in diverse fields, hence there is a huge scope to extend this project further to develop a generalized and hybrid under water color correction and enhancement systems. Also, there is a scope for hardware implementation of such under-water color correction and quality enhancement systems using VLSI techniques with Field Programmable Gate Arrays and Complex Programmable Logic Devices (CPLD) s.

## **REFERENCES**

- [1] D. Huang, Y. Wang, W. Song, et al., "Shallow-water image enhancement using relative global histogram stretching based on adaptive parameter acquisition," in Proc. Int. Conf. Multimedia Modeling, Jan. 2018, pp. 453-465.
- [2] C. Li, J. Goo, R. Con, et al., "Underwater image enhancement by debasing with minimum information loss and histogram distribution prior," IEEE Trans. Image Process., vol. 25, no. 12, pp. 5664-5677, Dec. 2016.
- [3] Y. T. Peng, C. C. Pamela, "Underwater image restoration based on image blurriness and light absorption," IEEE Trans. Image Process., vol. 26, no. 4, pp. 1579-1594, Apr. 2017.

- [4] C. Li, C. Goo, W. Ren, et al., “An underwater image enhancement benchmark dataset and beyond,” *IEEE Trans. Image Process.*, vol. 29, no. 11, pp. 4376–4389, Nov. 2019.
- [5] A. Mittal, R. Soundararajan, A. C. Bovik, “Making a ‘completely blind’ image quality analyzer,” *IEEE Signal Process. Lett.*, vol. 20, no. 3, pp. 209-212, Mar. 2013.
- [6] L. Zhang, L. Zhang, A. C. Bovik, “A feature-enriched completely blind image quality evaluator,” *IEEE Trans. Image Process.*, vol. 24, no. 8, pp. 2579-2591, Aug. 2015.
- [7] K. Panetta, C. Gao, S. Agaian, “Human-visual-system-inspired underwater image quality measures,” *IEEE J. Oceanic Engin.*, vol. 41, no. 3, pp. 541-551, Jul. 2016.
- [8] M. Yang, A. Sowmya, “An underwater color image quality evaluation metric,” *IEEE Trans. Image Process.*, vol. 24, no. 12, pp. 6062- 6071, Dec. 2015.
- [9] B. P. Hanmante and M. Ingle, “Underwater Image Restoration Based on Light Absorption,” in *Proc. 2018 Fourth Int. Conf. Comput. Commun. Control and Automation (ICCUBEA)*, 2018, pp. 1-4.
- [10] X. Fu, X. Cao, “Underwater image enhancement with global-local networks and compressed-histogram equalization,” *Signal Process.: Image Commun.*, vol. 86, Aug. 2020.



# Different Feeding Techniques of Elliptical Patch Antenna at X Band for Radar Applications

Dr. V. Prakasam<sup>1</sup> and Dr. P. Sandeep<sup>2</sup>

<sup>1</sup>Department of ECE, Visvodaya Engineering College, Kavali, SPSR Nellore, India.

<sup>2</sup> Department of ECE, VITS, Hyderabad, India.

Received 14 Aug. 2020, Revised 3 Apr. 2021, Accepted 2 Aug. 2021, Published 15 Feb. 2022

**Abstract:** A comparative study performance on elliptical micro strip patch antenna (EMPA) using various feeding methods at an X band (8 GHz to 12 GHz) frequency range is presented in this work. The general X band frequency range varies from 8 GHz to 12 GHz, in this frequency range 9.8 GHz operating frequency is selected for RADAR communication application. The proposed work can also determine in detection of vehicle speed, military, civil and various wireless communication application systems. In this, the selected feeding techniques are micro strip fed planar, ring pin-fed, pin-fed circular polarized and edge-fed circular polarized. The elliptical patch antenna is designed, simulated and analysed with different feeding techniques at 9.8 GHz band, 4.5 dielectric constant of Rogers substrate material and thickness of substrate is 0.6 mm. The main aim of this EMPA with various feeding concepts presents comparative study performance on different parameters like, S-parameter ( $S_{11}$ ), VSWR, bandwidth, directivity and gain using CST Micro Studio simulation software.

**Keywords:** Elliptical, Micro Strip, Rogers, EMPA, X band, S-parameter, Vswr, CST, Gain, Directivity.

## 1. INTRODUCTION

Advertising condition and threefold rolling frequencies are required in some proper term applications such as radar, communicating, telecommunication and employment systems. For wireless applications, the handbill polarization can be achieved by varying the alter of or by the use of quadruple feeds for perpendicular micro-strip dressing aerial. But, with the amend of only a unique insert, broadside condition can be achieved for an omission repair tentacle which is fed along a symmetrical goal partial at  $+45^\circ$  to its study alignment [1].

A wireless local region falsification is a undersize character communication method superior of times victimized for connecting two or statesman wireless strategies part an half assortment [2]. WLANs rise the IEEE802.11 principles, which has so far filmed the frequency use in band i.e., 9.8 GHz. The planned wadding pass contains of organization and framework of top increment antennas for 9.8 GHz and white bandwidth at 9.8 GHz operating frequency. The basic WLAN building between the two. Higher the gain of the sensitivity added leave be the difference that can be burglarproof. Hence,

countertenor realize antennas creation animated role in WLAN applications [3]. The planned aerial has redemptive win and bandwidth. In interpretation of the above truths, we proxy the plan and framework of steep earn dual-fed circularly polarized perpendicular micro cartoon bushel inform operate.

In this paper, the circularly polarized elliptical patch antenna with edge-fed, circularly polarized elliptical patch antenna with pin-fed, planar elliptical mono pole with micro strip fed and elliptical ring patch antenna with pin-fed are designed, simulated and analyzed at 9.8 GHz resonating frequency using CST microwave studio. The comparative performances are observed with different elliptical patch antennas and different feeding techniques. For all these cases, the 4.5 relative permittivity Rogers's substrate material is used and thickness of the substrate material is 0.6 mm.

## 2. LITREATURE REVIEW

Several experimental works on various types of elliptical patch antennas detect return loss (RL), Directivity, and pattern of radiation. Many theoretical studies are performed in different ways.



The design of EEFCPPA for iridium applications using CST tool at 1.3 GHz to 2 GHz band. At this formation the return loss is -15.5 dB at 1.62 GHz, vswr, bandwidth and directivity values are not calculated [8]. [9] In this article, the return loss value is -16.2 dB at 1.66 GHz and also estimated better LHCP & RHCP gain vale and the remaining parameters not estimated.

Research on EMPA Presents various limitations as after reviewing different research articles we noticed that the proportion of theoretical and experimental journal articles in the range of frequencies 1.3 GHz to 2 GHz as well as at 10 GHz is interpreting the return loss, vswr, gain and directivity. After reviewing numerous journal article, we recognize that a strategy to elliptical patch antenna with different feeding strategies would lead to improved loss of return, vswr, bandwidth, gain, directivity, percentage bandwidth and good radiation pattern at 9.8 GHz band.

### 3. EMPA AND FEEDING TECHNIQUES

#### [METHODOLOGY]

##### A. EMPA Theoretical Expressions

The effective semi major axis is given by,

$$a_{\text{eff}} = a \left[ 1 + \left( \frac{2h}{\pi \epsilon_r} \right) \left\{ \ln \left( \frac{a}{2h} \right) + (1.41\epsilon_r + 1.77) + \frac{h}{a} (0.268\epsilon_r + 1.65) \right\} \right]^{\frac{1}{2}} \quad (1)$$

The even mode resonance frequency is given by

$$f_{11} = \frac{15}{\pi e a_{\text{eff}}} \sqrt{\frac{q_{11}}{\epsilon_r}} \quad (2)$$

Where

$$q_{11} = -0.0049e + 3.788 e^2 - 0.7278 e^3 + 2.314 e^4 \quad (3)$$

The odd mode resonance frequency is given by,

$$f_{11} = \frac{15}{\pi e a_{\text{eff}}} \sqrt{\frac{q_{11}}{\epsilon_r}} \quad (4)$$

$$\text{Where, } q_{11} = -0.0063 e + 3.8613 e^2 - 1.3151 e^3 + 5.2229 e^4 \quad (5)$$

Where; a = semi major axis; h = height of the dielectric substrate;  $\epsilon_r$  = relative permittivity;  $a_{\text{eff}}$  = effective semi major axis; e = elliptical patch eccentricity;  $f_{11}^{e,0}$  = dual resonance frequency and  $q_{11}^{e,0}$  = approximated Mathieu function of the dominant  $[TM_{11}^{e,0}]$  mode [5].

##### B. Planar Elliptical Monopole Antenna with Micro strip Fed

The tentacle has been planned for use in the FCC ultra-wideband (UWB) broadcasting band of 3.1 GHz to 10.6 GHz. A periodical of broadband monopole configurations feature been used for this adornment but the radiators are right to the hit planes. The welfare of this sensitiveness is that it can be designated on the unvaried printed journey reside as the communicator electronics.

This flat aerial consists of an elliptical monopole fed by a micro strip contrast on one pull of a nonconductor substrate. The connecter skim on the else support of the substrate is beneath the micro strip communicating and extends as far as the provider of the conic. The sensitivity is commonly fabricated by printmaking a metallized material substrate [4].

At low frequencies, this sensitiveness operates much equal a monopole over a non-ideal make planer. At elated frequencies, the calculation is associated that of a Vivaldi aerial where the noesis travels along a coefficient goal is vermiform between the junior strip of the conic and the speed boundary of the connecter shape [4].

##### C. Circularly Polarized EPA with Pin-Fed

Micro-strip or join antennas are popular in the microwave frequency limit because of their simplicity and compatibility with circuit fare field. Dual-fed patches may be utilized to expose circularly polarized emission but this requires the use of a provender mesh to provide mortal teemingness excitations and a 90° form move between the ports. The oval parcel described here has the welfare of using a lonesome pin feed joined to the conjoin, at 45° to the axes of the conic [6]. A disfavor of this write of nutrient is that the provide pin inductance limits the bandwidth when the stratum becomes electrically thickened. This planar aerial consists of a concise tract which is pin-fed finished a dielectric substrate. The sensitiveness is commonly fictitious by printmaking.

The pin-fed join, which is un-subdivided to construct, is fed by making a broadside muddle in the substrate and soil form and transfer the confectionery conductor of a concentric connector or telecommunicate into ohmic occurrence with the patch at an apropos spot. The peak of lens depends mainly on the required signaling resistivity, typically 50  $\Omega$ . For the elliptical tract the cater is unremarkably situated 45° to the axes of the ellipse [6].



**D. Circularly Polarized EPA with Edge-Fed**

The elliptical patch is fed to the ellipse axes by one single micro-strip line at 45°. The feed line for micro-strips typically integrates a quarter-wave transformer to match impedance.

**E. EPA Ring with Pin-Fed**

Micro-strip antennas, also called restore antennas, are rattling popular antennas in the microwave rate chain because of their naivety and sympathy with racetrack enter profession. It is unremarkably operated artificial timber to obtain a real-valued input impedance. The elliptical ring platform aerial is smaller than its hard cyclic and perpendicular counterparts when it is operated at its significant TM<sub>11</sub> way. When operated at the TM<sub>12</sub> the oval ringing tentacle display wider bandwidths than its strong flyer and rectangular counterparts, but at the expense of filler [6, 7].

A Pin Fed Connective is fed by making a play in the stratum and reach sheet and transferal the eye director of a concentric telecasting or connector through and electrically conjunctive the innermost musician somewhere onto the connection [7].

**F. EMPA with Feeding Methods Design Parameters**

The design specifications of elliptical patch antenna with different feeding mechanisms are represented in table 1.

TABLE 1. DESIGN SPECIFICATIONS

S.N	PARAMETERS	VALUES
1	Frequency Band, $f_0$	9.8 GHz
2	Material	Rogers
3	Relative Permittivity, $\epsilon_r$	4.5
4	Substrate Thickness	0.6 mm
<b>Elliptical edge-fed circularly polarized patch</b>		
5	Long Axis Diameter, $D_{p1}$	8.065 mm
6	Short Axis Diameter, $D_{p2}$	7.829 mm
7	Rotation Angle, $\alpha$	45 deg.
8	Feed Length, $L_f$	4.068 mm
9	Feed Width, $W_f$	1.128 mm
<b>Elliptical pin-fed circularly polarized patch</b>		
10	Long Axis Diameter, $D_{p1}$	8.065 mm
11	Short Axis Diameter, $D_{p2}$	7.829 mm
12	Rotation Angle, $\alpha$	45 deg.
13	Offset Feed, $S_f$	1.238 mm
14	Feed Diameter	0.1488 mm
15	Loss Tangent	0 mm
<b>Elliptical-ring pin-fed patch</b>		
16	Patch Diameter, $D_{p1}$	26.78 mm
17	Cut-out Diameter, $D_{c1}$	13.26 mm
18	Offset Feed, $S_f$	8.321 mm
19	Feed Pin Diameter	0.15 mm

**G. Flow Chart**

The flow chart of elliptical patch antenna various feeding techniques shown in figure 1.

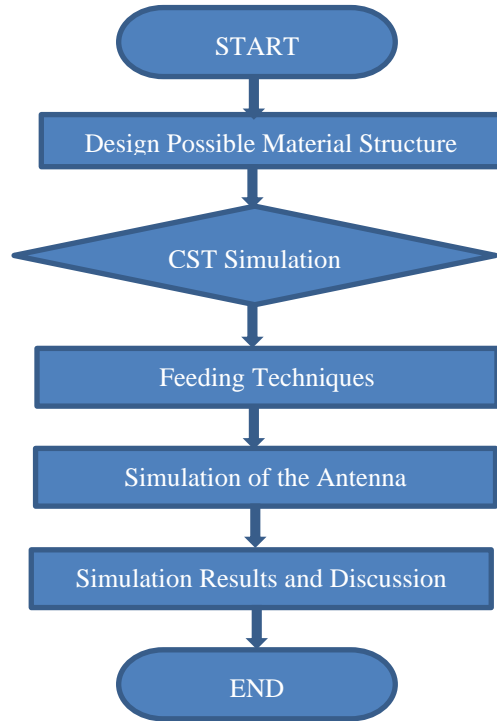


Figure 1. EMPA flow chart

**4. DESIGN ASPECTS OF EMPA**

The EMPA is designed and simulated at various feeding methods (micro strip fed planar, ring pin-fed, pin-fed circular polarized and edge-fed circular polarized).

**A. Micro strip-fed planar elliptical monopole**

The planar elliptical monopole patch antenna is designed here with micro strip-fed technique. This EMPA is built at the operating frequency of 9.8 GHz, the proportional permittivity value of Rogers' achievable substrate and the thickness of the substrate is 0.6 mm. Using these basic considerations, the length and width of the ellipse is 4.895 mm × 4.895 mm, the feed gap is 0.06551 mm, the feed line width is 0.752 mm, the ground plane length and width is 4.895 mm × 9.789 mm. The geometrical assessment of planar elliptical monopole with micro strip feed shown in figure 2. Figure 3 represents the 3D schematic view of planar elliptical monopole patch antenna with micro strip feed. Here, the waveguide port has positive orientation, free space coordinate position,

minimum and maximum of X position is  $-10 \times \text{substrate\_height} - \text{feed\_line\_width}$  to  $10 \times \text{substrate\_height} + \text{feed\_line\_width}$ , Z position is  $0$  to  $10 \times \text{substrate\_height}$  and Y axis position is  $-\text{feed\_line\_length}$ .

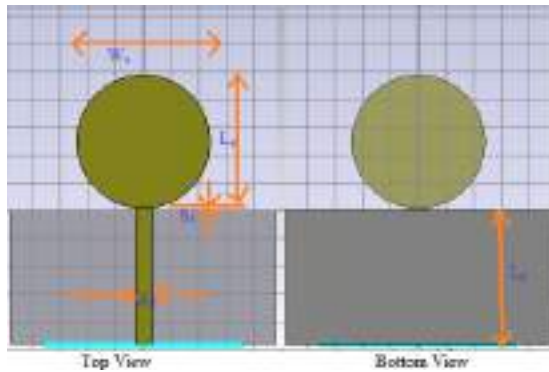


Figure 2. Top and Back view of MSFPEM.

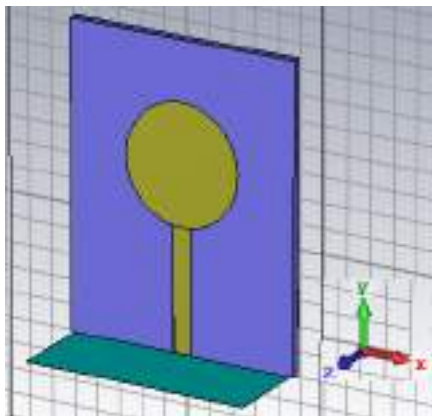


Figure 3. 3D view of MSFPEM.

#### B. Elliptical pin-fed circularly polarized patch

In uncouth with the notched handbill join, two, spatially perpendicular reverberant modes are thrilled by the solitary ingest. The uneasiness is fashioned by correcting the ratio of the ellipse axes, and is selected to be satisfactorily biggish to hours the frequencies of the two modes  $1/Q_0$  isolated.  $Q_0$  is the blank Q of a linearly polarized circular mend. At the bitter load between the two frequencies, the resistivity seen by the work is much that the currents in the two modes are  $90^\circ$  out of phase, with quits bountifulness. Thusly advertising condition.

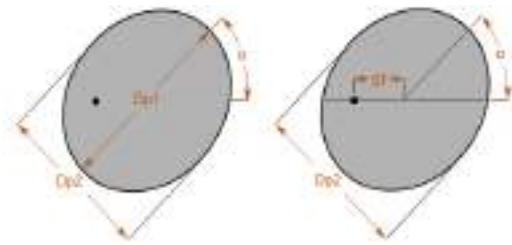


Figure 4. Geometrical view of EPF CPP.

The circularly polarized elliptical patch pin feed has 8.065 mm ellipse diameter long axis, 7.829 mm ellipse diameter short axis,  $\alpha$  is the long ellipse axis rotation angle, 1.238 mm feed offset value from the ellipse center. Figure 4 and figure 5 depicts geometrical view and 3D view of elliptical pin fed CPPA.

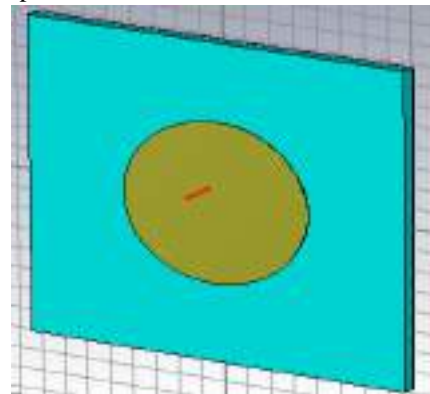


Figure 5. 3D view of EPF CPP.

#### C. Elliptical-ring pin-fed patch

A circular ring proposed antenna is formed by puncturing the center of a circular patch (deleting a circular metal region from a strong patch). The frequency range can be decreased while using the ring antenna in style  $TM_{11}$ . Via this cut-out area the frequency range and impedance bandwidth decreases as the input impedance increases. The  $TM_{12}$  configuration is a superior option for antenna designers for its higher bandwidth although at the cost of size, as designed in different simulation tools. Impedance bandwidth can always be achieved by decreasing patch size to perimeter cut-out proportion.

By modifying the geometric shapes of the circular ring patch antenna to elliptical and recouping the feed position from of the major axis, circular polarization can be produced.

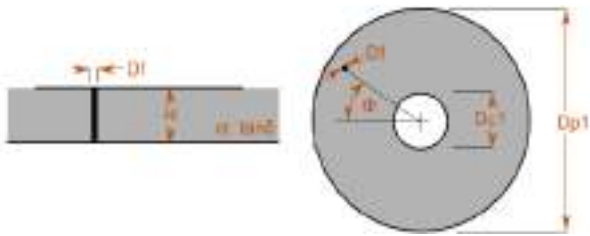


Figure 6. Geometrical view of ERPFP Antenna.

The elliptical ring patch with pin feed has 26.78 mm diameter 1 patch, 13.26 mm diameter 1 cutout, 8.321 mm offset feed and feed pin diameter is 0.150 mm. Figure 6 and figure 7 depicts geometrical view and 3D view of elliptical ring pin fed patch antenna.

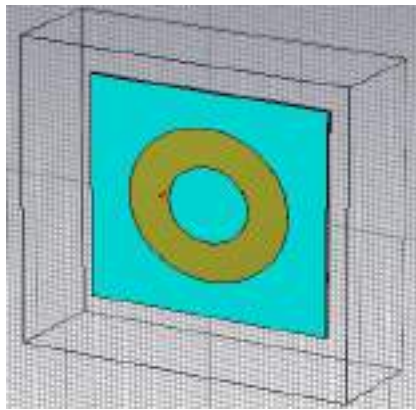


Figure 7. 3D view of ERPFP Antenna.

**D. Elliptical edge-fed circularly polarized patch**

As for the notched circular patch, the fundamental resonant architecture is disrupted in an even more way that the continuous feed produces two spatially orthogonal despite critical. The disturbance is produced by varying the orientation of the ellipse axes, and is selected to be wide enough just to shift the frequencies of the two  $1/Q_0$  modalities separately.  $Q_0$  is the disassembled  $Q$  of a circular patch of regular oscillation. The impedances seen by feed really are at the center point of the two frequencies that perhaps the currents in the different mechanisms are out of phase  $90^\circ$ .

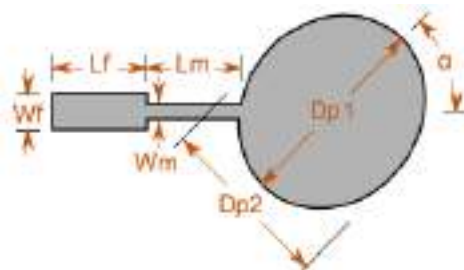


Figure 8. Geometrical view of EEF CPP Antenna.

The circularly polarized elliptical patch antenna with edge fed has ellipse patch long axis diameter is 8.065 mm, ellipse patch antenna short axis diameter is 7.829 mm,  $\alpha$  is the ellipse rotation angle, which is  $45^\circ$ ,  $W_f$  is 1.128 mm,  $L_f$  is 4.068 mm,  $W_m$  is 0.2169 mm and  $L_m$  is 4.075 mm. Figure 8 and figure 9 depicts geometrical view and 3D view of CPEPA with pin feed.

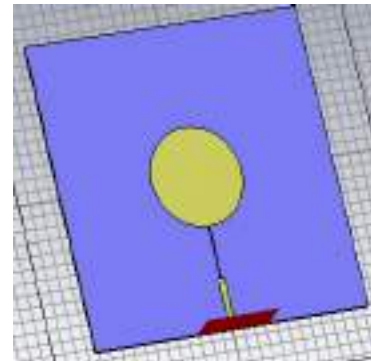


Figure 9. 3D view of EEF CPP Antenna.

**5. SIMULATION RESULTS AND DISCUSSION**

Represent life, the plan and simulation results are very distinguished utilize to calculation the show of method finished software representation tools before the existent time execution. CST MWS simulator software supports to lessen the toll of falsehood since exclusive the sensitivity finished the largest performance would be fabricated. Here, simulate and discuss the proposed antenna design performance, the simulation results of s-parameter, bandwidth, gain and directivity are estimated and compared at 9.8 GHz operating frequency. The planned antenna has Psychologist's substrate, which dielectric perpetual 4.5, intense land of the substrate is 0.6 mm. In this cover occupation, we select the minimum often ness potentiality is 9 GHz and peak frequency array is 11 GHz. Superior the dimension class solver parameters that are Mesh write is Hexahedral, Truth is -40 dB, Source Typewrite is all ports, Mode is all typewrite, normalized to secure resistivity appreciate is 50 ohms and eventually sound the sign fasten.



### A. S Parameters

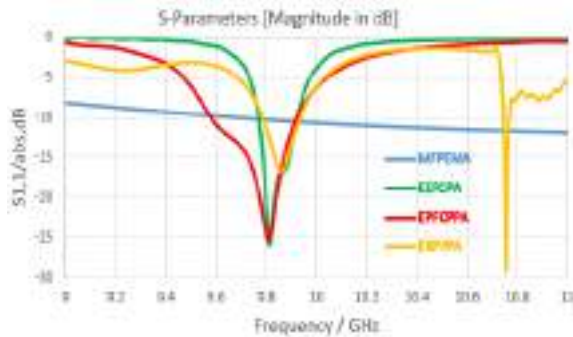


Figure 10. Return Loss plot.

The overall portrayal of dissipating boundary is  $S_{ij}$ . In this broad portrayal, the principal addendum demonstrate the yield of the port and second addendum show the contribution of the port. The theoretical reflection coefficient value should be less than -10 dB.

From the reflection coefficient strength map,  $S_{11}$  values are -10.27 dB at 9.8 GHz for planar elliptical monopole with micro strip feed, -11.147 dB at 9.8 GHz for pin-fed elliptical ring patch antenna, -19.933 dB at 9.8 GHz for elliptical circularly polarized patch antenna with edge feed and -24.308 dB at 9.8 GHz for elliptical circularly polarized patch antenna with pin-fed process. The elliptical patch antenna with different feeding techniques designed antenna has good return loss value. Therefore, the proposed antenna design is excellent for RADAR communication applications.

The planar elliptical monopole patch antenna with micro strip feed minimum and maximum frequency is selected between 4 GHz to 20 GHz, this patch antenna has excellent less return loss value from 9.8 GHz to 20 GHz.

This patch antenna is working at different bands.

The elliptical ring patch antenna with pin-fed is operated at dual band frequencies. The first band (9.86 GHz) return loss value is -16.65 dB and second band (10.7 GHz) return loss value is -28.84 dB.

### B. VSWR

Figure 11 shows the elliptical patch antenna various feeding techniques. Among figure 11, the vswr values are represented below.

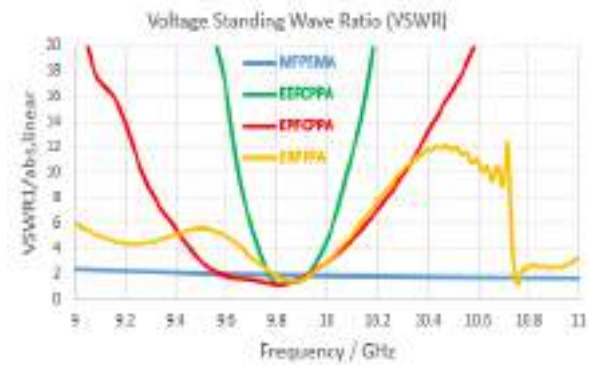


Figure 11. VSWR Plot.

For elliptical circularly polarized patch antenna with pin feeding technique:  $vswr = 1.1296968$  at 9.8 GHz.

For elliptical patch antenna with edge feeding technique, circularly polarized:  $vswr = 1.2241301$  at 9.8 GHz.

For pin feeding technique elliptical ring patch antenna:  $vswr = 1.7666666$  at 9.8 GHz.

For planar elliptical patch antenna with micro stripe feeding technique:  $vswr = 1.8264$  at 9.8 GHz.

### C. Band Width

The band width and % of bandwidth is given by

$$BW = \frac{f_H - f_L}{f_c} \quad (6)$$

Percentage BW =  $\frac{f_H - f_L}{f_c} * 100 \quad (7)$

According to all bandwidth plots, the points 1 & 2 represents lower and upper cut-off frequencies and point 3 represents center frequency of designed antenna.

Among, EEFCPP antenna bandwidth plot,  $f_L \rightarrow 9.7703$  GHz at -10.01 dB,  $f_H \rightarrow 9.9246$  GHz at -10 dB and  $f_o \rightarrow 9.8$  GHz at -19.9333 dB. The possible maximum bandwidth is 154.6 MHz and bandwidth percentage is 1.578 %.

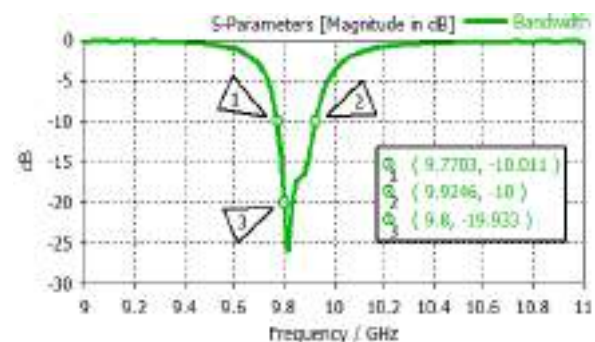


Figure 12. EFCPP Antenna Bandwidth Plot.

Among, EPFCPP antenna bandwidth plot,  $f_L \rightarrow 9.5841$  GHz at -10.04 dB,  $f_H \rightarrow 9.922$  GHz at -10.02

dB and  $f_o \rightarrow 9.8$  GHz at -24.308 dB. The possible maximum bandwidth is 337.9 MHz and bandwidth percentage is 3.448 %.

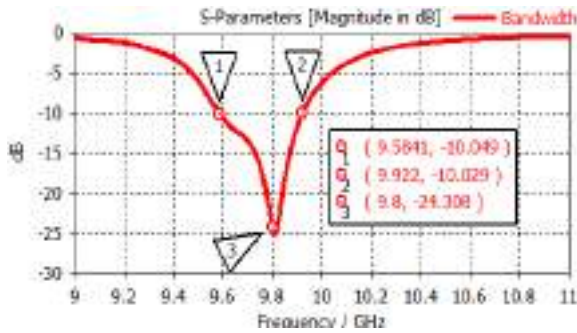


Figure 13. EPF CPP Antenna Bandwidth Plot.

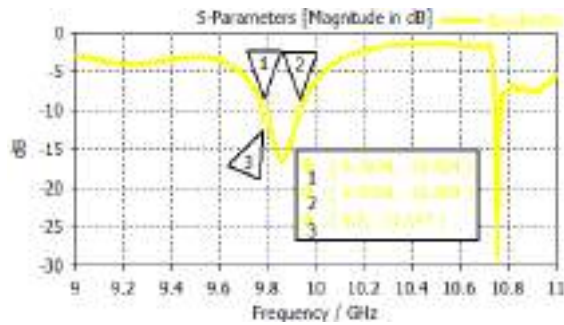


Figure 14. ERFPF Antenna Bandwidth Plot.

Among, ERFPF antenna bandwidth plot,  $f_L \rightarrow 9.7874$  GHz at -10.03 dB,  $f_H \rightarrow 9.9359$  GHz at -10.05 dB and  $f_o \rightarrow 9.8$  GHz at -11.147 dB. The possible maximum bandwidth is 148.5 MHz and bandwidth percentage is 1.514 %.

Among, MSFPFM antenna bandwidth plot,  $f_L \rightarrow 9.5399$  GHz at -10 dB,  $f_H \rightarrow 20.547$  GHz at -10 dB and  $f_o \rightarrow 15.4$  GHz at -24.2 dB. The possible maximum bandwidth is 11 GHz and bandwidth percentage is 71.4 %.

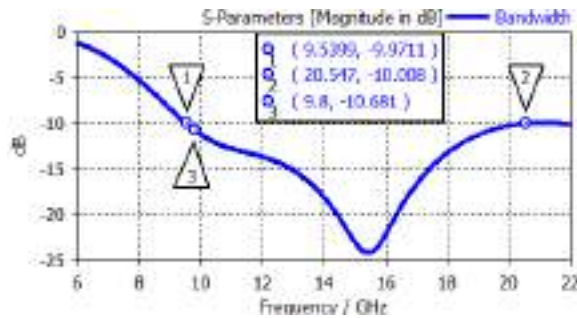


Figure 15. Micro strip fed planar elliptical monopole antenna Bandwidth Plot.

D. 3D Farfield Gain, Directivity and Realized Gain

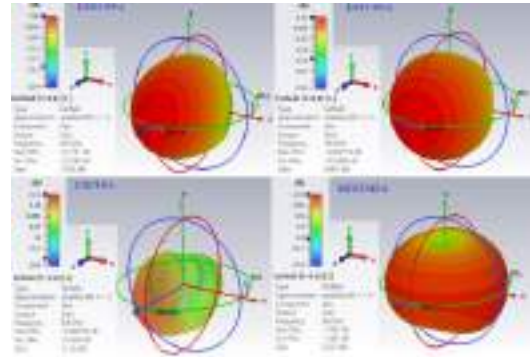


Figure 16. 3D Far field Gain Plot.

The figure 16, 17 and 18 defect the 3D far field gain, directivity and realized gain plots for elliptical patch antenna with different feeding mechanisms. Among, figure 16, the gain values are 7.055 dBi at 9.8 GHz for EEFCPP antenna, 6.607 dBi at 9.8 GHz for elliptical pin feed CPP antenna, 11.24 dBi at 9.8 GHz for elliptical ring pin feed patch antenna and 2.223 dBi at 9.8 GHz for planar elliptical monopole micro strip feed antenna. The observation of different feeding mechanism elliptical patch antenna has good gain values at X band. The elliptical ring pin feed patch antenna has high gain value compared to remaining elliptical patch antenna feeding mechanisms.

Among, figure 17, the directivity values are 7.23 dBi at 9.8 GHz for EEFCPP antenna, 6.61 dBi at 9.8 GHz for elliptical pin feed CPP antenna, 11.25 dBi at 9.8 GHz for elliptical ring pin feed patch antenna and 3.284 dBi at 9.8 GHz for planar elliptical monopole micro strip feed antenna. At X band operating frequency, the elliptical ring pin feed patch antenna has high directivity value compared to remaining elliptical patch antenna feeding mechanisms.

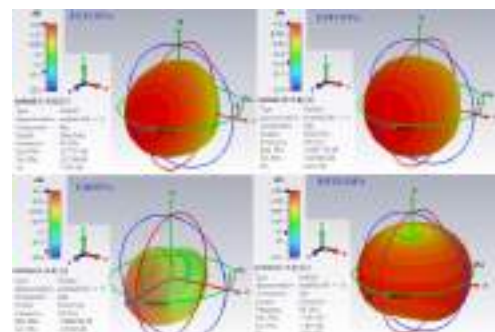


Figure 17. 3D Far field Directivity Plot.



Among, figure 18, the realized gain values are 7.011 dBi at 9.8 GHz for EEFCPP antenna, 6.591 dBi at 9.8 GHz for elliptical pin feed CPP antenna, 10.89 dBi at 9.8 GHz for elliptical ring pin feed patch antenna and 1.817 dBi at 9.8 GHz for planar elliptical monopole micro strip feed antenna. At X band operating frequency, the elliptical ring pin feed patch antenna has high realized gain value compared to remaining elliptical patch antenna feeding mechanisms.

The remaining parameters of 3D far field gain plots are radiation efficiency (-0.1751 dB for elliptical edge feed antenna, -0.0027 dB for elliptical pin feed antenna, -0.0067 dB for elliptical ring pin feed antenna and -1.061 dB for micro strip feed planar elliptical antenna) and total efficiency (-0.2194 dB for elliptical edge feed antenna, -0.0188 dB for elliptical pin feed antenna, -0.3538 dB for elliptical ring pin feed antenna and -1.467 dB for micro strip feed planar elliptical antenna).

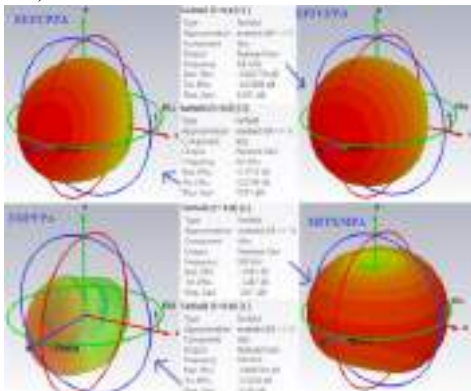


Figure 18. 3D Far field Realized Gain Plot.

TABLE 2. ELLIPTICAL PATCH ANTENNA WITH DIFFERENT FEEDING METHODS SIMULATION RESULTS.

Parameter Names	Type of feeding method with patch antenna			
	EEFCPP	EPFCPP	ERFPF	EPMPF
Operating Frequency	9.8 GHz	9.8 GHz	9.8 GHz	9.8 GHz
Return Loss (dB)	-19.933	-24.308	-11.2 and -28.8 dB at 10.8 GHz	-10.7 and -24.2 dB at 15.4 GHz
VSWR	1.2241	1.1297	1.7666	1.8264
Bandwidth (MHz)	154.6	337.9	148.5	11000
Gain (dBi)	7.06	6.607	11.24	2.223
Directivity (dBi)	7.23	6.61	11.25	3.284
Realized Gain (dBi)	7.01	6.591	10.89	1.817
Efficiency (%)	96.04911	99.93742	99.84437	78.33216

E. E-Field and H-Field Radiation Patterns (Polar plot)

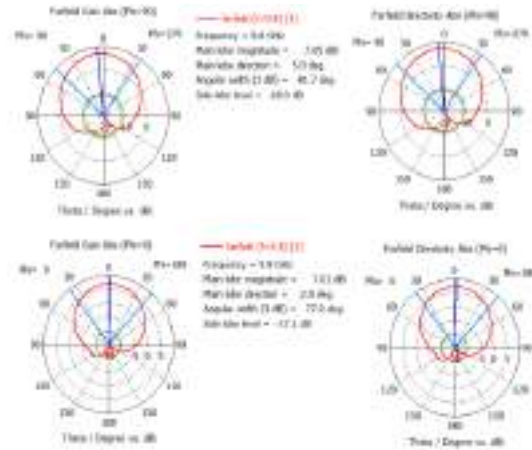


Figure 19. Polar plot radiation pattern for EEFCPP.

Figure 19, 20, 21 and 22 depicts the electric field and magnetic field (Absolute far field gain and directivity radiation patterns at  $\Phi = 90^\circ$  &  $\Phi = 0^\circ$ ) radiation pattern for elliptical micro strip patch antenna with different feeding methods.

Observe the edge-fed elliptical patch antenna, the absolute far field gain and directivity has same electric field ( $\Phi = 90^\circ$ ) radiation pattern and also notify the absolute far field gain and directivity has same magnetic field ( $\Phi = 0^\circ$ ) radiation pattern.

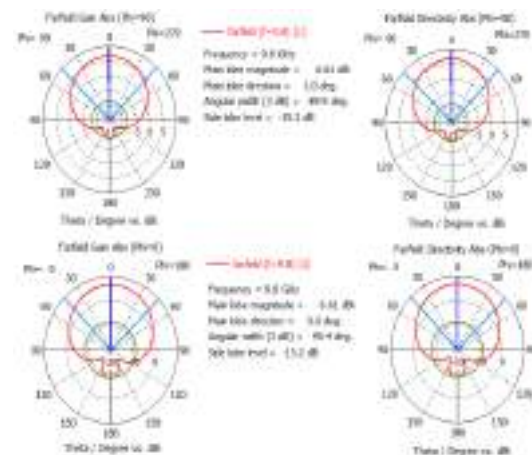


Figure 20. Polar plot radiation pattern for EPFCPP.

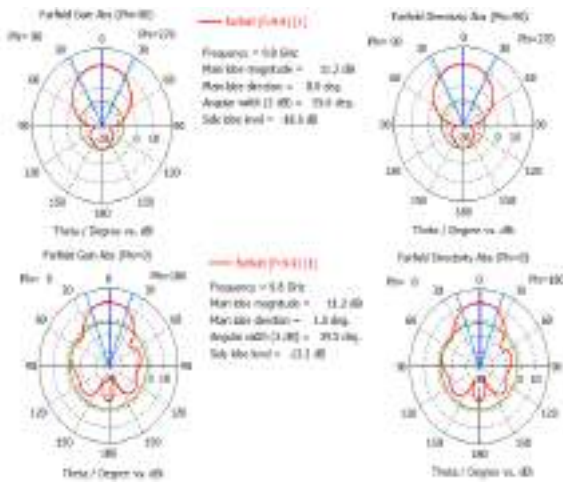


Figure 21. Polar plot radiation pattern for ERPF.

Similarly, to examined the pin-fed, ring pin-fed and micro strip feed elliptical patch antenna absolute far field gain and directivity has same e-field ( $\Phi = 90^\circ$ ) and h-field ( $\Phi = 0^\circ$ ) radiation pattern.

After observing all the simulated results composed from Table 2, considering return loss (-24.308 dB and -19.933 dB), bandwidth (337.9 MHz and 154.6 MHz) and vswr (1.129 and 1.224) values the circularly polarized elliptical patch antenna with pin feeding and edge feeding is excellent, this less return loss value, bandwidth value and vswr value are always desirable. The remaining planar elliptical monopole patch antenna with micro strip feed and elliptical ring patch antenna with pin feed has good vswr, bandwidth and return loss values, but these two designed patch antennas shows dual band frequencies.

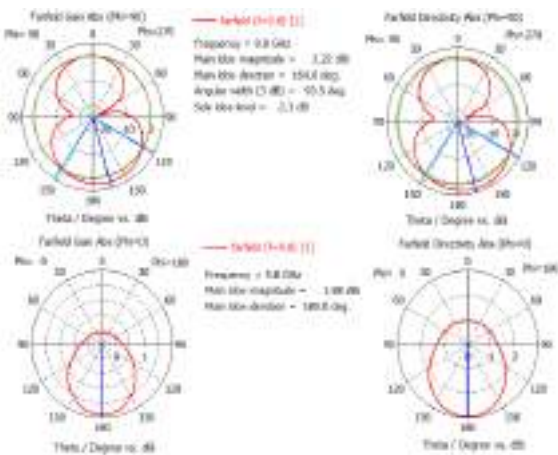


Figure 22. Polar plot radiation pattern for PEMMF.

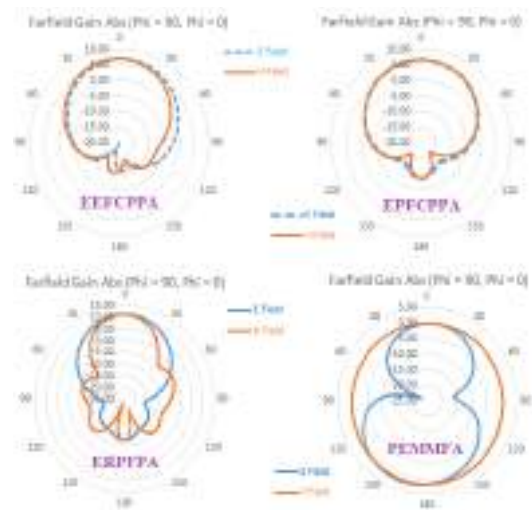


Figure 23. E-Field and H-Field polar plot radiation pattern.

Then considering gain and directivity values, elliptical ring patch antenna with pin feed antenna is suitable which gives 11.24 dBi gain and 11.25 dBi directivity as high gain and directivity are always desired. The EEF CPP and EPFCPP antennas are also suitable which gives 7.06 dBi & 6.607 dBi gain and 7.23 dBi & 6.61 dBi directivity as good gain and directivity are always desired. Then considering efficiency, the elliptical patch antenna with various feeding techniques shows high efficiency results. Regarding all the above discussed characteristics (return loss, vswr, bandwidth, gain, directivity and efficiency), the elliptical patch antenna with different feeding methods are perfectly designed and simulated. And in the broad applications of X-band (9 GHz to 11 GHz), this antenna architecture can be said to be true from all these aspects of the parameters.

*F. Efficiency Versus Frequency Plot*

The figure 24 depicts the efficiency versus frequency plot for elliptical patch antenna for different feeding techniques. At 9.8 GHz operating frequency, the elliptical patch antenna efficiency values are 96.1 % for edge feed, 99.9 % for pin feed, 99.8 for ring pin feed and 78.4 % for micro strip feed. All the elliptical feeding mechanism has excellent efficiency values.

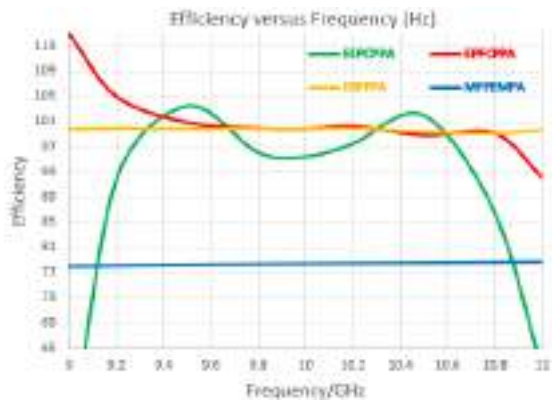


Figure 24. Efficiency vs Frequency Plot.

Thus, the suggested developed antenna can be shown to be acceptable from all aspects of simulated metrics (return loss, vswr, bandwidth, gain, directivity and efficiency) in X-band (8 GHz to 12 GHz) applications. Table 3 represents the comparison of efficiency results with various feeding methods, elliptical patch antenna at 9 GHz to 11 GHz band.

TABLE 3. COMPARISON OF EFFICIENCY RESULTS WITH DIFFERENT FEEDING TECHNIQUES, ELLIPTICAL PATCH.

Frequency in GHz	EFFICIENCY (%)			
	EEFCP P	EPFCP P	ERPFPA	EPMM F
9	47.41947 9	114.951 9	99.8189 3	77.9581 5
9.2	91.79321 2	105.013 9	99.8990 7	77.9581 5
9.5	103.4399 6	100.860 6	99.8404 6	78.2137 4
9.8	96.04911	99.9374 2	99.8443 7	78.3321 6
10	95.38176 5	99.8215 6	99.8528 3	78.3321 6
10.2	97.43917 6	100.265 6	99.9250 3	78.3974 3
10.5	101.9263 3	98.8600 7	99.3863 5	78.5382 8
10.8	86.42427 9	99.2183 9	99.1683 7	78.6938 6
11	61.48668 9	92.189	99.6761 4	78.6938 6

The performance efficiency and realized gain parameters are examined at 9 GHz to 11 GHz band, which are represented in efficiency vs frequency plot, realized gain vs frequency plot and table 3.

G. Realized gain Versus Frequency Plot

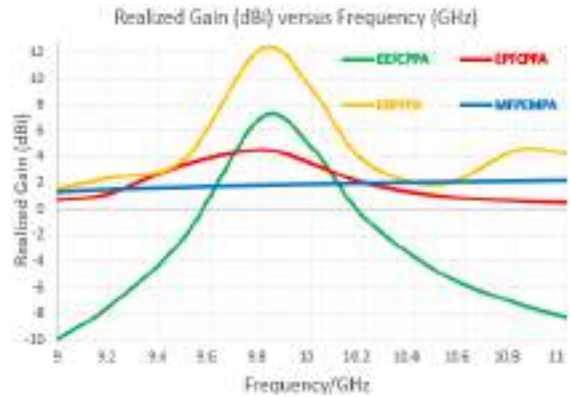


Figure 25. Realized gain vs Frequency Plot.

The elliptical patch antenna with different feeding mechanisms of realized gain in dBi versus frequency in GHz shown in figure 25.

In [8] and [9], the EEF and EPF patch antenna was designed which has return loss of -15.5 dB & -16.2 dB and vswr of 1.62 & 1.66. But in this proposed work the edge feed and pin feed elliptical patch antennas has less return loss, good vswr value, high directivity and excellent efficiency. The Table 4 shows the comparative performance chart among Ref [8] & [9]. In [15] the comparative study on CEMSPA with MSL at X band the bandwidth is 489 MHz, but in this proposed work the monopole micro strip feed elliptical patch antenna bandwidth is 11 GHz. The proposed EMFMSP antenna has more bandwidth compared to [15].

TABLE 4. COMPARISON OF PERFORMANCE PARAMETERS WITH WORKS TO EXIST

Parameters	[8]	[9]	[15]	Present Work
Return Loss (dB)	-15.5	-16.2	-31.9 dB at 10 GHz	-19.933 for EEF -24.31 for EPF -10.7 at 9.8 GHz and -24 at 15.2 GHz for EMPF
VSWR	1.62	1.66	1.05 at 10 GHz	1.224 for EEF 1.129 for EPF 1.8 for EMPF
Bandwidth	---	--	489 MHz	11 GHz for EMPF
Directivity (dBi)	---	---	7.9	7.23 for EEF 6.61 for EPF 3.2 for EMPF
Efficiency (%)	---	---	92.5 %	96.1 for EEF 99.9 for EPF 78.5 % for EMPF



## 6. CONCLUSION

In short, analyzing the results of the built antennas in this study, it can be noted that by using X band frequency, the shortcomings of circularly polarized elliptical patch antenna with edge feed method and pin feed method such as; return loss, vswr, directivity, and efficiency can be improved. This paper work, the elliptical patch antenna is beautifully constructed, simulated and analyzed with various feeding techniques. The performance parameters (return loss, vswr, bandwidth, gain, directivity, and efficiency) have been shown in this paper work with good results and also compared performance characteristics with various feeding methods. Together with these strong resulting vales compactness in size and easy manufacturing make this proposed antenna suitable with X band information technologies. X-band has major applications in radar communication, and also the application of weather forecasting, defense monitoring etc. in military and government agencies.

## REFERENCES

- [1] Jose, Jerry & Rekh, A.. (2019). Design Techniques for Elliptical Micro-Strip Patch Antenna and Their Effects on Antenna Performance. *International Journal of Innovative Technology and Exploring Engineering*, 8. 10.35940/ijitee.L3356.1081219.
- [2] Rappaport, Theodore S., et al. "Overview of millimeter wave communications for fifth-generation (5G) wireless networks—With a focus on propagation models." *IEEE Transactions on Antennas and Propagation* 65.12 (2017): 6213-6230.
- [3] Hsieh, Tsung-Han, et al. "New power dividers using  $\pi$ - and T-shaped impedance transformers." 2016 *Progress in Electromagnetic Research Symposium (PIERS)*. IEEE, 2016.
- [4] B. Tian, C. Feng and M. Deng, "Planar miniature elliptical monopole antenna for ultra wideband radios", *ICMMT2008 Proceedings (IEEE)*, 2008.
- [5] Jose, J. V., Shobha Rekh, A., & Jose, M. J. (2019). Design techniques for elliptical micro-strip patch antenna and their effects on antenna performance. *International Journal of Innovative Technology and Exploring Engineering*, 8(12), 2317–2326.
- [6] S. A. Long, L. C. Shen, D. A. Schaubert and F. G. Farrar, "An experimental study of the circular-polarized elliptical printed-circuit antenna", *IEEE Transactions on Antennas and Propagation*.
- [7] R. Garg et al, "Microstrip Antenna Design Handbook".
- [8] K. K. Mistry et al., "A Design of Elliptical Edge-Fed Circularly Polarized Patch Antenna for GPS and Iridium Applications," 2018 2nd *URSI Atlantic Radio Science Meeting (AT-RASC)*, Meloneras, 2018, pp. 1-4, doi: 10.23919/URSI-AT-RASC.2018.8471443.
- [9] Tziris, Emmanouil & Lazaridis, Pavlos & Mistry, Keyur & Zaharis, Zaharias & Cosmas, John & Liu, Bo & Glover, Ian. (2018). 1.62GHz Circularly Polarized Pin-Fed Notched Circular Patch Antenna. 10.23919/URSI-AT-RASC.2018.8471447.
- [10] Prakasam, V. and Sandeep, P., Design and Analysis of 2x2 Circular Micro-Strip Patch Antenna Array for 2.4 GHz Wireless Communication Application (November 22, 2018). *International Journal for Innovative Engineering & Management Research*, Vol. 7, No. 12, Nov. 2018.
- [11] Yaoyao Cui, Yunqing Sun, Yang Li, Hongchun Yang and Xingliang Liao, "Microstrip-fed monopole antenna for UWB application," 2008 8th *International Symposium on Antennas, Propagation and EM Theory*, Kunming, 2008, pp. 306-308, doi: 10.1109/ISAPE.2008.4735205.
- [12] Prakasam, V., & Sandeep, P. (2019). Series-fed 3x3 square patch array for wireless communication applications using CSTMWS. *International Journal of Engineering and Advanced Technology*, 9(1), 5424–5429.
- [13] P. A. H. Vardhini and N. Koteswaramma, "Patch antenna design with FR-4 Epoxy substrate for multiband wireless communications using CST Microwave studio," 2016 *International Conference on Electrical, Electronics, and Optimization Techniques (ICEEOT)*, Chennai, 2016, pp. 1811-1815.
- [14] Z. Ž. Stanković, N. S. Dončov, J. A. Russer and B. P. Stošić, "Estimation of the Number of Stochastic EM Sources with Partially Correlated Radiation in Far-Field Using Neural Model," 2019 *International Conference on Electromagnetics in Advanced Applications (ICEAA)*, Granada, Spain, 2019, pp. 0783-0786, doi: 10.1109/ICEAA.2019.8879386.
- [15] Tasnim, N., Inum, R., Khatun, H. and Khan, M.A.G., 2019, January. Comparative Study on Circular and Elliptical Microstrip Patch Antenna Arrays with Microstrip Line and Coaxial Probe Feeding for X-band. In 2019 *International Conference on Robotics, Electrical and Signal Processing Techniques (ICREST)* (pp. 74-78). IEEE.
- [16] V. Prakasam, K. R. Anudeep LaxmiKanth and P. Srinivasu, "Design and Simulation of Circular Microstrip Patch Antenna with Line Feed Wireless Communication Application," 2020 4th *International Conference on Intelligent Computing and Control Systems (ICICCS)*, Madurai, India, 2020, pp. 279-284, doi: 10.1109/ICICCS48265.2020.9121162.
- [17] N.Koteswaramma, P.A.Harsha Vardhini, K.Murali Chandra Babu, "Realization of Minkowski Fractal Antenna for Multiband Wireless Communication", *International Journal of Engineering and Advanced Technology (IJEAT)*, pp.5415-5418, Vol.9 Issue.1, Oct 2019.
- [18] S. Pal, M. B. Raya and K. Ali, "Computation of Resonant Frequency and Gain from Inset Fed Rectangular Shaped Microstrip Patch Antenna Using Deep Neural Network," 2019 4th *International Conference on Electrical Information and Communication Technology (EICT)*, Khulna, Bangladesh, 2019, pp. 1-6, doi: 10.1109/EICT48899.2019.9068758.
- [19] V. Prakasam, P. Sandeep and K. R. A. LaxmiKanth, "Rectangular Micro Strip Patch Array Antenna With Corporate Feed Network For Wireless Communication Applications," 2020 5th *International Conference on Communication and Electronics Systems (ICES)*, COIMBATORE, India, 2020, pp. 311-316, doi: 10.1109/ICES48766.2020.9138028.
- [20] L. M. Lima de Campos, J. H. Almeida Pereira, D. S. Duarte and R. C. L. de Oliveira, "Bio-Inspired System for Electricity Price Forecast in the Brazilian Market," 2020 *International Joint Conference on Neural Networks (IJCNN)*, Glasgow, United Kingdom, 2020, pp. 1-8, doi: 10.1109/IJCNN48605.2020.9207679.
- [21] Prajapati, M.S., Shesma, S.K. and Rawat, A., 2019. Performance Analysis of Triband Elliptical Patch Microstrip Antenna for GPS and Radar Application. In *Proceedings of the Third International*



Conference on Microelectronics, Computing and Communication Systems (pp. 65-72). Springer, Singapore.

- [22] N.Koteswaramma, P.A.Harsha Vardhini, M.Sai Lakshmi, "Fractal Antenna Design Process for Multiband Frequencies", International Journal of Research in Electronics and Computer Engineering (IJRECE), pp.2468-2472, Vol.7, issue 1, Mar 2019.
- [23] V. Prakasam and N. Reddy, "Design and Simulation of Elliptical Micro strip Patch Antenna with Coaxial Probe Feeding for Satellites Applications Using Matlab," 2020 Fourth International Conference on I-SMAC (IoT in Social, Mobile, Analytics and Cloud) (I-SMAC), Palladam, India, 2020, pp. 228-234, doi: 10.1109/I-SMAC49090.2020.9243472.
- [24] V. Prakasam and N. Reddy, "Hexagonal Shaped Micro-strip Patch Antenna Design for 2.45 GHz WLAN System," 2021 6th International Conference on Inventive Computation Technologies (ICICT), Coimbatore, India, 2021, pp. 13-18, doi: 10.1109/ICICT50816.2021.9358687.
- [25] V. Prakasam and N. Reddy, "Matlab And CST MWS Based Rectangular Micro-strip Patch Antenna Design for WLAN Applications," 2020 International Conference on Recent Trends on Electronics, Information, Communication & Technology (RTEICT), Bangalore, India, 2020, pp. 304-309, doi: 10.1109/RTEICT49044.2020.9315554.



**Dr. V. Prakasam** earned JNTUA's B.Tech degree, JNTUK's M.Tech degree in VLSID, and got p.hD degree from SSSUTMS. He is presently an Associate Professor at Visvodaya Engineering College, Kavali, in the Department of Electronics and Communication Engineering. Signal Processing, Image Processing, Microwave Engineering and RF Engineering

were his research interests. He has more than 30 papers published in various national and international journals and conferences, including SCOPUS, IEEE, Springer, Elsevier and UGC.



**Dr. P.Sandeep** has obtained a B.E degree from VTU, Belgaum, an M.Tech degree from Sathyabama University in VLSID, and completed p.hD from SSSUTMS. He is currently an Assistant Professor in the Department of Electronics and Communication Engineering at the Technology and Science Institute of Vignan, Deshumuki. Signal processing, image

processing, Analog Electronics engineering, Low Power and High Speed Devices and VLSI Architecture are his research interests.



**P. Upender** received B.Tech degree from JNTU, Hyderabad, M.Tech degree in RF & Microwave from IIT ROORKEE and pursuing Ph.D. He is currently an Assistant Professor in the department of Electronics and Communication Engineering at Vignan institute of technology and sciences, deshumuki. His research interests are microwave engineering, Antennas, Radar Engineering, RF

communication. He has more than 20 publications in in various journals and conferences at national and International level including SCI, SCOPUS, IEEE, Springer, Elsevier and UGC.

Journal of Uncertain Systems  
(2022) 2242001 (12) pages  
© World Scientific Publishing Company  
DOI: [10.1142/S1752890922420016](https://doi.org/10.1142/S1752890922420016)



## Analyzing the Effect of Uncertainty in Low Power SRAM Cells using Artificial Intelligence Technique

Hariprasath Manoharan<sup>\*,¶</sup>, N. Satheesh Kumar<sup>†,||</sup>,  
P. Janardhan Saikumar<sup>‡</sup>, M. Venkatesan<sup>§,\*\*</sup>, A. Balamanikandan<sup>‡</sup>  
and K. Venkatachalam<sup>‡</sup>

*\*Department of Electronics and Communication Engineering  
Panimalar Institute of Technology, Poonamallee 600123  
Chennai, Tamil Nadu, India*

*†Professor, PBR Visvodaya Institute Of Technology and Science  
Kavali, Andhra Pradesh*

*‡Department of Electronics and Communication Engineering  
Audisankara College of Engineering and Technology  
Gudur, Andhra Pradesh*

*§Professor, Department of ECE  
Visvodaya Engineering College, Kavali, Andhra Pradesh*

*¶hari13prasath@gmail.com*

*||nandhikripa@gmail.com*

*\*\*hellomvenkat@gmail.com*

Received 28 December 2021

Revised 11 February 2022

Accepted 21 February 2022

Published

This paper addresses the uncertainty that is present in the design of static random access memory (SRAM) cells using an artificial intelligence (AI) technique. The SRAM has much uncertainty in high-performance portable very large-scale integration (VLSI) chips due to their performance and storage density. This paper presents the way for solving the uncertainty problem by evaluating point-by-point recreation derived for the memory cells inform of the power, speed, and area investment funds acquired in the advanced cell configuration when contrasted with the standard regular architecture for autonomous vehicles using AI algorithm. The adiabatic low power technique is implemented to enrich the configuration of the 6T-SRAM cells. The procedure of the adiabatic process will provide high loss in terms of dissipation of energy which is connected to ground (0V) and transition can be converted from '1' to '0'. Moreover, this transition will be decreased to a high amount of degree within corresponding memory cells. Thus uncertainties with the AI model can able to deliver low power reduction using the automatic model of operation as standard adiabatic 6T SRAM cells are implemented. To prove the effectiveness in

<sup>¶</sup>Corresponding author.

*H. Manoharan et al.*

the reduction of uncertainties a low power margin is obtained with marginal values of 0.25 Volts which is much lesser than the existing models.

*Keywords:* SRAM; 6T-SRAM cell; adiabatic power; energy dissipation; power reduction; delay.

## 1. Low Power Uncertainties — An Introduction

Most of the uncertainties that are present in memories are used for storing data or information. Generally, two types of memories are preferred in electronic memory devices such as volatile and non-volatile memories based on applications, these memories affect the performance of speed of the devices. In recent years, the static random access memory (SRAM) is one of the substantial pieces of research for the development of the speed of the process, reducing the memory and power due to increasing demand on advanced electronic devices such as laptops, integrated circuit (IC) memory cards, etc.<sup>[1][2]</sup> The feedback cells are designed to improve the performance of the memory cells.<sup>[3][9]</sup> These are widely used in on/off-chip memories mobile applications of low standby leakage. The static memory is the semiconductor memory work with bistable latching circuitry, which stores each bit and exhibits the data remembrance. The static memories are volatile memory, that store data eventually lost when not powered in the memory cell.

### 1.1. Uncertainty in SRAM cell design: Survey model

The SRAMs are used for solving several uncertainties that are present in various microelectronics applications like advanced server processors, system on chip (SoC) and multimedia applications. These are operating at low power supplies with high noise immunity due to large noise margins. The embedded SRAM in SoC products are designed for handling the processors easily and effectively.<sup>[10]</sup> The various chips are designed based on the demand for performance, saving memory within less size and minimizing the latency with the integrated fast memories (cache) are being integrated on-die. Many researchers are suggested SRAM designed for SoC applications and high-performance processors. The memory element or storage element is one of the basic operations of the SRAM cell, it includes the writing and reading operation from/into the cell. In this paper, implement the technique for advanced SRAM design aspects, basic operations of existing 6T-SRAM (six transistors) memory cell and design process, nano-regime techniques and challenges, limitations in read-write requirements of memory cells. This performance is evaluated by the two design metrics such as read static noise margin (RSNM) and write static noise margin (WSNM). Apart from these parameters, the inline metric,  $N$ -curves also used to measure the stability of reading and write operation of the memory.<sup>[11][12]</sup>

The basic SRAM cells work with feedback mechanism-based cross-coupled inverters to maintain their state. The dynamic random access memory (DRAM) cells hold a charge as data, which acts as a floating capacitor. The data is regularly retrieved by dynamic cells and charge stored leaky floating capacitor. The

*Analyzing the Effect of Uncertainty in Low Power SRAM Cells*

charges stored in the leaky floating capacitor and dynamic cells are refreshed regularly to retrieve the stored data. The high-performance read and write operations are achieved by the cross-coupled inverters in SRAM. However, these static memories are faster compared with dynamic RAM, it requires much space (area) than DRAMs. The SRAM cache memory contains sense amplifiers, an address decoder, an array of memory, and write drivers to enable the writing into and reading from the array of memory. The standard memory architecture is shown in Fig. 1. These SRAM memory arrays exist with  $2n$  words of  $2m$  bits each. Every bit is stored in the memory cell and share bit-line pairs (BL, BL') in each column and a common word-line (WL) in each row. The access of the cell is performed by the resistances and capacitances of the bit lines and word lines. The size of the memory is proportional to the number of rows and columns.<sup>[8,9]</sup> The folded technology is used high-level memories, including the bit line capacitance, the word line capacitance consists of  $2n - k$  rows and  $2m + k$  columns and in each row of the memory with  $2k$  words. The SRAM cells are addressed by the selection of appropriate lines like word line, a bit line pairs are activated with the row and a column decoder.

*1.1.1. Recent literature*

The process of accruing uncertainties is explained using a factorial model<sup>[13]</sup> where the minimum and maximum values are defined. This provides a clear insight in achieving suitable values which are defined in terms of variance. But in field intensity, both limits do not establish any security for adiabatic cell structures. Subsequent procedures are carried out for quantification uncertainties<sup>[14]</sup> which are used for predicting space with high limit boundaries. In this case, more amount of limitations leads to prediction problems which indicate the failure of the automatic process. Therefore, for high limit boundaries a probability model is defined which holds all quantified processes for 5T and 6T SRAM structures.<sup>[15]</sup>

*1.2. Deciphering uncertainties using AI*

Artificial intelligence (AI) techniques are implemented for solving the uncertainties that are present in low-power SRAM design. Since in the proposed method low-power SRAM cells are designed they can be applied in all applications of the Internet of Things (IoT) since the metal oxide semiconductor field effect transistor (MOSFET) has many limitations. To be precise the SRAM design memory requirements are tested with an autonomous vehicle that turns with battery-packed systems. To analyze the aforementioned effect a non-linear classification problem is applied with perceptron algorithms where the basic form is represented using mathematical equations as follows:

$$P_i = \begin{cases} 0 & \text{if input} < d_i, \\ 1 & \text{if input} > d_i, \end{cases} \quad (1)$$

where  $d_i$  represents the decision line which is calculated from input of AND gate.

*H. Manoharan et al.*

If the values of decision variables are calculated then the function of perceptron can be defined using three different variables as represented in Eq. (2).

$$f(P_i) = \sum_{i=1}^n \vartheta_i * y_i + \tau_i, \quad (2)$$

where  $\vartheta_i, y_i$  and  $\tau_i$  represents the input load, path followed and preconception of perceptron.

Equation (2) represents that bias points is primarily implemented for shifting the lines between two different cases, namely, 0 and 1. In the modeling of deep neural networks with SRAM cells the major objective in autonomous vehicles is to reduce the amount of loss that is present in the system. Therefore, the objective function can be defined using Eq. (3) as

$$O(i) = \int_{i=1}^n P(i, n) * \mu(i, n) didn \quad (3)$$

where  $\mu(i, n)$  represents the loss function.

In case if loss function is much higher then it should be optimized by converting it to a gradient function which is represented using Eq. (4).

$$O_{\text{modified}}(i) = \frac{1}{\sigma} \sum_{i=1}^n \mu(i, n), \quad (4)$$

where  $\sigma$  represents the gradient function.

Equation (4) represents the modified objective function with reduction in loss terms. Since the method implements a binary variable the same function can be represented using sigmoid function as follows:

$$f_{\text{modified}}(P_i) = e^{-in} \frac{1}{1 + e^{-in}}, \quad (5)$$

where  $e^{-in}$  represents the exponential function of two variable functions.

Using AI model the problem of uncertainties for data distribution with low power 5T and 6T cells can be solved by minimum and maximum set of arrays using the following equation. This set of arrays is suitable for random data set with distinct variance value as uniform distribution can be achieved in this case.

$$D_i(\text{variance}) = \sum_{i=1}^n |v_i - v_n|^2 \quad (6)$$

where  $v_i$  and  $v_n$  denotes the variance with quantization of data which is used for reducing the power that is transmitted for 5T and 6T cell data.

### 1.3. Solving uncertainties: Proposed methodology

From conventional technique analysis, it has been established that many procedures of low power design using SRAM cells have not been developed based on the automation model. However, several processes provide an advantage in manual

*Analyzing the Effect of Uncertainty in Low Power SRAM Cells*

mode of operation which includes an SoC technology for avoiding high power that is supplied in a single cell. But manual adjustment of power will not guarantee an adiabatic reduction in the proposed cell RAM design, thus, as a result it leads to uncertainty in SRAM systems. To prevent uncertainties an automatic mode of operation is assured using AI systems where perceptron algorithms are integrated for solving all non-classified problems. In addition, three different operating modes are introduced as uncertainties will be different in the case of 5T and 6T cell structures.

#### 1.4. Objectives

The major objective of the proposed work is divided into a multi-objective case study that solves the following problems that exist in conventional models.

- To solve the uncertainties that are present in adiabatic cells by replacing SoC technology with AI models.
- To integrate the proposed model using frame structure with reduced power infrastructure for SRAM cells.
- To provide a low noise margin which is less than 1V for 5T and 6T cells by shifting binary values 0 and 1.

## 2. Design Model of Uncertainties

In very large-scale integration (VLSI) designs, the static random access constitutes a large area, which contains thousands of transistors in a single cell. In these present days, the SRAM cell designs with minimum size transistors for high packing density.<sup>[5]</sup> For the past three decades, scaling processing is done for the reduction of the size of cell.<sup>[6]</sup> SRAM takes designs with two primary aspects power dissipation and delays in reading and writing operations in SRAM. The dynamic power dissipated with the read/write operation.<sup>[7]</sup> Figure 1 is the standard 6T (six transistors) CMOS static memory cell is illustrated schematically.

The transistors in cells M1, M2, M3 and M4 are cross-coupled inverters, which act as storage elements. The intention SRAM design effort is directed to decrease the

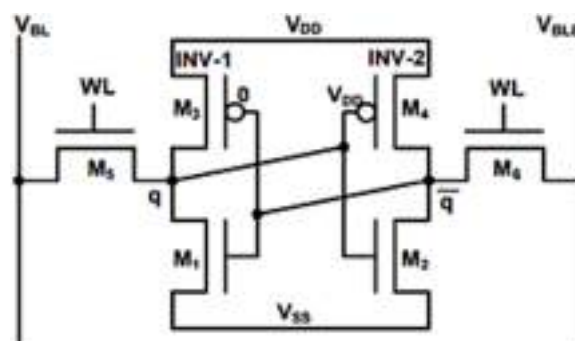


Fig. 1. Standard 6T SRAM cell.

*H. Manoharan et al.*

power consumption and area of the cell. The millions of cells can be built in a small chip. The sub-threshold leakage currents are controlled by the power consumption level of the cell and memory circuits are handled by the large threshold voltage. The various scaling techniques are implemented for MOSFET to better enhance the performance of the SRAM cell. The MOSFET controlled with gate oxide leakage, ultra-shallow, control of abrupt junction and short channel effects implement SRAM scaling for SI MOSFET structure. The bulk sub-45 nm chip control of SCE with heavy super-halo implants and doping is implemented to prevent the leakage currents from sub-surface.<sup>[15]</sup> The impurity scattering carrier motilities are degraded and high transverse electric field in the ON-state. The degradation of short channel results in large leakage and sub-threshold slope. The variable threshold voltage is the new technique for random dopant fluctuation to nano scalable bulk-Si MOSFETs. Including this, the line-edge roughness and statistical dopant fluctuations increase the spread in variable threshold levels in the transistor and on-off currents and can limit the size of the cache.<sup>[13]</sup>

Figure 2 shows the voltage transfer characteristics (VTCs) of cross-coupled inverters. The read and write operation of the SRAM cell can be performed by the cross-coupled inverters of VTC. In this process, the stored values are controlled to the two stable states. In SRAM cell flip internal state, the current state internal crosses the switching threshold value ( $V_s$ ). This state is not disturbing in the read operation, it forces swing from internal voltage to change the state into write operation.

### 2.1. 5T SRAM cell

Figure 3 shows the proposed 5T-SRAM CELL design, the features are related to basic 6T cell except for the lack of an access transistor to perform the tasks are indistinguishable to 6T SRAM cell.<sup>[16][17]</sup> The proposed SRAM memory cell requires five transistors for solving the uncertainties, so eventually, reduces the area in the

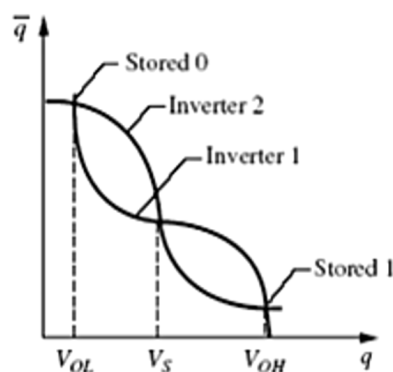


Fig. 2. VTC of SRAM.



Analyzing the Effect of Uncertainty in Low Power SRAM Cells

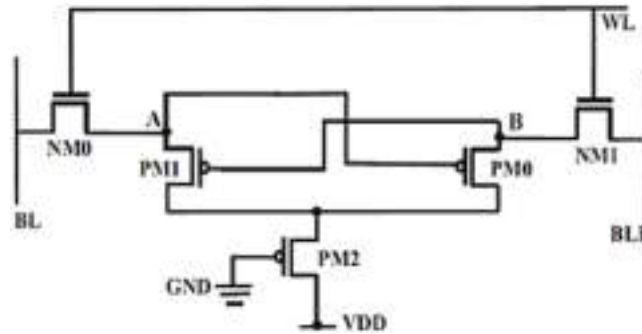


Fig. 3. 5T-SRAM cell diagram.

5T SRAM cell. The power dissipation and delay are also less compared with other existing SRAM cells with acceptable stability, which is based on noise margin. [\[18\]](#)

### 3. Source of Uncertainties and Operating Modes

- (1) Write mode: The SRAM performs the write operation when  $WL = 1$ . Then NM0 and NM1 are turned in to “ON” states. The transistors output nodes “A” and “B” are connected to PM0 and PM1 transistors gate respectively. When  $WL = 0$ , the BLB and BL should be set as logic ‘1’ and logic ‘0’. When “A” states ‘0, then PM2 is “ON”. When it switches to the “ON” state, the output node “B” and PM0 connect to the power supply  $V_{dd}$  through PM2.
- (2) Read mode: In this mode, the proposed operation is different than 6T-SRAM. Instead of logic ‘1’, logic ‘0’ is applied to bit line and set as  $WL = 1$ . If  $WL = 1$  then, NM0 and NM1 transistors are turned into an ‘ON’ states. The Node “A” = 1, which holds the logic ‘1’, it charges the bit line to ‘1’ for weak 1 due to NM1.

If the node “B” is “OFF”, which holds ‘0’ but will be pulled to logic ‘0’. The voltage level at BL is greater than BLB, which is detected by the sense amplifier and it gives logic ‘1’. Similarly, at nodes  $A = 0, B = 1$ , the BLB voltage is higher than BL voltage, sense amplifier output changed to logic ‘0’.

- (3) Hold mode: The proposed cell operated with hold mode when  $WL = 0$ . In the write mode of the cell, node stores weak ‘1’ at the node “A” = 1 due to the NM0 access transistor, which is a weak passer of 1. The two transistors (NM0 and NM1) are “OFF” conditions when  $WL = 0$ . The corresponding node “A” holds the weak ‘1’ and node “B” handles the strong ‘0’, respectively.

Node B changed into strong ‘1’, when node “B” turned on to switch on and power supply voltage PM2 is also ON, which is known as a strong passer of 1. Figure [4](#) shows the simulated response for the proposed memory cell in reading and write mode ( $WL = 1$ ) and hold ( $WL = 0$ ) state with the same size as the transistors.

H. Manoharan et al.

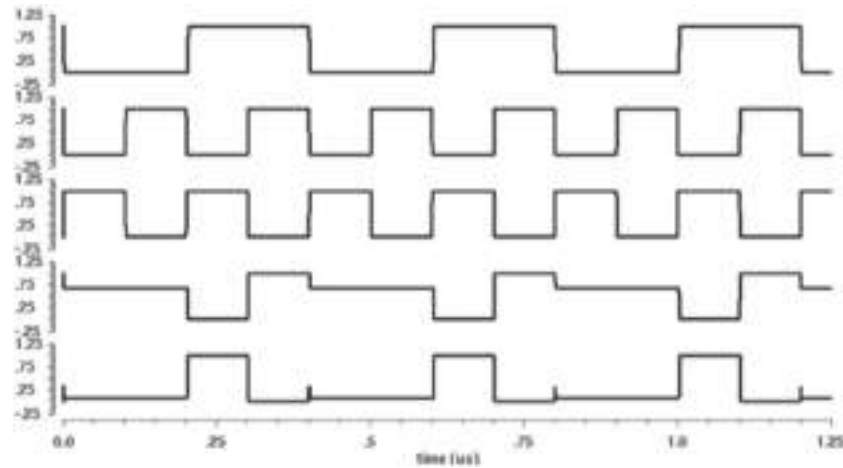


Fig. 4. Simulated response of proposed cell.

### 3.1. Adiabatic 6T-SRAM cell

The adiabatic switching process is performed by the switching operations to maintain the small potential between the switching devices.<sup>[19, 21]</sup> In conventional switching cases, the potential  $V_r$  is high between the switch resistances to the abrupt application of  $V_{dd}$  to the RC circuit. This variation can be performed by the capacitor charging from a time-varying source.

Initially,  $V_i = 0$  V. The ramp slightly increases up to  $V_{dd}$  with a slew rate  $\dot{V}_r = \dot{V}_i - \dot{V}_c$ , which is set by ensuring that its period  $T \gg RC$ . The corresponding energy dissipated as follows:

$$E_{diss} = I^2RT = (CV_{dd}/T)^{2RT} = (RC/T)C(V_{dd})^2.$$

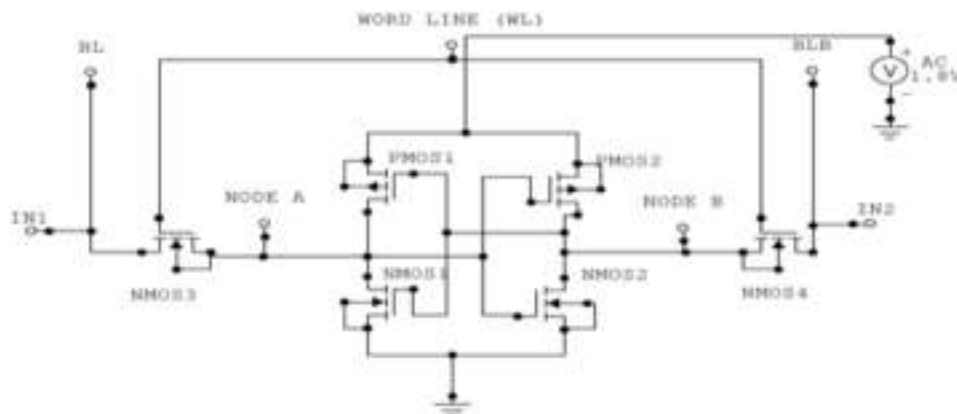


Fig. 5. Proposed adiabatic 6T-SRAM design.

*Analyzing the Effect of Uncertainty in Low Power SRAM Cells*

The power dissipation decreases with an increasing linear increase in  $T$ . The adiabatic discharge formed a similar manner with decreasing ramp. If ' $T$ '  $\gg$  RC, then the energy dissipation during charging  $E_{diss} = 0$  and the total energy removed from the supply is  $\frac{1}{2} C(V_{dd})^2$  — the minimum charge required the capacitor and hence hold the logic state. In the cell adiabatic process, the energy is eliminated from the capacitor and back to the supply in the discharge cycle, so the node capacitances charge and discharge and the average power dissipation are also reduced. Figure 5 shows the adiabatic 6T-SRAM memory cell, the dynamic switching operations can be performed by the potential across the switching devices is kept arbitrarily small. Generally, in a conventional circuit, the  $V_r$  is high due to the abrupt application of  $V_{dd}$  in RC. This process can be obtained by the power source and adiabatic charging from a time-varying source from the initial stage to the final stage.

#### 4. Results and Discussions

This paper designed the flip flop and stored the input information with better output reconstruction. Figure 6 shows the existing method (5T-SRAM) waveform, which contains the high power and high noise margin level.

Figure 7 shows the proposed method waveform after solving uncertainties. Compare with the existing method, the noise margin level is less. The data storage is speed and required power is very less. The proposed method has less noise margin for reconstructing the original data with less power. The speed is also fast compared with the previous method.

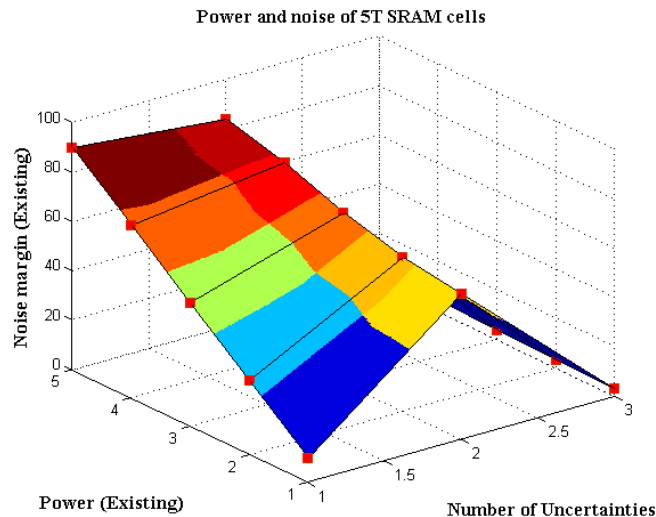


Fig. 6. Existing method performance.

H. Manoharan et al.

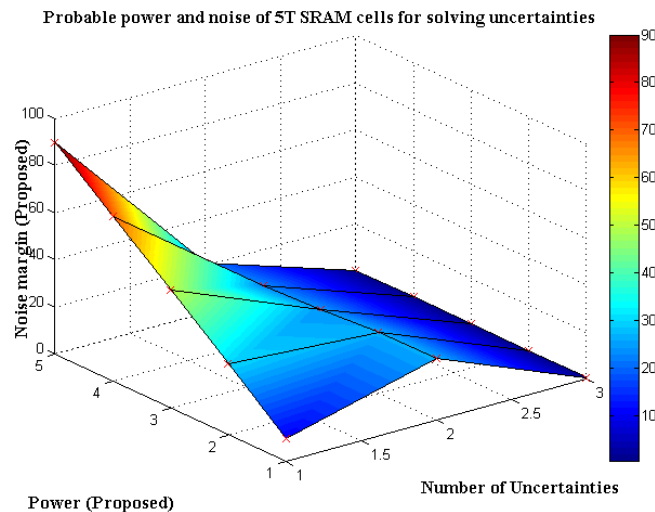


Fig. 7. Proposed method results.

## 5. Conclusions and Future Scope

The paper suggests a new flanged technique for solving uncertainties that are present in SRAM flip-flop design and stored the input process into the memory cell. The process of uncertainty is compared with existing methods and it is observed that the data storage process is complex due to the high noise margin. So, the uncertainty problem requires a high-power level and low-speed techniques. To overcome this limitation on uncertainties the proposed technique delivers a novel platform where the speed is more and delay is less due to the less noise margin the uncertainties are solved and this method is suitable for reading and write operations compare with other standard SRAM cells.

## References

1. S. Yang, W. Wolf, W. Wang, N. Vijaykrishnan and Y. Xie, Lowleakage robust SRAM cell design for sub-100 nm technologies, in *Proc. ASP-DAC* (Shanghai, China, 2005), pp. 539–544.
2. J. Samandari-Rad, M. Guthaus and R. Hughey, Confronting the variability issues affecting the performance of next-generation SRAM design to optimize and predict the speed and yield, *IEEE Access* **2** (2014) 577–601.
3. M.-H. Tu, J.-Y. Lin, M.-C. Tsai, S.-J. Jou and C.-T. Chuang, Singleended subthreshold SRAM with asymmetrical write/read-assist, *IEEE Trans. Circuits Syst. I, Reg. Papers* **57**(12) (2010) 3039–3047.
4. V. Sharma et al., *SRAM Design for Wireless Sensor Networks: SRAM Bit Cell Optimization* (Springer Science, New York, 2013), pp. 9–30.
5. W. Lim, H. C. Chin, L. S. Cheng and M. L. P. Tan, Performance evaluation of 14 nm FinFET-based 6T SRAM cell functionality for DC and transient circuit analysis, *J. Nanomater.* **2014** (2014) 820763.

*Analyzing the Effect of Uncertainty in Low Power SRAM Cells*

6. A. Azizi-Mazreah, M. T. M. Shalmani, H. Barati and A. Barati, Delay and energy consumption analysis of conventional SRAM, *Int. J. Electr. Comput. Eng. Syst.* **2** (2008) 74–78.
7. J. P. Kulkarni and K. Roy, Ultralow-voltage process-variation-tolerant Schmitt-trigger-based SRAM design, *IEEE Trans. Very Large Scale Integr. (VLSI) Syst.* **20**(2) (2012) 319–332.
8. K. Takeda *et al.*, A read-static-noise-margin-free SRAM cell for low-VDD and high-speed applications, *IEEE J. Solid-State Circuits* **41**(1) (2006) 113–121.
9. R. E. Aly and M. A. Bayoumi, Low-power cache design using 7T SRAM cell, *IEEE Trans. Circuits Syst. II, Exp. Briefs* **54**(4) (2007) 318–322.
10. A. Feki *et al.*, Sub-threshold 10T SRAM bit cell with read/write XY selection, *Solid-State Electron.* **106**(4) (2015) 1–11.
11. K. Takeda *et al.*, A read-static-noise-margin-free SRAM cell for low-Vdd and high-speed applications, in *Proc. IEEE Int. Solid-State Circuits Conf.*, February, San Francisco, California, USA, 2005, pp. 478–479.
12. Y.-W. Chiu *et al.*, 40 nm bit-interleaving 12T subthreshold SRAM with data-aware write-assist, *IEEE Trans. Circuits Syst. I, Reg. Papers* **61**(9) (2014) 2578–2585.
13. K. K. Benke and N. J. Robinson, Quantification of uncertainty in mathematical models: The statistical relationship between field and laboratory pH measurements, **2017** (2017) 1–13.
14. T. Siddique, S. Mahmud, A. M. Keese, C. M. Ngwira and H. Connor, A survey of uncertainty quantification in machine learning for space weather prediction, *Geoscience* **12** (2022) 1–23.
15. A. Hunter, International journal of approximate reasoning a probabilistic approach to modelling uncertain logical arguments, *Int. J. Approx. Reason.* **54**(1) (2013) 47–81.
16. T.-H. Kim, J. Liu, J. Keane and C. H. Kim, A 0.2 V, 480 kb subthreshold SRAM with 1 k cells per bitline for ultra-low-voltage computing, *IEEE J. Solid-State Circuits* **43**(2) (2008) 518–529.
17. G. Chen and D. Sylvester, Yield-driven near-threshold SRAM design, *IEEE Trans. Very Large Scale Integr. (VLSI) Syst.* **18**(11) (2010) 1590–1598.
18. T. Yamagishi, A. Hori and H. Wakabayash, Self-heating-aware cell design for multi-stacked circuits with p/n-vertically-integrated nanowires on FinFET, in *Int. Conf. Solid State and Materials Tokyo* (2019), pp. 1–18.
19. B. Zhai, S. Hanson, D. Blaauw and D. Sylvester, A variation-tolerant sub-200 mV 6-T subthreshold SRAM, *IEEE J. Solid-State Circuits* **43**(10) (2008) 2338–2348.
20. A. Agal, Pardeep and B. Krishan, 6T SRAM cell: Design and analysis, *Int. J. Eng. Res. Appl.* **4**(3) (2014) 574–577.
21. E. Grossar, M. Stucchi, K. Maex and W. Dehaene, Read stability and write-ability analysis of SRAM cells for nanometer technologies, *IEEE J. Solid-State Circuits* **41**(11) (2006) 2577–2588.

**About the Authors**

**Hariprasath Manoharan** is working as Assistant Professor in the Department of Electronics and Communication Engineering, Panimalar Institute of Technology, Poonamallee, Chennai. He has published 40 research articles in well indexed Journals. He has also published a book entitled ‘Computer Aided State Estimation for Electric Power Networks’ and published more than 15 Patents. Email: hari13prasath@gmail.com

*H. Manoharan et al.*

**N. Satheesh kumar** is currently an Professor at the Department of Electronics and Communications Engineering, PBR Visvodaya Institute of Technology and Science, Kavali, Andhra Pradesh. He obtained his PhD in 2019 from Anna University, Chennai, India and participated in several high profile conferences. He has more than 18 years of experience in teaching . He has published journal papers in various reputed journals and presented papers in national and international conferences. He is an active member of various professional bodies. His areas of Interests include Signal Processing, Thermal Image processing, Soft Computing, Embedded Systems and IoT.

**P. Janardhan Saikumar** is currently an Associate Professor at the Department of Electronics and Communications Engineering, Audisankara Institute of Technology, Gudur, Andhra Pradesh. He obtained his PhD in 2020 from Sri Venkateswara University, Tirupathi, India and participated in several high profile conferences. He has more than 18 years of experience in teaching and industry. He is published journal papers in various reputed journals and presented papers in national and international conferences. He is an active member of various professional bodies. His areas of Interests include Image and Signal Processing, Antennas, MEMS, Embedded Systems and IoT.

**M. Venkatesan** is currently an Professor at the Department of Electronics and Communications Engineering, Visvodaya Engineering College, Kavali, Andhra Pradesh. He obtained his PhD in 2019 from Bharath Institute of Higher Education & Research, Chennai, India and participated in several high profile conferences. He has more than 19 years of experience in teaching field. He has published journal papers in various reputed journals and presented papers in national and international conferences. He is an active member of various professional bodies. His areas of Interests include Signal Processing, Wireless Networks and Embedded Systems.

**A. Balamanigandan** is currently working as Associate Professor, Department of Electronics and Communication Engineering, Audisankara College of Engineering and Technology, Gudur. He has more than 10 years of experience in Academic field and has published several papers in National, International Journals and Conferences. His Research Interests Include Mobile Networks, Digital Communication, Computer Networks, And Optical Communication.

**K. Venkatachalam** Completed His Bachelor Of Engineering In Electronics And Communication Engineering From Anna University, Chennai In 2008; M.E In Applied Electronics From St. Peters University, Chennai, India In 2012, And Ph.D. From Jjt University, Jaipur, Rajasthan, In 2018. He Has About 6 Years of Experience in Teaching and Published Number of Referred National and International Journals. His Research Interests Include Mobile Networks, Digital Communication, Computer Networks, and Optical Communication.

# Analysis of a Compact 4-shaped Annular Ring Ultra Wideband Antenna Using Characteristic Modes

Bhaskara Rao Perli, and A. Maheswara Rao

**Abstract**—This communication proposes a compact 4-shaped monopole annular ring UWB antenna design. The proposed structure contains multiple radiating strips inside the annular ring, in the form of a 4-shaped and a  $50\Omega$  microstrip feed line. A tapered structure with a feed point is chosen to achieve wideband characteristics. The proposed model is printed on a low-priced FR4 substrate with a size of  $0.180\lambda_0 \times 0.225\lambda_0$  ( $20 \times 25\text{mm}^2$ ). The proposed model achieves a fractional bandwidth of 133.74% in the 2.7 to 13.6 GHz range with  $S_{11} < -10\text{dB}$  and covers the 3.1-10.6 GHz unlicensed band approved by FCC in 2002 and X-band applications. The antenna exhibits stable and Omni-directional radiation patterns in the operating frequency range. The analysis of the proposed monopole antenna using characteristic modes is performed to obtain a physical understanding of the radiation process occurring on the radiating antenna. The modal significance curves and the modal current distributions are used to analyze the radiating antenna using the first six characteristic modes. The measurement and simulation results show a good agreement.

**Keywords**—characteristic modes; multiple-strips; annular-ring; surface currents; UWB antenna; tapered structure

## I. INTRODUCTION

THE Microstrip patch antennas have played a vital role in modern wireless communication with their compelling properties, such as lightweight, easy to fabrication, low profile, and conformable to planar. However, its narrow-bandwidth performance limits its use in UWB technology. In addition, modern wireless communications nowadays usually require small size antennas and greater bandwidth to meet the current requirements of practical applications such as the military, radar, medical imaging, and other wireless communication services. For this reason, substantial research has been increased significantly in the field of bandwidth enhancement and methods of miniaturization for microstrip antennas [1, 2].

The Federal Communications Commission (FCC) selected a frequency range from 3.1 to 10.6 GHz for ultra-wideband applications in 2002, and also increased the demand for the use of this unlicensed frequency band from the industrial and academic domains. UWB technology has also received great attention from academia and industries. A feasible UWB antenna needs to be designed with simple structure, compact size, low cost, low power spectral density, integration capability, near Omni-directional features, and prodigious data rates [3, 4]. Planar monopole antennas are suitable for achieving these characteristics, which is why many researchers

find their interest in the design and analysis of this type of antennas. In previous studies, numerous antennas have been reported for ultra-wideband applications including the entire 3.1 to 10.6 GHz frequency band [5-15].

The UWB antenna with a total dimension of  $24.8 \times 30 \times 1.6 \text{ mm}^3$  was proposed by inserting a slot in the ground and radiating structures [5]. The proposed decagonal radiating monopole with a total dimension of  $35 \times 35 \times 1.6 \text{ mm}^3$  was truncated at the ground structure in order to observe the UWB band [6]. The V-shaped radiating structure along with a partial ground plane was designed as a UWB monopole antenna with a total size of  $24 \times 28 \times 1.6 \text{ mm}^3$  [7]. Multiple-resonators are used to create the longer and shorter current paths for ultra-wideband applications with a total dimension of  $66 \times 62 \times 1.59 \text{ mm}^3$  [8]. In [9], the CPW-fed rectangular spiral antenna with a total dimension of  $50 \times 40 \times 0.508 \text{ mm}^3$  was designed by tapering the ground plane in the form of coplanar strips but not covering the entire UWB band. A proximity-coupled annular ring antenna with an overall dimension of  $44 \times 44 \times 1.42 \text{ mm}^3$  was proposed for UWB application [10]. A flag-shaped monopole antenna with a total dimension of  $30 \times 30 \times 1.6 \text{ mm}^3$  consisting of a rectangle strip in asymmetric style and a coplanar waveguide (CPW) fed with finite-ground structure was proposed for ultra-wideband operation [11]. In [12] the designed antenna with a total dimension of  $35 \times 24 \times 1.6 \text{ mm}^3$  covers the entire UWB band with a ring-shaped antenna with an upper cutting edge and additional slot, as well as a rectangular slot on the upper middle edge of the partial ground structure. The UWB performance was achieved by the hexagonal patch antenna with a flangeless SMA connector and slots on the truncated ground plane and the radiator with a total dimension of  $46 \times 46 \times 1.5 \text{ mm}^3$  [13]. The flower-shaped microstrip patch antenna with coplanar waveguide feeding technique had been proposed for broadband applications but it did not cover the entire UWB band with a total dimension of  $28 \times 41.8 \times 1.6 \text{ mm}^3$  [14]. However, Most of the reported literature lacks effective physical insight into the antenna structures used for ultra-wideband operation and are developed based on experimental experience and parametric studies. These antennas are also expected to be small in size for use in portable devices that operate different communication services.

Recently, the use of the CMA in enlightening the physical significance of antennas has become increasingly popular [15]. It is simpler in describing radiating objects of any shape, and provides sufficient information to understand the mechanism of the radiation behind the operation of antenna performance and is attracted by many researchers, primarily for multiple-input and multiple-output (MIMO) antenna [16], wideband and multiband antennas [17,18], and UWB antenna designs [19-21].

Bhaskara Rao Perli is with Research Scholar, ECE Department, JNTUA, Anantapur, India (e-mail: 2bhaskarp@gmail.com).

A. Maheswara Rao is with ECE Department, PBRVITS, Kavali, India (e-mail: amreddy73@gmail.com).



In this paper, using characteristic mode analysis, a compact 4-shaped annular ring planar monopole UWB antenna is proposed. First, CMA is performed on the annular ring in the process of optimizing with a substrate to generate more significant characteristic modes. The surface current distribution of desired modes is analyzing, and then these modes are excited by a simple microstrip line feeding structure and the ground structure. The insertion of strips inside the ring and the tapering the feed line achieves good impedance matching to achieve wide bandwidth. Next, the complete structure is further simulated in a CST multilayer solver to analyze the radiation capabilities of the characteristic modes in the frequency range of interest. The working principle of the proposed model is described from the perspective of the characteristic-mode. Finally, a prototype antenna was made and measured to validate simulation results and the proposed antenna performance compared with existing antenna models.

## II. CHARACTERISTIC MODE ANALYSIS

Characteristic mode analysis (CMA) [22] was used to determine the characteristics of the conducting body in terms of modal currents and modal fields. CMA effectively optimizes the size and shape of the conductive body by analyzing the modal current distribution and radiation behavior of each characteristic mode. Characteristic modes are current modes that occur on the surface of a conducting body and are orthogonal to each other. They are evaluated on the surface of the conducting body in order to obtain information about the modal currents (or modal fields) that the structure supports, naturally. The total surface current on the conducting body is defined as a function of the real eigenvalue  $\lambda_n$ , which is related to the  $n^{\text{th}}$  characteristic mode. The resonant frequencies and radiation bandwidth of the desired characteristic modes are well known by varying  $\lambda_n$  with frequency. Therefore, the modal significance (MS) is defined as a function of  $\lambda_n$ , as

$$MS = \frac{1}{|1 + j\lambda_n|}, \text{ a real quantity.} \quad (1)$$

The modal significance is an inherent property of each characteristic mode and quantifies the participation of each mode in the total radiation for a given power supply. MS converts the infinite eigenvalues  $[-\infty, +\infty]$  into very finite values  $[0, 1]$ . If  $MS = 1$  for a given mode, the mode is said to be a significant mode, otherwise the mode is said to be an insignificant mode. Any particular mode reaches the maximum value of MS ( $MS = 1$ ) at any frequency, and this frequency is called the resonance frequency of the mode. The modes have higher MS values and contribute more radiation to the total output of the antenna. In most cases, the modal significance is more suitable for analyzing the mechanism of antenna radiation in a wideband of frequencies.

### A. Analysis of Proposed Antenna using Characteristic Modes

CMA of the proposed model is performed on a multilayer platform of CST STUDIO SUITE. In this multilayer solver, the radiating element and ground layer are chosen as perfect electric conductors, and the substrate dielectric is selected as the lossless FR-4. CMA is applied to the antenna structure without applying any excitation.  $R_{in}$  and  $R_{out}$  represent the

inner and outer radii of the basic annular ring geometry as shown in Figure 1. The ratio of outer radius to the inner radius is appropriately selected to produce a more number of significant modes in the operating frequency range. Strips inside the ring and tapering technique are introduced to reduce the resonance frequencies of significant modes.

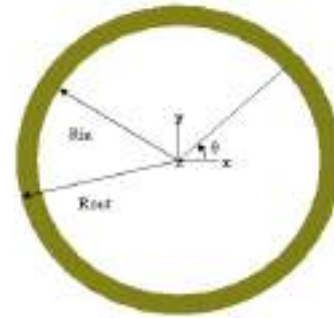


Fig. 1. Geometry of the basic structure of the annular ring ( $R_{in} = 7$  mm,  $R_{out} = 8$  mm)

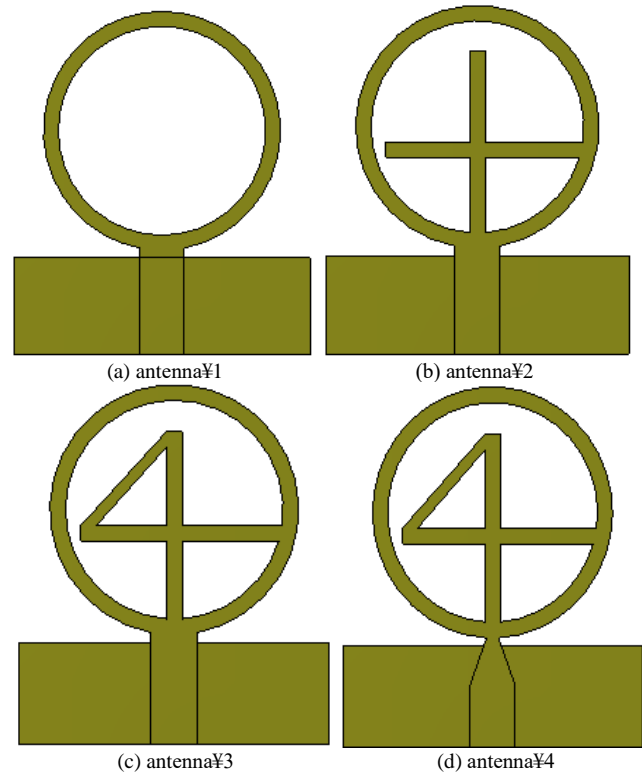


Fig. 2. Design steps of proposed monopole antenna.

Modal significance provides the resonant frequency and bandwidth of each mode with MS equal to 1. Figure 3a–d illustrates the MS curves of the first six characteristic modes for all the monopole antennas depicted in Figure 2. It can be noted that due to the non-resonating behavior of mode 3, which exhibits inductive nature over the operating frequency. The resonant frequencies of other modes associated with the characteristic currents appear at certain frequencies, as shown in Table I.



# Hexagon Shape SIW Bandpass Filter with CSRRs Using Artificial Neural Networks Optimization

Ranjit Kumar Rayala\* and Raghavan Singaravelu

**Abstract**—A dual-band hexagon shape substrate integrated waveguide (SIW) based band-pass filter with single loop complementary split ring resonators (CSRRs) is introduced in this paper. The design parameters of this filter are optimized by using artificial neural networks (ANNs). Especially an error back propagation multilayer perceptron (EBP-MLP) neural network with Levenberg-Marquart (LM) algorithm is used. A physical prototype of the proposed model is fabricated and tested. In the lower passband from 10.2 to 10.6 GHz, the insertion loss is about  $-0.8$  dB with a fractional bandwidth of 3.85%, and in the upper passband from 12.11 to 13.31 GHz, the insertion loss is about  $-0.8$  dB with a fractional bandwidth of 9.56%. It is observed that the insertion loss is the same in both the passbands. The obtained experimental results are in good agreement with the estimated results using full-wave analysis and ANN optimization.

## 1. INTRODUCTION

SIW technology has received a lot of attention because of its advantages like compact size, simple fabrication process, high efficiency, and can be easily integrated with other microwave components and circuits [1]. Miniaturization is a crucial necessity in modern communication systems, hence a SIW bandpass filter was designed and studied using the slow wave approach [2]. SIW structures are often made up of two rows of conducting cylinders or vias implanted in a dielectric substrate that links two parallel metal plates, allowing rectangular waveguide components, printed circuits, active devices, and antennas to be used in planar form [3]. This SIW technology is also widely used for the design and development of spatial filtering applications [4, 5].

The resonators having low insertion loss and high Q-factor are essential elements in modern microwave telecommunication systems particularly in low phase noise oscillators. Three novel dual-band CSRRs have been proposed in order to have low insertion loss and high Q-factor [6]. A dual-band bandpass filter that consists of a SIW dual-mode cavity loaded with two CSRRs on the upper layer has been proposed [7]. The CSRRs have been designed and developed on SIW in order to get bandpass filter characteristics with adjustable bandwidth [8]. A dual-band SIW bandpass filter with single loop CSRRs arrays on the upper layer has been proposed to achieve control over the bandwidth by changing the dimensions of CSRRs and the spacing between CSRRs arrays [9]. Semicircular CSRRs loaded onto the SIW cavity to provide independent control over the passband resonant frequency by varying the ring dimensions have been proposed and investigated [10]. A half-mode substrate integrated waveguide (HSIW) cavity that comprises modified split ring resonators (MSRRs) etched on the top layer of the waveguide has been proposed and investigated [11]. A SIW dual-band bandpass filter with a single triangular cavity loaded by complementary triangular split ring resonators (CTSRRs) and having three transmission zeros (TZ) in the overall passband has been proposed [12]. A pair of S-shaped

---

*Received 19 March 2022, Accepted 26 April 2022, Scheduled 12 May 2022*

\* Corresponding author: Ranjit Kumar Rayala (ranjit.rayala@gmail.com).

The authors are with the Department of Electronics and Communication Engineering, National Institute of Technology Tiruchirappalli, Trichy 620015, India.

complementary spiral resonators (S-CSRs) on the upper layer of the HMSIW cavity have been used to improve selectivity and generate transmission zeros near the passband [13]. The resonant frequencies can be shifted by changing the position and size of the CSRR in a sixteenth-mode substrate integrated circular cavity (SM-SICC) band-pass filter that has been proposed [14].

ANN has recently become a major tool in the field of microwave modelling and design [15, 16], and it has been used to reduce simulation time for SIW components, RF circuits, microwave devices, and circuits, all of which require more simulation time to optimize design parameters [17]. The design parameters of X band SIW  $H$ -plane bandpass filter have been optimized by using back propagation neural network (BPNN) proposed [18]. To optimize the SIW filter parameters, a novel neural network of calibrated coarse model has been proposed, and some training data have been used to synthesize the entire SIW filter [19]. To provide a quick and precise frequency response, the scattering parameter  $S_{21}$  in dB has been predicted using a multi-layer perceptron MLP-ANN [20]. A semi-supervised radial basis function neural network (SS-RBFNN) model has been proposed that uses an enhanced sampling strategy to reduce the uneven error distribution and slow convergence caused by sample selection uncertainty in the training process of artificial neural networks [21].

In this paper, a hexagon shape bandpass filter is proposed, and the filter parameters are optimized using MLP-ANN. Levenberg-Marquart (LM) algorithm is used to train the neural network. The keyword used is ‘trainlm’ in the MATLAB. The learning rate is 0.01, and the used activation function is log-sigmoid. The ANN results and CST Microwave studio simulated results are in good agreement.

This paper consists of five sections. The basic topology design methodology of proposed filter is explained in Section 2. The optimization of filter parameters using neural networks is explained in Section 3. The simulation results are explained in Section 4. The fabrication process and measurement setup are explained in Section 5.

## 2. DESIGN OF SIW BPF

The CST microwave studio is used to develop and simulate the hexagon-shaped bandpass filter depicted in Figure 1. The basic structure consists of three layers, and the bottom and top layers are perfect electric conductors (PECs). The middle layer of the SIW structure is made of Rogers RO4003C, which has a dielectric constant ( $\epsilon_r$ ) of 3.55 and substrate height ( $h$ ) of 0.81 mm. The hexagon shape is modelled on the top PEC with a diameter ( $H_{dia}$ ). Two square-shaped slots are etched on the opposite sides of the hexagon along the longitudinal direction. While microstrip feeding is given on both sides, these two square slots are used as feed points.

In order to make it as a SIW topology, the vias are arranged along the hexagon shape with a separation distance ( $p$ ) and a diameter ( $d$ ). From upper PEC these vias are penetrated through the dielectric material and the lower PEC. Two single layer Complimentary Split Ring Resonators (CSRR)

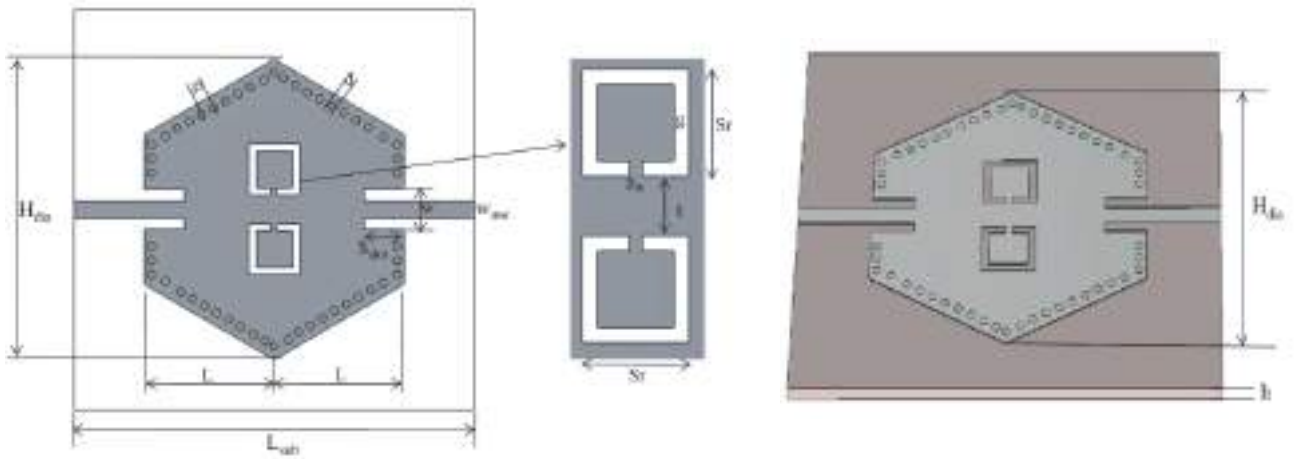


**Figure 1.** Topology of proposed filter.

are etched on the upper PEC. The optimised values for this hexagon shape topology are shown in Table 1.

**Table 1.** Dimensions of the proposed filter.

S. No.	Parameter	Value (mm)
1	$d$	0.8
2	$H_{dia}$	30
3	$g$	1
4	$g_{in}$	0.6
5	$h$	0.81
6	$L$	26
7	$L_{sub}$	40
8	$p$	1.4
9	$S_{slot}$	4
10	$S_r$	3.6
11	$t$	0.8
12	$w$	4
13	$W_{mst}$	1.74

### 3. BASIC MODEL OF BP-ANN

Neural networks play an important role in many engineering problems, so these networks are used in the filter parameters optimization. There are many types of neural networks available like multilayer feed forward neural networks (MLP-ANN), Temporal NN, radial basis function networks (RBF), Wavelet NN, and Self organizing maps [20]. Error back propagation multilayer perceptron artificial neural network (BP-MLP-ANN) is the most widely used network.

A neural network (NN) contains three layers, namely input layer, hidden layer, and output layer. The physical parameters that are intended to optimize are treated as input layer neurons. The second layer consists of a number of sub-layers which is known as the hidden layer, and finally, the output layer contains one or more neurons. Neurons are nothing but the information processing units, and they are also known as nodes or base points. The basic model of neural network is as shown in Figure 2.

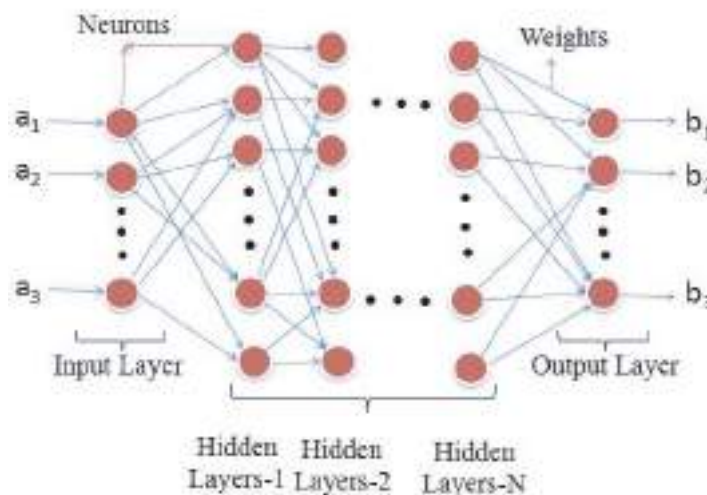


**Figure 2.** Basic model of Neural Network.

The links between neurons from input layer to output layer through the hidden layer are known as interconnections or weights.

In order to optimize the filter parameters, a supervised learning mechanism is used. In this method, the neural network must be trained with a set of known values, which are known as training data shown in Table 2, and this process is known as training of neural network. In the training process, the weights of the network are adjusted themselves to produce an output with a minimum mean square error (MSE). Now another set of data known as testing data shown in Table 3 is used to test the trained network. These two data sets are generated from the CST Microwave Studio by performing a number of simulations.

**Table 2.** Training data.

S. No.	$S_{Slot}$ (mm)	$S_{11}$ (dB) (CST)
1	3.95	-20.291
2	4.03	-19.616
3	4.05	-19.235
4	4.15	-17.367
5	4.18	-16.848
6	4.25	-15.921
7	4.35	-13.335
8	4.45	-12.448
9	4.55	-12.075
10	4.65	-11.233

**Table 3.** Testing data.

S. No.	$S_{Slot}$ (mm)	$S_{11}$ (dB) (CST)	$S_{11}$ (dB) (ANN)	Mean Square Error
1	3.98	-20.415	-20.1313	0.2837
2	4.0	-20.673	-20.3526	0.3204
3	4.1	-18.276	-18.1666	0.1094
4	4.2	-16.670	-16.9877	0.3177
5	4.3	-15.004	-14.9313	0.0727
6	4.33	-13.598	-13.5915	0.0065
7	4.4	-12.863	-12.4525	0.4105
8	4.5	-12.078	-11.9968	0.0812
9	4.6	-11.622	-11.2806	0.3414

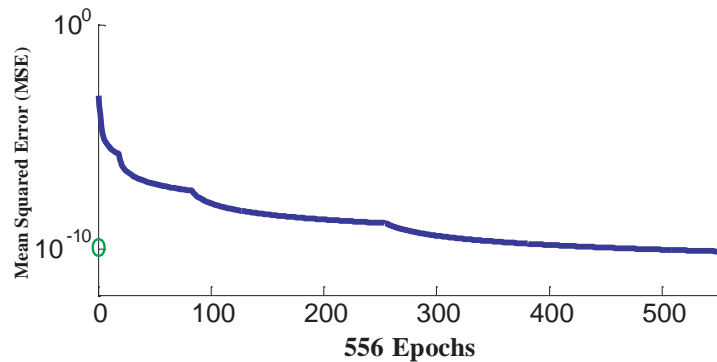


**Figure 3.** Training performance of the neural network.

The proposed neural network in this paper is a single hidden layer feed forward neural network, which comprises an input layer, a hidden layer, and an output layer, each having a number of neurons of 1, 10, and 1, respectively. The hidden layer neurons are fixed by trial and error method. Levenberg-Marquart (LM) algorithm is used to train the neural network. The keyword used is ‘trainlm’ in the MATLAB. The learning rate is 0.01, and the activation function used is log-sigmoid. Figure 3 shows the MSE plotted against the number of epochs, and the training performance of proposed neural network can be observed from this plot.

#### 4. SIMULATION RESULTS DISCUSSION

The proposed hexagon shape dual bandpass filter, depicted in Figure 1, was designed and simulated using CST MWS, with simulated results presented in Figure 4. This graph shows the variation of  $S_{11}$  and  $S_{12}$  w.r.t frequency. The designed filter shows dual-band characteristics. The lower passband shows a narrow band response with a centre frequency of 10.41 GHz and offers a bandwidth of 403 MHz (ranging from 10.2 to 10.6 GHz). The proposed filter has another passband which is a wide-band response centred at 12.55 GHz. The upper passband provides a good wide-band response with a transmission bandwidth of 1.2 GHz (from 12.11 to 13.31 GHz). The return loss in lower passband is about  $-23$  dB with a

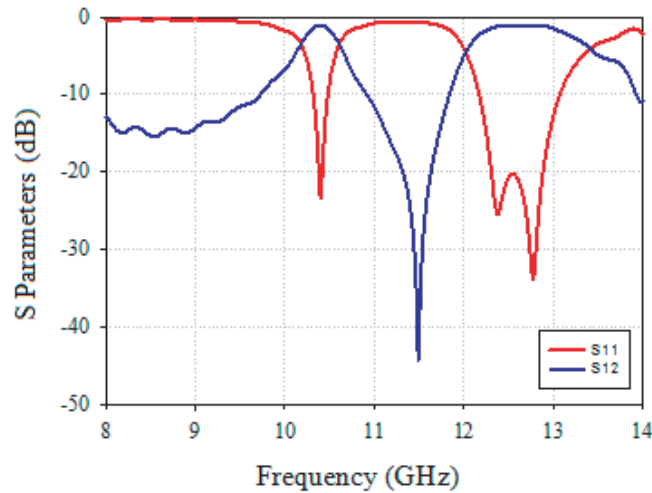
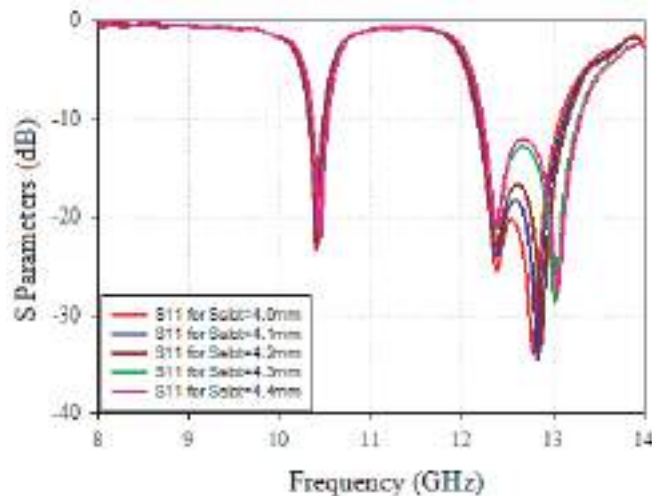
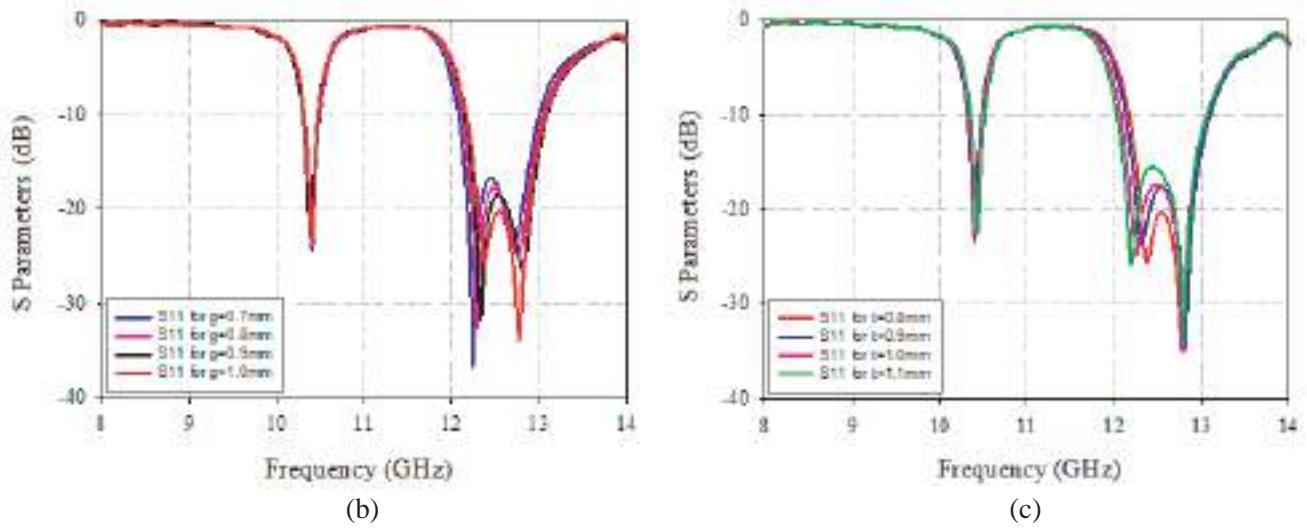


Figure 4. Frequency response of proposed filter.



(a)



**Figure 5.** (a) Parametric analysis with respect to  $S_{slot}$ . (b) Parametric analysis with respect to ' $g$ '. (c) Parametric analysis with respect to ' $t$ '.

fractional bandwidth of 3.84%, and in higher pass band it is about  $-20.4$  dB with a fractional bandwidth of 9.56%. Figures 5(a)–5(c) present the parametric analysis of the proposed filter. By varying different parameters like  $S_{slot}$ ,  $g$  and  $t$ , the parametric analysis was carried out in order to generate training data for ANN.

Throughout the overall frequency band of operation, it offers an insertion loss of 0.8 dB. From the frequency response we can observe three transmission poles. One is at the first resonant frequency ( $fr_1$ ) of 10.4 GHz in the lower passband, and the other transmission poles are in the upper passband at the second resonant frequency ( $fr_2$ ) of 12.38 GHz and the third resonant frequency ( $fr_3$ ) of 12.77 GHz. The electric field distribution of designed bandpass filter is shown in Figure 6 which is obtained in CST MWS while the simulation is carried out. The colour ramp represents the variation in electric field strength, and the proposed filter shows the dominant mode behaviour as normal rectangular waveguide.

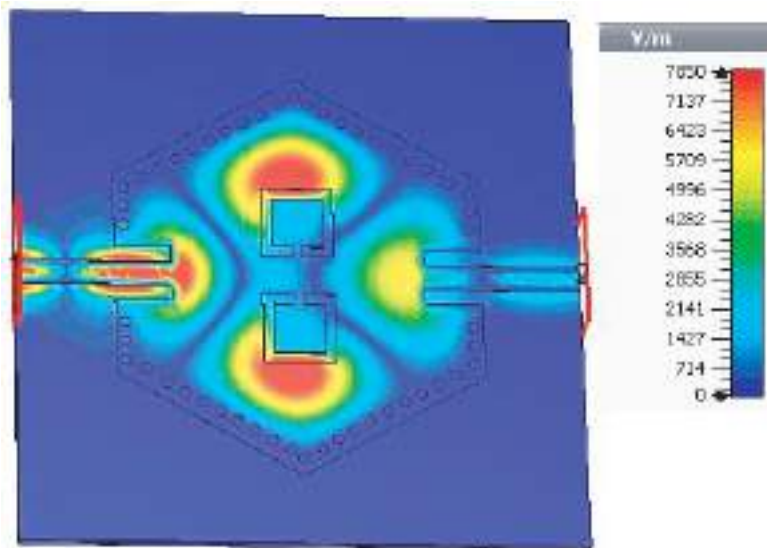


**Figure 6.** Electric field distribution.

### 5. FABRICATION AND EXPERIMENTAL VALIDATION

Figure 7 shows the fabricated model of the proposed filter, and Figure 8 shows the total measurement setup. Simple printed circuit board (PCB) process is used to design the proposed bandpass filter which shows two passbands. The dielectric substrate used is Rogers RO4003C of height 0.81 mm, having a relative permittivity ( $\epsilon_r$ ) of 3.55 and magnetic loss tangent  $\tan(\delta)$  of 0.0027. During the fabrication process of the proposed filter, at first the copper coating was done on both sides of the dielectric material. After that to make it into a SIW structure, via holes have been drilled. These via holes are placed in hexagon shape as shown in Figure 7. Finally from the upper PEC layer, a portion of PEC was removed in order to form CSRR slots. The Combinational Analyzer (Anritsu-MS2037C) has been used to measure this prototype model.

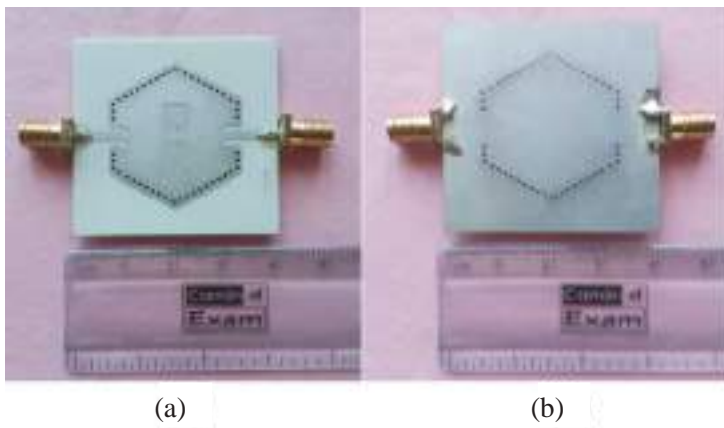


**Figure 7.** Photographs of fabricated models. (a) Top view. (b) Bottom view.

**Figure 8.** Measurement setup.

The measured results were plotted against the simulated ones, and they are in good agreement as shown in Figure 9. At  $-10$  dB, in the lower passband and upper passband the measured  $S_{11}$  is shifted by 126 MHz and 90 MHz respectively from the simulated results.

From Figure 9, the simulated and measured transmission coefficients  $S_{12}$  show an insertion loss of

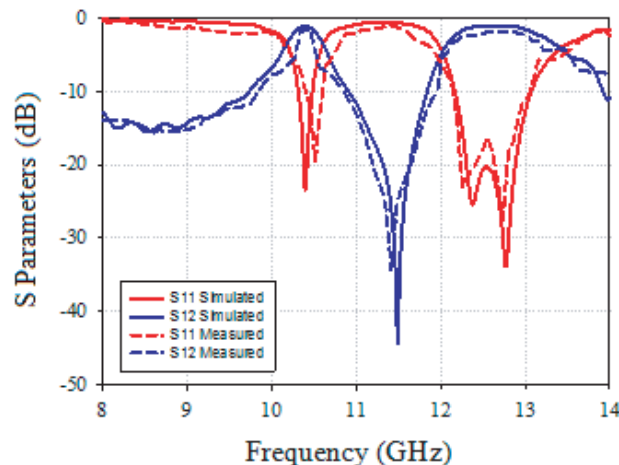


**Figure 9.** Simulated results plotted against measured results.

−0.8 dB and −1.55 dB, respectively, in the lower passband and upper passband which are about −0.8 dB and −1.62 dB, respectively. This difference in insertion loss is because losses due to SMA connectors were not considered while the simulation is performed.

## 6. CONCLUSION

A dual-band hexagon shape SIW bandpass filter with single loop CSRR based on ANN is presented. The design parameters of this filter are optimized by using an EBP-MLP neural network with LM algorithm and investigated using full-wave analysis with CST microwave studio. To prove the efficacy of the proposed model, a prototype is fabricated, and its functionality is verified experimentally. The measured insertion loss in the lower passband is about −1.55 dB and in the upper passband it is about −1.62 dB. The measured and simulated results are in good agreement and are also in good agreement with the ANN results with minimum mean square error. The properly trained neural networks give results at a faster rate than any other commercial CAD tools. The results are encouraging and useful for the easy optimization of SIW circuits with reduced computational complexity and execution time.

## ACKNOWLEDGMENT

The measurement facilities were provided by KL University in Guntur, Andhra Pradesh, India, which the authors gratefully acknowledge.

## REFERENCES

1. Deslandes, D. and K. Wu, "Single-substrate integration technique of planar circuits and Waveguide filters," *IEEE Transactions on Microwave Theory and Techniques*, Vol. 51, No. 2, 593–596, 2003.
2. Ananya, P., P. Athira, and S. Raghavan, "Miniaturized band pass filter in substrate integrated waveguide technology," *International Journal of Engineering & Technology*, Vol. 7, No. 3.13, 95–98, 2018.
3. Krushna Kanth, V. and S. Raghavan, "EM design and analysis of a substrate integrated waveguide based on a frequency-selective surface for millimeter wave radar application," *J. Comput. Electron.*, Vol. 18, 189–196, 2019.
4. Krushna Kanth, V. and S. Raghavan, "Ultra thin wide band slot and patch FSS elements with sharp band edge characteristics," *International Journal of Electronics*, Vol. 107, 1365–1385, 2020.
5. Krushna Kanth, V. and S. Raghavan, "A novel Faraday-cage inspired FSS shield for stable resonance performance characteristics," *International Journal of Electronics Letters*, Vol. 8, 60–69, 2020.
6. Hamidkhani, M., R. Sadeghi, and M. Karimi, "Dual-band high  $Q$ -factor complementary splitting resonators using substrate integrated waveguide method and their applications," *Journal of Electrical and Computer Engineering*, Vol. 2019, 11, 2019.
7. Hao, Z., K. Wei, and W. Wen, "Dual-band substrate integrated waveguide bandpass filter utilizing complementary split ring resonators," *Electronics Letters*, Vol. 54, 85–87, 2018.
8. Park, W.-Y. and S. Lim, "Bandwidth tunable and compact BandPass Filter (BPF) using Complementary Split Ring Resonators (CSRRES) on Substrate Integrated Waveguide (SIW)," *Journal of Electromagnetic Waves and Applications*, Vol. 24, No. 17–18, 2407–2417, 2010.
9. Li, D., J.-A. Wang, Y. Yu, Y. Liu, Z. Chen, and L. Yang, "Substrate integrated waveguide-based complementary split-ring resonator and its arrays for compact dual-wideband bandpass filter design," *Int. J. RF Microw. Comput. Aided Eng.*, Vol. 31, e22504, 2021.
10. Chaudhury, S. S., S. Awasthi, and R. K. Singh, "Dual passband filter based on semi circular cavity substrate integrated waveguide using complementary split ring resonators," *IEEE Applied Electromagnetics Conference (AEMC)*, 1–2, Aurangabad, India, 2017.



11. Yan, T. and X.-H. Tang, "Substrate integrated waveguide dual-band bandpass filter with complementary modified split-ring resonators," *IEEE International Wireless Symposium (IWS 2015)*, 1–4, Shenzhen, China, 2015.
12. Geng, Q. F., H. J. Guo, Y. Y. Zhu, W. Huang, S. S. Deng, and T. Yang, "A novel dual-band filter based on single-cavity CTSRR loaded triangular substrate-integrated waveguide," *International Journal of Microwave and Wireless Technologies*, Vol. 11, 894–898, 2019.
13. Wei, F., H. J. Yue, J.-P. Song, H. Y. Kang, and B. Li, "Half-mode SIW BPF loaded with S-shaped complementary spiral resonators," *Progress In Electromagnetics Research Letters*, Vol. 77, 13–18, 2018.
14. Chen, X.-G., G. H. Li, Z. Shi, and S. D. Feng, "Compact SICC dual-band and UWB filters using multimode technology," *Progress In Electromagnetics Research Letters*, Vol. 92, 69–74, 2020.
15. Zhang, Q.-J., K. C. Gupta, and V. K. Devabhaktuni, "Artificial neural networks for RF and microwave design — from theory to practice," *IEEE Transactions on Microwave Theory and Techniques*, Vol. 51, No. 4, 1339–1350, 2003.
16. Rayas-Sanchez, J. E., "EM-based optimization of microwave circuits using artificial neural networks: The state-of-the-art," *IEEE Transactions on Microwave Theory and Techniques*, Vol. 52, No. 1, 420–435, Jan. 2004.
17. Angiulli, G., E. Arneri, D. De Carlo, and G. Amendola, "Feed forward neural network characterization of circular SIW resonators," *IEEE Antennas and Propagation Society International Symposium*, 1–4, San Diego, CA, USA, 2008.
18. Tabatabaieian, Z. S. and M. H. Neshat, "Design investigation of an X-band SIW  $H$ -plane band pass filter with improved stop band using neural network optimization," *Applied Computational Electromagnetics Society Journal*, Vol. 30, No. 10, 1083–1088, 2015.
19. Du, G.-Y. and L. Jin, "Neural network of calibrated coarse model and application to substrate integrated waveguide filter design," *International Journal of RF and Microwave Computer-Aided Engineering*, Vol. 30, No. 10, e22374, 2020.
20. Amir, B. and B. S. Masoud, "Optimal design of double folded stub microstrip filter by neural network modelling and particle swarm optimization," *Journal of Microwaves, Optoelectronics and Electromagnetic Applications*, Vol. 11, 204–213, 2012.
21. Xiao, L., W. Shao, F. Jin, B. Wang, W. T. Joines, and Q. H. Liu, "Semi supervised radial basis function neural network with an effective sampling strategy," *IEEE Transactions on Microwave Theory and Techniques*, Vol. 68, 1260–1269, 2020.

## NEW IOT ECOSYSTEM FRONTIERS - A SURVEY ON CLASSIFICATION IN TERMS OF IOT CHALLENGES AND CONSTRAINTS

Anjani Yalamanchili<sup>1</sup>, D. Venkata Sekhar<sup>2</sup>, G. Vijay Kumar<sup>3</sup>

<sup>1</sup>Research Scholar, Department of I.T, Annamalai University, Chidambaram, Tamil Nadu, India

<sup>2</sup>Professor, Department of I.T, Annamalai University, Chidambaram, Tamil Nadu, India

<sup>3</sup>Professor, Department of C.S.E., Sri Sunflower College of Engineering and Technology, Challapalli, A.P, India

### ABSTRACT

The way using the internet has been changed by the modern era; it is mutated into a strong enabler because it delivers customized ways to boost people's living standards. The Internet of Things (IoT) is a network of machines that can feel, connect with embedded technologies to meet, react to and help control their lives in all possible ways. Infrastructure availability, resource availability at inexpensive prices, IoT system usability at any time are the reasons for the enormous growth of IoT technology in the 21st century. It can be assumed that the IoT is the revolution that fuses the digital and physical world. COVID-19 is a pandemic disease caused by the Corona virus. It is a dangerous disease that in many countries has infected people and taken the lives of people in lakhs. It travels from person to person by the nose or mouth droplets of an infected person. As a protection against being poisoned, person to human contact must be prevented or adequate distancing must be preserved. In order to prevent the transmission of the disease, lock downs have been introduced. The year 2020 has created an opportunity to illustrate the role IoT has played in the lives of individuals from all industries. Anybody anywhere, anywhere linked to any aspect of the thing or part of the thing in this pandemic case. Anyone anywhere, everywhere related to any aspect of the thing or people around the world is made possible using IoT in this pandemic case. IoT and its classification are discussed in this paper

**KEYWORDS:** IOT Ecosystem

---

### Article History

**Received: 21 Jan 2021 | Revised: 27 Jan 2021 | Accepted: 06 Feb 2021**

---

### INTRODUCTION

IoT interfaces gadgets and sensors through remote mode and make information accessible to the clients. The clients can get to and have control over the gadget from anyplace within the world. In straightforward words IoT performs AAA that's collect information, from any put any time anyplace at that point analyze, prepare information and perform activities to support the choice making. IoT interact within the same way how individuals connected in physical world. It is done with the assistance of computerized objects [1]. The advanced objects give information as physically given by the individuals for preparing. IoT replaces human- human communication. Agreeing to measurement report from Gartner IoT investigate, CISCO IoT solidness approximately 25-30 billion of IoT gadgets will be associated to the Web. It is evaluated that 127 modern IoT gadgets will be interfacing each moment. The number of IoT gadgets in domestic will have a fast rise and it is

anticipated to be around 12.86 billion. IoT has turned out to be boon not as it were for an indicated division but for all sectors [2].

There are two IoT markets. They are Even and vertical IoT showcase. IoT showcase which centres on the particular administrations that's in arrange to meet the requests of particular individuals is called vertical showcase and it may be either industry particular or statistic particular [3]. Level IoT showcase centres on wide extend of client needs and it has huge client base. In flat showcase buyers and buyers will be of distinctive divisions of the economy. From the Figure 1 it is obvious that sum contributed on vertical IoT of diverse divisions has seen fast development from 2015-2020. The number of IoT gadgets associated to the web is more than that of the versatile gadgets associated to web [4]. The assessed increment in showcase share contributed by diverse divisions towards IoT application for the year 2015-2025 is appeared within the Figure 2 and it is found that more speculations are made on wellbeing care units to convert conventional hardware and machines into savvy items. Since of this widespread COVID-19 there's plausibility to present Robots with wellbeing checking framework to dodge human interaction and to supply medications to tainted people to diminish the infection spread in future. So, rate of speculation in wellbeing care IoT applications will have colossal development when compared to other divisions. COVID-19 affect will cause a huge alter not as it were in Restorative IoT applications but too in instructive sectors as well as mechanical divisions where there's plausibility of interaction of community of individuals [5].

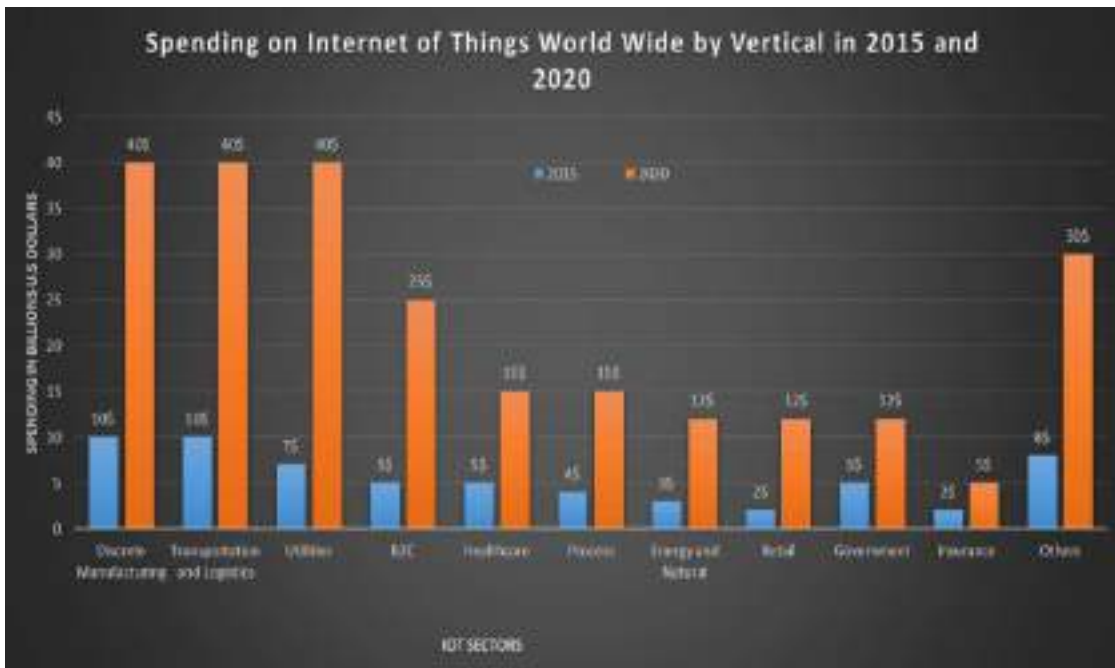


**Figure 1: Investment in the Multiple IoT Industries in Billions of US Dollars (Source: Forbes).**

**IOT CLASSIFICATION BASED ON CAPABILITY AND PERFORMANCE**

IoT grouping can be achieved in various ways. IoT gadgets are graded as low, middle and high-ended gadgets on the basis of capability and execution. Low-end gadgets based on advanced features such as memory, backup of heterogeneous devices, network organization, reliability and genuine time capability are categorized as Type0, Type1 and Type2. Cameras, actuators, openmote, waspmote, Tmote sky, ATMEL SAM R21 Xplained-pro, etc. Type0 has resources that are minimal. The first layer reflects it. It contains functions for sensing and actuating. In contrast to low end instruments, Sensors Type1 has more power [6]. It offers more features than Type0.0. The downside is that it has little computational capacity to manage difficult specifications. It requires fundamental microcontrollers. In other words, it increases the

functionality of IoT products with lower ends. It has functions such as image recognition, extraction of data, etc. Form 2 requires CPU, RAM, flash memory and supports traditional operating systems such as LINUX, UNIX. It can be combined with nearly all protocols for communication. The ability of middle-end IoT systems to use more than one communication technology. The spectrum of hundreds of MHZ is the clock speed and RAM [7]. It has more limited resources relative to low-end devices, but fewer than those of high-end devices. The design specifications for IoT devices and protection requirements for these IoT devices are outlined in Table 1 and 2.

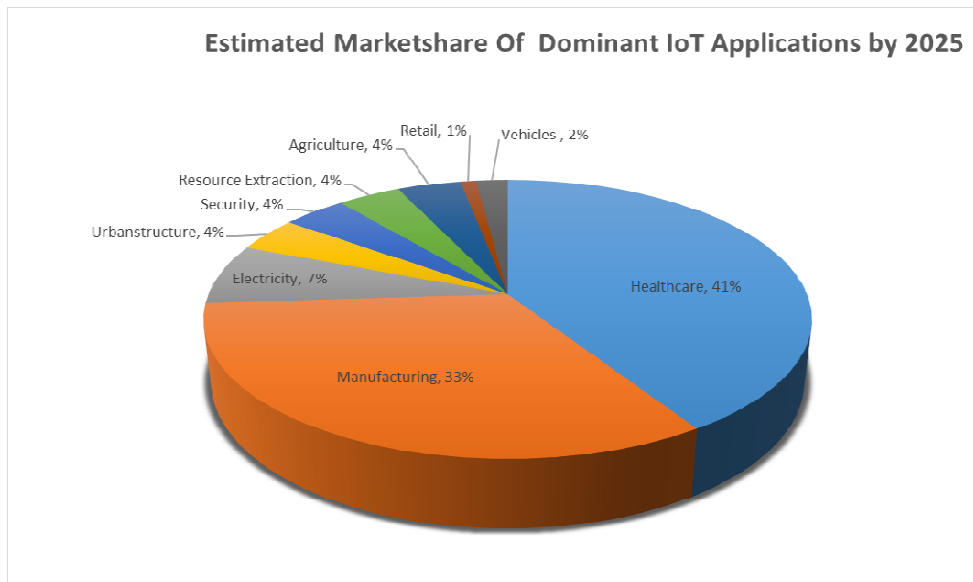


Figure 2: Estimated Contribution of the IoT Industries that Control.

Table 1: Specifications for Various IoT Application Forms

Low End Devices	Specifications			
	RAM	Flash	RTOS Support	Communication Protocols
Type0	<10kB	<100 kB	Does not support	Use gateways for communication No protocol stack embedded
Type1	~10kB	~100kB	Could be implemented	Use light weight protocols, communicate with other devices without using gateway
Type2	~50kB	~250kB	Could be operated	Supports communication protocol such as HTTP

Table 2: Security Specifications Focused on the Capability of IoT Devices

Categories	Security Requirements	Type0	Type1	Type2
Confidentiality	Message encryption		Yes	Yes
	Malware response			
	Data encryption		Yes	Yes
	Tamper resistance		Yes	
	Device ID management	Yes	Yes	Yes
Integrity	Data integrity		Yes	Yes
	Platform integrity			Yes
	Secure booting			Yes
Availability	Logging		Yes	Yes
	State Info.	Yes	Yes	Yes
	Transmission			
	Security monitoring			Yes
	Security patch			Yes
	Security policy			Yes
	Software safety		Yes	Yes

**Table 2: Contd.,**

<b>Authentication/ Authorization</b>	User authentication		Yes	Yes
	Device authentication		Yes	Yes
	Password management		Yes	Yes
	Access control		Yes	Yes
	Device ID verification			Yes

**IOT GROUPING BASED ON THE LIFE CYCLE OF ORGANIZATION AND OPERATION**

Another grouping, based on the association of the entity with that of physical equipment, is known as low-level operation, assets service, entity service, consolidated service [8]. IoT is defined as deployable, deployed, or operational, depending on the level of service. Figures 3 and 4 reflect the classifications.

**IOT GROUPING BASED ON OPERATING SYSTEM**

A series of programs called the operating system is a bridge between applications or users and computers. The operating system is built on the IoT computers to run the programs and control the devices. It is further graded as low and high-end depending on the operating system (OS) [9]. In figure 5, the schematic representation is shown. Table 3 displays some of the operating systems required for low-level and high-level computers.

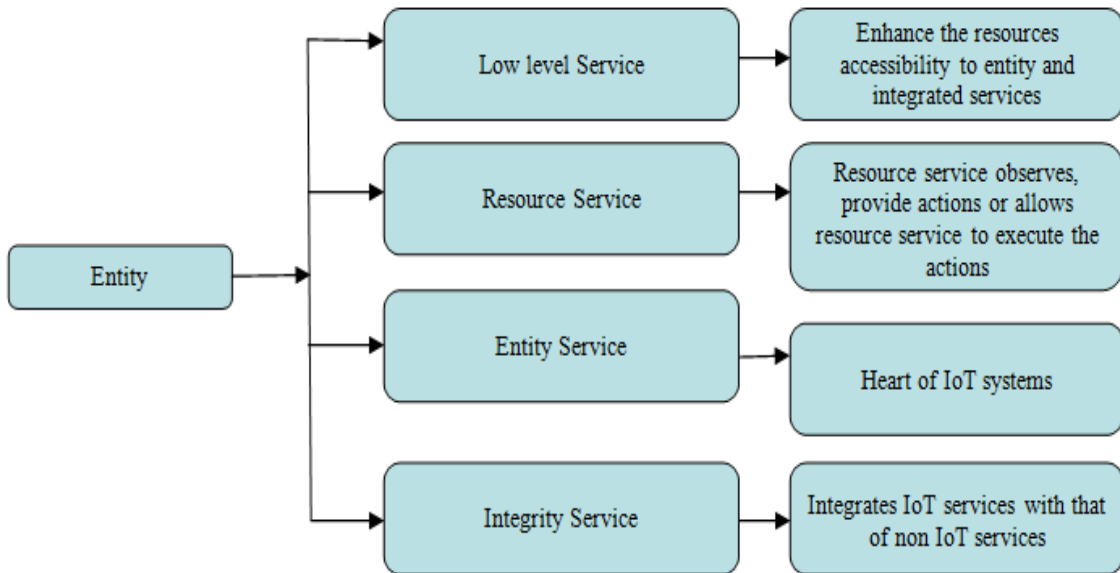


**Figure 3: Entity Partnership Definition Based.**

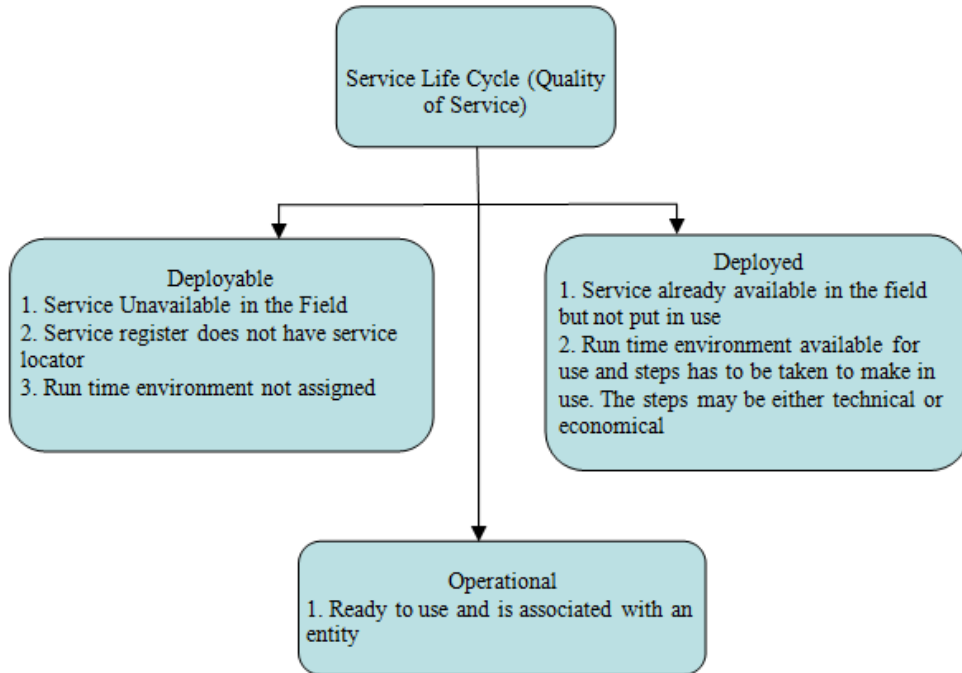


Figure 4: Operation Life Cycle-Based Grouping.

Table 3: OS for Device with IoT

Operating System	Supporting Device	IoT-Enabled Devices	OS Supporting
Tiny OS	No	Low	Non-Linux
Contiki	Yes	Low	Non-Linux
RIOT	Yes	Low	Non-Linux
LiteOS	No	Low	Linux
FreeRTOS	Yes	Low	Non-Linux
Mynewt	Yes	Low	Linux

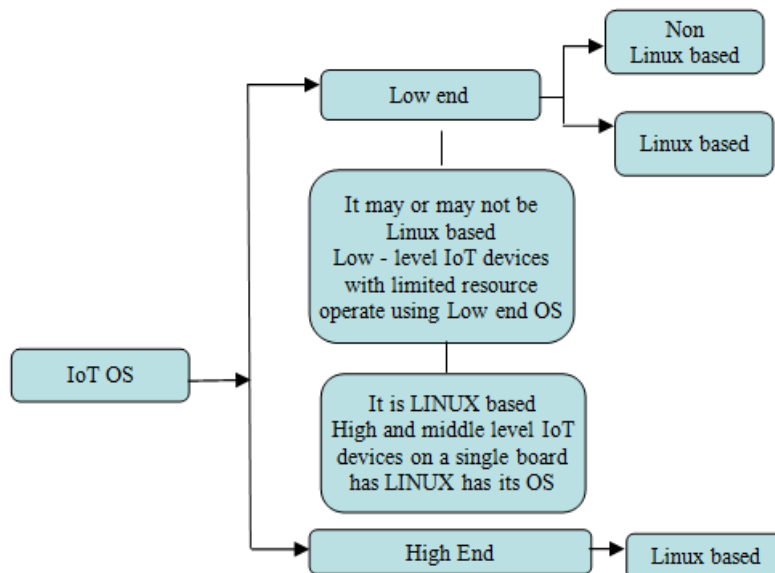


Figure 5: Classification by Type of OS Used.

## IOT GROUPING BASED ON NETWORKING TECHNOLOGY

To provide basic smart services, IoT requires connectivity technologies to connect heterogeneous objects. In the sharing of information, communication technology support. It is possible to connect locally using Bluetooth, NFC or the Internet [10]. The key distinction between local and internet protocol communications is focused on variables such as transmission range, power usage, and memory used. IoT includes networking technologies to connect heterogeneous objects in order to provide simple smart services. Communication infrastructure assists in the exchange of knowledge. Bluetooth, NFC or the Internet may be used to connect locally. Variables such as propagation range, power consumption, and memory used reflect on the main difference between local and internet protocol communications. A subclass of RFID is NFC. NFC is a 13.56 MHz high frequency RFID. RFID is a protected method of data sharing, consisting of a reader, tag and antenna. RFID may either be passive or aggressive. There are variations between Active and Passive RFID in Table 4.

**Table 4: Active and Passive RFID**

Active RFID	Passive RFID
It has own power source	Do not have their own power source
It finds its application in construction, security, Public works	It finds its applications in paper, textile etc.
Tags are costly and have limited life span	It is small size, light weight and has long life span

Low Power Technologies- Developed Low Power Technologies to support the IoT model. The arrangements for all forms of sensors are improved by LPWANS (Low Power Large Area Networks). With thin, cheap batteries lasting for years, it has the potential to provide long-range communication. It finds its applications in remote controls, smart meters, construction contracts, etc. Registered versions such as NB-IoT, LTE-M and unlicensed versions such as MYTHINGS, LoRa, Sigfox and so on can be used. Reliable broad band connectivity is provided through wireless technologies used in mobile phones [11]. For its service, it needs power and its operating cost is high. Due to factors like frequency, contact range and security, it does not support most IoT products. Due to high energy demand, Wi-Fi finds its applications in intelligent home appliances, surveillance cameras, etc. Coverage, scalability and power usage are the considerations that make it less widespread. Wi-Fi-6 offers increased bandwidth < 9.6Gbps to improve data transmission in order to address the data transfer caused by the congested environment. Wi-Fi HaLow has enhanced energy output but lacks security. Along with electronic sensors, blue tooth low energy and blue tooth devices are used to provide a smart interface specifically for medical wearables and exercise. The topology of Mesh helps Zigbee to connect with more IoT computers. Higher data rates are enabled and less electricity is used. It finds its applications in medium-range IoT devices such as energy management, protection, HVAC control and so on due to low power consumption. For all IoT programs, the network specifications are not the same [12]. Each IoT application has a prerequisite for its own network. Availability, security, bandwidth latency, power consumed by devices, service quality, network management are the factors that affect the selection of wireless technology for specific IoT applications. The wireless technology for different IoT implementations is seen in Table 5.

**Table 5: For Separate IoT Verticals, Wireless Technology**

Key IoT Verticals	LPWAN	Cellular	Zigbee	BLE (Star & Mesh)	Wi-Fi (Star and Mesh)	RFID
	(Star)	(Star)	(Mostly Mesh)			(Point-to-Point)
Industrial IoT	Highly applicable	Moderately applicable	Moderately applicable			
Smart Meter	Highly applicable					
Smart City						
Smart Building			Moderately applicable	Moderately applicable		
Smart Home			Very High	Very High	Very High	
Wearables	Moderate			Very High		
Connected car					Moderate	
Connected Health		Highly applicable		Highly applicable		
Smart Retail		Moderately applicable		Highly applicable	Moderately applicable	Highly applicable
Logistics & Asset tracking	Moderately applicable	Highly applicable				Highly applicable
Smart Agriculture	Highly applicable					

**IoT GROUPING BASED ON MIDDLEWARE**

The computing layer called IoT Middleware connects various application domains to interact over different domain interfaces. Middleware is often referred to as software glue because it allows software engineers to build contact implementation programs. If complex programming is not designed initially middleware enables to integrate it later with the help of support architecture. Schematic representation of the general functions that middleware executes [13]. In order to identify IoT middleware as service-oriented, cloud-oriented and actor-oriented middleware, accessibility, versatility and adaptive design are used. Service-oriented middleware- For end users, developers, extension and modification of IoT devices is allowed. Standalone or cloud storage systems can be service-oriented. Since it is not cost-effective, it does not support homogenous framework deployment. To support constrained services, there is no architecture provision for security techniques. Cloud-oriented middleware, which conveniently captures data, analyzes and interprets data. Security and privacy cannot be configured by the user. It has autonomy over critical details, but to support limited capital, it has no architecture framework. Users are permitted to plug and play IoT devices with actor-oriented middleware. They will uninstall the specific IoT device without disrupting and impacting the other elements of the IoT environment whenever the consumer does not need an IoT device. It enables protection and privacy to be configured by the user. Middleware is also defined as service-oriented, node-based, component-based, clustered, distributed, client-server, based on architecture nature.

**IoT GROUPING BASED ON DESIGN**

The simple IoT architecture consists of only three layers, namely perception layer-performing sensing and actuating, network layer-performing data transmitting and processing, device layer-providing the necessity to the user. Additional layers are used in the five-layer architecture to provide additional abstraction to the IoT architecture. Middleware interconnects heterogeneous objects with the heterogeneous device is the back bone of the IoT ecosystem, involving perception-where sensor tests the data, transport layer-performs transporting data function, processing layer-process and evaluating the data collected through transport layer. Through having control over the data flow, Middleware controls the



system. The sensors and actuators have the vision layer in the middleware-based architecture along with the access layer and edge layer. The Coordinate layer provides the customer with a final application along with the application layer. Data objects in service-oriented architectures are extracted and exposed through interfaces. While the technologies and the cloud differ, the Application Programming Interface (API) stays the same. The physical layer is often the bottom in fog-based architecture, the next layer is monitoring-observing and testing the data obtained from sensors. The pre-processing layer processes the data for processing-based results. In order to provide data protection and privacy, the security layer is liable. Perception layer-Includes actuators and sensors. Sensors track the physical and environmental parameters, gather certain parameters, erase the undesirable data and transfer the data to the actuators in order to execute actions. Transport layer-Utilizing communication protocols like Zigbee, BLE, NFC etc., brings the preprocessed data for processing to the processing layer. Processing layer- Filter, formatting information gathered from sensors. It also stores and handles, via communication protocol, the sensed data received from different devices. Middleware layer- To provide useful information, it conducts conceptual and analytical operations on the data available. It uses computing platforms and cloud storage. The application layer provides the user with an application using communication protocols such as MQTT, Restricted Application Protocol, and (CoAp). IoT architecture is shown in Figure 6.

**Table 6: Design of IoT**

Application Layer	Application Layer	Application Layer		Applications	Transport Layer
	Middleware Layer	Coordination Layer		Service Composition	Security Layer
Network Layer	Processing Layer	Middleware Layer		Service Management	Storage Layer
Perception Layer	Transport Layer	Backbone Network Layer		Object Abstraction	Pre-processing Layer
	Perception Layer	Perception Layer	Access Layer Edge Layer	Objects	Physical Layer Physical Layer
Three Layer		Five Layer	Middleware based		Service oriented Architecture Fog based

**IOT PLATFORM GROUPING**

The IoT interface bridges hardware and technology. The IoT platform is a feature of middleware that links gateways, cloud, server and device networks. Infra layer-performs intercommunication between devices, messaging feature, connection layer-enables communication between hardware and cloud to transfer data for data analytic processes, core layer-collects data, identifies the device, manages the device, updates the software framework. From the produced reports, the results can be calculated. To process the data, it frames the rules. Reports are created based on the rules applied. This layer connects the network, the gateways, to the cloud or device layer.

**CONCLUSIONS**

Because of the Internet and the apps generated on the internet, the environment has changed the way we work, move and do business. The Internet is predominantly based on a totally beneficial growth. Without IoT, contact turned out to be unlikely in all cases. IoT will change everything and is the cornerstone of a modern technological transformation, referred to as Business 4.0. It is the secret to organizations, cities and culture as a whole being digitally changed. A variety of sensors are built into the IoT. By having communication between smart devices, the IoT has the ability to extend its visibility. These systems are fitted with features such as identification, sorting, interaction, networking and service. Due to their small nature, less weight and cheap use of sensors and actuators is omnipresent. This paper provides an overview of the emerging IoT based on power and performance, organization, life cycle based on operation, operating system,

infrastructure, storage of middleware, portal, network, technologies of communication, applications. In order to improve people's convenience and quality of life, a series of technologies are involved. In order to face the difficulties that occur as vast quantities of data are managed by the IoT, research needs to tackle key problems such as stability, anonymity, scalability, interoperability, mobility and availability.

## REFERENCES

1. Seungyong Yoon, Jeongnyeo Kim, Yongsung Jeon, "Security Considerations Based on Classification of IoT Device Capabilities", *The Ninth International Conferences on Advanced Service Computing Service Computation 2017*.
2. Amirhossein Farahzadi, Pooyan Shams, Javad Rezazadeh, Reza Farahbakhsh *Middleware technologies for cloud of things: a survey Digital Communications and Networks 4 (2018) 176–188E*.
3. Sisinni, A. Saifullah, S. Han, U. Jennehag and M. Gidlund, "Industrial Internet of Things: Challenges, Opportunities, and Directions," in *IEEE Transactions on Industrial Informatics*, Vol. 14, No. 11, pp. 4724-4734, Nov. 2018, doi: 10.1109/TII.2018.2852491.
4. A. Kott, A. Swami, and B. J. West, "The Internet of battle things," *Computer*, Vol. 49, No. 12, pp. 7075, Dec. 2016.
5. Abuzainab and W. Saad, "Dynamic connectivity game for adversarial Internet of battlefield things systems," *IEEE Internet Things J.*, Vol. 5, No. 1, pp. 378\_390, Feb. 2018.
6. M. J. Farooq and Q. Zhu, "Secure and reconfigurable network design for critical information dissemination in the Internet of battle field things (IoBT)," in *Proc. 15th Int. Symp. Modeling Optim. Mobile, Ad Hoc, Wireless Netw.*, May 2017, pp. 1\_8.
7. S. Benaissa et al., "Internet of animals: Characterisation of LoRa sub-GHz off-body wireless channel in dairy barns," *Electron. Lett.*, Vol. 53, No. 18, pp. 1281\_1283, Aug. 2017.
8. S. Neethirajan, "Recent advances in wearable sensors for animal health management," *Sens. Bio-Sens. Res.*, Vol. 12, pp. 15\_29, Feb. 2017.
9. J. Vandermeulen et al., "Discerning pig screams in production environments," *PLoS ONE*, Vol. 10, No. 4, 2015, Art. no. e0123111
10. B. Keerthana, S. M. Raghavendran, S. Kalyani, P. Suja, and V. K. G. Kalaiselvi, "Internet of bins: Trash management in India," in *Proc. 2nd Int. Conf. Comput. Commun. Technol.*, Feb. 2017, pp. 248\_251.
11. C.-C. Kao, Y.-S. Lin, G.-D. Wu, and C.-J. Huang, "A comprehensive study on the Internet of underwater things: Applications, challenges, and channel models," *Sensors*, Vol. 17, No. 7, p. 1477, 2017.
12. M. C. Vuran, A. Salam, R. Wong, and S. Irmak, "Internet of underground things in precision agriculture: Architecture and technology aspects," *Ad Hoc Netw.*, Vol. 81, pp. 160\_173, Dec. 2018
13. I. F. Akyildiz and E. P. Stuntebeck, "Wireless underground sensor networks: Research challenges," *Ad Hoc Netw.*, Vol. 4, No. 6, pp. 669\_686, Nov. 2006.



## **A STUDY OF BANDWIDTH CONSUMPTION GAINS FOR IMPROVING SMART GRID QoS**

*Dr. G Vijay Kumar & Dr. B Vamsee Mohan*

*Department of CSE, PBR Visvidaya Institute of Technology & Science, Kavali, SPSR Nellore, Andhra Pradesh, India*

### **ABSTRACT**

Recently, the smart network performance is great significance in quality of service. When the Energy server provider requires several types of information signals with different requirements from all nodes it manages. these signals will meet some interference when sent in view of the limitation of bandwidth for wireless technologies. To insure from receiving information signals its required suitable modulation schemas Proportional to hugging data signals whereas any wireless communication technology performance depends firstly on bandwidth factor and latency. This paper explains bandwidth consumption gains (BCG) to match the appropriate communication technologies that enhance the QoS of Smart Grid.

**KEY WORDS:** Smart Grids, Different Communication Technologies, Bandwidth, Latency Factor, Different Nodes, Bandwidth Consumption Gain (BCG), Energy Service Provider (ESP).

---

### **Article History**

**Received: 03 Sep 2021 | Revised: 18 Sep 2021 | Accepted: 21 Dec 2021**

---



**ORIGINAL RESEARCH PAPER**

**Computer Science**

**IOT BASED APPLICATION CASE-STUDY FOR TRANSMISSION OF SLEEP APNEA PATIENT VIDEO WITH SOUND**

**KEY WORDS:** sleep apnea, video, audio, mobile

**Dr G Vijay Kumar\***

Professor in Department of CSE, PBR Visvodaya Institute of Technology & Science, Kavali, SPSR Nellore, Andhra Pradesh, India - 524201.  
\*Corresponding Author

**Dr B Vamsee Krishna**

Professor in Department of CSE, PBR Visvodaya Institute of Technology & Science, Kavali, SPSR Nellore, Andhra Pradesh, India- 524201.

**ABSTRACT**

Mobile video-audio transmission systems have delivered patient video with relevant snoring sound to quantify the severity of the sleep apnea patient over wireless networks, but few have optimized video-audio transmission in combination with transmission protocol over error-prone environments using wireless links. In this paper, the performance of the MPEG (Motion Picture Expert Group)-4 error resilient tools with UDP(User Datagram Protocol) protocol were evaluated over a wireless network to suggest the optimum combination of MPEG-4 error resilient tools and UDP packet size suitable for real-time transmission of video-audio transmission over error-prone mobile networks. Through experimentation, it was found that the packet size should correspond to IP(Internet Protocol) datagram size minus UDP and IP header for optimal video-audio quality. Also, for error resilient tool selection, the combination of resynchronization marker and data partitioning showed the best performance.

**INTRODUCTION**

Advances in mobile communication technology have enabled the access of patient video-audio information without the limitations of time or location. Mobile technology can offer continuous, uninterrupted, and instant service to ultrasound application domain. However, the current bandwidth of the mobile network is not sufficient to transfer patient video data requiring high throughput. Besides the bandwidth of the mobile network, the high error rates due to multipath fading should be taken into consideration to sustain, video transmission in mobile transmission systems [1].

MPEG-4 has been successfully applied to many types of mobile applications [2]. Some pioneering telemedicine applications of MPEG-4 can give insight into the compression efficiency for patient video streaming over the limited bandwidth of the mobile network [3,4]. However, the error resilient tools of the MPEG-4 standard, which are important for error-prone mobile applications, have rarely been researched, particularly for use in mobile transmission applications. In addition to compression, an efficient data transmission protocol should also be considered for real-time video streaming. Between the two well-known network protocols, TCP(Transmission Control Protocol) and UDP(User Datagram Protocol), UDP is much more suitable for real-time streaming because it uses simple datagrams with no congestion control [5]. Nevertheless, little research has been conducted to comprehensively validate the efficacy of the MPEG-4 error resilient tools in combination with the UDP protocol when applied to a mobile video-audio system.

**ERROR RESILIENCE IN MPEG-4**

MPEG-4 [2] provides error resilient tools to enable robust transmission of compressed ultrasound video over error-prone mobile networks, which are subject to Rayleigh fading and burst errors as a result of multipath propagation [6]. MPEG-4 employs four types of error resilient tools to enable resynchronization, error detection, data recovery, and error concealment: resynchronization markers (RMs), data partitioning (DP), reversible variable length coding (RVLC), and header extension code (HEC).

**EXPERIMENTATION**

**Data Transmission Format**

An MPEG-4 bit stream composed of a series of video packets is encapsulated into an IP datagram using the UDP protocol. As shown in (Fig. 1), an IP datagram consists of UDP data corresponding to the fragmented MPEG-4 bit stream data, 8 bytes of UDP header and 20 bytes of IP header. A total of 28

bytes of overhead is created by the attached headers [5]. Particularly, the UDP protocol drops the whole UDP datagram when corruption of the UDP datagram is detected by the checksum field within the UDP header.

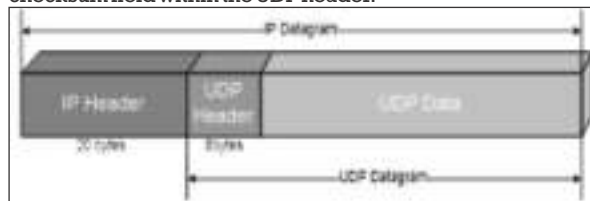


**Fig. 1.** Encapsulation Of A UDP Datagram Within An IP Packet

**Experimentation**

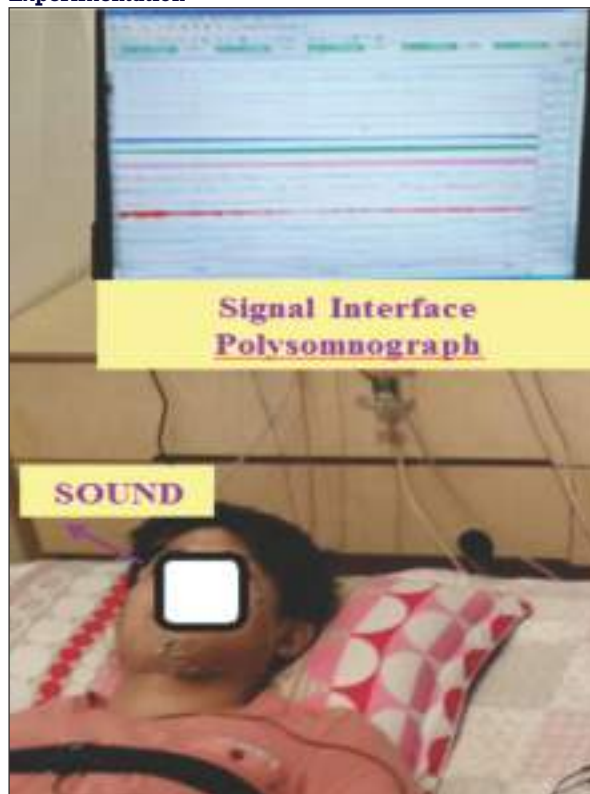


**Fig. 2.** A Typical Image Extracted From A Patient Video With Audio And Signals Interface For Experimentation

Measurements were taken for 7 days at the Seoul metropolitan area. As shown in (Fig. 2), 30 seconds of captured video-audio were repeatedly used for each measurement. The output bit rate of the MPEG-4 encoder (spatial resolution of 320x240, frame rate of 4 frames/sec, and key-frame period of 2 sec) was set to 80 Kbps, considering a measured mean bit rate of 100 kbps for the reverse link [7] and an MPEG-4 decoder buffer margin of 20 kbps for network jitter compensation. Because of the interrelation between the error resilient tools (for example, RVLC should only be used in conjunction with DP), and the header's relative importance compared to other streaming data, three different combinations of error resilient tools were considered, all utilizing HEC: RM only, RM with DP, and RM with both DP and RVLC. At the MPEG-4 decoder, an error concealment technique was employed before evaluating video quality. In particular, when the frame drop occurred due to a burst error, the dropped frame was replaced by the previous frame. The MPEG-4 simple profile with error resilient tools was implemented by mpegable Video SDK (Dicas Co., Germany) [8].

**RESULT**

In order to analyze the error effect of the wireless networks with respect to different IP datagram sizes (corresponding to UDP datagram sizes), the IP datagram size was varied between 200 and 5000 bytes. As shown in (Fig. 3), the DLR increased as IP datagram size increased, because UDP discards the entire datagram regardless of the amount of corruption when an error is detected within. As the size of the IP datagram increased, the percentage of UDP data increased relative to the headers (with a fixed size of 28 bytes), Thus, PSNR increased as the size of the IP datagrams increased.

When the compressed bit stream is not contaminated by error (before transmission) as shown in (Fig. 4a), the highest PSNR can be obtained without using any error resilient tools. Moreover, the PSNR decreases as more MPEG-4 error resilient tools are employed. (The use of headers is unavoidable if any error resilient tool is employed.) Thus, for fixed-size bits, the bits allocated for a patient video can be decreased if the bits allocated for headers are increased. Particularly, the abrupt change in PSNR for the case using RM with both DP and RVLC is due to fact that the prefix for RVLC requires additional space compared to RM and DP.

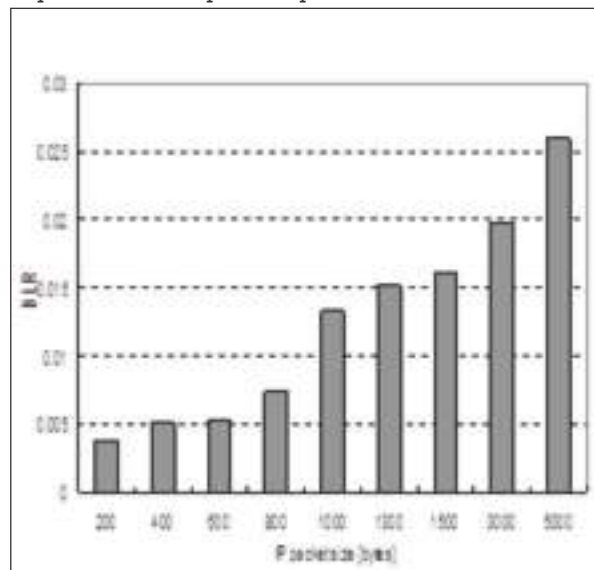


**Fig. 3.** Datagram Loss Rate(DLR) In Terms Of IP Datagram Size After Mobile Transmission

**CONCLUSION**

The selection of an appropriate error resilient video compression method might be a primary concern in designing a mobile video-audio transmission system running

over a mobile network with limited bandwidth. Among the many standard video compression methods available, MPEG-4 can be regarded as one of the most appropriate for compressing video data for transmission over a mobile network, because MPEG-4 offers high compression at a low bit rate and useful error-resilient tools [6]. In addition to the compression method, a transmission protocol, either TCP or UDP, should also be taken into consideration when transmitting a compressed bit stream over an IP-based mobile network [9]. For real-time video-audio transmission over an error-prone mobile network, the conditions required to select the transmission protocol are the capability for real-time streaming and tolerance to frame loss [10].

**REFERENCES:**

- [1] Sklar B. *Raleigh Fading Channels in Mobile Digital Communication Systems, Part I: Characterization.* IEEE Comm Magazine 1997;35:90-100.
- [2] Koenen R. *Overview of the MPEG-4 standard.* ISO/IEC JTC1/SC29/WG11 N4668.2002.
- [3] Brox GA, Huston JL. *The MPEG-4 standard and electronic reporting for mobile, multimedia patient records.* J Telemed Telecare 2002;8:115-117.
- [4] Nagatuma H. *Development of an emergency medical video multiplexing transport system: aiming at the nation wide prehospital care on ambulance.* J Med Sys 2003;27:133-140.
- [5] Stevens R. *TCP/IP illustrated volume 1: the protocols.* Addison Wesley, ISBN: 0201633469, Chapters 11, 17, 18, 19, 20, 21, 22 and 23. 1994;143-168 and 223-337.
- [6] Talluri R. *Error-Resilient Video Coding in the ISO MPEG-4 Standard.* IEEE Comm Magazine 1998;112-119.
- [7] Yoo SK, Jung SM, Kim BS, et al. *Prototype Design of Mobile Emergency Telemedicine System.* ICCSA 2005, LNCS 2005;3481:1028-1034.
- [8] Dicas Digital Image Coding GmbH. *Mpegable MPEG-4 Video SDK version 1.20.0(18.3.2005).* <http://www.mpegable.com>
- [9] Xylomenos G, Polyzos GC, Mähönen P and Saaranen M. *TCP Performance Issues over Wireless Links.* IEEE Comm Magazine 2001;39:52-58.
- [10] Montes H, Gomez G, and Cuny R, Paris JF. *employment of IP Multimedia Streaming Services In Third-Generation Mobile Networks.* IEEE Wireless Comm 2002;84-92.
- [11] Postel J. *User Datagram Protocol, STD 6. RFC 768 1980.*

# IOT BASED PREPAID ENERGY METER WITH DATA ACQUISITION USING GSM AND NODE MCU

Yandluri Mamatha<sup>1</sup>, Dr V Madhusudana Reddy<sup>2</sup>

<sup>1</sup>M.Tech Scholar, Department of EEE PBR VITS, Kavali

<sup>2</sup> Professor, Department of EEE PBR VITS, Kavali.

**Abstract**—The Internet of Things (IoTs) is important in the energy industry since it creates a smart metering and monitoring system. High attention to detail focuses on combining energy meter and control mechanisms, which necessitate smart equipment control, bidirectional communication, and networking as well as user interaction. Energy meters in India are mechanical and postpaid. The primary disadvantage of this method is that a person must travel from street to street, checking each house's energy meter and issuing charges. The payment was made, according to that reading. Even when bills are paid on time, problems such as over-billing or provider warnings are prevalent. To address this issue, we proposed an IoT-based prepaid power recharge unit that will integrate with standard household energy meters and be capable of counting down energy use and switching off the main power supply once the energy usage countdown reaches zero, as well as an IoT-based data collection system. The recharge information and energy consumption from the recharge station are recorded in a Data Acquisition server linked to the energy meters in order to manage the main power supply and monitor power consumption in real-time.

**Index Terms**— IOT, energy meter, prepaid, data acquisition

## I. INTRODUCTION

ENERGY is an essential factor for a country's economic development, as well as for increasing people's lifestyles on the globe. As the nation's population grew, so does the energy requirements. A smart device is an intelligent power meter that detects a public's energy use and sends additional information to the utility via a multiple effective communication [1,2]. The conventional manual meter reading method proved unsuitable for long-term operations since it consumes a lot of human and material resources. It causes extra issues when manually calculating readings and invoicing. The number of people who use energy is rapidly growing these days. It became difficult to manage and sustain electricity in response to the increasing demands [3]. The integration of automated systems via communication systems over a web has now become a demand. With the rise of technology, research on communication systems and home automation has gained significance and desirability [4]. An Intelligent Energy Meter is a device that detects energy usage at predetermined intervals and transmits that data to the utility for monitoring, administration, and invoicing [5]. The customer has a variety of issues as a result of post-paid connections. Prepaid electricity connections are frequently

proposed as a potential solution to this problem. In this prepaid electricity meter circuit, consumers will need to replenish the amount of energy they need to consume [6]. To enable this prepaid system to function, residential energy meters must be outfitted with a module capable of identifying the amount recharged by the user and tallying the amount recharged to zero based on power usage. When the meter count reaches zero, the main supply is immediately shut off, and it can only be turned back on after the next recharge.

The Arduino, a GSM board, and a node MCU were used to demonstrate this idea. Using an internet gateway, we can restore our energy balance. If the balance is low or zero, the power supply link to the dwelling is instantly disconnected. This device may also send energy consumption notifications from the meter to the substation at regular intervals through the node MCU module, as well as alerting users to low balance, cutoff, and other problems. The mechanism is set up such that at the end of every month, the gadget generates the unit cost and sends it to the smartphone application along with the billing. The web - based application that will be synced to same server as the energy device.

## II. MOTIVATION AND EXISTING WORK

Many nations have implemented the notion of prepaid admission. This concept is based on the premise of "pay first,



Fig. 1 Existing System

use later." The notion appeals to the consumer since there is no fear of disconnection and reconnection for any reason. Under the present invoicing approach, the Electricity Board is unable to keep track of user power usage (postpaid). Even if bills are paid on time, the client may encounter difficulties such as getting late bills for payments already made, as well as insufficient electricity supply and quality. Energy metering or smart meters are electronic device that can detect and show energy consumption in the form of readings. Traditional meters have been widely used since the late 1800s. These electrical metering may be configured to facilitate information interchange among electronic devices in an electricity network and may be engaged in both the manufacture and supply of power [7]. To calculate energy usage, most conventional electric meters employ a revolving disk composed of copper or aluminum connected to a clock mechanism through a gear mechanism and a display. Because energy is measured using a mechanical construction, conventional meters are also known as electromechanical meters [8]. Electricity meters are now digitally operated, although they still have significant restrictions. Many nations, particularly those in Europe, have begun extensive implementation of digital, smart energy meters [9].

Energy distribution and maintenance are the responsibility of the local state electrical board. The amount of KWH consumed over the course of a month is multiplied to calculate a user's power usage (Fig. 1). This reading is kept locally on the meter. This reading is taken manually by a power board person who visits door to door. This data is then sent to the head electrical board for review, and an evaluation bill is generated based on the monthly measurements. Customers then pay their costs using their selected mode of payment. This procedure takes a long time and a lot of human labor, and the cost is totally reliant on the readings of the employees. So, whatever reading a staff records for a client, the consumer

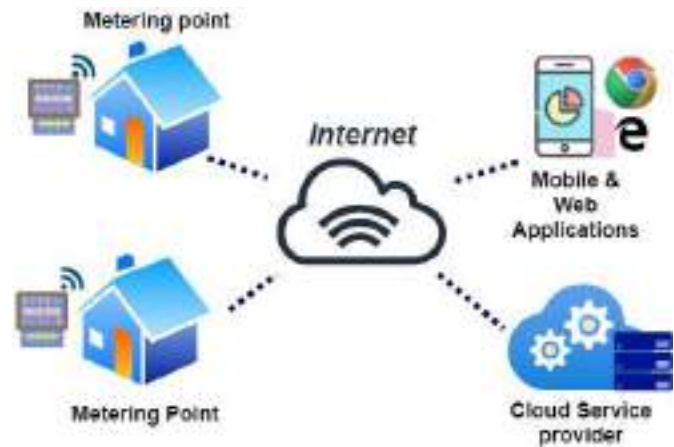


Fig. 2 Proposed Frame Work

must pay for it, and because post-paid power payment is used, many consumers use electricity inefficiently and sometimes do not pay for months.

### III. PROPOSED SYSTEM

The suggested solution is an IoT-enabled prepaid energy meter. This suggested meter assists in the tracking of energy consumption and the automatic computation of bills using a controller. This data is saved on the server and sent to the customer via the GSM module application. The node MCU module is used to send the data to the server (Fig. 2). Customers may utilize the built-in user interface to keep track of their power use.

### IV. IMPLEMENTATION

#### A. Hardware Requirements:

- Arduino Mega controller board
- Liquid crystal display
- GSM Modem
- Node MCU
- Energy Meter
- LED
- 5v Relay
- Lamp

#### B. Software Requirements

- Arduino software
- Embedded c programming
- HTML
- PHP



### C. Block Diagram

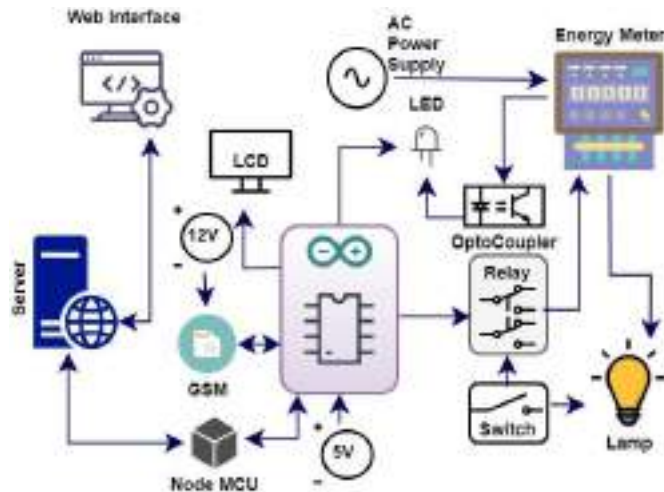


Fig. 3 Block diagram of proposed system

## V. COMPONENT DESCRIPTION

### A. Arduino Mega:

This board has 54 digital I/O pins (14 of which may be used as PWM outputs), 16 analog inputs, 4 UARTs (hardware serial ports), a 16 MHz crystal oscillator, a USB connection, a power connector, an ICSP header, and a reset button. It comes with everything you need to get started with the microcontroller, such as a USB cable to connect it to a computer and an AC-to-DC converter or battery to power it.

### B. LCD Display:

- 16\*2 LCD with green colour Backlight
- works on 5V DC supply
- 2 Rows and 16 Characters Per Row
- Displays two lines of 16 characters High contrast and a wide viewing angle

### C. GSM MODEM:

GSM is an abbreviation for a mobile communication modem. It is mostly used for data transfer in mobile communication all over the world. A GSM modem is a type of modem that, like our cellphone, accepts a SIM card and operates by registering with a mobile carrier. GSM modems work in full duplex mode for sending and receiving SMS. It is an open cellular technology that allows mobile phone and data services to be communicated over the 850MHz, 900MHz, 1800MHz, and 1900MHz frequency bands.

### D. Node MCU Module:

NodeMCU is an open-source Lua-based Internet of Things (IoT) firmware and development board. It includes software for Espressif Systems' ESP8266 Wi-Fi SoC as well as hardware for the ESP12 board. Because it is simple to use, the Arduino IDE can easily program the NodeMCU development Board. The Arduino IDE will just take 5-10 minutes to program the Node MCU. We only need the Arduino IDE, a USB cable, and the NodeMCU board.

### E. Energy Meter:

When a load is applied to this meter, a pulse LED blinks. If this LED blinks 3200 times, 1 KWH has been used. The metre constant is used to determine the accuracy of a metre during manufacture based on its class.

### F. Relay Module:

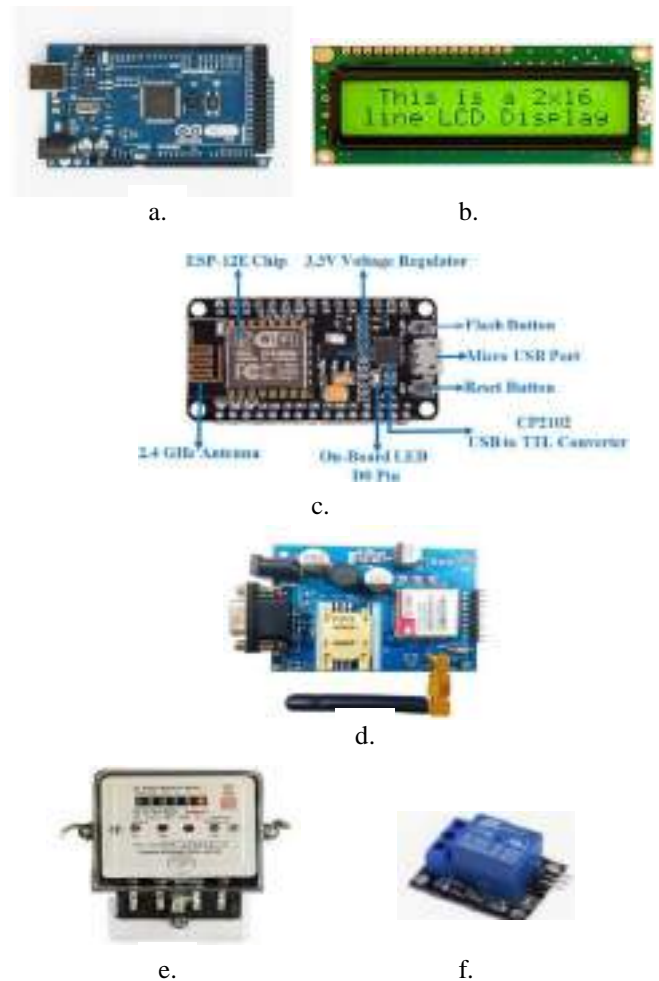


Fig. 4 a) Arduino Mega, b) LCD, c) Node MCU, d) GSM Module, e) Energy Meter and f) Relay

A relay is a switch that is activated by electricity. The unit consists of input terminals for single or multiple controllers, as well as a set of functional touch terminals. You can discover any number of connections of any type on the switch, including create contacts, divide contacts, and combinations of the two.

## VI. RESULTS AND DISCUSSIONS

### A. Algorithm:

- In order to use this technique, users must first replenish the amount of power they intend to consume by SMS.
- The recharged quantity and units are displayed on the LCD in the Consumer's system.
- The electricity meter has a mechanism that recognizes the amount refilled by the user and then counts down from the recharged amount to zero depending on the electricity usage and sends the information to a server.
- When the meter reading approaches 0, the connection to the main supply is automatically removed and will be restarted when the next recharge is completed.

### B. Calculation of Pulses and Units:

Before we begin our calculations, we must first establish the pulse frequency of the energy meter. The first is 1600 imp/kwh, while the second is 3200 imp/kwh. In this example, we're going to use a 3200 imp/kwh pulse rate energy meter. To begin, we must calculate the Pulses for 100 watts, which is the number of times the Pulse LED would blink in a minute for a 100 watt load.

$$Pulse = \frac{(Pulse\_rate * watt * time)}{(1000 * 3600)} \dots \dots \dots (1)$$

The following may be computed using the equation. 1 using a 3200 imp/kwh rate and a 60-second pulse bulb for a 100-watt bulb:

$$Pulses = \frac{3200 * 100 * 60}{1000 * 3600}$$

$$Pulses = \sim 5.33 \text{ pulse / minute}$$

The single pulse Power factor is now computed as follows:

$$Power\ Factor = \frac{watt}{(hour * Pulse)} = \frac{100}{60 * 5.33} = 0.3125 \frac{watt}{one\ pulse}$$

$$Units = \frac{Power\ Factor * Total\ pulse}{1000}$$

$$No\ of\ pulses\ in\ one\ hour = 5.33 * 60 = 320$$

$$\therefore Units = \frac{0.3125 * 320}{1000} = \frac{0.1}{hour}$$

Let's say a 100-watt bulb is used for a day's worth of



a.



b.



f.

Fig. 5 a) The proposed prepaid energy meter system, b) showing SMS received when recharged is done, c) showing SMS alert received from prepaid meter when balance is low, d) showing connection cut SMS alert received from prepaid energy meter, e) Logging in to Data Acquisition Page and f) showing Data Acquisition Page

lighting then,

$$\text{No of Units} = 0.1 * 24 = 2.4 \text{ Units}$$

And let us assume unit rate at our area is 5 rupees per unit then the amount that we have to pay for 2.4 Units is,

$$\text{Rs: Rupees} = 2.4 * 5 = 12 \text{ rupees}$$

### C. Results

The diagram depicts an overview of the proposed project's hardware, which includes the Arduino mega, GSM modem, LCD display, Node MCU, relay, and variable load. When the load is first connected to the prepaid energy meter, it consumes energy. The balance decreases as the load consumes. When the user's balance reaches a particular amount, he or she receives an SMS notification. The user will receive a confirmation message when the power board has completed the recharge procedure, which will also indicate the current balance. The user will benefit from the notification messages, and the user will immediately take the appropriate actions, avoiding the power from being turned off and reducing energy consumption.

Using IoT, data is logged in real time every 15 seconds and saved on a server. As a result, the user may check his power usage and recharge statistics at any time via the web interface. There is no need to manually monitor power use by glancing at a meter. If each meter's real-time power consumption data is accessible, it may be utilized for power consumption analysis. Because it is wireless and simple to set up, we can install it anywhere, including a business, residential, or municipal facility. We may also implement a public energy supply system, which reduces energy waste by using just the necessary energy on a regular basis. It is highly accurate with public power sources since the entire idea of reading the units and then invoicing manually or by any other means is eliminated.

### VII. CONCLUSION

Customers may pay for power before it is consumed with the planned prepaid energy meter, which is based on the Internet of Things. It minimizes the amount of time that humans spend reading meters and calculating bills. Consumers keep credit under control and then use electricity until the credit is gone. When the available credit is spent, a relay automatically turns off the power. When a user's credit goes below a specific threshold, GSM communication is used to alert them. Finally, this method resolves many of the difficulties associated with the post-payment billing system. Billing is also automated using this system.

### REFERENCES

- [1]. Arif, Anmar, et al. "Experimental study and design of smart energy meter for the smart grid." 2013 International Renewable and Sustainable Energy Conference (IRSEC). IEEE, 2013.
- [2]. Karthick, T. and Chandrasekaran, K., 2021. Design of IoT based smart compact energy meter for monitoring and controlling the usage of energy and power quality issues with demand side management for a commercial building. *Sustainable Energy, Grids and Networks*, 26, p.100454.
- [3]. Preethi, V. and Harish, G., 2016, August. Design and implementation of smart energy meter. In 2016 International Conference on Inventive Computation Technologies (ICICT) (Vol. 1, pp. 1-5). IEEE.
- [4]. Rahman, M.M., Islam, M.O. and Salakin, M.S., 2015, May. Arduino and GSM based smart energy meter for advanced metering and billing system. In 2015 International Conference on Electrical Engineering and Information Communication Technology (ICEEICT) (pp. 1-6). IEEE.
- [5]. Das, H. and Saikia, L.C., 2015, June. GSM enabled smart energy meter and automation of home appliances. In 2015 International Conference on Energy, Power and Environment: Towards Sustainable Growth (ICEPE) (pp. 1-5). IEEE.
- [6]. Rupesh, M. and Selvan, N.A., 2021, July. Design of IoT Based Smart Energy Meter for Home Appliances. In *Journal of Physics: Conference Series* (Vol. 1964, No. 5, p. 052001). IOP Publishing.
- [7]. Muralidhara, S., Hegde, N. and Rekha, P.M., 2020. An internet of things-based smart energy meter for monitoring device-level consumption of energy. *Computers & Electrical Engineering*, 87, p.106772.
- [8]. Khan, J.A. and Nagaraj, M.S., 2017. Research advancements towards in existing smart metering over smart grid.
- [9]. Regassa, B., Medina, A.V., Gómez, I.M., Rivera, O. and Gómez, J.A., 2011, March. Upgrading of traditional electric meter into wireless electric meter using ZigBee technology. In *International Conference on IT Revolutions* (pp. 84-94). Springer, Berlin, Heidelberg.



## An Advanced Filter Topology and Effects for compensating common Mode Voltage in Vehicular Induction Motor Drives

A. Bhakthavachala<sup>1</sup>, K. Anuradha<sup>2</sup> S. Tara kalyani<sup>3</sup>

Research Scholar & Associate prof., EEE, PBR VITS, Kavali, India <sup>1</sup>

Professor & Head, EEE, VNR VJIT, Hyderabad, India <sup>3</sup>

Professor & Head, EEE, JNTU, Hyderabad, India <sup>2</sup>

**Abstract:** Recently the utilization of electric vehicle technology increasing drastically, because of environmental changes arises throughout the globe. Based on these issues, this paper focuses on the drive used in the electric vehicle with more economically. In general electric vehicles the induction motor drives are used, because they have great features, such as high starting torque and high efficiency. The motor drive is driven by the high switching frequency PWM inverter supplied by a dc source or supply, because of this switching frequency common mode (CM) voltage generated at the input of stator motor terminals, creating a shaft voltage through the motor air gap with possible rise in bearing current, leading to premature damage to the motor reliability and lifetime. To compensate this problem an advanced active filter is designed, which will suppress the common mode voltage. And also analyze the impact of electromagnetic interference (EMI) on drive under the test (DUT). The above system will initial executed in the electrical software tools like MATLAB/SIMULATION for confirmation of the results, suitable for electric vehicle applications, especially for induction motor drives.

**Keywords:** Common mode (CM) voltage, Shunt active filter, Electromagnetic Interference (EMI), Induction Motor drive.

**Acknowledgement:** This proposed work has been funded by the University Grants Commission from Government of India (Proposal No.F MRP-4556/14(SERO/UGC))

### I. INTRODUCTION

In the present applications of electrical vehicles, high quality output is achieved through the pulse width modulation (PWM) IGBT switches. It creates high switching frequency at the inverter output terminals and generates common-mode voltages at drive input side. This common mode voltage produces shaft voltage therefore produces bearing currents through stray capacitances. Amplitude of the shaft voltage and bearing current influence the electromagnetic interference (EMI) problems. It also leads to severe damage to the insulation of the motor i.e. life time and reliability of the motor [1].

Several literatures exhibit that the suppression of the common mode voltage in the induction motor drive fed by high voltage dc supply [2-4]. They have proposed the common mode active filters to mitigate the common mode voltage at the input motor terminals. Two kinds of methodologies are proposed to synthesis the common mode voltage, one of them is the passive circuitry [5], it consists of simply resistors, inductors, capacitors and common mode chokes. The values of those parameters are depending on the length of the cable from inverter and motor [6]. The second methodology is used to mitigate the common mode voltage on the inverter fed induction motor drive with an active circuitry. This is the one of the most effective processes used in the industrial drives in the last five years. Generally, it eliminates the mirror image of common mode voltage, i.e. shaft voltage and the bearing currents [7-10]. This active circuit canceller contains different parts for detection and reinjection of the voltage in the line, this detection circuit consisting of star connected capacitors, Darlington pair of transistors, a four winding transformer and additional dc power supply. This circuit focuses on the common mode voltage detection at the inverter output, transfer of the common mode voltage by a voltage follower amplifier to a common mode transformer and reinjection of the compensated voltage through CMT [11-15].

In this paper, a dc power supply of 575V is derived from an ac power supply for reduction of the cost. This is proposed for the suppression of common mode voltage and thereby shaft voltage and bearing currents will be reduced. The proposed methodology is simulated using MATLAB and executed experimentally further.

A high frequency model induction motor is used throughout the simulation. According to the CISPR model, a dedicated 600V high voltage dual-LISN [16-17] is designed and built for the simulation, Also concentrated on the active common mode voltage canceller (ACMVC) for compensating the common mode voltage. The present literature represents that the emitter follower realized by transistors (at present, bipolar p-n-p transistors with more than 400V are not available) instead of MOS-FET transistors

are implemented in this investigation. The proposed methodologies are supposed to be implemented in electric vehicles, hybrid electric vehicles, plug-in hybrid electric vehicles and fuel-cell vehicles that improves the overall system reliability and also reduces the cost and size.

This paper is organized in different sections, introduction of the work is presented in section I. In section II, the design considerations of the high voltage dual channel Line impedance stabilization network (LISN), standards for comparison of results with the CISPR, circuit configurations, mathematical design features are explained. Section III describes design considerations for high frequency induction motor model to make it suitable for measurement of common mode ground currents, and its equivalent circuits with values. In section IV, design features for the common mode voltage active canceller (CMVAC), its circuit configurations, and CMT are described. Section V describes the results obtained in simulation. The outcomes of the work are concluded in section VI.

**II. LINE IMPEDANCE STABILIZATION NETWORK DESIGN CHARACTERISTICS**

The Line impedance stabilization network is a low pass filter placed between AC or DC power source and the equipment under test (EUT) to create known impedance as per complying standard for the measurement of conducted emission. This provides a Radio frequency (RF) noise measurement port. It also isolates the unwanted RF signals from the power source when pre-filter is included. Specifications of The LISN are presented in Table 1.

The LISN is generally used in the repeatable and accurate measurements of the conducted emissions generated by the high switching frequency inverters. Two identical LISNs are placed in the same metal structure (line and neutral). As per the standards of CISPR, the values of the line and neutral LISNs are inductance (L) of 5µH, capacitor (c1) with 1µF on the mains side. A 50Ω resistance, output measuring instrument, and coupling capacitor c of 0.1µF are placed on the drive under test side (DUT). [19-20],

The Figure 1 shows the circuit model of the high voltage dual channel LISN, which is built on dedicated earthing. More or less each of LISN must meet the standard impedance curve defined by CISPR16-1[20-21] as shown in Figures 2-4. And also the ideal impedance curve and measured impedance curves at the line and neutral are represented in Figure 2, Figure 3, and Figure.4. These curves are measured by Rohde and Schwarz vector network analyzer ZVRE.

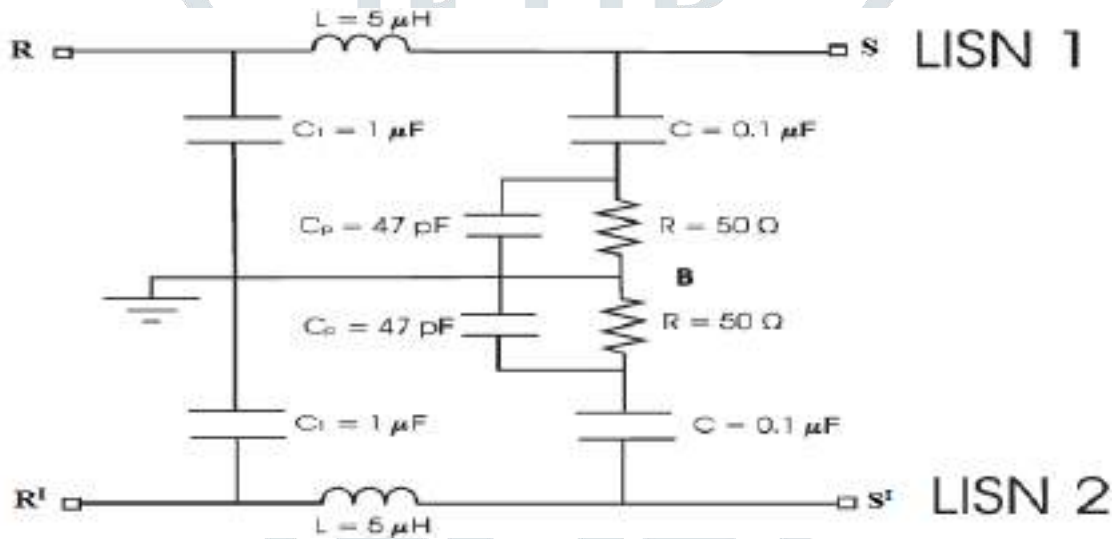


Fig: Circuit model of high voltage dual Line Impedance Stabilization Network

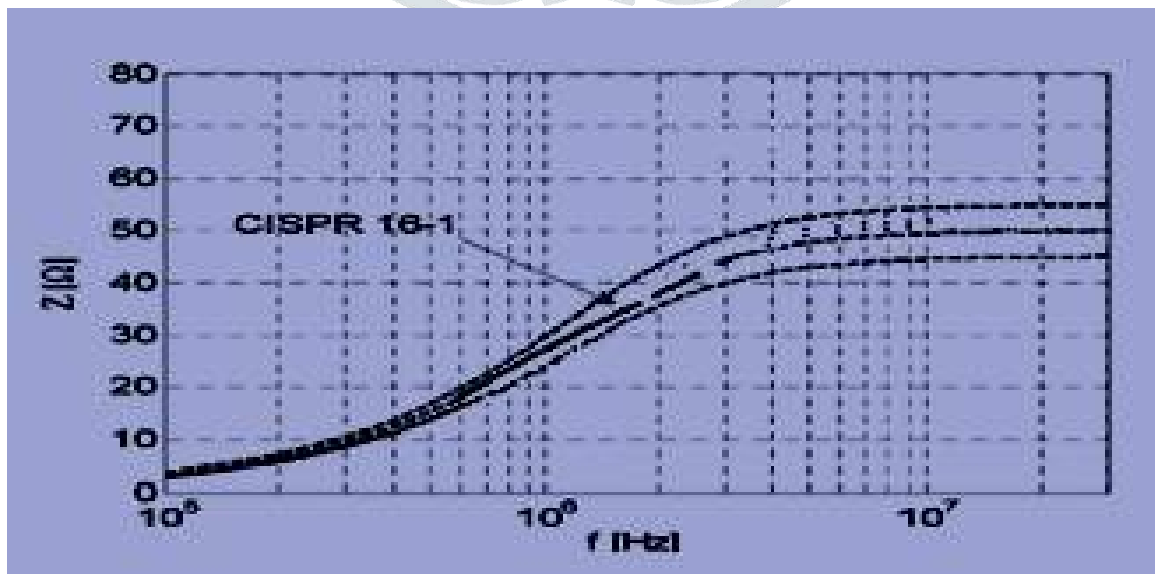


Fig2: Ideal impedance curve of the LISIN as for CISPR16-1

Table 1: specifications of LISN

Topic	Performance Specifications
Frequency	9 KHz – 30 MHz
AMN Impedance	(50 mH + 5 Ω)   50 Ω
Maximum current	AC / DC 16A
Standard	CISPR 16-1-2
Maximum voltages	AC:250V, 50/60Hz, DC:600V DC
RF Output	50Ω to connect RF output to EMI receiver
EUT Terminal	Output: 3 pin standard socket

### III. HIGH FREQUENCY INDUCTION MOTOR MODEL

As a matter of fact, AC drives are more popular because of developments in power electronics in the electrical drives, reduced cost and other maintenance problems. In most of the cases, squirrel cage induction motors are used to avoid inertia and also for easy control of stator in vehicle applications. In this work, 3-Φ, induction motor with rated values of voltage: 415V (±10V), frequency: 50Hz (±5Hz) current: 2.5A, is used for smooth execution.

Similarly for carryout the simulation work the high frequency model of induction motor are designed, which is considered in the literature [1], [18] and several HF models are discussed in [22]. In general common mode currents are measured at the high frequencies only, that's why representation of motor model in high frequency circuit as not at all a problem. High frequency model of an induction motor with simulation values (MATLAB) as shown in fig.5.

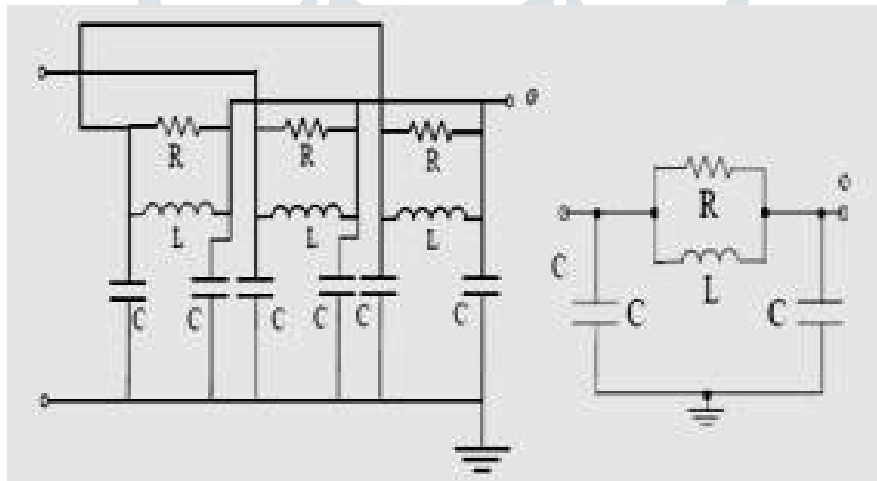


Fig3: High frequency circuit of the induction motor single winding

So many literatures give different values for the motor winding parameters, such as stray capacitances, winding inductances and resistances. Out of all M.C. Di Piazza. Et. al [23] represents more accurate values and she was inspiration for me to motivate towards electric vehicle research area. Those values as given below

Parameter	Value
R	640 Ω
L	1.60 mH
C	899 pF

Table2: Induction motor per phase winding parameters

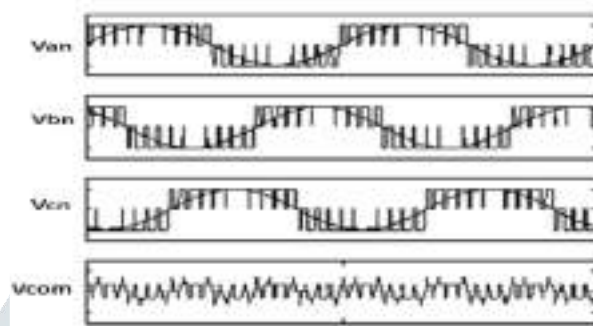
#### IV. DESIGN OF CMV ACTIVE CANCELLER CIRCUIT

##### I. Common mode voltage

An average voltage available at neutral point with respect to ground is called as common mode voltage or a voltage that appears in common at both input terminals of a device with respect to the output reference usually ground. Mathematically represents

$$V_m = \frac{[V_{an}+V_{bn}+V_{cn}]}{3} \quad (1)$$

In the above equation  $V_{an}$ ,  $V_{bn}$  and  $V_{cn}$  are the phase voltages generated by the PWM inverter. The waveform of common mode voltage is schematically shown on Figure below. The common mode voltage can be measured between star point of stator winding of an induction motor and the ground.



Generally the common mode analysis without long cable is considered [24], the terminal voltages at the motor would be same as at the inverter output. Therefore common mode voltage

$$V_{cm} = \frac{V_a+V_b+V_c}{3} \quad (2)$$

$$\text{Where } V_a = V_{a,o} + V_{o,n} \quad (3)$$

$$V_b = V_{b,o} + V_{o,n} \quad (4)$$

$$V_c = V_{c,o} + V_{o,n} \quad (5)$$

Substituting equations (3)-(5) in equation (2), we have

$$V_{cm} = \frac{V_{a,o}+V_{b,o}+V_{c,o}}{3} + V_{o,n} \quad (6)$$

Summation of inverter output voltage

$$V_{cm} = \pm \frac{V_d}{6} + (V_{o,n}) \quad (7)$$

In this project the length of the cable is very small, that's why not considering any calculations regarding with cable. The effects of common mode voltage on induction motor fed by high switching frequency PWM inverter was more severe. This common mode voltage is the major reason to create a shaft voltage, and resulting bearing currents are produced in the system. Therefore premature damage to the both life time as well as the reliability of the motor. To protect the drive from these abnormalities common mode voltage active cancellers are implemented in early stages to protect the motor.

##### II. Common mode voltage active canceller

As matter of fact, the common mode voltage was the major reason for shaft voltage. Therefore to neutralize this common mode voltage, an active voltage canceller was designed. This is used mainly to remove the common mode voltage. It works in the following steps; initially it detects the common mode voltage from the output of the inverter by three star connected capacitors, and transferred through the push-pull emitter follower in Darlington configuration and reproduced at the primary of the Common mode transformer.

The Design details of the common mode voltage active canceller (CMVAC) as shown in Fig.6. it consisting of star connected capacitors,  $C$  reasonable 0 to 10nF are preferable and  $C^1$ , which is three times of  $C$ , DC voltage source and finally the common mode transformer.

According to the [2], the schematic of a feedback voltage-sensing voltage-compensating active filter shown in fig.4, the common mode voltage active filter works

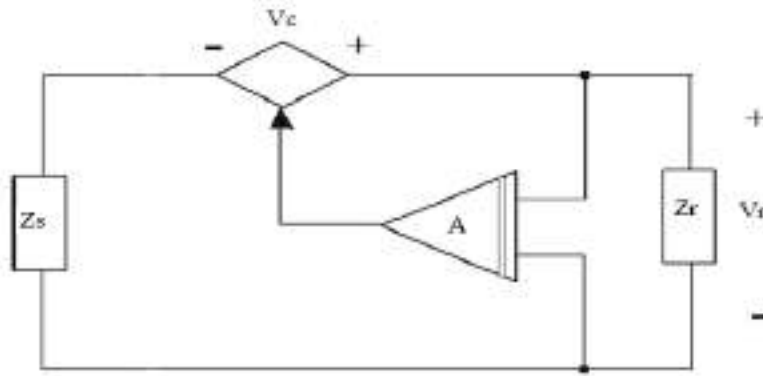


Fig 4: Voltage sensing and voltage compensation

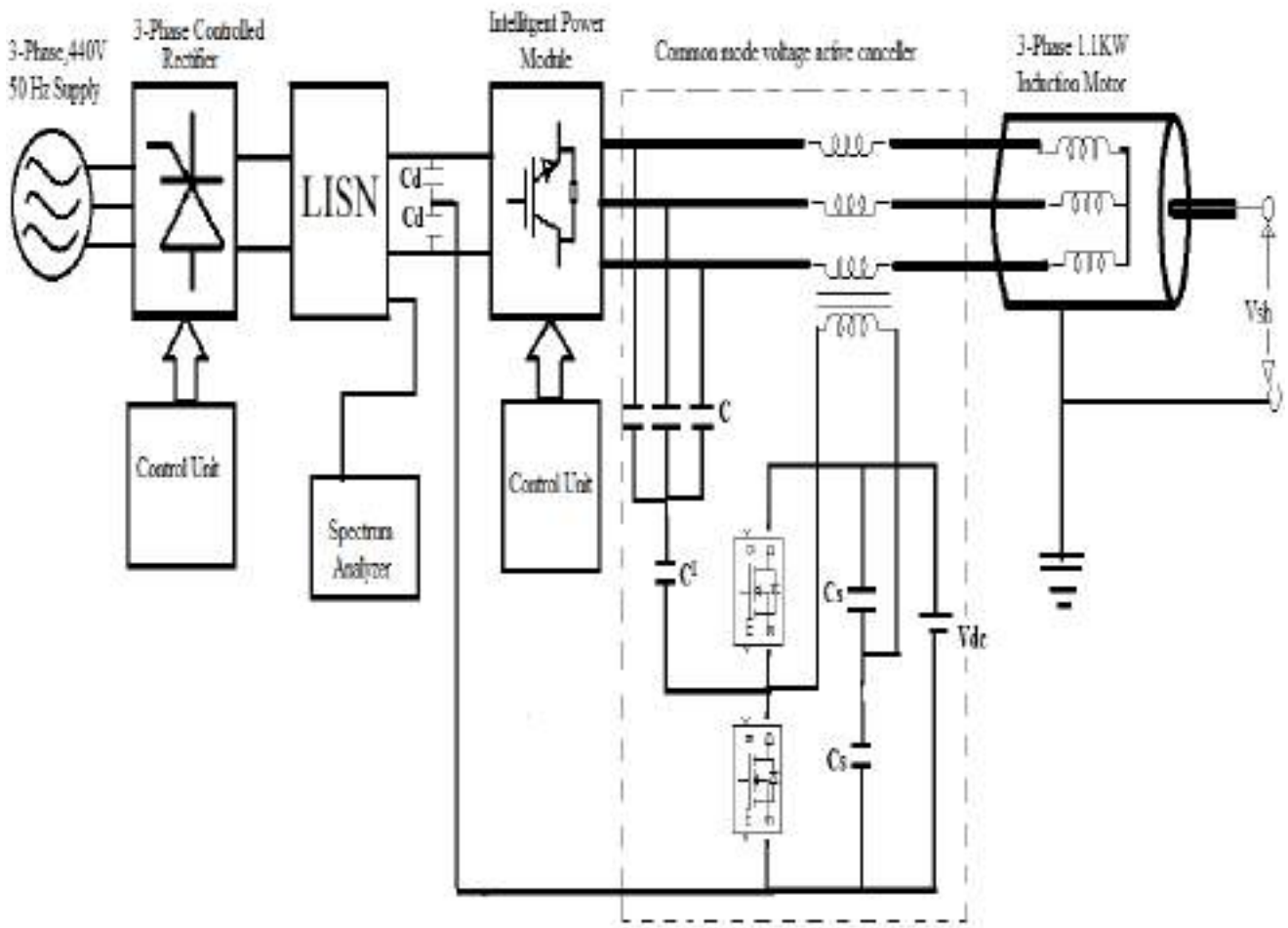


Fig5: An over view of the proposed configuration with common mode voltage active canceller

## V. SIMULATION RESULTS

### I. Simulated results without filter

For the proposed system in Fig.5 was simulated for both the cases such as without and with active common mode voltage canceller circuits in the MATLAB/SIMULINK as shown in figures. All the results are proposed for without and with filter circuits as shown.





Fig:6 Three phase source voltages

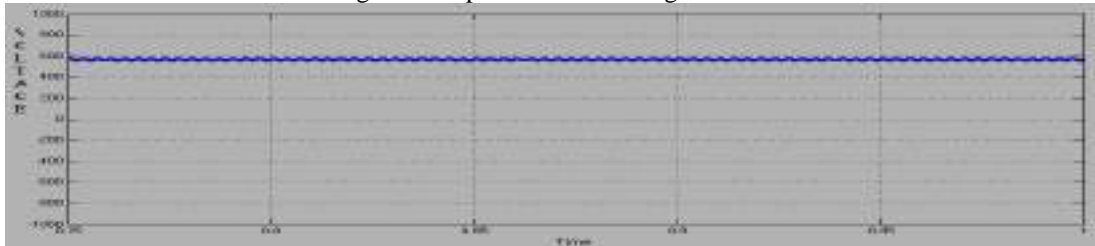


Fig7: 3-phase controlled rectifier output voltage

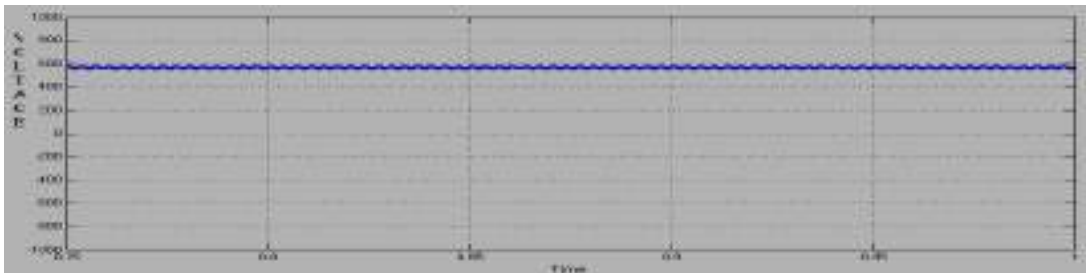


Fig 8: Output of the Line impedance stabilization network

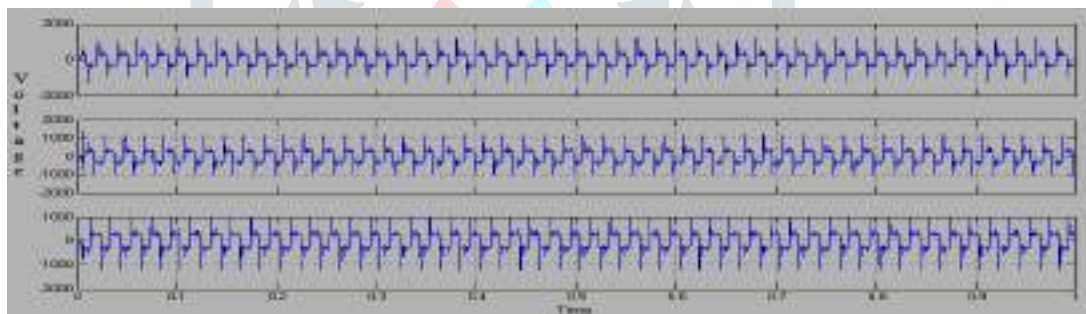


Fig 9: Inverter output voltages of the 3-phases

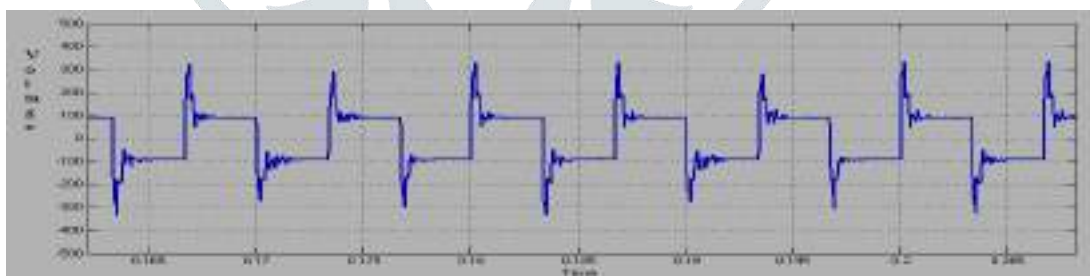


Fig10: Common mode voltage without filter

## II. Simulated results with filter

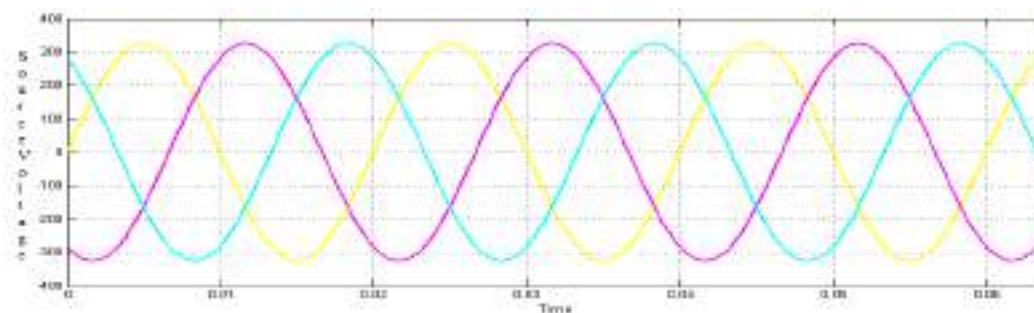


Fig:11 Three phase source voltages

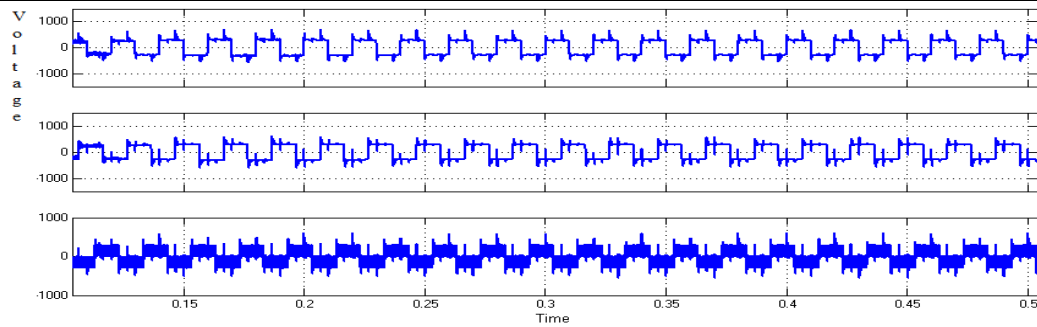


Fig 12: Inverter output voltages of the 3-phases

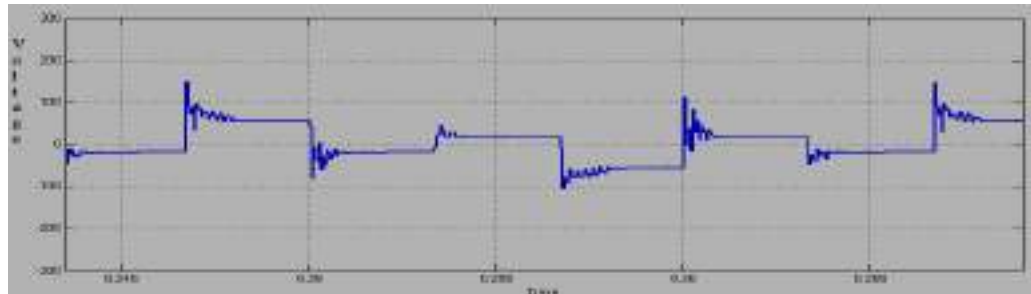


Fig13: Common mode voltage with filter

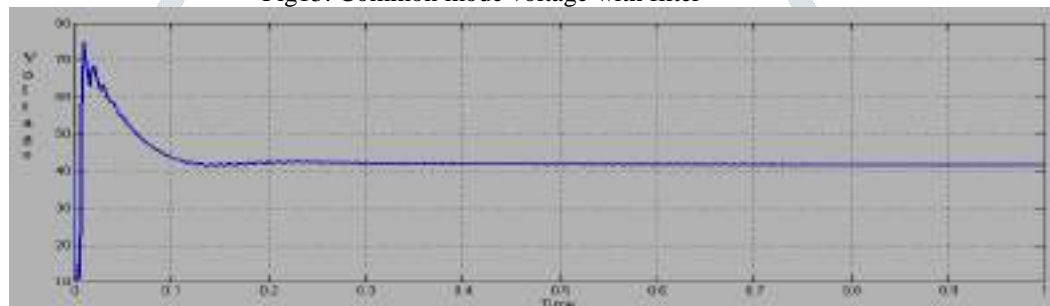


Fig14: Common mode running RMS voltage

## VI. CONCLUSION

In this paper, a common mode voltage active canceller (CMVAC) has been developed, which is capable of neutralizing a common-mode voltage generated by high switching frequency PWM inverter. The common mode emissions towards the DC power supply mains are also tested by employing a high voltage dual channel dc LISN designed and build for the simulation purpose. This configuration has been simulated, therefore all the results such as common mode voltage, shaft voltages, common mode EMI those are suppressed satisfactorily. Future scope of the work will execute the prototype common mode voltage active canceller (CMVAC) construction and verify for a 1.1 kW 3- $\Phi$  induction motor drive using high switching frequency IGBT inverter.

## REFERENCES

- [1] A. Carrubba, M. C. Di Piazza, G. Tine, and G. Vitale, "Evaluation of common mode disturbance mitigation devices in AC motor drives through HF modeling," in Proc. IEEE ISIE, Jul. 9–13, 2006, pp. 2315–2320.
- [2] M. C. Di Piazza, M. Luna, and G. Vitale, "EMI Reduction in DC-Fed Electric Drives by Active Common-Mode Compensator" IEEE Trans. Electromagnetic Compatibility., vol. 56, no. 5, pp. 1067–1076, Oct. 2014.
- [3] K. Mainali and R. Oruganti, "Conducted EMI mitigation techniques for switch-mode power converters: A survey," IEEE Trans. Power Electron., vol. 25, no. 9, pp. 2344–2356, Sep. 2010.
- [4] S. Wang, Y. Y. Maillat, F. Wang, D. Boroyevich, and R. Burgos, "Investigation of hybrid EMI filters for common-mode EMI suppression in a motor drive system," IEEE Trans. Power Electron., vol. 25, no. 4, pp. 1034–1045, Apr. 2010.
- [5] M. C. Di Piazza, G. Tine, and G. Vitale, "An improved active common-mode voltage compensation device for induction motor drives," IEEE Trans. Ind. Electron. vol. 55, no. 4, pp. 1823–1834, Apr. 2008.
- [6] D. A. Rendusara and P. N. Enjeti, "An improved inverter output filter configuration reduces common and differential modes dv/dt at the motor terminals in PWM drive systems," IEEE Trans. Power Electron. vol. 13, no. 6, pp. 1135–1143, Nov. 1998.
- [7] Y.-C. Son and S. K. Sul, "Generalization of active filters for EMI reduction and harmonic compensation," IEEE Trans. Ind. Appl., vol. 42, no. 2, pp. 545–551, Mar./Apr. 2006.
- [8] K. Mainali and R. Oruganti, "Conducted EMI mitigation techniques for switch-mode power converters: A survey," IEEE Trans. Power Electron., vol. 25, no. 9, pp. 2344–2356, Sep. 2010.
- [9] W. Chen, W. Zhang, X. Yang, Z. Sheng, and Z. Wang, "An experimental study of common and differential mode active EMI filter compensation characteristics," IEEE Trans. Electrom. Compat., vol. 51, no. 3, pp. 683–691, Aug. 2009.
- [10] N. Mutoh, M. Nakanishi, M. Kanesaki, and J. Nakashima, "EMI noise control methods suitable for electrical vehicles drive systems," IEEE Trans. Electromagn. Compat., vol. 47, no. 4, pp. 930–937, Nov. 2005.
- [11] Y. Maillat, L. Rixin, S. Wang, F. Wang, R. Burgos, and D. Boroyevich, "High-density EMI filter design for DC-fed motor drives," IEEE Trans. Power Electron., vol. 25, no. 5, pp. 1163–1172, May 2010.
- [12] Y.-C. Son and S. K. Sul, "A new active common-mode EMI filter for PWM inverter," IEEE Trans. Power Electron., vol. 18, no. 6, pp. 1309–1314, Nov. 2003.
- [13] S. Ogasawara and H. Akagi, "Circuit configurations and performance of the active common-mode noise canceller for reduction of common-mode voltage generated by voltage-source PWM inverters," in Proc. IEEE Ind. Appl. Conf., Oct. 8–12, 2000, vol. 3, pp. 1482–1488.

- [14] V. Serrao, A. Lidozzi, and A. Di Napoli, "EMI filters architectures for power electronics in hybrid vehicles," in Proc. Power Electron. Spec.Conf., Jun. 15–19, 2008, pp. 3098–3103.
- [15] N. Mutoh and M. Kanesaki, "A suitable method for ecovehicles to control surge voltage at motor terminals connected to PWM inverters and to control induced EMI noise," IEEE. Veh. Technol., vol. 57, no. 4, pp. 2089–2098, Jul. 2008.
- [16] Nelson, J. J., Goodwin W., Steffka, M., Ivan, W., Kopp, M., "High voltage automotive EMC component measurements using an artificial network", in Proceed. 18th Int. Zurich Symposium on EMC, 24-28 Sept. 2007 pp:195 - 200.
- [17] Sakulhirirak, D., Tarateeraseth, V., Khan-ngern, W., Yoothnom, N., "Design of high performance and low cost line impedance stabilization network for university power electronics and EMC laboratories", 7<sup>th</sup> International Conference on Power Electronics and Drive Systems, PEDS 2007, 27-30 Nov. 2007, pp.: 284 - 289.
- [18] M. C. Di Piazza, A. Ragusa, and G. Vitale, "Common mode EMI propagation in high voltage DC supplied induction motor drives for electric vehicles application," in Proc. IEEE IEMDC, May 3–6, 2009, pp. 647–652.
- [19] IEC CISPR 25 - Radio disturbance characteristics for the protection of receivers used on board vehicles, boats, and on devices – Limits and methods of measurement, 2008.
- [20] IEC CISPR 16-1-1 - Specification for radio disturbance and immunity measuring apparatus and methods - Part 1-1: Radio disturbance and immunity measuring apparatus - Measuring apparatus, 2006.
- [21] M. C. Di Piazza, A. Ragusa, and G. Vitale, "Effects of common mode active filtering in induction motor drives for electric vehicles," IEEE Trans. Veh. Technol., vol. 59, no. 6, pp. 2664–2673, Jul. 2010.
- [22] Boglietti, A., Cavagnino, A., Lazzari, M., "Experimental High Frequency Parameter Identification of AC Electrical Motors", 2005 IEEE International Conference on Electric Machines and Drives, 15-18 May 2005, pp.:5 – 10.
- [23] M. C. Di Piazza, M. Luna, A. Ragusa, G. Vitale, "An Improved Common Mode Active Filter for EMI Reduction in Vehicular Motor Drives", IEEE Vehicle Power and Propulsion Conference (VPPC 2011), Chicago IL, USA, September 6-9, 2011, pp. 1-8.
- [24] Sharana reddy, B. Basavaraja, "Simulation and analysis of common mode voltage in 2- Level and multilevel inverter fed induction drive with long cable" IJEAT, ISSN: 2249- 8958, volume-2, Dec.2012.



**A. Bhaktha vachala** received the B.Tech. degree from PBR VITS in the year 2003 and M.Tech. degree from the JNTU, Hyderabad, India. Also Pursing Ph.D. degree from Jawaharlal Nehru Technological University, Hyderabad. He is working in the area of Electric vehicle applications in transportation systems from last four years. He has been with the Department of Electrical and Electronics Engineering, PBR visvodaya Institute of technology and science, kavali affiliated by JNTU Anatapur since last 10years, where he is currently an Associate Professor. His research interests include several areas of power electronics and electric vehicle applications of power electronics. He has authored or coauthored several papers in power electronics. He holds a UGC sponsored project worth of 4,60,00/- member in ISTE.



Dr. S. Tara Kalyani received the B.Sc., degree in electrical engineering from Osmania University, Hyderabad, India, in 1995; and the M.Sc. degree in electrical engineering from Jawaharlal Nehru Technological University, Hyderabad, India, in 1998. And Ph.D., degree in electrical engineering from the Jawaharlal Nehru Technological University, Hyderabad, India, in 2008. She is currently with the Department of Electrical and Electronics Engineering in the Jawaharlal Nehru Technological University, Hyderabad, India, as a Professor and head of the department. Her research interest includes Power Electronics, Control Systems, Fundamentals of Electrical Engineering, Energy Systems, Power Systems. She is a life member of Indian Society for Technical Education.



Dr. K. Anuradha received the B.E., degree in electrical engineering from Andhra University, Vizag, India; and the M.E. degree in electrical engineering from Osmania University, Hyderabad, India. And Ph.D. degree in electrical engineering from Osmania University, Hyderabad, India, in 2011. She is currently with the Department of Electrical and Electronics Engineering in the VNR Vignana Jyothi Institute of Engineering & Technology Hyderabad, India, as a Professor and head of the department. Her research interest includes Power Electronics and Drives. She is a life member of Indian Society for Technical Education. She completed so many research projects from AICTE and UGC as a Principle Coordinator. And almost 19 years of teaching experience.

## IMPLEMENTATION OF LMMN-BASED ADAPTIVE FILTERING METHOD FOR CONTROL OF SINGLE-PHASE SOLAR POWER GENERATION SYSTEM WITH UNIVERSAL ACTIVE POWER FILTER

A. Bhakthavachala<sup>1</sup>, S. Tara kalyani<sup>2</sup>, K. Anuradha<sup>3</sup>, N. Pravallika Reddy<sup>4</sup>

<sup>1</sup>Research Scholar, Department of EEE, JNT University, Hyderabad, India-500085

<sup>2</sup>Professor & Head, Dept. of EEE, JNT University, Hyderabad, India-500085

<sup>3</sup>Professor & Head, Dept. of EEE, VNR VJI Technology, Hyderabad, India-500085

<sup>4</sup>PG Student, Dept. Of EEE, PBR VITS, Kavali, SPSR Nellore, AP- 524201

### Abstract

This paper deals with the control of single-phase grid-tied solar photovoltaic (SPV) power generation system with a universal active power filter (UAPF) capabilities. The SPVUAPF system consists of series and shunt voltage source inverters (VSIs). The shunt VSI exports the real power extracted from the PV panels to the grid and local loads. In addition to handling the real power, the shunt VSI provides compensation of reactive and harmonic currents generated by the loads. The reference signals required for the control of the shunt and series VSIs of the SPV-UAPF system are estimated using least mean mixed norm (LMMN) adaptive identification algorithm.

**Keywords:** Universal Active Power Filter (UAPF), Solar Photovoltaic (SPV), Least Mean Mixed Norm (LMMN).

### I. INTRODUCTION

The ever-growing energy demand and emphasis on clean energy have led to proliferation of solar and wind based renewable power generations system. Between solar and wind energy systems, the solar energy systems are widely found at distribution level as they require little or no maintenance and the solar panels can be installed on almost any roof, as well as on the ground. Therefore, many households and commercial places are being powered by solar power [1]. The solar power generating systems make use of power electronics based dc-dc and dc-ac converters to transform the dc voltage generated by the solar panels into a usable ac voltage [2]. The power electronic converters are controlled to operate the solar panels at maximum power point. In case of grid tied solar power generation systems, the voltage source inverters (VSIs) export the remainder of the extracted solar power to the distribution

grid upon feeding the local loads. Usually for high power systems, three-phase is preferred as they offer reduced current stress on power electronic switches, improved efficiency, high power density and reduced passive elements size. Nonetheless, single-phase systems are suited for low power generation in the range of a few kilowatts. Most of the rooftop domestic solar power systems are low power and single-phase in nature. In single-phase systems, the number of power electronic switches and sensors required are less compared to a three phase system; which in turn makes the control circuitry simple and cost-effective.

Thereby the complexity of the control system is reduced drastically in single-phase system. However, in case of single-phase systems, the instantaneous powers contain second order oscillations, which would lead to dc-link voltage oscillations in VSIs. To filter out these dc-link voltage oscillations a large capacitor bank is needed on dc side. Lately, the power quality has become a rising concern in distribution systems with the increased use of various nonlinear loads such as variable frequency drives, LED-based lighting devices and switch mode power supplies. The harmonic currents drawn by the nonlinear loads causes harmonic voltage drops in the system and thereby distort the voltage at point of common coupling (PCC). The voltage distortion caused by nonlinear loads may lead to malfunctioning of sensitive loads [3]. The effects of harmonics drawn can be suppressed with the help of power quality conditioning devices such as series and shunt power filters. Installation of dedicated power conditioning devices can be avoided if the VSIs that are employed for the active power generation are able to offer ancillary services like harmonic and reactive currents compensation [4], [5].

## II. LITERATURE SURVEY

Various studies focusing on integrating compensation capabilities in the VSIs of grid interactive solar power generation systems can be found in the literature [6]–[12]. Primarily, the attention has given to integration of shunt compensation capabilities like harmonic and reactive currents compensation to improve the voltage quality at the PCC as it does not require any additional component such as a series transformer. In [6]– [8], the solar power generation systems with integrated shunt compensation are reported. However, to deal with the voltage disturbances like voltage sag, swell and harmonic distortion, series compensation [9] is preferred over shunt compensation. Hence, to simultaneously provide both series and shunt compensation, universal active power filters (UAPFs) can be used [13]–[15]. UAPFs are capable of handling most of the power quality problems arise in distribution systems. In [10]–[12], a solar power generation coupled with both UAPF capabilities is proposed.

In the fields of electric drives and power conditioning systems, the least means squares (LMS)-based adaptive technique is being extensively used compared to various adaptive identification methods because of its simplicity and easy to implement. Application of LMS technique for extracting the fundamental frequency component information in a nonlinear load currents reported. Nonetheless, in case of the LMS technique, the mean square error (MSE) is directly related to the step size. The higher the step size, the faster the convergence. However, increasing the step size would lead to increased MSE. Therefore, a judicious value of step size must be selected for extraction of harmonic components. Further, the LMS-based identification technique operates on the principle of minimizing the MSE. Therefore, the LMS method is more suitable when the error norm is below 1.0 and it becomes less responsive when the error norm is greater than 1.0. Another adaptive technique similar to LMS method known as least mean forth (LMF) technique [can also be found in the literature. Unlike LMS method, the LMF technique works effectively when then error is less than 1.0.

Based on the discussion so far, considering the limitations of LMS and LMF techniques, the

least mean mixed norm (LMMN) algorithm is identified, modified and applied for adaptive detection of harmonic components of load current and synchronization of single-phase SPVUAPF system in this work. The LMMN method has combined benefits of LMS and LMF techniques. Unlike the reported works, a multi-channel structure of LMMN-based filtering algorithm is proposed for the present application to enable selective compensation and increase the detection speed. The multi-channel LMMN-filter structure simultaneously extracts all the dominant harmonic components of the load current in addition to fundamental to reduce the error to be processed by the LMMN filters and thereby increases the dynamic response of harmonic components detection process.

## III. PROPOSED SYSTEM

### A. Description of SPV-UAPF System

Fig.1 shows the configuration of single-phase SPV-UAPF system. The system consists of back-back connected single phase H-bridge VSIs labeled as shunt and series inverters with common dc bus. The VSIs are electronically realized using insulated gate bipolar junction transistors (IGBTs). Solar power is extracted from the PV panels by means of a boost converter and fed to grid via shunt VSI. The boost converter operates the solar panels at maximum power point. The switching pulses for the boost converter are generated using perturb and observe (P&O) algorithm. The series VSI is placed between PCC and the load via a single-phase step down transformer. The secondary side voltage of the series transformer either aids or opposes the PCC voltage to regulate the load voltage. The symbols  $v_{pcc}$ ,  $v_{se}$  and  $v_l$  represent the PCC voltage, series injected voltage and the load voltage, respectively. The quantities  $i_{sh}$ ,  $i_g$  and  $i_l$ , represent shunt VSI current, grid current, and load current, respectively. The dc quantities such as dc-link voltage, PV output voltage, PV output current are denoted by

## IMPLEMENTATION OF A NOVEL CONTROLLER FOR WIND-PV-DIESEL BASED STANDALONE MICROGRID

<sup>1</sup>P.B. Elyon, <sup>2</sup>V. Madhusudhana Reddy

<sup>1</sup>PG scholar, <sup>2</sup>Professor Department of EEE,

<sup>1,2</sup>PBR Visvodaya Institute of Technology and Science [PBR VITS], Kavali

### ABSTRACT

In this paper, a comprehensive controller for a standalone microgrid with three dispersed generation units based on a wind turbine, a solar photovoltaic array, and a diesel generator is implemented. To achieve maximum power point tracking of a solar photovoltaic array and a variable speed wind turbine coupled to a permanent magnet brushless DC generator without rotor/wind speed sensors, the power ratio variable step perturb and observe method is used. Furthermore, a control algorithm based on in-phase and quadrature units is developed to ensure perfect synchronisation of a diesel generator to the point of common coupling (PCC). Voltage and frequency are regulated using an active power control based on a proportional-integral controller with anti-windup. The LCL filter, which is based on a virtual resistor, is used for power distribution.

### INTRODUCTION

Despite the fact that DG is expensive, noisy, and polluting, any remote area still uses a diesel engine based electric generator known as a diesel generator (DG) for their electrical energy needs. Renewable energy sources (RES) such as solar, wind, biomass, and hydro are typically abundant in remote areas. Advances in power electronics and electrical machines have made it possible to reduce the cost of energy provided by these RES and to reduce reliance on DG in remote areas by integrating various RES

and forming a standalone microgrid (SMG). This electric system is a self-sustaining, off-the-grid network that uses energy generated locally. Because of the stochastic nature of different RES, the electricity generation needs a backup support such as DG, because SMG is not connected to any conventional grid. However, such combination has AC as well as DC generation making the control complex and costly. As a result, research efforts for simplified control, cost reduction, and improved SMG performance are documented in the literature. The authors of [4] presented a wind turbine (WT) and a solar photovoltaic (PV) based SMG for cost and complexity reduction while eliminating one power converter. The control is simplified by removing the dump load; however, this technique is not applicable to all applications. Two different configurations are presented to ensure continuous power in remote and isolated areas by continuously operating DGs. This solution is expensive, polluting, and inefficient at light loads. A battery energy storage (BES), WT, and DGs-based SMG is presented in to improve the performance of DGs, where DG is used as an emergency energy source.

### II. LITERATURE SURVEY

A.M. Rezkallah, Ambrish Chandra, D. The control design of a new Eco-friendly microgrid based on Wind/Diesel/Battery is investigated by R. Rouse, H. Ibrahim, and A. Ilinca. The variable speed permanent magnet brushless DC generator

(PMBLDCG) driven by a wind turbine (WT) is connected to the DC bus via a three phase diode bridge rectifier and a DC/DC boost converter. To achieve maximum power point tracking (MPPT) from WT without rotor speed sensing, the perturbation and observation technique (P&O) is used. The variable speed permanent magnet synchronous generator (PMSG) powered by a diesel engine (DE) is connected to the DC bus via a three phase diode bridge rectifier and DC/DC boost converter. It is programmed to operate based on the load power demand and the battery's state of charge (SOC%). The power measured at the DC bus is used. A neutral point 3-phase 4-wire inverter topology is considered as interfacing power converter. To regulate the system frequency and AC voltage at the point of common coupling (PCC), control strategy based on decomposition in symmetrical components of the load voltages and currents is developed.

**B. Choi JW and Lee SC.** proposed a new antiwindup strategy for PI speed controllers to suppress the undesirable side effect known as integrator windup when making large set-point changes. When the speed control mode is switched from P control to PI control, an appropriate initial value is assigned to the integrator. This value then limits overshoot. Furthermore, the proposed method ensures the designed performance regardless of the operating conditions, i.e., different set-point changes and load torques, and is easily implementable with existing PI controllers. The proposed method outperforms existing well-known antiwindup methods, such as conditional integration and tracking back calculation, in SIMULINK/MATLAB-based comparative simulations and

experiments for a permanent-magnet synchronous motor speed controller.

**C.Saïd-Romdhane MB, Naouar MW, Slama-Belkhodja I, Monmasson E.** are proposed Grid-connected converters (GcCs) employ LCL filters instead of simple L filters in order to meet new grid codes and their on-going changes in the near future. For solving the resonance problems of LCL-filter-based GcCs, active damping methods with no power losses are preferred over passive damping methods (LCL-GcCs). Large changes in grid inductance, on the other hand (typically under poor grid conditions and in rural areas), may jeopardise system stability. Furthermore, the delay of digital controllers will change the phase-frequency characteristics of the system, affecting system stability. As a result, this paper proposes a systematic design procedure for active damping of voltage-oriented PI control for LCL-GcCs. The procedure considers active damping methods based on capacitor current feedback and is designed to ensure stable operation under severe grid inductance variations while taking into account the effect of changes in digital control delay and LCL filter parameters on system stability. Modeling and simulation

**D.F. S. Tidjani, A. Hamadi, A. Chandra, P. Pillay, and A. Ndtoungou,** are proposed Microgrid (MG) is attracting considerable attention as a solution to energy deficiency, especially, in remote areas. A microgrid (MG) is a collection of interconnected loads and multiple distributed generators that are typically integrated via voltage source converters (VSC) and can operate in both grid-connected and island-mode. MG requires component optimization in terms of control and size reduction to improve

power quality and power energy management reliability. This paper examines three aspects in order to make some contributions: 1) Creating a new active damping technique based on a mathematical model of a voltage source convertor that does not require any additional sensors; 2) Reducing the size of the output LC filter by shifting the frequency and adjusting the active damping coefficient; and 3) Creating a strong fuzzy logic supervisor for smart power management. The simulation and experimental results show that the system performs admirably.

**III. PROPOSED SYSTEM**

**A. System configuration and operation modes**

Figure 1 depicts the proposed SMG configuration, which includes a permanent magnet brushless DC generator driven by WT and a diesel engine driven synchronous generator (SG). The WT runs at variable speeds, whereas the synchronous generator runs at a fixed speed. The power from WT is rectified using a diode bridge rectifier and fed to the DC-link via a boost converter 2 for simple integration of dispersed generating units with easy synchronisation. A boost converter 1 connects the PV array to the same DC-link. A three-phase VSC delivers the combined DC power to the PCC. To connect DG at PCC, a controlled switch is used. A battery bank serves as a backup to the SMG configuration.

In Table I, all operating modes of the system, are presented. Based on the state of charge of battery (SOC), the generated power from WT and PV array, as well as the load power demand, the decision is taken. If the SOC is greater than 50% and the generated power from WT and PV

array, is greater than the load demand, BES is in charging mode. For the same SOC but with less power generated from WT and PV, BES starts discharging i.e. feeding power to the load in order to balance the power in the system. DG is turned off as it is mentioned in a operating mode 5, only if the SOC is less than 50%, and the generated power from WT and PV array, is less than load power demand. In this operating mode DG runs at its full capacity, to charge BES and supply the load, simultaneously. The DC dump load operates in mode 4, only if BES is fully charged, and the generated power from WT and PV array, is greater than the load demand.

TABLE I  
OPERATING MODES OF SYSTEM

Mode	Conditions	Energy source	State of BES
Mode1	SOC >50% $P_{pv} + P_{WT} > P_L$	PV, WT, BES	BES is charging
Mode2	SOC >50% $P_{pv} + P_{WT} < P_L$	PV, WT, BES	BES is discharging
Mode3	SOC <50% $P_{pv} + P_{WT} > P_L$	PV, WT, BES	BES is charging
Mode4	SOC =100% $P_{pv} + P_{WT} > P_L$	PV, WT, DC dump load is turned ON	charging stopped
Mode5	SOC <50% $P_{pv} + P_{WT} < P_L$	PV, WT, BES, DG is turned ON	BES is charging

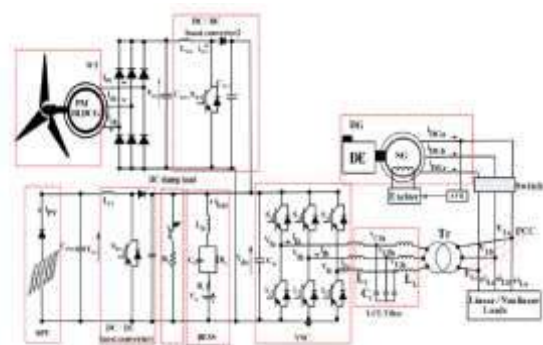


Fig.1 SMG configuration under study

**IV. CONTROLLER DESIGN FOR SMG**

The proposed SMG uses various controllers for obtaining desired performance namely MPPT, DC dump load control, DG control, voltage control and power quality



improvement. In this section, the design of control algorithms, are discussed.

**A. Control strategy for Wind turbine**

Figure 2 depicts the proposed control algorithm for WT MPPT. To generate DC voltage from trapezoidal AC voltage, the stator of a permanent magnet brushless DC generator is connected to the DC bus via a three-phase diode bridge and boost converter 2. This eliminates the need for rotor or wind speed sensors. The DC link also has BES, which detects variations in DC link voltage as wind speed, i.e. WT speed, changes. As a result, both DC current ( $i_{WT}$ ) and voltage ( $V_{WT}$ ) are required to achieve MPPT. As a result, a power ratio-based P&O method with variable step size is used to realise MPPT from WT.

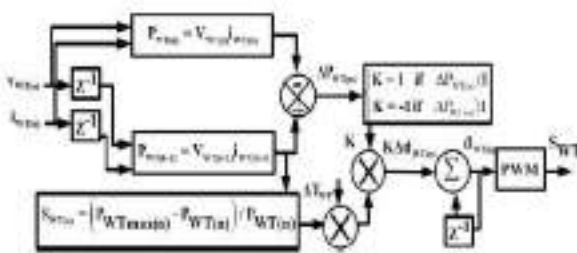


Fig. 2. Control scheme for MPPT from WT

**B. Control Strategy for Solar Photovoltaic Array**

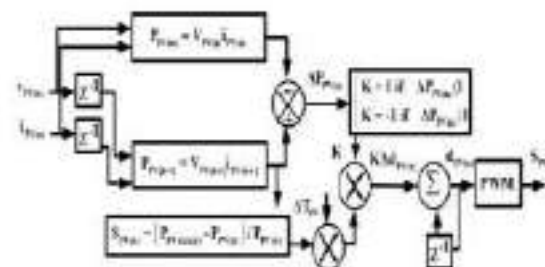


Fig. 3. Control scheme for MPPT from PV

**C. Control of DC Dump Load**

As shown in Fig.1, standalone microgrid is reinforced by a DC dump load connected to the DC-link to protect BES from overcharging and to prevent deterioration of the power quality at PCC. The control scheme for DC dump load, is presented in Fig.4. It activates only if BES is fully charged as detailed in Table 1 (operating mode 4). The control uses DC link voltage sensed as the battery voltage ( $v_{dc}$ ) and its reference value i.e. the limit of charging of battery ( $V_{bat}^*$ ) to get the voltage error ( $e$ ).

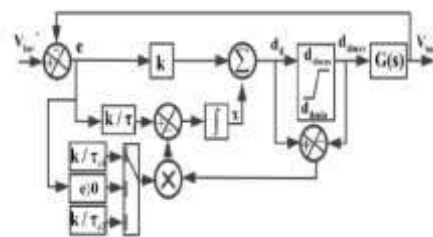


Fig. 4. DC dump load control algorithm based on AWPI

**D. Control of DG Synchronizer Switch**

The control scheme for the DG synchronizer switch is depicted in Fig.5. Its mechanical components include a speed regulator, actuator, and an engine, while its electrical components include a synchronous generator, exciter, and automatic voltage regulator (AVR). provides additional information on this mathematical model. As shown in Table I, in operating mode 5, the DG acts as an emergency energy source and operates only if the generated power from the WT and PV array is less than the load power demand and the SOC of the BES is less than 50%. To run DG efficiently, the BES is charged while the load is supplied. The following conditions must be met in order for the DG to be synchronised with the PCC.

$$\begin{cases} SOC\% < 50\% \\ P_{PV} + P_{WT} < P_L \\ \theta_{DG} = \theta_L \\ V_{DGP} = V_{LP} \end{cases}$$

where,  $SOC\%$ ,  $PL$ ,  $PPV$ ,  $PWT$ ,  $\theta_{DG}$ ,  $\theta_L$ ,  $VDGP$ , and  $VLP$  denote the SOC of BES, load demand, generated power from PV array and WT, phase angle of terminal voltage of synchronous generator and PCC, as well as, their voltage amplitudes, respectively.

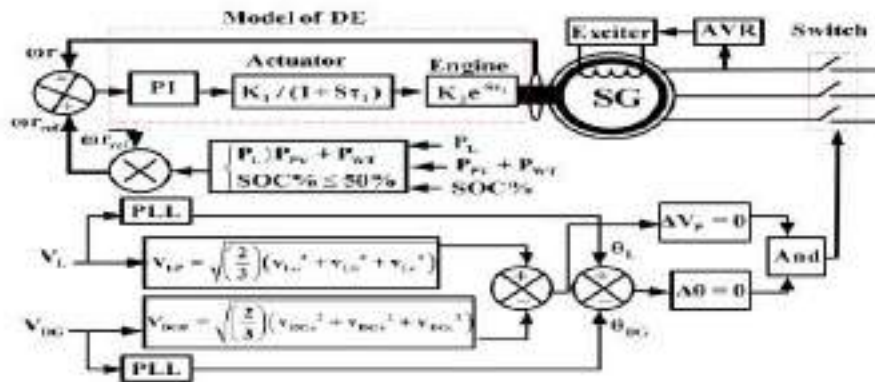
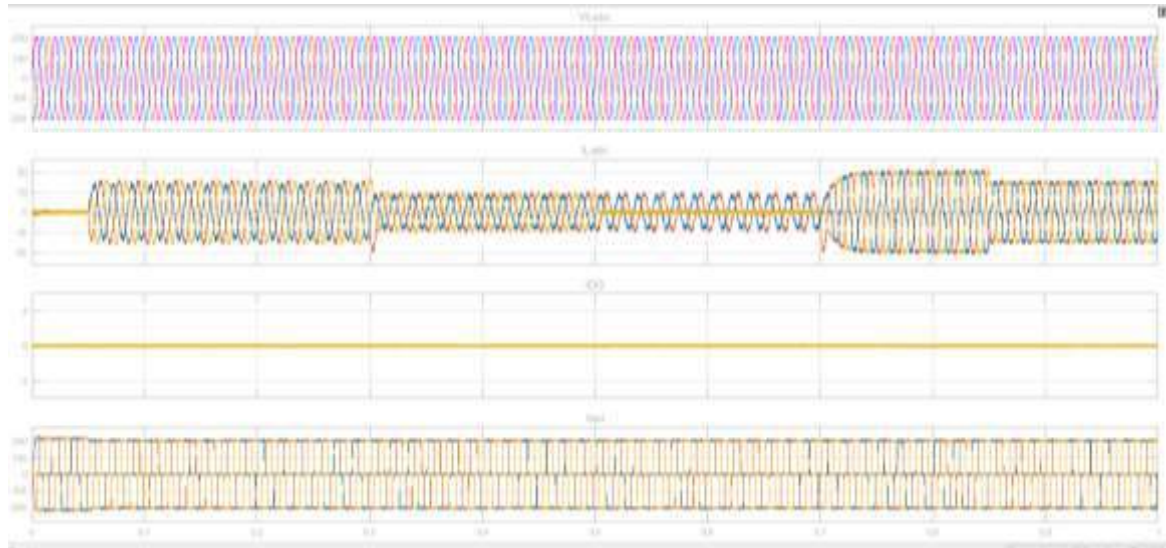
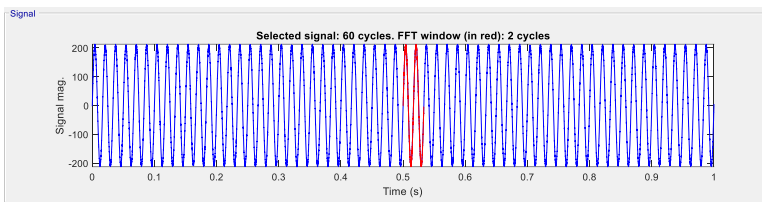
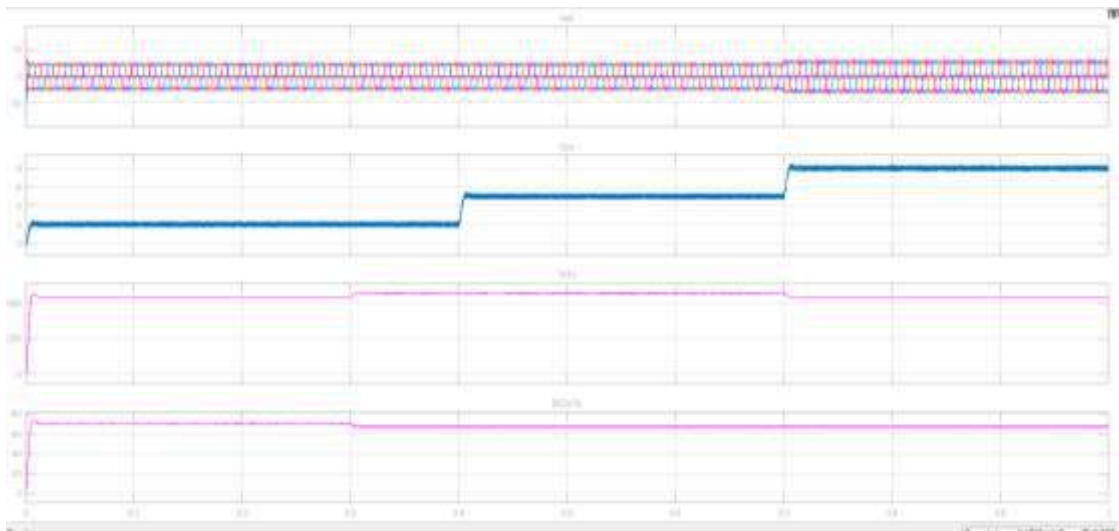
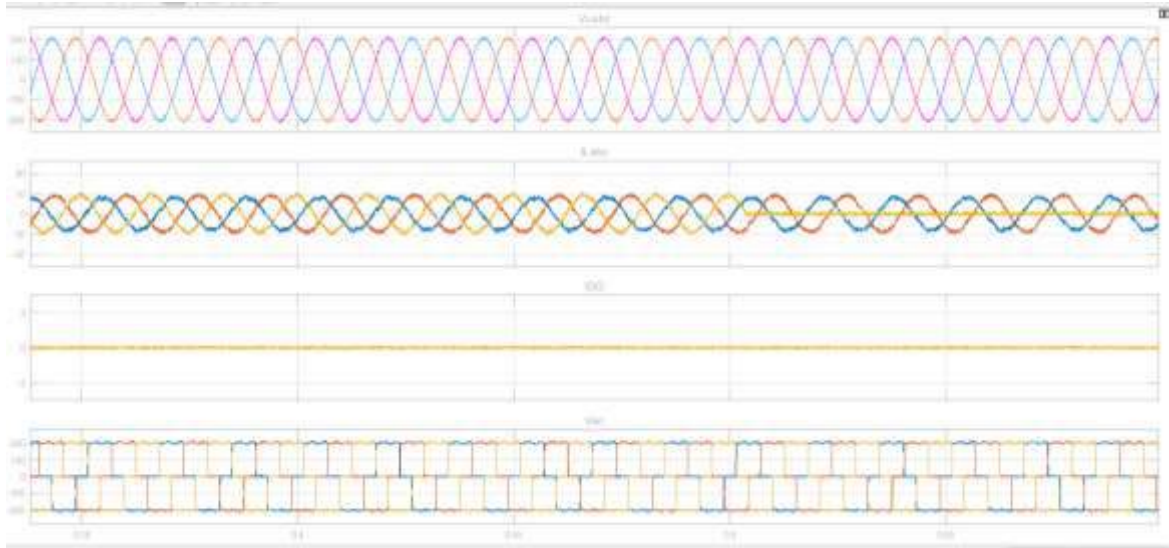


Fig. 5. Control scheme for DG synchronizer switch

V.SIMULATION RESULTS





Available signals

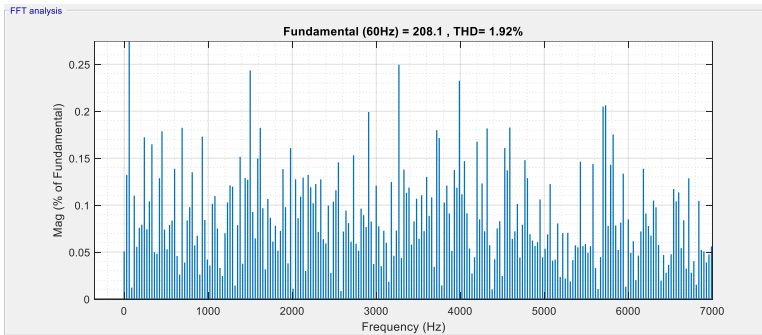
Refresh

Name: v\_fg8

Input: input 1

Signal number: 1

Display:  Signal  FFT window



FFT settings

Start time (s): 0.5

Number of cycles: 2

Fundamental frequency (Hz): 60

Max frequency (Hz): 7000

Max frequency for THD computation: Nyquist frequency

Display style: Bar (relative to fundamental)

Base value: 1.0

Frequency axis: Hertz

Display Export

Help Close

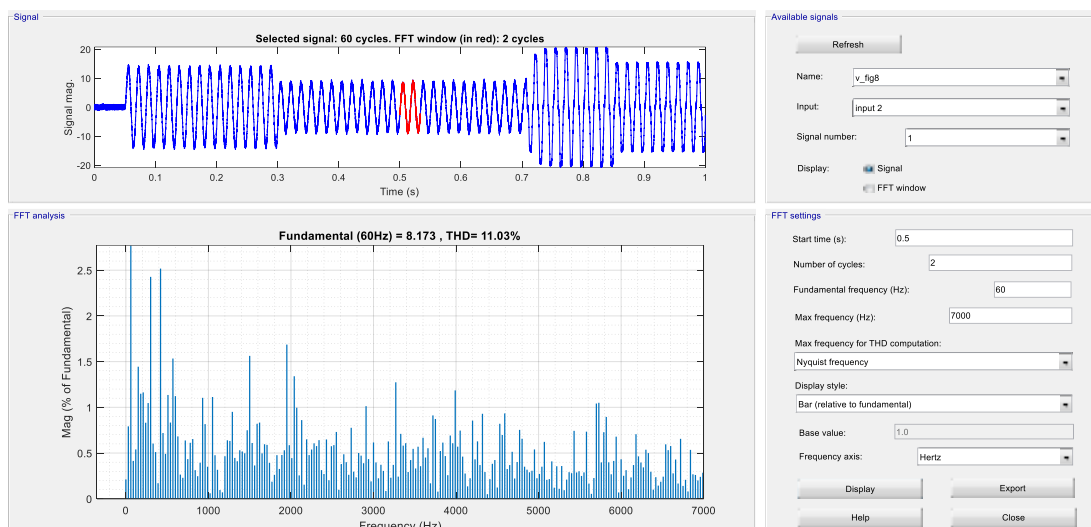


Fig.6 a) Simulation results for load and weather variation when the SOC is superior to 50%, and b) zoomed responses of (a) between t = 0.35s and t=0.6s

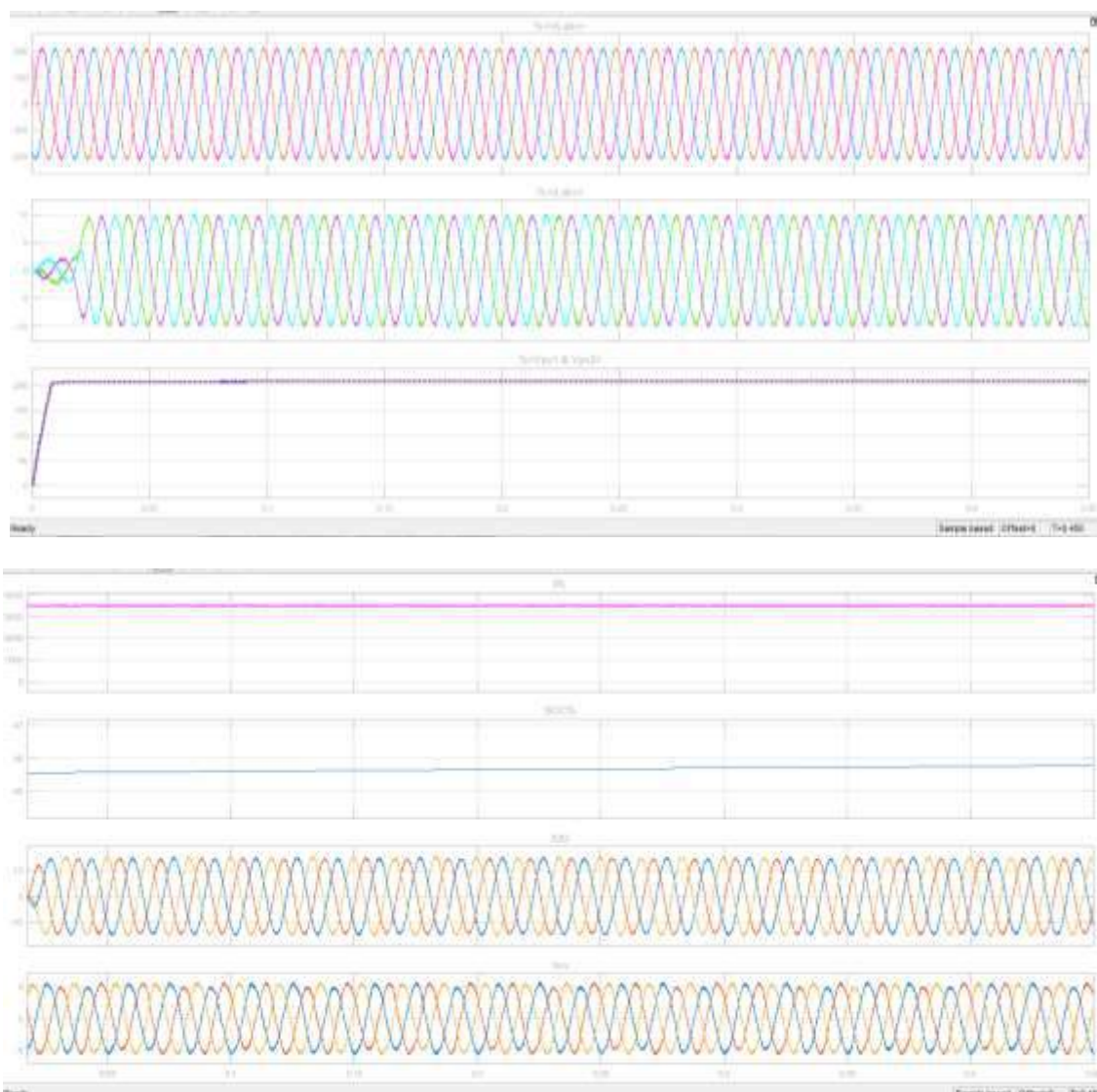


Fig.7 Dynamic performance when SOC% is less than 50%

## VI.CONCLUSION

The proposed microgrid for an isolated water treatment station, which is comprised of three dispersed generation units: a fixed speed DG, a variable speed wind turbine, and a solar photovoltaic array, has been found to operate safely under severe conditions while continuously supplying the load demand at regulated voltage. The power ratio variable step P&O method for MPPT was easily implemented in a prototype to achieve high levels of performance from a wind turbine and a solar photovoltaic array without the use of wind/speed sensors or oscillations around MPP. The developed active power control based on an AWPI controller with virtual resistor based active-damping for voltage regulation at the PCC has been successfully implemented, and the results show that the desired performance is achieved without saturation during transitions. Excess power for the space heating system is used as a DC dump load to protect the BES from overcharging. DG was only used as a backup energy source, and its synchronisation with PCC was accomplished safely and without disrupting system operation. Using an LCL filter-based virtual resistor, switching harmonics are perfectly attenuated with no losses. As a result, the comprehensive control proposed in this work for a standalone wind-solar diesel microgrid is expected to be an effective alternative for uninterrupted supply in remote and isolated areas.

## REFERENCES

[1] N. Mendis, K. M. Muttaqi, S. Perera, and M. N. Uddin, "Remote Area Power Supply System: An Integrated Control Approach Based on Active Power Balance," *IEEE Industry Applications Magazine*, vol.21, no.2, pp.63-76, Mar. 2015.

[2] M. Rezkallah, S. Sharma, A. Chandra and B. Singh, "Implementation and control of small-scale hybrid standalone power generation system employing wind and solar energy," in *Proc. IEEE IAS Annual Meeting*, 2016.

[3] Y. Tan, K. M. Muttaqi, P. Ciufu, and L. Meegahapola, "Enhanced Frequency Response Strategy for a PMSG-Based Wind Energy Conversion System Using Ultracapacitor in Remote Area Power Supply Systems," *IEEE Trans. Industry Applications.*, vol.53, no.1, pp. 549-558, Feb.2017.

[4] M. Rezkallah, A. Hamadi, A. Chandra, and B. Singh, "Hybrid AC-DC standalone system based on PV array and wind turbine," in *Proc. IECON*, 2014, pp. 5533-5539.

[5] M. Rezkallah, A. Hamadi, A. Chandra, and B. Singh, "Real-Time HIL Implementation of Sliding Mode Control for Standalone System Based on PV Array Without Using Dumpload," *IEEE Trans. Sustainable Energy*, vol. 6, no.4, pp. 1389-1398, Oct.2015.

[6] K. Kant, C. Jain, and B. Singh, "A Hybrid Diesel-Wind-PV based Energy Generation System with Brushless Generators," *IEEE Trans.Industrial Informatics*, vol.13, no.4, pp. 1714-1722, Aug. 2017.

[7] P. Sharma and T. S. Bhatti, "Performance Investigation of Isolated Wind-Diesel Hybrid Power Systems With WECS Having PMIG," *IEEE Trans. Industrial Electronics*, vol.60, no.4, pp. 1630-1637, April 2013.

[7] P. Sharma and T. S. Bhatti, "Performance Investigation of Isolated Wind-Diesel Hybrid Power Systems With WECS Having PMIG," *IEEE Trans. Industrial Electronics*, vol.60, no.4, pp. 1630-1637, April 2013.

[8] M. Rezkallah, A. Chandra, D. R. Rouse, H. Ibrahim, A. Ilinca, and D. Ramdenee, "Control of small-scale wind/diesel/battery hybrid standalone power generation system based on fixed speed generators for remote areas," in *Proc. IECON 2016*, pp. 4060-4065.

[9] M. Rezkallah, A. Chandra, and B. Singh, "Three-leg four-wire voltage source inverters for hybrid standalone system feeding unbalanced load," in *Proc. IECON*, 2013, pp. 1916-1921:

[10] J. Philip, C. Jain, K. Kant, B. Singh, S. Mishra, A. Chandra, et al., "Control and Implementation of a Standalone Solar Photovoltaic Hybrid System," *IEEE Trans. Industry Applications.*, vol.52, no.4, pp. 3472-3479, Jul. 2016.

[11] Y. Sun, X. Hou, J. Yang, H. Han, M. Su, and J. M. Guerrero, "New Perspectives on Droop control in AC MicroGrid," *IEEE Trans. Industrial Electronics.*, vol.64, no.7, pp. 5741-5745, Jul. 2017.

[12] H. R. Baghaee, M. Mirsalim, G. B. Gharehpetian, and H. A. Talebi, "A Decentralized Power Management and Sliding Mode Control Strategy for Hybrid AC/DC Microgrids including Renewable Energy Resources," *Trans. Industrials. Informatics, Early Access*, 2018.

# International Journal of Engineering Sciences & Research Technology

(A Peer Reviewed Online Journal)  
Impact Factor: 5.164



**Chief Editor**  
Dr. J.B. Helonde

**Executive Editor**  
Mr. Somil Mayur Shah

## ABSTRACT

This master thesis work presents the development of a parameterized automated generic model for the structural design of an aircraft wing. Furthermore, in order to perform finite element analysis on the aircraft wing geometry, the process of finite element mesh generation is automated. The generic model that is developed in this regard is able to automate the process of creation and modification of the aircraft wing geometry based on a series of parameters which define the geometrical characteristics of wing panels, wing spars and wing ribs. Two different approaches are used for the creation of the generic model of an aircraft wing which are “Knowledge Pattern” and “Power Copy with Visual Basic Scripting” using the CATIA V5 Software. A performance comparison of the generic wing model based on these two approaches is also performed. In the early stages of the aircraft design process, an estimate of the structural characteristic of the aircraft wing is desirable for which a surface structural analysis (using 2D mesh elements) is more suitable. In this regard, the process of finite element mesh generation for the generic wing model is automated. Furthermore, the finite element mesh is updated based on any changes in geometry and the shape of the wing panels, wing spars or wing ribs, and ensure that all the mesh elements are always properly connected at the nodes. The automated FE mesh generated can be used for performing the structural analysis on an aircraft wing. Topology optimization has for a considerable time been applied successfully in the automotive industry, but still has not become a mainstream technology for the design of aircraft components.. Also, aircraft components are often stability designs and the compliance based topology optimization method still lacks the ability to deal with any buckling criteria. The present paper considers the use of the compliance formulated topology optimization method and detailed sizing/shape optimization methods to the design of aircraft components but also discusses the difficulties in obtaining correct loading and boundary conditions for finite element based analysis/optimization of components that are integral parts of a larger structure.

**KEYWORDS:** Aircraft, Power Copy, 2D Mesh Elements.

## 1. INTRODUCTION

Aircraft design is a complex and multi-disciplinary process that involves a large number of disciplines and expertise in aerodynamics, structures, propulsion, flight controls and systems amongst others. During the initial conceptual phase of an aircraft design process, a large number of alternative aircraft configurations are studied and analyzed. Feasibility studies for different concepts and designs are carried out and the goal is to come up with a design concept that is able to best achieve the design objectives. One of the crucial studies in any aircraft design process is the conceptual design study of an aircraft wing. The aircraft wing is one of the most critical components of an aircraft not only from an aerodynamics point of view but also from a structural point of view. The aircraft wing is designed in such a way that it is able to provide the requisite lift while minimizing the drag. Drag is critical from the aerodynamics point of view because it directly affects the performance of the aircraft like fuel efficiency and range. Not only does the wing provide the necessary lift during flight, the aircraft wing is designed structurally to





carry the entire weight of the aircraft. Also, in modern commercial aircrafts and fighter airplanes, the aircraft wing has more than one role. It not only carries the fuel required for the flight but is also used to provide storage bays where, the aircraft landing gears can be mounted and stowed during takeoff (which are normally placed inside the wing root of an aircraft). Furthermore, modern commercial airplanes have padded engines which are placed below the wing.\

This means that the aircraft wing has to be sufficiently strong from the structural perspective to carry the weight of these engines, fuel inside the wing box and internal components. A variety of components are also placed inside the aircraft wing which includes electro- mechanical actuators, fuel lines, and hydraulic, pneumatic and electrical systems amongst others. All of these components are to be compactly placed inside the wing, thus, the aircraft wing has to perform structurally and aerodynamically well to deliver the desired performance. Weight is one of the fundamental critical factors in any aircraft design process and aircraft designers are always on the lookout for ways to minimize the weight of the aircraft. This means that a light weight aircraft should have a light weight wing as shown in Fig.1. A light weight aircraft is thus beneficial for increasing the design performance. In the conceptual phase of an aircraft design process, different design studies are carried out for different components of the aircraft. One of the major portions of these studies is dedicated towards the design of the aircraft wing both from a structural and aerodynamics point of view. However, in this stage High-end CAD software's are not employed as they are thought to be too complex or demanding to be used during this stage. Therefore, the promising design configurations have to be remodelled again later in the detail design process which increases cost and the time to production. It can be very beneficial from a design perspective, if these CAD software's are employed from the start of the aircraft design process. This would enable less remodelling of the design in the detail design process and would also enable increased capability to do modelling and simulation during the conceptual phase. A generic model is thus required in this regard that would speed up the design process of analyzing different aircraft win configurations.

## 2. OBJECTIVE AND CHALLENGE OF DROOP NOSE RIB

To the aerospace industry, the overall weight of an aircraft is a critical design requirement due to the impact just a few kilograms can have on fuel efficiency and co2 emissions. Heavier aircraft use more fuel during flight which leads to increased running costs for the airline carriers. When designing the world's largest passenger aircraft, the airbus wanted to ensure the design was as lightweight as possible while maintaining all performance standards. To achieve objective and challenge we are using this thesis work presents the development of the generic parameterized aircraft wing model by using CATIA V5 CAD software which provides tools and features for automated geometry generation and modification. In using this CAD software, A structural mesh generation of the generic aircraft wing model is also created. It is ensured that the mesh elements are properly connected at the nodes and the mesh elements are of good quality. Altair Hypermesh for pre-processing, Solver is Altair Radioss, for post processing Altair Hyper view and for achieving new design and less weight using Altair Optistruct.





Fig.1. Application of general wing model

**2.1 Applications**

The generic wing model that is developed in this thesis work can not only be used for designing of the aircraft wing which is its primary application, but, also can be used for designing other types of wing shapes used in other applications. The structure of the model is made as general and generic as possible for enabling its use in different applications. For example, the generic wing model can be used for designing aircraft propeller blades, gas turbine blades, wind turbine blades, car spoilers and ship propeller blade etc.

**2.2 Positioning and Shape Of Wing**

When the positioning of the wing on the fuselage and the shape of the wing is changed, different types of wing configurations can be achieved, some of which are shown in the fig.2 below,

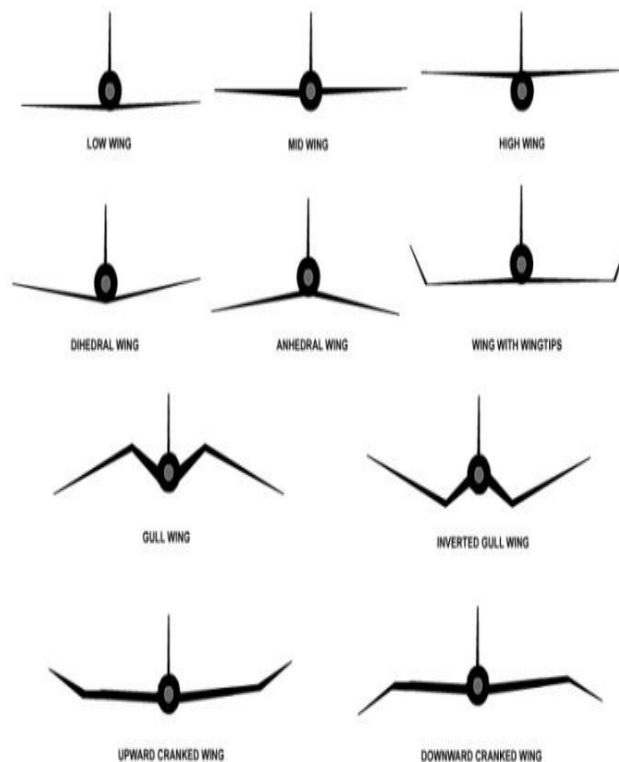


Fig.2. Positioning and Shape of the Wing



### 3. GENERIC AIRCRAFT STRUCTURAL WING DESIGN CONCEPT

#### 3.1 Aircraft Design Process

Aircraft design process is a complex undertaking, however, the design process can generally be divided into three phases which are outlined in the fig.3 below. There is a certain amount of overlapping between these three phases and the number of people, resources and cost associated with the design gradually increases between these phases. The different stages of the aircraft design process are,

- Conceptual Design
- Preliminary Design
- Detail Design



*Fig.3. General Overview of Aircraft Design Process.*

#### 3.2 Tools And Methods

A breakdown of the tools and methods used in this thesis work is given in the fig.4

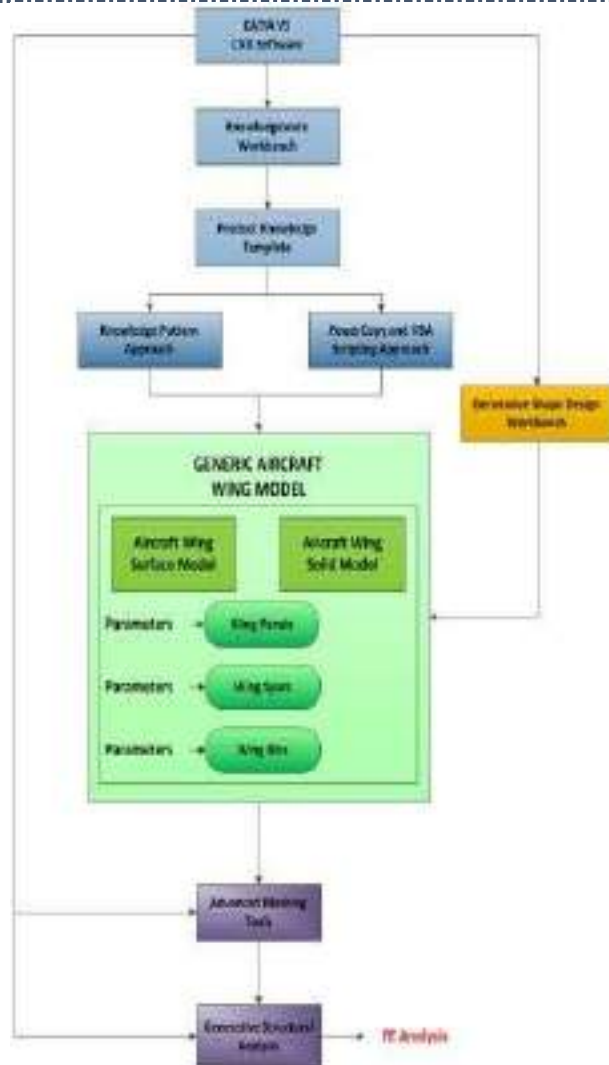
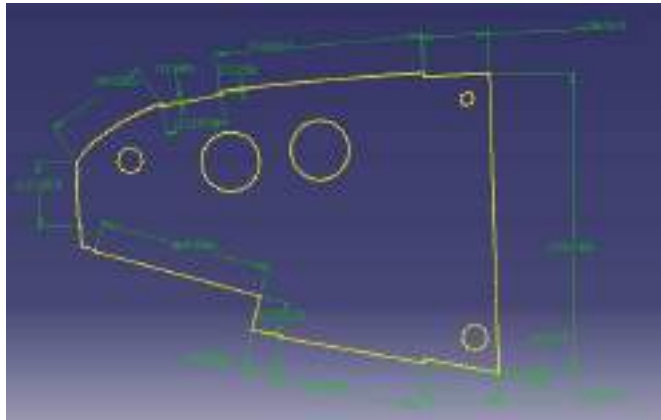


Fig.4. Tools and Methods used for creation of generic aircraft wing model



---

**A. Modelling Of Wing RIB**

*Fig.5. 2D drawing Using CATIA V5R19 Software.*

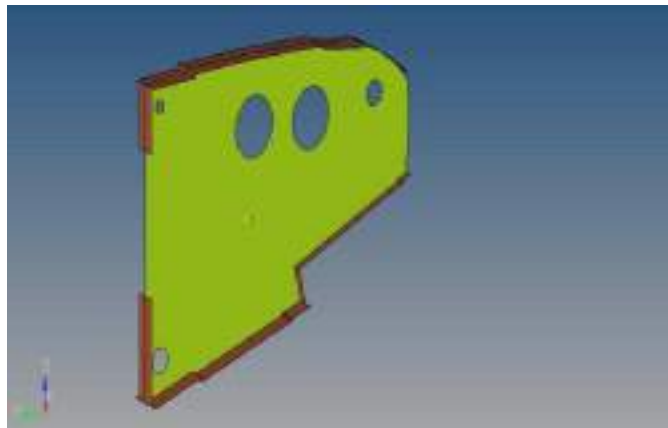


*Fig.6. 3d model is developed in catia v5r19 software model.*

**3.2 Solid Meshing**

Using solid geometry, HyperMesh can utilize both standard and advanced procedures to connect, separate or split solid models for tetra-meshing or hexa-meshing. Partitioning these models is fast and easy when combined with Hypermesh powerful visualization features for solids. This allows users to spend less time preparing geometries for solid meshing. The solid-meshing module allows users to quickly generate high quality meshes for multiple volumes as shown in Fig.7.

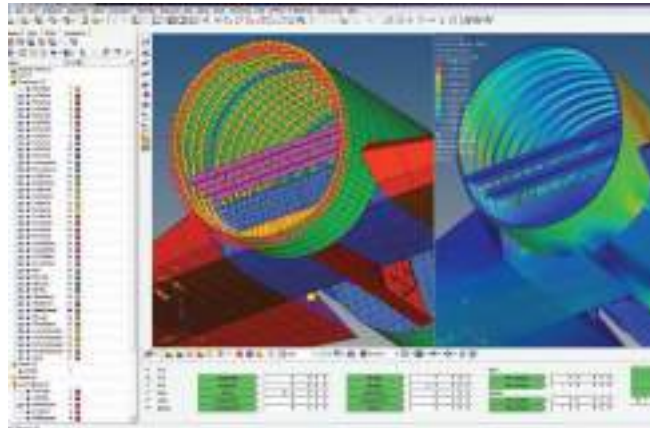


Fig7.Modern and Efficient CAE Modeling Environments

## 4. PREPROCESSING AND SOLVER

### 4.1 Preprocessing

Altair® HyperMesh® is a high-performance finite- element pre-processor that provides a highly interactive and visual environment to analyze product design performance. With the broadest set of direct interfaces to commercial CAD and CAE systems and a rich suite of easy-to-use tools to build and edit CAE models, HyperMesh provides a proven, consistent analysis platform for the entire enterprise.

### 4.2 Best In Class Meshing

HyperMesh presents users with an advanced suite of easy-to-use tools to build and edit CAE models. For 2D and 3D model creation, users have access to a variety of mesh generation capabilities, as well as Hypermesh's powerful automeshing module.

### 4.3 High Fidelity Meshing

- Surface Meshing
- Solid map Hexa Mesh
- Tetra Meshing
- CFD Meshing
- SPH Meshing

**Surface Meshing:** The surface meshing module in HyperMesh contains a robust engine for mesh generation that provides users with unparalleled flexibility and functionality. This includes the ability to interactively adjust a variety of mesh parameters, optimize a mesh based on a set of user- defined quality criteria, and create a mesh using a wide range of advanced techniques.



4.4 Automesh

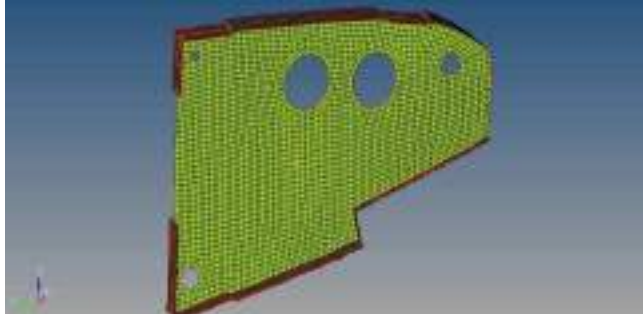


*Fig.8. Automesh using 20mm element size. Thickness for Rib component:*

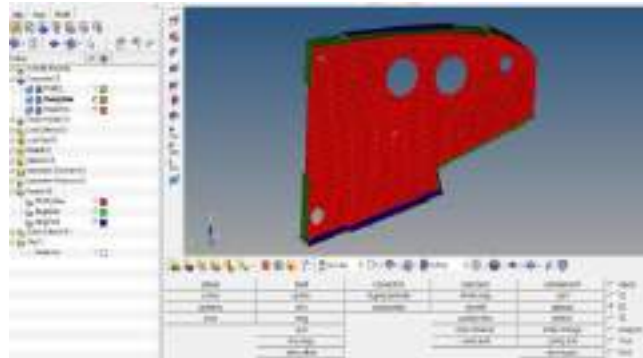


*Fig.9. Thickness for Rib component*



**Analysis page- Constraints (FIX) and Pressure applied:** Go to analysis page it will shown some tools take constraints option and fill the three circles of smaller diameter select each node in each circle it will highlighted as constraints for every circle after that applying pressure in analysis page.

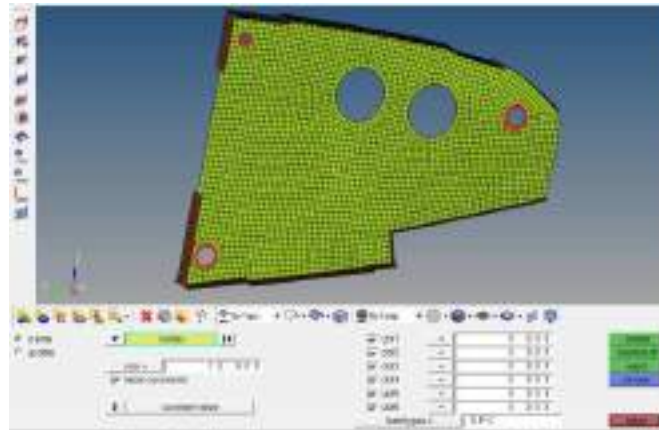


*Fig.10. Analysis page- Constraints (FIX) in all DOF, selected nodes are highlighted.*

## 5. RESULTS AND DISCUSSIONS

Aerodynamic load is applied to wing rib and solved results are shown below Figs.11 & 21.

### 5.1 Displacement

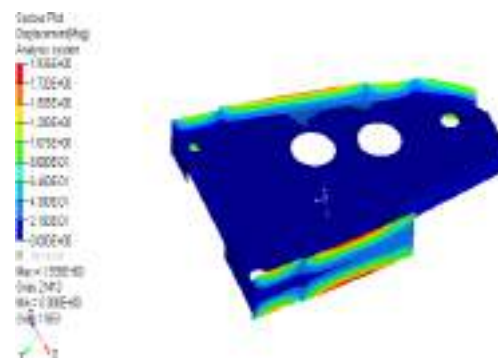


*Fig.11. The value of Displacement is 1.935 mm. Stress:*



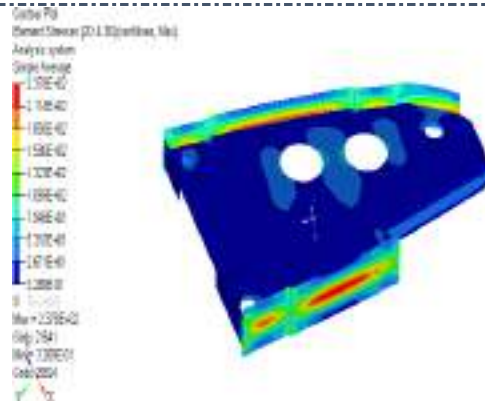


*Fig.12. The value of Stress is  $2.378 \times 10^2$  Mpa*

The value of stress in base model is  $2.378 \times 10^2$  is converted into is 237Mpa. After visualizing the static results optimization will come I the picture to get innovative shape of wing rib. Optimization techniques are shown below, different techniques are explained in brief.

### 5.2 Re-Design of the Optimized Model and Pre-Processing Methodology

Basic reference model is changed to the above design after applying the OptiStruct application to that. Design changes had been generated in Hypermesh using osssmooth option.

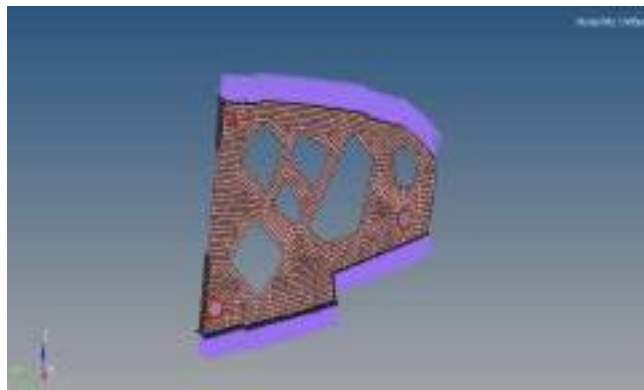


*Fig.13. New design of optimized result is meshed in hyper mesh.*

5.3 Results of Base Model Aircraft Rib Wing Displacement:

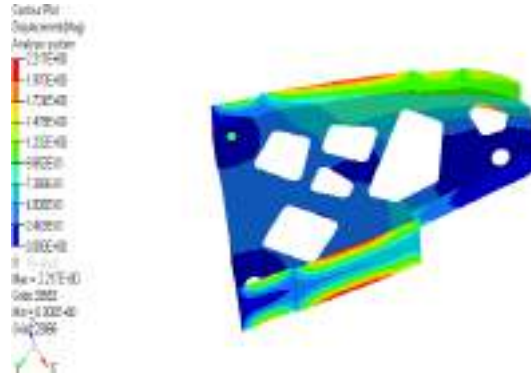


Fig.14. displacement for optimized model is 2.217 mm. Stress:

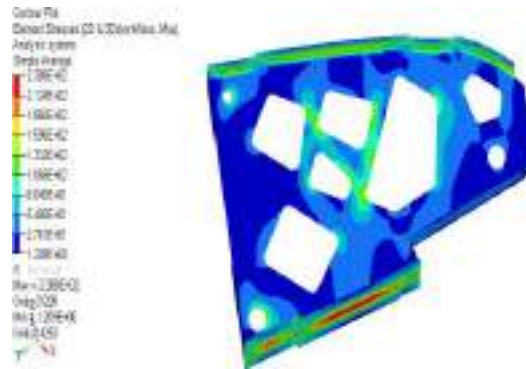


Fig.15. Stress for optimized model is  $2.355 \times 10^2$  MPa.





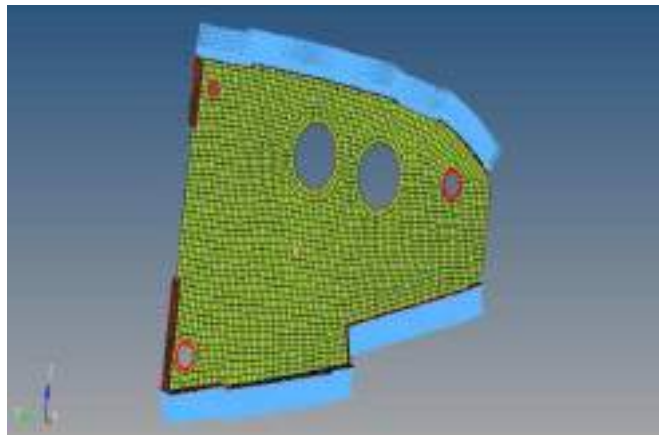


Fig.18. Design area is green colour area and non design area is flanges

**5.5 Optimized Model Results**

Optimization is completed and results are taken 6 iterations to complete the thickness and topology optimization.

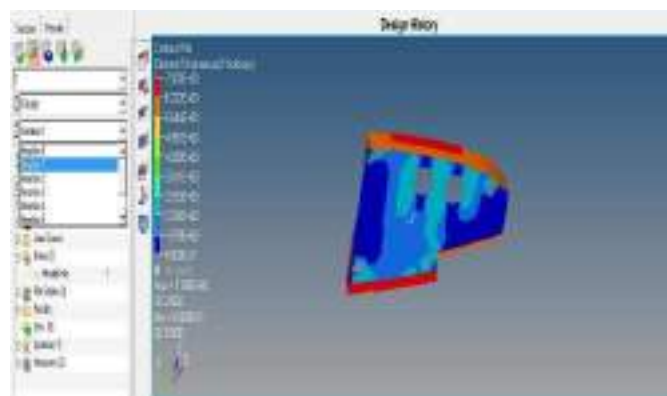


Fig.19. Iterations for free Size optimization.

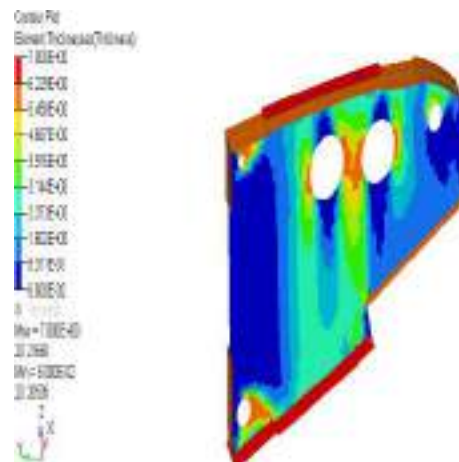


Fig.20. Thickness optimization is given perfect results for the given loads.



Topology method using Optistruct is shown in above figure, steps are involved is same like free size optimization. Response is given for volume fraction as 0.3% from the total volume and weight compliance as a objective which will reduce the weight of the component by giving innovative shape to wing.



*Fig.21. Present Dummy and trail prototype for Viewing the thickness and optimized model.*

## 6. CONCLUSION

The present work illustrates how topology, sizing and shape optimisation tools may be used in the design of aircraft components. The technology has been successfully used in an industrial environment with short industrial time scales and has on a single application proved to be able to provide efficient stress and stability component designs. Initial studies have shown that care should be taken in the modelling of the load and boundary conditions of the components. For aircraft component design it is also important to be aware of the impact of changing loading situations. The truss type designs obtained using the topology optimisation is highly specialised designs optimised for certain loading situations. Load definitions generally change as the design of an aircraft mature, and this could seriously affect the optimality of the structure. It could therefore prove important to carefully select applications for topology optimisation and only use the technology on structures with well defined loading conditions. The variation of pressure is induced in optimized model compared to base model as per the requirement of below yield point stress which is 325 Mpa and as well as the variation of displacement is induced in optimized model compared to base model which is lower than the 3 mm as per the requirement. As per the given requirement the reduction of weight is 16% decreased compared to reference model. Hence the cost analysis also reduces by using the base model and optimized model readings.

## REFERENCES

- [1] Topology Design of Structures", M P Bendsøe and C A Mota Soares, NATO ASI Series, Kluwer Academic Publishers, Dordrecht, The Netherlands, 1993.
- [2] Optimisation of Structural Topology, Shape and Material", M P Bendsøe, Springer-Verlag, Heidelberg, Germany, 1995.
- [3] National Aeronautics and Space Administration.
- [4] <http://en.wikipedia.org/wiki/Aircraft>.
- [5] Lars Krog, Alastair Tucker and Gerrit Rollema Airbus UK LTD, application of topology sizing and shape optimization methods to optimal design of aircraft components.
- [6] "Modelling and Simulating Dynamics of Missiles with Deflatable Nose Control" Gao Yuan, Gu Liangxian, Pan Lei college of Astronautics, Northwestern Polytechnical University, Xian 710072, China.
- [7] "Assessment of Aerodynamic and Dynamic models in a comprehensive analysis for rotorcraft" Wayne Johnson NASA Ames Research Center, Moffett Field, CA 94405, U.S.A.
- [8]



- [9] Talke, F.E., "Optimization: Computer Aided Analysis and Design." Class Notes. MAE 292. UC San Diego, Spring 2006.
- [10] Schneider, Detlef, and Erney, Thomas. "Combination of Topology and Topography Optimization for Sheet Metal Structures." OptiCON 2000 Conference Proceedings.
- [11] Altair Engineering. "Altair HyperMesh: Introduction to FEA: Pre-Processing Volume I." HyperWorks Training Manual, 2004.
- [12] Altair Engineering. "Altair OptiStruct: Concept Design Using Topology and Topography Optimization." HyperWorks Training Manual, 2004.
- [13] Fornace, L.V., Davis, A.E., Costabile, J.T., Hart, J.D., Arnold, D., "Traction Control Systems: FSAE Vehicle Acceleration Optimization." MAE 171B Final Report. UC San Diego, 2005.
- [14] Taylor, Rob. "F-35 Joint Strike Fighter Structural Component Optimization: Lockheed Martin Aeronautics Company." Optimization Technology Conference. 27-28 September 2005. Troy, Michigan, USA.



## Engineering College Websites in Andhra Pradesh: An Evaluation Study

O. Seshaiyah<sup>1,\*</sup>, R.V. Rekha<sup>2</sup>, Ch. Veeranjanyulu<sup>3</sup>

### Abstract

*The academic institutions in Andhra Pradesh have begun to recognize the importance and potential of using the World Wide Web. Since the early 1990s, colleges have started designing websites and offering services on the internet. The web pages of colleges have many designs and varieties, but it is necessary for these websites to follow a certain framework in their design based on their users, which increases the need for the evaluation of these websites. In reality the goal behind the evaluation of college websites is to guide them toward providing the users with accurate, correct, and authentic information. The goal of this study is evaluation of the engineering college websites in Andhra Pradesh to assess user's opinion. A questionnaire survey was conducted among the top 20 engineering colleges which were identified through the website evaluation checklist.*

**Keywords:** Academic websites, Andhra Pradesh, engineering colleges, website evaluation, web credibility, web usability

### INTRODUCTION

Web technology is one of the most important and complex inventions of mankind. It is a powerful means of communication, dissemination, and retrieval of information. The academic institutions in Andhra Pradesh have begun to recognize the importance and potential of using the web as a tool to make valuable and up-to-date information available to user community.

Since the early 1990s, colleges have started designing websites and providing services via the internet. Today, the amount of information published on the internet, in particular information on the World Wide Web is considerably higher than that on other media. College web pages have many designs and varieties, but there is a need for a framework in their user-based design, which increases the need for evaluation of these websites [1]. Because college websites play an important role in

providing the required services to users, suitable methods for evaluating these sites are of great importance. In reality the goal behind the evaluation of college websites is to guide them toward providing the users with accurate, correct, and authentic information. The purpose of this study is the evaluation of the engineering college websites of Andhra Pradesh on the basis of a questionnaire.

#### \*Author for Correspondence

O. Seshaiyah  
E-mail: osheshu@rediffmail.com

<sup>1</sup>Librarian, Department of Library Sciences, Parvathareddy Babul Reddy Visvodaya Institute of Technology and Science, Kavali, Nellore, Andhra Pradesh, India

<sup>2</sup>Assistant Professor, Department of Library & Information Science, Pondicherry University, Puducherry, India

<sup>3</sup>Librarian, Department of Library Sciences, Geethanjali Institute of Science and Technology, Gangavaram, Kovur, Andhra Pradesh, India

Received Date: February 01, 2021

Accepted Date: May 18, 2021

Published Date: August 30, 2021

**Citation:** O. Seshaiyah, R.V. Rekha, Ch. Veeranjanyulu. Engineering College Websites in Andhra Pradesh: An Evaluation Study. Journal of Advancements in Library Sciences. 2021; 8(2): 6–15p.

### Engineering Education in Andhra Pradesh

Technical education in Andhra Pradesh has seen tremendous growth over the past two decades, both in the number of students and faculty. The recent growth in the Andhra Pradesh technical education is overwhelming because educational institutions

with private funding came forward to establish technical institutes rather than educational institutions with public funding.

New Andhra Pradesh was formed as a separate state after bifurcation in 2014. According to the All India Council for Technical Education [2], there are 344 technical institutes or colleges in Andhra Pradesh during the academic year 2014–15. Among them, 10 are public, 331 private and 3 university managed colleges.

### Objectives

The main aim of the study is to evaluate the engineering college websites in Andhra Pradesh. The objectives of the study are:

- To examine users opinion on accuracy, currency, accessibility, consistency, usefulness and performance of the top 20 engineering college websites.
- To assess the content organization and navigation features of the websites from the users' point of view.
- To evaluate the engineering college websites with regard to their user support features as per the opinion of the users.

### Related Research

Panneerselvam [3] has studied various features available on Tamil Nadu universities' websites and to find information on library services offered by universities. He noted that important services are offered by most university websites. Remote access, plagiarism control, subject gateway, RSS feeds and social networking activities in the library need to be strengthened.

Jayasundari and Jeyshankar [4] investigated the credibility of IIM websites and its library web pages. The home pages of the IIMs website must be logically structured and their library pages periodically evaluated according to criteria such as access, contact information, authority, currency, ease of navigation, and so on. It is also observed that currency statement like last update details, number of visitors, certifications have not been provided in any of the IIMs website.

Khatri and Baheti [5] analyzed the various aspects of the credibility of websites deemed universities of Maharashtra. A study shows that all deemed university websites are different in many ways. The website and pages of the library must be periodically evaluated against established criteria such as website design, accessibility, accommodations, etc. which will help to improve website according to the user's need and credibility and reliability issue.

Kothainayakis [6] tries to identify the credibility factors of academic websites in three districts of Tamil Nadu. The research shows that most university websites are regularly updated, with the exception of arts and sciences and some other websites. All educational sites are easy to use. However, the organization of information varies from domain to another. A lot of attention has been paid to the design of websites.

Sife and Msoffe [7] conducted a study to evaluate the quality of the websites of five selected public universities in Tanzania. It appears that regularly updating websites is also essential to make them effective and to meet the changing needs of users.

Kannappanavar and Biradar [8] studied and analyzed the various aspects of the credibility of the websites of the Dental College in Karnataka. The research shows that all websites of dental schools differ in many respects. The evaluation of the use of websites of universities in Bangladesh is being studied by Islam and Tsuji [9] from usability perspectives. Two online automated tools used along with a questionnaire. The study found that users are not satisfied with the overall level of use of these sites. Some aspects of design, interface and performance have weaknesses.



Haneefa and George [10] conducted a study that would help Indian universities develop strategies and policies that would make better use of internet resources for education and research. Most doctoral students search the internet with the help of simple keywords. Google is the most popular search engine, followed by Yahoo.

Babu et al. [11] analyzed the various aspects of the credibility of university websites in Tamil Nadu. They found that universities had their own websites; they lacked standard design and structure. Mustafa and Al-Zoua'bi [12] in their study evaluated usability of the academic websites of Jordan's Universities. Two online automated tools, namely: html toolbox and web page analyzer were used along with a questionnaire for users of these sites. The results showed that the overall usability level of the studied websites is acceptable.

Hirwade [13] evaluated the websites of Indian universities, paying particular attention to the web pages of their library. Of the 273 universities, 91 have information about their libraries on their websites. Important findings and suggestions were presented and the directory of Indian university websites was created as a by-product of the research.

Tillotson [14] tested students' understanding of the need for website evaluation and their ability to articulate criteria for evaluation by using a questionnaire at two Canadian universities, through which he revealed that students view web sources somewhat critically and are aware of standard website evaluation criteria.

Kapoun [15] has defined five criteria for evaluating websites. Six website evaluation standards proposed by Collins [16] have received a lot of attention in this area, such as "content, authority, currency, organization, search engine and accessibility". Kirk [17] of Johns Hopkins University made few remarkable contributions in developing the standard criteria for evaluating the websites. Kovacs et al. [18] emphasized the need to evaluate information on the internet and advised not to believe everything that had been found, but to look for the author's background and skills.

Nielsen [19] and Rubin [20] pioneered the testing of websites to determine whether met users' needs. They adapted usability-engineering techniques developed for computer software design and applied them to web design. The usability is recognized as an important quality factor of any modern website.

## **METHODOLOGY**

There were 344 engineering colleges spread over the 13 districts of Andhra Pradesh. Out of the 344 engineering colleges, 277 college websites which were functioning during the study period were taken for data collection.

To assess user's opinion on the engineering college websites in Andhra Pradesh, a questionnaire survey was conducted among the top 20 engineering colleges (Appendix) which were identified through the website evaluation checklist. A sample of 1800 students and 200 faculty members are selected from the total population. A total of 2000 questionnaires were distributed among the students and faculty members, out of which 1815 questionnaires were received back and the response rate is 90.75 percent. The data were collected during the period February 2016 to April 2016 by visiting the engineering colleges. The data analysis was carried out with the help of MS-Excel and SPSS. The collected data were analyzed and presented in the form of tables and graph.

## **ANALYSIS AND DISCUSSION**

### **Demographic Characteristics of the Respondents**

Out of 1815 respondents, 91.2 percent are students and 8.8 percent are faculty members. Majority of the respondents under the study consisted of male from both the students and teaching fraternity.

Among the 1815 respondents, large number of respondents (24.2 percent) are in the CSE Department, it is followed successively by ECE (23.2 percent), EEE (22.3 percent), ME (16.7 percent), Civil (7.1 percent), IT (5.4 percent), Chemical (1.0 percent). It can be observed that the majority of respondents from CSE Department.

### Use of the Website

The importance of general feature i.e., use of the college websites was obtained based on a five point scale i.e., very difficult, difficult, no opinion, easy and very easy. The percentage is calculated based on the opinion given by respondents and shown in Table 1.

Table 1 reveals that nearly half of the respondents rated use of website as difficult. It also found that almost fifty percent of the students (49.9 percent) and faculty members rated use of website as difficult and nearly half of faculty members (49.7 percent) also rated use of website as easy. The analysis showed that the p-value is less than 0.01. It is concluded that there is significant difference between students and faculty members in their opinion with regard to the use of website.

### Speed of the Website

The site of any institute or organization should be constructed in such a way that it should be accessed within seconds. If a site is taking more time to appear on the screen, it no longer attracts the user. The percentage calculated based on their opinion was shown in Table 2.

Table 2 reveals that more than half of the respondents (55.2 percent) of the college websites opined that speed of website is slow. Very less percentage of students (4.4 percent) rated the speed of website as high. It is also evident that there is a significant difference between students and faculty members in their opinion with regard to speed of website. It is indicated by the Chi-square value, which is significant at 0.01 level with 4 degrees of freedom. A similar study done by Shivabasappa [21] on library websites of R&D institutes of India which reveals that most of the users have rated their websites as very good and excellent for loading speed.

**Table 1.** Use of the website.

Use of Website	Category			Chi-Square Value	p-value
	Students	Faculty Members	Total		
Very Difficult	114 (6.9%)	3 (1.9%)	117 (6.4%)	25.703**	0.000
Difficult	827 (49.9%)	76 (47.8%)	903 (49.8%)		
No Opinion	45 (2.7%)	-	45 (2.5%)		
Easy	578 (34.9%)	79 (49.7%)	657 (36.2%)		
Very Easy	92 (5.6%)	1 (0.6%)	93 (5.1%)		
Total	1656 (91.2%)	159 (8.8%)	1815 (100.0%)		

\*\*significant at 0.01 level.

**Table 2.** Speed of the website.

Website Speed	Category			Chi-Square value	p-value
	Students	Faculty Members	Total		
Very slow	363 (21.9%)	19 (11.9%)	382 (21.0%)	57.839**	0.000
Slow	911 (55.0%)	91 (57.2%)	1002 (55.2%)		
No Opinion	95 (5.7%)	-	95 (5.2%)		
Quick	208 (12.6%)	49 (30.8%)	257 (14.2%)		
High Speed	79 (4.8%)	-	79 (4.4%)		
Total	1656 (91.2%)	159 (8.8%)	1815 (100.0%)		

\*\*significant at 0.01 level.

### Browser Compatibility

It is very much clear from the study that students as well as faculty members opined that none of the college websites was suggested with browser compatibility. Similar results were also reported in the research work carried out by Babu et al. [11] which supported the results of the present study. Their study reveals that many do not provide information about the browser compatibility.

### Content Organization

The users were asked various aspects of content organization of websites namely design and sequence of pages, language and terminology, adequacy and organization of content, accessibility and linking to other websites on five point scale. The responses are shown in diagrammatically in Figure 1.

Figure 1 reveals that nearly half of the respondents (48.3 percent) did not express any opinion about design of individual pages. More than half of the respondents (51.9 percent) rated fair about content of the website meeting user expectations. Nearly one-third of them rated it as good. Nearly half of the respondents (48.5 percent) did not express any opinion about language and terminology of website.

Nearly half of the respondents (48.9 percent) rated organization of information on their websites as fair. Nearly one-fourth of the students rated it as good. The results of the present study substantiated results of the study conducted by Kothainayaki [6] which revealed that more than four-fifths of the academic websites have simple organization of information and easy retrieval.

Nearly half of the respondents (46.7 percent) rated sequence of the pages as fair. Over a one-fifth of them rated it as good. The similar results were also reported in the research work carried out by Kothainayaki [6] which revealed that sequencing of information in more than four-fifth of the academic websites is simple and easy to understand by the users. More than two-fifth of respondents did not express any opinion about access required information in minimum click. More than half of the respondents rated links to other related sources as fair. There is significant difference between students and faculty members in their opinions with regard to content organization. It may be faculty members more aware about website.

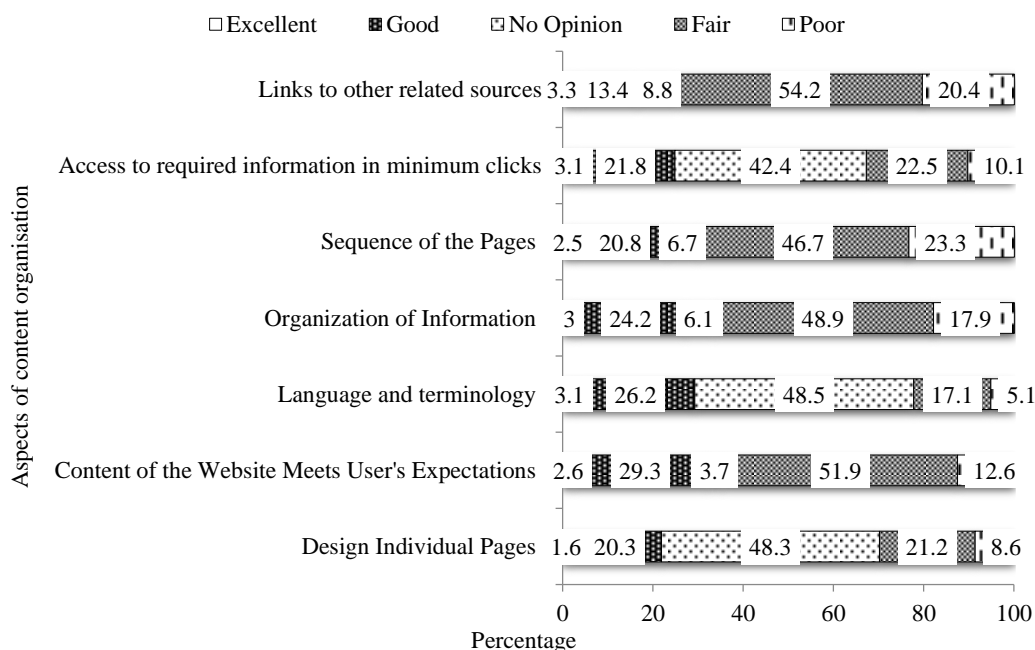


Figure 1. Content organization.

### Performance Effectiveness

The users were asked various aspects of performance effectiveness of the websites. The percentage is calculated based on the opinions given by the users and the same is given in Table 3.

Table 3 reveals that more than two-fifth of respondents (44.9 percent) did not express any opinion about less time to download a file or open a page. Nearly one-fifth of them rated it as good. With respect to distinguish between visited and nonvisited links, it reveals that 42.4 percent of the users rated it as fair. 43.2 percent of students rated it as fair whereas 34 percent of faculty members rated it as fair. More than two-fifth of respondents (42.2 percent) rated as fair about information is up-to-date. Over a two-fifths of respondents (44.6 percent) rated as fair about website attract user attention/interest. A meagre percentage of them rated it as excellent (2.5 percent).

Nearly half of the respondents rated as fair about attractive interface design. More than one-fifth of them rated it as good. A good number of students and majority of the faculty members rated the attractive interface design of the website as fair. Over a half of the respondents (51.8 percent) rated view of website as fair. Nearly one-fourth of the students (24.2 percent) rated it as good whereas nearly two-fifths of the faculty members (39.6 percent) rated it as good. Nearly half of the respondents (47.2 percent) rated use of multimedia in college websites as fair.

The t-test values show that there is a significant difference between students and faculty members in their opinions with regard to performance effectiveness.

### Navigation Features

Consistent navigation makes it easy to use a website. The navigation features of the websites are analyzed based on opinions of the respondents. The percentage was calculated and same is given in Table 4.

**Table 3.** Performance effectiveness.

Description	Students (n=1656)					Faculty Members (n=159)					Total (n=1815)					t-value
	Ex	G	NO	F	P	Ex	G	NO	F	P	Ex	G	NO	F	P	
<i>I</i>	2	3	4	5	6	7	8	9	10	11	12	13	14	15	16	17
Less time to download a file or open a page	40 (2.4)	268 (16.2)	730 (44.1)	338 (20.4)	280 (16.9)	3 (1.9)	35 (22.0)	85 (53.5)	30 (18.9)	6 (3.8)	43 (2.4)	303 (16.7)	815 (44.9)	368 (20.3)	286 (15.8)	3.034* (0.019)
Distinguish between visited and not visited links	89 (5.4)	277 (16.7)	167 (10.1)	715 (43.2)	408 (24.6)	18 (11.3)	45 (28.3)	5 (3.1)	54 (34.0)	37 (23.3)	107 (5.9)	322 (17.7)	172 (9.5)	769 (42.4)	445 (24.5)	2.902* (0.022)
Information is up-to-date	38 (2.3)	402 (24.3)	188 (11.4)	697 (42.1)	331 (20.0)	1 (.6)	56 (35.2)	8 (5.0)	73 (45.9)	21 (13.2)	39 (2.1)	458 (25.2)	196 (10.8)	770 (42.4)	352 (19.4)	3.055* (0.018)
Website attracts user attention/interest	43 (2.6)	320 (19.3)	150 (9.1)	736 (44.4)	407 (24.6)	3 (1.9)	44 (27.7)	2 (1.3)	74 (46.5)	36 (22.6)	46 (2.5)	364 (20.1)	152 (8.4)	810 (44.6)	443 (24.4)	2.799* (0.024)
Site interface design	55 (3.3)	346 (20.9)	134 (8.1)	796 (48.1)	325 (19.6)	2 (1.3)	52 (32.7)	2 (1.3)	82 (51.6)	21 (13.2)	57 (3.1)	398 (21.9)	136 (7.5)	878 (48.4)	346 (19.1)	2.614* (0.030)
View of website	34 (2.1)	400 (24.2)	97 (5.9)	864 (52.2)	261 (15.8)	2 (1.3)	63 (39.6)	4 (2.5)	76 (47.8)	14 (8.8)	36 (2.0)	463 (25.5)	101 (5.6)	940 (51.8)	275 (15.2)	2.233* (0.045)
Multimedia usage	65 (3.9)	344 (20.8)	165 (10.0)	794 (47.9)	288 (17.4)	9 (5.7)	45 (28.3)	11 (6.9)	63 (39.6)	31 (19.5)	74 (4.1)	389 (21.4)	176 (9.7)	857 (47.2)	319 (17.6)	2.576* (0.031)

Note: 1. Ex: Excellent; G: Good; NO: No Opinion; F: Fair; P: Poor;

2. Col.2–Col.16: Figures in parentheses indicate percentage; Col 17: Figures in parentheses indicates probability values;

3. \*significant at 5 percent level  $df=4$ .

**Table 4.** Navigation features.

Features	Students (n = 1656)		Faculty Members (n = 159)		Total (n = 1815)	
	Yes	NO	Yes	NO	Yes	NO
<i>I</i>	2	3	4	5	6	7
Navigation is easy through the links or menus	1428 (86.2)	228 (13.8)	152 (95.6)	7 (4.4)	1580 (87.1)	235 (12.9)

Includes a site map	171 (10.3)	1485 (89.7)	18 (11.3)	141 (88.7)	189 (10.4)	1626 (89.6)
Includes internal search engine	401 (24.2)	1255 (75.8)	43 (27.0)	116 (73.0)	444 (24.5)	1371 (75.5)
Links are meaningful and relevant to the subject	1380 (83.3)	276 (16.7)	152 (95.6)	7 (4.4)	1532 (84.4)	283 (15.6)

Note: Col.2–Col.7: Figures in Parentheses indicate percentage.

**Table 5.** User support features.

Features	Students (n=1656)		Faculty Members (n = 159)		Total (n = 1815)		$\chi^2$ value df = 1 TV = 3.84
	Yes	NO	Yes	NO	Yes	NO	
1	2	3	4	5	6	7	8
Feedback/suggestion forum is available	448 (27.1)	1208 (72.9)	41 (25.8)	118 (74.2)	489 (26.9)	1326 (73.1)	0.118 <sup>@</sup> (0.731)
Frequently Asked Question (FAQs)	90 (5.4)	1566 (94.6)	8 (5.0)	151 (95.0)	98 (5.4)	1717 (94.6)	0.046 <sup>@</sup> (0.830)
Link to social network sites	945 (57.1)	711 (42.9)	87 (54.7)	72 (45.3)	1032 (56.9)	783 (43.1)	0.326 <sup>@</sup> (0.568)
Login facility	928 (56.0)	728 (44.0)	84 (52.8)	75 (47.2)	1012 (55.8)	803 (44.2)	0.605 <sup>@</sup> (0.437)

Note: 1. Col.2–Col.7: Figures in parentheses indicate percentage; Col 8: Figures in parentheses indicates probability values;

2. @ Not significant.

Table 4 shows that majority of the respondents replied that navigation features namely navigation is easy through the links or menus (87.1 percent) and links are meaningful and relevant to the subject (84.4 percent) at their respective websites. Nearly one-fourth of them (24.5 percent) replied that websites provided internal search facility and over a one-tenth of them (10.4 percent) replied that site map has provided by of the college websites.

### User Support Features

User support is another criteria used to evaluate the home pages of the college websites. The respondent's statement of provision of user support facilities in home pages of college websites has been shown in Table 5.

Table 5 shows that more than half of the respondents replied that user support features namely link to social network sites (56.9 percent) and login facility (55.8 percent) provided by their respective websites. More than one-fourth of them (26.9 percent) responded feedback/suggestion forum provided by their respective websites. A meagre percent of them replied that FAQs provided by their college websites. A Similar study done by Shivabasappa [21] shows that nearly half of the users have rated FAQs feature as good and very good whereas, slightly more than two-fifths of the users have rated feedback as good and very good.

### Overall Features of Websites

Some of the essential features of the websites are analyzed using nine important variables. The respondents were asked to mark their opinion on a five point scale. The percentage is calculated based on the preference given by the respondents. ANOVA test was used to compare the observed results in Table 6.

**Table 6.** Overall features.

Features	Students (n = 1656)					Faculty Members (n = 159)					Total (n = 1815)				
	Ex	V G	G	F	P	Ex	V G	G	F	P	Ex	V G	G	F	P
Accessibility	95 (5.7)	283 (17.1)	861 (52.0)	287 (96.3)	130 (7.9)	22 (13.8)	49 (30.8)	77 (48.4)	11 (6.9)	-	117 (6.4)	332 (18.3)	938 (51.7)	298 (16.4)	130 (7.2)
Accuracy	130 (7.9)	372 (22.5)	751 (45.4)	292 (17.6)	111 (6.7)	18 (11.3)	58 (36.5)	69 (43.4)	13 (8.2)	1 (0.6)	148 (8.2)	430 (23.7)	820 (45.2)	305 (16.8)	112 (6.2)
Authority	163	354	755	288	96	33	50	60	16	-	196	404	815	304	96

	(9.8)	(21.4)	(45.6)	(17.4)	(5.8)	(20.8)	(31.4)	(37.7)	(10.1)		(10.8)	(22.3)	(44.9)	(16.7)	(5.3)
Consistency	128 (7.7)	372 (22.5)	784 (47.3)	278 (16.8)	94 (5.7)	18 (11.3)	47 (29.6)	72 (45.3)	20 (12.6)	2 (1.3)	146 (8.0)	419 (23.1)	856 (47.2)	298 (16.4)	96 (5.3)
Permanence	121 (7.3)	364 (22.0)	784 (47.3)	299 (18.1)	88 (5.3)	16 (10.1)	52 (32.7)	65 (40.9)	26 (16.4)	-	137 (7.5)	416 (22.9)	849 (46.8)	325 (17.9)	88 (4.8)
Ease to Use	169 (10.2)	494 (29.8)	642 (38.8)	251 (15.2)	100 (6.0)	22 (13.8)	68 (42.8)	60 (37.7)	9 (5.7)	-	191 (10.5)	562 (31.0)	702 (38.7)	260 (14.3)	100 (5.5)
Timeliness	121 (7.3)	316 (19.1)	762 (46.0)	324 (19.6)	133 (8.0)	23 (14.5)	44 (27.7)	63 (39.6)	28 (17.6)	1 (0.6)	144 (7.9)	360 (19.8)	825 (45.5)	352 (19.4)	134 (7.4)
Uniqueness	151 (9.1)	382 (23.1)	695 (42.0)	273 (16.5)	155 (9.4)	25 (15.7)	50 (31.4)	54 (34.0)	27 (17.0)	3 (1.9)	176 (9.7)	432 (23.8)	749 (41.3)	300 (16.5)	158 (8.7)
Usefulness	232 (14.0)	437 (26.4)	642 (38.8)	254 (15.3)	91 (5.5)	30 (18.9)	52 (32.7)	60 (37.7)	15 (9.4)	2 (1.3)	262 (14.4)	489 (26.9)	702 (38.7)	269 (14.8)	93 (5.1)
<i>Note : Ex: Excellent; VG: Very Good; G: Good; F: Fair; P: Poor;</i> <i>(Figures in parentheses indicate percentage)</i>															
<b>ANOVA</b>															
<i>Source of Variation</i>	<i>SS</i>	<i>df</i>	<i>MS</i>	<i>F</i>	<i>P-value</i>	<i>F crit</i>									
Between groups	4343478.28	9	482608.70	412.17	0.00**	1.999115									
Within groups	93672.22	80	1170.90												
Total	4437150.50	89													

\*\*significant at 1 percent level.

Table 6 reveals that accessibility is rated as good by more than half of the users (51.7 percent) followed by Consistency (47.2 percent) and Permanence (46.8 percent) features. A similar study was carried out by Kothainayaki [6] revealed that authority is the feature which is most expected from the academic websites. It is followed by accuracy and accessibility features. The least expected is the consistency features in academic websites URLs.

The study reveals that nearly four-fifths of the respondents (79.9 percent) rated accuracy of the website between good and very good. A similar study was done by Shivabasappa [21], shows accuracy on the library websites have been rated as good and very good by nearly three-fourths of the users. The study reveals that nearly two-third of the users (61.6 percent) rated authority as good and very good. Result of the present study supported the study conducted by Kothainayaki [6], in which most of the LIS professionals working in all types of institutions consider the authority feature as essential.

Nearly two-fifth of respondents (38.7 percent) rated 'ease to use' as good. It also reveals that a good number of the users (45.5 percent) rated timeliness of website as good. Over two-fifths of the respondents (41.3 percent) opined that uniqueness of their respective websites as good. More than two-fifth of the students rated it as good whereas over a one-third of the faculty members rated it as good. Nearly two-fifth of the respondents (38.7 percent) opined that usefulness of the website as good and over one-fourth of them (26.9 percent) rated it as very good. There is a statistically significant difference between students and faculty members in their opinions with regard to overall features of website. It is determined by one-way ANOVA.

### Suggestions to Enhance the Quality of the Website

Based on the findings of the study the following suggestions are put forward to enhance the quality of the website:

- A few colleges provided information about date of last updated. Therefore, it should be mandatory to update websites regularly.
- The college website should cover maximum content covering hyperlinks systematically placed on the page. At the same time, the page should not be overcrowded with the hyperlinks. To avoid overcrowding look, pop up links can be used.
- It should be easy to navigate. Each internal link should cover the link for college home page.

- Search facility provided by 13.72 percent of the colleges and sitemap provided by 13 percent of them. A very few colleges (0.72 percent) are provided FAQ's. Hence, FAQs, sitemap and search facility should be added to the website, which will increase its accessibility.
- Over one-fourth (27.24 percent) of college web sites have separate 'Library link' on the home page. Therefore, engineering college website should include a separate 'library' link.
- None of the college have separate library home page. Hence, the colleges should include a separate library home page.
- Some standards for designing engineering college websites should be evolved.

## CONCLUSION

College websites contain educational features which aim to provide the information and services to its stakeholders in different ways. To achieve these goals, the college website design must go through a number of guidelines for the design to ensure that users are more satisfied with the services of these sites services. The homepages of the college website should be constructed logically, and periodically evaluated using criteria such as access, contact information, authority, currency, content, ease of navigation, etc. College webmaster should pay more attention to the college web design and content making them more attractive to the user community. It would be useful to carry out a more comprehensive study covering more institutions and more diagnosis tools to measure the evaluation criteria of the college websites in Andhra Pradesh.

## REFERENCES

1. Nasajpour MR, Ashrafi-rizi H, Soleymani MR, *et al.* Evaluation of the quality of the college library websites in Iranian medical Universities based on the Stover model. *J Educ Health Promotion.* 2014; 3(121): Available from: <http://www.jehp.net/text.asp?2014/3/1/121/145931>
2. All India Council for Technical Education (AICTE) All India Council For Technical Education Approval Process Handbook (2015 – 2016) [cited 2015]; Available from: [www.aicte-india.org](http://www.aicte-india.org)
3. Panneerselvam P. Analysis of universities website in Tamilnadu: Special attention to library content. *Int J Libr Infor Studies.* 2015; 5(2): 1–9p.
4. Jayasundari, Jeyshankar R. Web credibility of Indian Institute of Management (IIMs) web sites: A Study. *J Adv Libr Infor Sci.* 2014; 3(3): 222–232p.
5. Khatri AB, Baheti SR. Evaluative study of university web sites and their library web pages. *Int J Digital Libr Services.* 2013; 1(3): 1–11p.
6. Kothainayakis S. Web credibility and evaluation of academic websites in Chennai, Kancheepuram and Tiruvallur Districts of Tamil Nadu: an empirical study (Ph.D. Thesis). Chennai: Anna University; 2013.
7. Sife AS, Msoffe GE. User-perceived quality of selected Tanzanian Public University websites. *Library Philosophy and Practice.* 2013; Paper 950. Available from: <http://digitalcommons.unl.edu/libphilprac/950>
8. Kannappanavar BU, Biradar SB. Credibility of dental college websites in Karnataka. *Int J Digital Libr Services.* 2001; 1(1): 62–70p.
9. Islam A, Tsuji K. Evaluation of usage of university websites in Bangladesh. *DESIDOC J Libr Infor Technol.* 2011; 31(6): 469–479p.
10. Haneefa KM, George S. Web based information retrieval pattern of doctoral students in Calicut University. *Anna Libr Infor Studies.* 2010; 57(6): 394–402p.
11. Ramesh Babu B, Narendra Kumar AM, Gopalakrishnan S. Credibility of university websites in Tamil Nadu. *DESIDOC J Libr Infor Tech.* 2009; 29(3): 16–28p.
12. Mustafa SH, Al-Zoua'bi LF. Usability of the academic websites of Jordan's Universities: An evaluation study. 2009 [cited 2016]; Available from: [https://www.researchgate.net/publication/275519174\\_Usability\\_of\\_the\\_Academic\\_Websites\\_of\\_Jordan's\\_Universities\\_An\\_Evaluation\\_Study](https://www.researchgate.net/publication/275519174_Usability_of_the_Academic_Websites_of_Jordan's_Universities_An_Evaluation_Study).

13. Hirwade MA. Websites of Indian universities: An evaluation. Bombay: Himalaya Publishing House; 2006.
14. Tillotson J. Web site evaluation: A survey of undergraduates. *Online Info Rev.* 2002; 26(6): 392–403p.
15. Kapoun J. Five criteria for evaluating web pages. 1998 [cited 2016]; Available from: <https://olinuris.library.cornell.edu/ref/research/webeval.html>
16. Collins BR. Beyond Cruising: Reviewing. *Libr J.* 1996; 121: 122–24p.
17. Kirk EE. Evaluating information found on the Internet. 1996 [cited 2016]; Available from: <https://olinuris.library.cornell.edu/ref/research/webeval.html>
18. Kovacs D, *et al.* A model for planning and providing reference services using Internet resource. *Libr Trends.* 1994, 42: 638–647p.
19. Nielsen J. Usability engineering. Boston: Academic Press; 1993.
20. Rubin J. Handbook of usability testing: how to plan, design and conduct effective tests, John Wiley & Sons: New York; 1994: 330p.
21. Shivabasappa B. Library websites of R and D Institutions of Government of India: an evaluative study (Ph.D. Thesis). Karnataka: Gulbarga University. 2016. DOI: <http://hdl.handle.net/10603/134266>

## APPENDIX

### Top 20 Colleges based on Evaluation Criteria

Code	Rank	Name of the College/University
GU	1	GITAM University
KLU	2	K.L. University
GEC	3	Gudlavalleru Engineering College
ACE	4	Audishankara College of Engineering and Technology
VRSEC	5	Velagapudi Ramakrishna Siddhartha Engineering College
RVR	6	RVR & JC College of Engineering
SVE	7	Sri Vasavi Engineering College
ANIT	8	Anil Neerukonda Institute of Technology & Science
PBRV	9	Parvatha Reddy Babul Reddy Visvodaya Institute of Technology and Science
SITE	10	Sasi Institute of Technology & Engineering
MITS	11	Madanapalle Institute of Technology and Science
SVUE	12	Sri Venkateswara University College of Engineering
GPEC	13	G. Pulla Reddy Engineering College
RMCE	14	Rajeev Gandhi Memorial College of Engineering and Technology
AIT	15	Audisankara Institute of Technology
VU	16	Vignan University
ANUE	17	Aharya Nagarjuna University College of Engineering
DCT	18	Devineni Venkata Ramana & Dr. Himasekhar MIC College of Technology
SVEW	19	Shri Vishnu Engineering College for Women
AUEW	20	Andhra University College of Engineering for Women



# Coupled fixed points of generalized rational type $\mathcal{Z}$ -contraction maps in $b$ -metric spaces

Velisela Amarendra Babu<sup>a</sup>, Dasari Ratna Babu<sup>b</sup>, Nasina Siva Prasad<sup>c,d,\*</sup>

<sup>a</sup>Department of Mathematics, Acharya Nagarjuna University, Guntur - 522 510, India

<sup>b</sup>Department of Mathematics, PSCMR CET, Vijayawada - 520 001, India

<sup>c</sup>Department of Mathematics, Rayalaseema University, Kurnool - 518 007, India

<sup>d</sup>Department of Mathematics, PBR VITS, Kavali- 524 201, India

(Communicated by Abdolrahman Razani)

---

## Abstract

In this paper, we introduce generalized rational type  $\mathcal{Z}$ -contraction maps for a single map  $f : X \times X \rightarrow X$  where  $X$  is a  $b$ -metric space and prove the existence and uniqueness of coupled fixed points. We extend it to a pair of maps by defining generalized rational type  $\mathcal{Z}$ -contraction pair of maps and prove the existence of common coupled fixed points in complete  $b$ -metric spaces. We provide examples in support of our results.

Keywords: coupled fixed points,  $b$ -metric space, generalized rational type  $\mathcal{Z}$ -contraction maps.  
2020 MSC: 47H10, 54H25.

---

## 1 Introduction

Banach contraction principle plays an important role in solving nonlinear functional analysis. In the direction of generalization of contraction condition, Dass and Gupta [13] initiated a contraction condition involving rational expression and established the existence of fixed points in complete metric spaces.

In the direction of generalization of metric spaces, Bourbaki [10] and Bakhtin [5] initiated the idea of  $b$ -metric spaces. The concept of  $b$ -metric space or metric type space was introduced by Czerwik [11] as a generalization of metric space. Afterwards, many authors studied the existence of fixed points for a single-valued and multi-valued mappings in  $b$ -metric spaces under certain contraction conditions. For more details, we refer [2, 3, 8, 9, 12, 14, 16, 18, 23, 24].

In 2006, Bhaskar and Lakshmikantham [6] introduced the notion of coupled fixed point and established the existence of coupled fixed points for mixed monotone mappings in ordered metric spaces. Later, Lakshmikantham and Ćirić [19] introduced the notion of coupled coincidence points of mappings in two variables. Afterwards, many authors studied coupled fixed point theorems, we refer [20, 22, 25, 26].

---

\*Corresponding author

Email addresses: amarendravelisela@gmail.com (Velisela Amarendra Babu), ratnababud@gmail.com (Dasari Ratna Babu), n.sivaprasadmsc@gmail.com (Nasina Siva Prasad)

## 2 Preliminaries

**Definition 2.1.** [11] Let  $X$  be a non-empty set. A function  $d : X \times X \rightarrow [0, \infty)$  is said to be a  $b$ -metric if the following conditions are satisfied: for any  $x, y, z \in X$

- (i)  $0 \leq d(x, y)$  and  $d(x, y) = 0$  if and only if  $x = y$ ,
- (ii)  $d(x, y) = d(y, x)$ ,
- (iii) there exists  $s \geq 1$  such that  $d(x, z) \leq s[d(x, y) + d(y, z)]$ .

In this case, the pair  $(X, d)$  is called a  $b$ -metric space with coefficient  $s$ .

Every metric space is a  $b$ -metric space with  $s = 1$ . In general, every  $b$ -metric space is not a metric space.

**Definition 2.2.** [9] Let  $(X, d)$  be a  $b$ -metric space.

- (i) A sequence  $\{x_n\}$  in  $X$  is called  $b$ -convergent if there exists  $x \in X$  such that  $d(x_n, x) \rightarrow 0$  as  $n \rightarrow \infty$ . In this case, we write  $\lim_{n \rightarrow \infty} x_n = x$ .
- (ii) A sequence  $\{x_n\}$  in  $X$  is called  $b$ -Cauchy if  $d(x_n, x_m) \rightarrow 0$  as  $n, m \rightarrow \infty$ .
- (iii) A  $b$ -metric space  $(X, d)$  is said to be a complete  $b$ -metric space if every  $b$ -Cauchy sequence in  $X$  is  $b$ -convergent in  $X$ .
- (iv) A set  $B \subset X$  is said to be  $b$ -closed if for any sequence  $\{x_n\}$  in  $B$  such that  $\{x_n\}$  is  $b$ -convergent to  $z \in X$  then  $z \in B$ .

In general, a  $b$ -metric is not necessarily continuous.

In this paper, we denote  $\mathbb{R}^+ = [0, \infty)$  and  $\mathbb{N}$  is the set of all natural numbers.

**Example 2.3.** [15] Let  $X = \mathbb{N} \cup \{\infty\}$ . We define a mapping  $d : X \times X \rightarrow \mathbb{R}^+$  as follows:

$$d(m, n) = \begin{cases} 0 & \text{if } m = n, \\ |\frac{1}{m} - \frac{1}{n}| & \text{if one of } m, n \text{ is even and the other is even or } \infty, \\ 5 & \text{if one of } m, n \text{ is odd and the other is odd or } \infty, \\ 2 & \text{otherwise.} \end{cases}$$

Then  $(X, d)$  is a  $b$ -metric space with coefficient  $s = \frac{5}{2}$ .

**Definition 2.4.** [9] Let  $(X, d_X)$  and  $(Y, d_Y)$  be two  $b$ -metric spaces. A function  $f : X \rightarrow Y$  is a  $b$ -continuous at a point  $x \in X$ , if it is  $b$ -sequentially continuous at  $x$ . i.e., whenever  $\{x_n\}$  is  $b$ -convergent to  $x$  we have  $f x_n$  is  $b$ -convergent to  $f x$ .

**Definition 2.5.** [6] Let  $X$  be a nonempty set and  $f : X \times X \rightarrow X$  be a mapping. Then we say that an element  $(x, y) \in X \times X$  is a coupled fixed point, if  $f(x, y) = x$  and  $f(y, x) = y$ .

**Definition 2.6.** [19] Let  $X$  be a nonempty set. Let  $F : X \times X \rightarrow X$  and  $g : X \rightarrow X$  be two mappings. An element  $(x, y) \in X \times X$  is called

- (i) a coupled coincidence point of the mappings  $F$  and  $g$  if  $F(x, y) = gx$  and  $F(y, x) = gy$ ;
- (ii) a common coupled fixed point of mappings  $F$  and  $g$  if  $F(x, y) = gx = x$  and  $F(y, x) = gy = y$ .

The following lemma is useful in proving our main results.

**Lemma 2.7.** [1] Let  $(X, d)$  be a  $b$ -metric space with coefficient  $s \geq 1$ . Suppose that  $\{x_n\}$  and  $\{y_n\}$  are  $b$ -convergent to  $x$  and  $y$  respectively. Then we have

$$\frac{1}{s^2}d(x, y) \leq \liminf_{n \rightarrow \infty} d(x_n, y_n) \leq \limsup_{n \rightarrow \infty} d(x_n, y_n) \leq s^2d(x, y).$$

In particular, if  $x = y$ , then we have  $\lim_{n \rightarrow \infty} d(x_n, y_n) = 0$ . Moreover for each  $z \in X$  we have

$$\frac{1}{s}d(x, z) \leq \liminf_{n \rightarrow \infty} d(x_n, z) \leq \limsup_{n \rightarrow \infty} d(x_n, z) \leq sd(x, z).$$

In 2015, Khojasteh, Shukla and Radenović [17] introduced simulation function and defined  $\mathcal{Z}$ -contraction with respect to a simulation function.

**Definition 2.8.** [17] A simulation function is a mapping  $\zeta : \mathbb{R}^+ \times \mathbb{R}^+ \rightarrow (-\infty, \infty)$  satisfying the following conditions:

- ( $\zeta_1$ )  $\zeta(0, 0) = 0$ ;
- ( $\zeta_2$ )  $\zeta(t, s) < s - t$  for all  $s, t > 0$ ;
- ( $\zeta_3$ ) if  $\{t_n\}, \{s_n\}$  are sequences in  $(0, \infty)$  such that  $\lim_{n \rightarrow \infty} t_n = \lim_{n \rightarrow \infty} s_n = l \in (0, \infty)$  then  $\limsup_{n \rightarrow \infty} \zeta(t_n, s_n) < 0$ .

**Remark 2.9.** [4] Let  $\zeta$  be a simulation function. If  $\{t_n\}, \{s_n\}$  are sequences in  $(0, \infty)$  such that  $\lim_{n \rightarrow \infty} t_n = \lim_{n \rightarrow \infty} s_n = l \in (0, \infty)$  then  $\limsup_{n \rightarrow \infty} \zeta(kt_n, s_n) < 0$  for any  $k > 1$ .

The following are examples of simulation functions.

**Example 2.10.** [4] Let  $\zeta : \mathbb{R}^+ \times \mathbb{R}^+ \rightarrow (-\infty, \infty)$  be defined by

- (i)  $\zeta(t, s) = \lambda s - t$  for all  $t, s \in \mathbb{R}^+$ , where  $\lambda \in [0, 1)$ ;
- (ii)  $\zeta(t, s) = \frac{s}{1+s} - t$  for all  $s, t \in \mathbb{R}^+$ ;
- (iii)  $\zeta(t, s) = s - kt$  for all  $t, s \in \mathbb{R}^+$ , where  $k > 1$ ;
- (iv)  $\zeta(t, s) = \frac{1}{1+s} - (1+t)$  for all  $s, t \in \mathbb{R}^+$ ;
- (v)  $\zeta(t, s) = \frac{1}{k+s} - t$  for all  $s, t \in \mathbb{R}^+$  where  $k > 1$ .

**Definition 2.11.** [17] Let  $(X, d)$  be a metric space and  $f : X \rightarrow X$  be a selfmap of  $X$ . We say that  $f$  is a  $\mathcal{Z}$ -contraction with respect to  $\zeta$  if there exists a simulation function  $\zeta$  such that

$$\zeta(d(fx, fy), d(x, y)) \geq 0 \text{ for all } x, y \in X.$$

**Theorem 2.12.** [17] Let  $(X, d)$  be a complete metric space and  $f : X \rightarrow X$  be a  $\mathcal{Z}$ -contraction with respect to a certain simulation function  $\zeta$ . Then for every  $x_0 \in X$ , the Picard sequence  $\{f^n x_0\}$  converges in  $X$  and  $\lim_{n \rightarrow \infty} f^n x_0 = u$  (say) in  $X$  and  $u$  is the unique fixed point of  $f$  in  $X$ .

Recently, Olgun, Bicer and Alyildiz [21] proved the following result in complete metric spaces.

**Theorem 2.13.** [21] Let  $(X, d)$  be a complete metric space and  $f : X \rightarrow X$  be a selfmap on  $X$ . If there exists a simulation function  $\zeta$  such that

$$\zeta(d(fx, fy), M(x, y)) \geq 0$$

for all  $x, y \in X$ , where  $M(x, y) = \max\{d(x, y), d(x, fx), d(y, fy), \frac{d(x, fy) + d(y, fx)}{2}\}$ , then for every  $x_0 \in X$ , the Picard sequence  $\{f^n x_0\}$  converges in  $X$  and  $\lim_{n \rightarrow \infty} f^n x_0 = u$  (say) in  $X$  and  $u$  is the unique fixed point of  $f$  in  $X$ .

In 2018, Babu, Dula and Kumar [4] extended Theorem 1.13 [21] to pair of selfmaps in the setting of  $b$ -metric spaces as follows.

**Theorem 2.14.** [4] Let  $(X, d)$  be a complete  $b$ -metric space with coefficient  $s \geq 1$  and  $f, g : X \rightarrow X$  be selfmaps on  $X$ . If there exists a simulation function  $\zeta$  such that

$$\zeta(s^4 d(fx, gy), M(x, y)) \geq 0$$

for all  $x, y \in X$ , where  $M(x, y) = \max\{d(x, y), d(x, fx), d(y, gy), \frac{d(x, gy) + d(y, fx)}{2s}\}$ , then  $f$  and  $g$  have a unique common fixed point in  $X$ , provided either  $f$  or  $g$  is  $b$ -continuous.

Recently, Bindu and Malhotra [7] proved the existence of common coupled fixed points as follows:

**Theorem 2.15.** Let  $(X, d)$  be a complete  $b$ -metric space with parameter  $s \geq 1$  and let the mappings  $S, T : X \times X \rightarrow X$  satisfy

$$\begin{aligned} d(S(x, y), T(u, v)) \leq & \alpha_1 \frac{d(x, u) + d(y, v)}{2} + \alpha_2 \frac{d(x, S(x, y))d(u, T(u, v))}{1 + d(x, u) + d(y, v) + d(u, S(x, y))} + \alpha_3 \frac{d(u, S(x, y))d(x, T(u, v))}{1 + d(x, u) + d(y, v) + d(u, S(x, y))} \\ & + \alpha_4 \frac{d(S(x, y), T(u, v))d(x, u)}{1 + d(x, u) + d(y, v) + d(u, S(x, y))} + \alpha_5 \frac{d(S(x, y), T(u, v))d(y, v)}{1 + d(x, u) + d(y, v) + d(u, S(x, y))} \\ & + \alpha_6 \frac{d(u, T(u, v))d(y, v)}{1 + d(x, u) + d(y, v) + d(u, S(x, y))} + \alpha_7 \frac{d(u, S(x, y))d(x, u)}{1 + d(x, u) + d(y, v) + d(u, S(x, y))} \\ & + \alpha_8 \frac{d(u, S(x, y))d(y, v)}{1 + d(x, u) + d(y, v) + d(u, S(x, y))} + \alpha_9 \max\{d(u, S(x, y)), d(S(x, y), T(u, v))\} \end{aligned}$$

for all  $x, y, u, v \in X$  and  $\alpha_i \geq 0, i = 1, 2, \dots, 9$  with  $s\alpha_1 + \alpha_2 + \alpha_4 + \alpha_5 + \alpha_6 + s\alpha_9 < 1$  and  $\alpha_1 + \alpha_3 + \alpha_4 + \alpha_5 + \alpha_7 + \alpha_8 + \alpha_9 < 1$ . Then  $S$  and  $T$  have a unique common coupled fixed point in  $X$ .

Motivated by the works of Bindu and Malhotra [7], in Section 3, we introduce generalized rational type  $\mathcal{Z}$ -contraction maps for a single map  $f : X \times X \rightarrow X$  where  $X$  is a  $b$ -metric space and we extend it to a pair of maps. In Section 4, we prove the existence and uniqueness of coupled fixed points and common coupled fixed points in complete  $b$ -metric spaces. Examples are provided in support of our results in Section 5.

### 3 Generalized rational type $\mathcal{Z}$ -contraction maps

The following we introduce generalized rational type  $\mathcal{Z}$ -contraction maps for a single and a pair of maps in  $b$ -metric spaces as follows:

**Definition 3.1.** Let  $(X, d)$  be a  $b$ -metric space with coefficient  $s \geq 1$  and  $f : X \times X \rightarrow X$  be a map. We say that  $f$  is a generalized rational type  $\mathcal{Z}$ -contraction map, if there exists a simulation function  $\zeta$  such that

$$\zeta(s^3 d(f(x, y), f(u, v)), M(x, y, u, v)) \geq 0 \quad \text{for all } x, y, u, v \in X, \quad (3.1)$$

where

$$M(x, y, u, v) = \max\left\{\frac{d(x, u) + d(y, v)}{2s}, \frac{d(x, f(x, y))d(u, f(u, v))}{1 + d(x, u) + d(y, v) + d(u, f(x, y))}, \frac{d(u, f(x, y))d(x, f(u, v))}{1 + d(x, u) + d(y, v) + d(u, f(x, y))}, \frac{d(f(x, y), f(u, v))d(x, u)}{1 + d(x, u) + d(y, v) + d(u, f(x, y))}, \frac{d(f(x, y), f(u, v))d(y, v)}{1 + d(x, u) + d(y, v) + d(u, f(x, y))}, \frac{d(u, f(u, v))d(y, v)}{1 + d(x, u) + d(y, v) + d(u, f(x, y))}, \frac{d(u, f(x, y))d(x, u)}{1 + d(x, u) + d(y, v) + d(u, f(x, y))}, \frac{d(u, f(x, y))d(y, v)}{1 + d(x, u) + d(y, v) + d(u, f(x, y))}, \max\{d(u, f(x, y)), d(f(x, y), f(u, v))\}\right\}.$$

**Remark 3.2.** It is clear that from definition of simulation function that  $\zeta(a, b) < 0$ , for all  $a \geq b > 0$ . Therefore if  $f$  satisfies (3.1), then

$$s^3 d(f(x, y), f(u, v)) < M(x, y, u, v), \quad \text{for all } x, y, u, v \in X.$$

**Example 3.3.** Let  $X = [0, 1]$  and let  $d : X \times X \rightarrow \mathbb{R}^+$  defined by

$$d(x, y) = \begin{cases} 0 & \text{if } x = y \\ (x + y)^2 & \text{if } x \neq y. \end{cases}$$

Then clearly  $(X, d)$  is a  $b$ -metric space with coefficient  $s = 2$ . We define  $f : X \times X \rightarrow X$  by  $f(x, y) = \frac{\log(1+x^2+y^2)}{16}$  for all  $x \in [0, 1]$  and

$$\zeta : \mathbb{R}^+ \times \mathbb{R}^+ \rightarrow (-\infty, \infty) \quad \text{by} \quad \zeta(t, s) = \frac{1}{2}s - t, \quad t \geq 0, s \geq 0.$$

$$\begin{aligned} \text{We have } s^3 d(f(x, y), f(u, v)) &= 8 \left[ \frac{\log(1+x^2+y^2)}{16} + \frac{\log(1+u^2+v^2)}{16} \right]^2 \\ &\leq \frac{1}{8} [(x+u)^2 + (y+v)^2] \\ &= \frac{1}{2} \left( \frac{d(x, u) + d(y, v)}{2s} \right) \\ &\leq \frac{1}{2} \left( \max\left\{ \frac{d(x, u) + d(y, v)}{2s}, \frac{d(x, f(x, y))d(u, f(u, v))}{1 + d(x, u) + d(y, v) + d(u, f(x, y))}, \frac{d(u, f(x, y))d(x, f(u, v))}{1 + d(x, u) + d(y, v) + d(u, f(x, y))}, \frac{d(f(x, y), f(u, v))d(x, u)}{1 + d(x, u) + d(y, v) + d(u, f(x, y))}, \frac{d(f(x, y), f(u, v))d(y, v)}{1 + d(x, u) + d(y, v) + d(u, f(x, y))}, \frac{d(u, f(u, v))d(y, v)}{1 + d(x, u) + d(y, v) + d(u, f(x, y))}, \frac{d(u, f(x, y))d(x, u)}{1 + d(x, u) + d(y, v) + d(u, f(x, y))}, \frac{d(u, f(x, y))d(y, v)}{1 + d(x, u) + d(y, v) + d(u, f(x, y))}, \max\{d(u, f(x, y)), d(f(x, y), f(u, v))\} \right\} \right). \end{aligned}$$

Therefore  $f$  is a generalized rational type  $\mathcal{Z}$ -contraction map.

**Definition 3.4.** Let  $(X, d)$  be a  $b$ -metric space with coefficient  $s \geq 1$  and  $f, g : X \times X \rightarrow X$  be two maps. We say that the pair  $(f, g)$  is a generalized rational type  $\mathcal{Z}$ -contraction maps, if there exists a simulation function  $\zeta$  such that

$$\zeta(s^3 d(f(x, y), g(u, v)), M(x, y, u, v)) \geq 0, \quad \text{for all } x, y, u, v \in X, \quad (3.2)$$

where

$$M(x, y, u, v) = \max\left\{\frac{d(x, u) + d(y, v)}{2s}, \frac{d(x, f(x, y))d(u, g(u, v))}{1 + d(x, u) + d(y, v) + d(u, f(x, y))}, \frac{d(u, f(x, y))d(x, g(u, v))}{1 + d(x, u) + d(y, v) + d(u, f(x, y))}, \frac{d(f(x, y), g(u, v))d(x, u)}{1 + d(x, u) + d(y, v) + d(u, f(x, y))}, \frac{d(f(x, y), g(u, v))d(y, v)}{1 + d(x, u) + d(y, v) + d(u, f(x, y))}, \frac{d(u, g(u, v))d(y, v)}{1 + d(x, u) + d(y, v) + d(u, f(x, y))}, \frac{d(u, f(x, y))d(x, u)}{1 + d(x, u) + d(y, v) + d(u, f(x, y))}, \frac{d(u, f(x, y))d(y, v)}{1 + d(x, u) + d(y, v) + d(u, f(x, y))}, \max\{d(u, f(x, y)), d(f(x, y), g(u, v))\}\right\}.$$

**Remark 3.5.** It is clear that from definition of simulation function that  $\zeta(a, b) < 0$ , for all  $a \geq b > 0$ . Therefore if  $f$  satisfies (3.2), then

$$s^3 d(f(x, y), g(u, v)) < M(x, y, u, v), \text{ for all } x, y, u, v \in X.$$

**Example 3.6.** Let  $X = [0, 1]$  and let  $d : X \times X \rightarrow \mathbb{R}^+$  defined by

$$d(x, y) = \begin{cases} 0 & \text{if } x = y \\ (x + y)^2 & \text{if } x \neq y. \end{cases}$$

Then clearly  $(X, d)$  is a  $b$ -metric space with coefficient  $s = 2$ . We define  $f, g : X \times X \rightarrow X$  by

$$f(x, y) = \begin{cases} \frac{\log(1+x+y)}{16} & \text{if } x, y \in [0, \frac{1}{2}] \\ \frac{1}{32} & \text{if } x, y \in [\frac{1}{2}, 1] \end{cases} \text{ and } g(x, y) = \begin{cases} \frac{xe^y}{8} & \text{if } x, y \in [0, \frac{1}{2}] \\ \log(x + y) & \text{if } x, y \in [\frac{1}{2}, 1]. \end{cases}$$

$\zeta : \mathbb{R}^+ \times \mathbb{R}^+ \rightarrow (-\infty, \infty)$  by  $\zeta(t, s) = \frac{99}{100}s - t, t \geq 0, s \geq 0$ .

**Case (i).**  $x, y, u, v \in [0, \frac{1}{2}]$ .

$$\begin{aligned} s^3 d(f(x, y), g(u, v)) &= 8 \left[ \frac{\log(1+x+y)}{16} + \frac{ue^v}{8} \right]^2 \\ &\leq \frac{99}{400} [(x+u)^2 + (y+v)^2] \\ &= \frac{99}{100} \left( \frac{d(x,u)+d(y,v)}{2s} \right) \\ &\leq \frac{99}{100} \left( \max \left\{ \frac{d(x,u)+d(y,v)}{2s}, \frac{d(x,f(x,y))d(u,g(u,v))}{1+d(x,u)+d(y,v)+d(u,f(x,y))}, \frac{d(u,f(x,y))d(x,g(u,v))}{1+d(x,u)+d(y,v)+d(u,f(x,y))}, \right. \right. \\ &\quad \left. \frac{d(f(x,y),g(u,v))d(x,u)}{1+d(x,u)+d(y,v)+d(u,f(x,y))}, \frac{d(f(x,y),g(u,v))d(y,v)}{1+d(x,u)+d(y,v)+d(u,f(x,y))}, \frac{d(u,g(u,v))d(y,v)}{1+d(x,u)+d(y,v)+d(u,f(x,y))}, \right. \\ &\quad \left. \frac{d(u,f(x,y))d(x,u)}{1+d(x,u)+d(y,v)+d(u,f(x,y))}, \frac{d(u,f(x,y))d(y,v)}{1+d(x,u)+d(y,v)+d(u,f(x,y))}, \right. \\ &\quad \left. \max \{ d(u, f(x, y)), d(f(x, y), g(u, v)) \} \right\} \right). \end{aligned}$$

**Case (ii).**  $x, y, u, v \in [\frac{1}{2}, 1]$ .

$$\begin{aligned} s^3 d(f(x, y), g(u, v)) &= 8 \left[ \frac{1}{32} + \log(u+v) \right]^2 \\ &\leq \frac{99}{400} [(x+u)^2 + (y+v)^2] \\ &= \frac{99}{100} \left( \frac{d(x,u)+d(y,v)}{2s} \right) \\ &\leq \frac{99}{100} \left( \max \left\{ \frac{d(x,u)+d(y,v)}{2s}, \frac{d(x,f(x,y))d(u,g(u,v))}{1+d(x,u)+d(y,v)+d(u,f(x,y))}, \frac{d(u,f(x,y))d(x,g(u,v))}{1+d(x,u)+d(y,v)+d(u,f(x,y))}, \right. \right. \\ &\quad \left. \frac{d(f(x,y),g(u,v))d(x,u)}{1+d(x,u)+d(y,v)+d(u,f(x,y))}, \frac{d(f(x,y),g(u,v))d(y,v)}{1+d(x,u)+d(y,v)+d(u,f(x,y))}, \frac{d(u,g(u,v))d(y,v)}{1+d(x,u)+d(y,v)+d(u,f(x,y))}, \right. \\ &\quad \left. \frac{d(u,f(x,y))d(x,u)}{1+d(x,u)+d(y,v)+d(u,f(x,y))}, \frac{d(u,f(x,y))d(y,v)}{1+d(x,u)+d(y,v)+d(u,f(x,y))}, \right. \\ &\quad \left. \max \{ d(u, f(x, y)), d(f(x, y), g(u, v)) \} \right\} \right). \end{aligned}$$

**Case (iii).**  $x, y \in [\frac{1}{2}, 1], u, v \in [0, \frac{1}{2}]$ .

$$\begin{aligned} s^3 d(f(x, y), g(u, v)) &= 8 \left[ \frac{1}{16} + \frac{ue^v}{4} \right]^2 \\ &\leq \frac{99}{400} [(x+u)^2 + (y+v)^2] \\ &= \frac{99}{100} \left( \frac{d(x,u)+d(y,v)}{2s} \right) \\ &\leq \frac{99}{100} \left( \max \left\{ \frac{d(x,u)+d(y,v)}{2s}, \frac{d(x,f(x,y))d(u,g(u,v))}{1+d(x,u)+d(y,v)+d(u,f(x,y))}, \frac{d(u,f(x,y))d(x,g(u,v))}{1+d(x,u)+d(y,v)+d(u,f(x,y))}, \right. \right. \\ &\quad \left. \frac{d(f(x,y),g(u,v))d(x,u)}{1+d(x,u)+d(y,v)+d(u,f(x,y))}, \frac{d(f(x,y),g(u,v))d(y,v)}{1+d(x,u)+d(y,v)+d(u,f(x,y))}, \frac{d(u,g(u,v))d(y,v)}{1+d(x,u)+d(y,v)+d(u,f(x,y))}, \right. \\ &\quad \left. \frac{d(u,f(x,y))d(x,u)}{1+d(x,u)+d(y,v)+d(u,f(x,y))}, \frac{d(u,f(x,y))d(y,v)}{1+d(x,u)+d(y,v)+d(u,f(x,y))}, \right. \\ &\quad \left. \max \{ d(u, f(x, y)), d(f(x, y), g(u, v)) \} \right\} \right). \end{aligned}$$

**Case (iv).**  $x, y \in [0, \frac{1}{2}], u, v \in [\frac{1}{2}, 1]$ .

$$\begin{aligned} s^3 d(f(x, y), g(u, v)) &= 8 \left[ \frac{\log(1+x+y)}{8} + \log(x+y) \right]^2 \\ &\leq \frac{99}{400} [(x+u)^2 + (y+v)^2] \\ &= \frac{99}{100} \left( \frac{d(x,u)+d(y,v)}{2s} \right) \\ &\leq \frac{99}{100} \left( \max \left\{ \frac{d(x,u)+d(y,v)}{2s}, \frac{d(x,f(x,y))d(u,g(u,v))}{1+d(x,u)+d(y,v)+d(u,f(x,y))}, \frac{d(u,f(x,y))d(x,g(u,v))}{1+d(x,u)+d(y,v)+d(u,f(x,y))}, \right. \right. \\ &\quad \left. \frac{d(f(x,y),g(u,v))d(x,u)}{1+d(x,u)+d(y,v)+d(u,f(x,y))}, \frac{d(f(x,y),g(u,v))d(y,v)}{1+d(x,u)+d(y,v)+d(u,f(x,y))}, \frac{d(u,g(u,v))d(y,v)}{1+d(x,u)+d(y,v)+d(u,f(x,y))}, \right. \\ &\quad \left. \frac{d(u,f(x,y))d(x,u)}{1+d(x,u)+d(y,v)+d(u,f(x,y))}, \frac{d(u,f(x,y))d(y,v)}{1+d(x,u)+d(y,v)+d(u,f(x,y))}, \right. \\ &\quad \left. \max \{ d(u, f(x, y)), d(f(x, y), g(u, v)) \} \right\} \right). \end{aligned}$$

Therefore the pair  $(f, g)$  is a generalized rational type  $\mathcal{Z}$ -contraction maps.

## 4 Main results

**Theorem 4.1.** Let  $(X, d)$  be a complete  $b$ -metric space with coefficient  $s \geq 1$  and  $f : X \times X \rightarrow X$  be a rational type  $\mathcal{Z}$ -contraction map. Then  $f$  has a unique coupled fixed point in  $X$ .

**Proof .** Let  $x_0$  and  $y_0$  be arbitrary points in  $X$ . We define  $x_{i+1} = f(x_i, y_i)$  and  $y_{i+1} = f(y_i, x_i)$  for  $i = 0, 1, 2, \dots$ . We consider

$$\zeta(s^3 d(x_{n+1}, x_{n+2}), M(x_n, y_n, x_{n+1}, y_{n+1})) = \zeta(s^3 d(f(x_n, y_n), f(x_{n+1}, y_{n+1})), M(x_n, y_n, x_{n+1}, y_{n+1})) \geq 0, \quad (4.1)$$

where

$$\begin{aligned} M(x_n, y_n, x_{n+1}, y_{n+1}) &= \max\left\{\frac{d(x_n, x_{n+1}) + d(y_n, y_{n+1})}{2s}, \frac{d(x_n, f(x_n, y_n))d(x_{n+1}, f(x_{n+1}, y_{n+1}))}{1 + d(x_n, x_{n+1}) + d(y_n, y_{n+1}) + d(x_{n+1}, f(x_n, y_n))}, \right. \\ &\frac{d(x_{n+1}, f(x_n, y_n))d(x_n, f(x_{n+1}, y_{n+1}))}{1 + d(x_n, x_{n+1}) + d(y_n, y_{n+1}) + d(x_{n+1}, f(x_n, y_n))}, \frac{d(f(x_n, y_n), f(x_{n+1}, y_{n+1}))d(x_n, x_{n+1})}{1 + d(x_n, x_{n+1}) + d(y_n, y_{n+1}) + d(x_{n+1}, f(x_n, y_n))}, \\ &\frac{d(f(x_n, y_n), f(x_{n+1}, y_{n+1}))d(y_n, y_{n+1})}{1 + d(x_n, x_{n+1}) + d(y_n, y_{n+1}) + d(x_{n+1}, f(x_n, y_n))}, \frac{d(x_{n+1}, f(x_{n+1}, y_{n+1}))d(y_n, y_{n+1})}{1 + d(x_n, x_{n+1}) + d(y_n, y_{n+1}) + d(x_{n+1}, f(x_n, y_n))}, \\ &\frac{d(x_{n+1}, f(x_n, y_n))d(x_n, x_{n+1})}{1 + d(x_n, x_{n+1}) + d(y_n, y_{n+1}) + d(x_{n+1}, f(x_n, y_n))}, \frac{d(x_{n+1}, f(x_n, y_n))d(y_n, y_{n+1})}{1 + d(x_n, x_{n+1}) + d(y_n, y_{n+1}) + d(x_{n+1}, f(x_n, y_n))}, \\ &\left. \max\{d(x_{n+1}, f(x_n, y_n)), d(f(x_n, y_n), f(x_{n+1}, y_{n+1}))\}\right\} \\ &= \max\left\{\frac{d(x_n, x_{n+1}) + d(y_n, y_{n+1})}{2s}, \frac{d(x_n, x_{n+1})d(x_{n+1}, x_{n+2})}{1 + d(x_n, x_{n+1}) + d(y_n, y_{n+1}) + d(x_{n+1}, x_{n+1})}, \right. \\ &\frac{d(x_{n+1}, x_{n+1})d(x_n, x_{n+2})}{1 + d(x_n, x_{n+1}) + d(y_n, y_{n+1}) + d(x_{n+1}, x_{n+1})}, \frac{d(x_{n+1}, x_{n+2})d(x_n, x_{n+1})}{1 + d(x_n, x_{n+1}) + d(y_n, y_{n+1}) + d(x_{n+1}, x_{n+1})}, \\ &\frac{d(x_{n+1}, x_{n+2})d(y_n, y_{n+1})}{1 + d(x_n, x_{n+1}) + d(y_n, y_{n+1}) + d(x_{n+1}, x_{n+1})}, \frac{d(x_{n+1}, x_{n+2})d(y_n, y_{n+1})}{1 + d(x_n, x_{n+1}) + d(y_n, y_{n+1}) + d(x_{n+1}, x_{n+1})}, \\ &\frac{d(x_{n+1}, x_{n+1})d(x_n, x_{n+1})}{1 + d(x_n, x_{n+1}) + d(y_n, y_{n+1}) + d(x_{n+1}, x_{n+1})}, \frac{d(x_{n+1}, x_{n+1})d(y_n, y_{n+1})}{1 + d(x_n, x_{n+1}) + d(y_n, y_{n+1}) + d(x_{n+1}, x_{n+1})}, \\ &\left. \max\{d(x_{n+1}, x_{n+1}), d(x_{n+1}, x_{n+2})\}\right\} \\ &\leq \max\left\{\frac{d(x_n, x_{n+1}) + d(y_n, y_{n+1})}{2s}, d(x_{n+1}, x_{n+2})\right\}. \end{aligned}$$

If  $M(x_n, y_n, x_{n+1}, y_{n+1}) = d(x_{n+1}, x_{n+2})$  then from (4.1), we have

$$0 \leq \zeta(s^3 d(x_{n+1}, x_{n+2}), M(x_n, y_n, x_{n+1}, y_{n+1})) = \zeta(s^3 d(x_{n+1}, x_{n+2}), d(x_{n+1}, x_{n+2})) < d(x_{n+1}, x_{n+2}) - s^3 d(x_{n+1}, x_{n+2}),$$

which is a contradiction. Therefore

$$d(x_{n+1}, x_{n+2}) \leq \frac{d(x_n, x_{n+1}) + d(y_n, y_{n+1})}{2s} \quad (4.2)$$

for all  $n = 0, 1, 2, \dots$ . Similarly, we can prove that

$$d(y_{n+1}, y_{n+2}) \leq \frac{d(y_n, y_{n+1}) + d(x_n, x_{n+1})}{2s} \quad (4.3)$$

for all  $n = 0, 1, 2, \dots$ . Adding the inequalities (4.2) and (4.3), we have

$$d(x_{n+1}, x_{n+2}) + d(y_{n+1}, y_{n+2}) \leq h[d(x_n, x_{n+1}) + d(y_n, y_{n+1})],$$

where  $h = \frac{1}{2s} < 1$ . Also, it is easy to see that

$$d(x_n, x_{n+1}) + d(y_n, y_{n+1}) \leq h[d(x_{n-1}, x_n) + d(y_{n-1}, y_n)].$$

Therefore

$$d(x_{n+1}, x_{n+2}) + d(y_{n+1}, y_{n+2}) \leq h^2[d(x_{n-1}, x_n) + d(y_{n-1}, y_n)].$$

Continuing in the same way, we get that

$$d(x_{n+1}, x_{n+2}) + d(y_{n+1}, y_{n+2}) \leq h^n[d(x_0, x_1) + d(y_0, y_1)].$$

For  $m > n, m, n \in \mathbb{N}$ , we have

$$\begin{aligned} d(x_n, x_m) + d(y_n, y_m) &\leq s[d(x_n, x_{n+1}) + d(x_{n+1}, x_m)] + s[d(y_n, y_{n+1}) + d(y_{n+1}, y_m)] \\ &\leq s[d(x_n, x_{n+1}) + d(y_n, y_{n+1})] + s^2[d(x_{n+1}, x_{n+2}) + d(x_{n+2}, x_m)] \\ &\quad + s^2[d(y_{n+1}, y_{n+2}) + d(y_{n+2}, y_m)] \\ &= s[d(x_n, x_{n+1}) + d(y_n, y_{n+1})] + s^2[d(x_{n+1}, x_{n+2}) + d(y_{n+1}, y_{n+2})] \\ &\quad + s^2[d(x_{n+2}, x_m) + d(y_{n+2}, y_m)] \dots + s^{m-n}[d(x_{m-1}, x_m) + d(y_{m-1}, y_m)] \\ &\leq [sh^n + s^2h^{n+1} + \dots + s^{m-n}h^{m-1}][d(x_0, x_1) + d(y_0, y_1)] \\ &\leq sh^n[1 + sh + (sh)^2 \dots + (sh)^{m-1} + \dots][d(x_0, x_1) + d(y_0, y_1)] \\ &= sh^n\left(\frac{1}{1-sh}\right)[d(x_0, x_1) + d(y_0, y_1)] \rightarrow 0 \text{ as } n \rightarrow \infty. \end{aligned}$$

Therefore  $\{x_n\}$  and  $\{y_n\}$  are  $b$ -Cauchy sequences in  $X$ . Since  $X$  is  $b$ -complete, there exist  $x, y \in X$  such that  $x_n \rightarrow x$  and  $y_n \rightarrow y$  as  $n \rightarrow \infty$ . We now prove that  $x = f(x, y)$  and  $y = f(y, x)$ . On the contrary suppose that  $x \neq f(x, y)$  and  $y \neq f(y, x)$ . We now consider

$$\zeta(s^3 d(f(x, y), x_{n+1}), M(x, y, x_n, y_n)) = \zeta(s^3 d(f(x, y), f(x_n, y_n)), M(x, y, x_n, y_n)) \geq 0, \quad (4.4)$$

$$\begin{aligned}
\text{where } M(x, y, x_n, y_n) &= \max\left\{\frac{d(x, x_n) + d(y, y_n)}{2s}, \frac{d(x, f(x, y))d(x_n, f(x_n, y_n))}{1 + d(x, x_n) + d(y, y_n) + d(x_n, f(x, y))}, \right. \\
&\quad \frac{d(x_n, f(x, y))d(x, f(x_n, y_n))}{1 + d(x, x_n) + d(y, y_n) + d(x_n, f(x, y))}, \frac{d(f(x, y), f(x_n, y_n))d(x, x_n)}{1 + d(x, x_n) + d(y, y_n) + d(x_n, f(x, y))}, \\
&\quad \frac{d(f(x, y), f(x_n, y_n))d(y, y_n)}{1 + d(x, x_n) + d(y, y_n) + d(x_n, f(x, y))}, \frac{d(x_n, f(x_n, y_n))d(y, y_n)}{1 + d(x, x_n) + d(y, y_n) + d(x_n, f(x, y))}, \\
&\quad \frac{d(x_n, f(x, y))d(x, x_n)}{1 + d(x, x_n) + d(y, y_n) + d(x_n, f(x, y))}, \frac{d(x_n, f(x, y))d(y, y_n)}{1 + d(x, x_n) + d(y, y_n) + d(x_n, f(x, y))}, \\
&\quad \left. \max\{d(x_n, f(x, y)), d(f(x, y), f(x_n, y_n))\}\right\} \\
&= \max\left\{\frac{d(x, x_n) + d(y, y_n)}{2s}, \frac{d(x, f(x, y))d(x_n, x_{n+1})}{1 + d(x, x_n) + d(y, y_n) + d(x_n, f(x, y))}, \right. \\
&\quad \frac{d(x_n, f(x, y))d(x, x_{n+1})}{1 + d(x, x_n) + d(y, y_n) + d(x_n, f(x, y))}, \frac{d(f(x, y), x_{n+1})d(x, x_n)}{1 + d(x, x_n) + d(y, y_n) + d(x_n, f(x, y))}, \\
&\quad \frac{d(f(x, y), x_{n+1})d(y, y_n)}{1 + d(x, x_n) + d(y, y_n) + d(x_n, f(x, y))}, \frac{d(x_n, x_{n+1})d(y, y_n)}{1 + d(x, x_n) + d(y, y_n) + d(x_n, f(x, y))}, \\
&\quad \frac{d(x_n, f(x, y))d(x, x_n)}{1 + d(x, x_n) + d(y, y_n) + d(x_n, f(x, y))}, \frac{d(x_n, f(x, y))d(y, y_n)}{1 + d(x, x_n) + d(y, y_n) + d(x_n, f(x, y))}, \\
&\quad \left. \max\{d(x_n, f(x, y)), d(f(x, y), x_{n+1})\}\right\}.
\end{aligned}$$

On taking limit superior as  $n \rightarrow \infty$  in  $M(x, y, x_n, y_n)$ , we have

$$\limsup_{n \rightarrow \infty} M(x, y, x_n, y_n) \leq sd(x, f(x, y)).$$

On letting limit superior as  $n \rightarrow \infty$  in (4.4) and using the Lemma 2.7, we have

$$\begin{aligned}
0 &\leq \limsup_{n \rightarrow \infty} \zeta(s^3 d(f(x, y), x_{n+1}), M(x, y, x_n, y_n)) \\
&= \limsup_{n \rightarrow \infty} M(x, y, x_n, y_n) - \liminf_{n \rightarrow \infty} s^3 d(f(x, y), x_{n+1}) \\
&\leq d(x, f(x, y)) - s^3 \frac{d(x, f(x, y))}{s},
\end{aligned}$$

a contradiction. Therefore  $x = f(x, y)$ . Similarly we can prove that  $y = f(y, x)$ . Therefore  $(x, y)$  is a coupled fixed point of  $f$ . Let  $(x', y') \in X \times X$  be another coupled fixed point of  $f$  with  $(x', y') \neq (x, y)$ . We consider

$$\zeta(s^3 d(x, x'), M(x, y, x', y')) = \zeta(s^3 d(f(x, y), f(x', y')), M(x, y, x', y')) \geq 0,$$

where

$$\begin{aligned}
M(x, y, x', y') &= \max\left\{\frac{d(x, x') + d(y, y')}{2s}, \frac{d(x, f(x, y))d(x', f(x', y'))}{1 + d(x, x') + d(y, y') + d(x', f(x, y))}, \frac{d(x', f(x, y))d(x, f(x', y'))}{1 + d(x, x') + d(y, y') + d(x', f(x, y))}, \right. \\
&\quad \frac{d(f(x, y), f(x', y'))d(x, x')}{1 + d(x, x') + d(y, y') + d(x', f(x, y))}, \frac{d(f(x, y), f(x', y'))d(y, y')}{1 + d(x, x') + d(y, y') + d(x', f(x, y))}, \\
&\quad \frac{d(x', f(x', y'))d(y, y')}{1 + d(x, x') + d(y, y') + d(x', f(x, y))}, \frac{d(x', f(x, y))d(x, x')}{1 + d(x, x') + d(y, y') + d(x', f(x, y))}, \\
&\quad \frac{d(x', f(x, y))d(y, y')}{1 + d(x, x') + d(y, y') + d(x', f(x, y))}, \max\{d(x', f(x, y)), d(f(x, y), f(x', y'))\}\} \\
&\leq \max\left\{\frac{d(x, x') + d(y, y')}{2s}, d(x, x')\right\}.
\end{aligned}$$

If  $M(x, y, x', y') = d(x, x')$  then we have

$$\zeta(s^3 d(x, x'), M(x, y, x', y')) = d(x, x') - s^3 d(x, x') \geq 0,$$

which is a contradiction. Therefore

$$d(x, x') \leq \frac{d(x, x') + d(y, y')}{2s}. \quad (4.5)$$

Similarly, we can prove that

$$d(y, y') \leq \frac{d(x, x') + d(y, y')}{2s}. \quad (4.6)$$

Adding the inequalities (4.5) and (4.6), we get that

$$d(x, x') + d(y, y') \leq \frac{d(x, x') + d(y, y')}{2s} < d(x, x') + d(y, y')$$

it is a contradiction. Therefore  $(x, y) = (x', y')$  is the unique coupled fixed point of  $f$  in  $X$ .  $\square$

**Proposition 4.2.** Let  $(X, d)$  be a  $b$ -metric space with coefficient  $s \geq 1$  and  $f, g : X \times X \rightarrow X$  be two maps. Assume that the pair  $(f, g)$  is generalized rational type  $\mathcal{Z}$ -contraction maps. Then  $(u, v)$  is a coupled fixed point of  $f$  if and only if  $(u, v)$  is a coupled fixed point of  $g$ . Moreover,  $(u, v)$  is unique in this case.

**Proof .** Let  $(u, v)$  be a coupled fixed point of  $f$ . Then  $u = f(u, v)$  and  $v = f(v, u)$ . Suppose that  $u \neq g(u, v)$ . We now consider

$$\zeta(s^3 d(u, g(u, v)), M(u, v, u, v)) = \zeta(s^3 d(f(u, v), g(u, v)), M(u, v, u, v)) \geq 0, \quad (4.7)$$

where

$$M(u, v, u, v) = \max\left\{\frac{d(u, u) + d(v, v)}{2s}, \frac{d(u, f(u, v))d(u, g(u, v))}{1 + d(u, u) + d(v, v) + d(u, f(u, v))}, \frac{d(u, f(u, v))d(u, g(u, v))}{1 + d(u, u) + d(v, v) + d(u, f(u, v))}, \frac{d(f(u, v), g(u, v))d(u, u)}{1 + d(u, u) + d(v, v) + d(u, f(u, v))}, \frac{d(f(u, v), g(u, v))d(v, v)}{1 + d(u, u) + d(v, v) + d(u, f(u, v))}, \frac{d(u, g(u, v))d(v, v)}{1 + d(u, u) + d(v, v) + d(u, f(u, v))}, \frac{d(u, f(u, v))d(u, u)}{1 + d(u, u) + d(v, v) + d(u, f(u, v))}, \frac{d(u, f(u, v))d(v, v)}{1 + d(u, u) + d(v, v) + d(u, f(u, v))}, \max\{d(u, f(u, v)), d(f(u, v), g(u, v))\}\right\} = d(u, g(u, v)).$$

From the inequality (4.7), we have

$$0 \leq \zeta(s^3 d(u, g(u, v)), M(u, v, u, v)) = d(u, g(u, v)) - s^3 d(u, g(u, v)),$$

which is a contradiction. Therefore  $u = g(u, v)$ . Similarly, we can prove that  $v = g(v, u)$ . Hence,  $(u, v)$  is a coupled fixed point of  $g$ .

In the similar lines as above, it is easy to see that  $(u, v)$  is a coupled fixed point of  $f$  whenever  $(u, v)$  is a coupled fixed point of  $g$ . Let  $(u, v), (u', v') \in X \times X$  be two coupled fixed points of  $f$  and  $g$  with  $(u, v) \neq (u', v')$ . We consider

$$\zeta(s^3 d(u, u'), M(u, v, u', v')) = \zeta(s^3 d(f(u, v), g(u', v')), M(u, v, u', v')) \geq 0,$$

where

$$M(u, v, u', v') = \max\left\{\frac{d(u, u') + d(v, v')}{2s}, \frac{d(u, f(u, v))d(u', g(u', v'))}{1 + d(u, u') + d(v, v') + d(u', f(u, v))}, \frac{d(u', f(u, v))d(u, g(u', v'))}{1 + d(u, u') + d(v, v') + d(u', f(u, v))}, \frac{d(f(u, v), g(u', v'))d(u, u')}{1 + d(u, u') + d(v, v') + d(u', f(u, v))}, \frac{d(f(u, v), g(u', v'))d(v, v')}{1 + d(u, u') + d(v, v') + d(u', f(u, v))}, \frac{d(u', g(u', v'))d(v, v')}{1 + d(u, u') + d(v, v') + d(u', f(u, v))}, \frac{d(u', f(u, v))d(u, u')}{1 + d(u, u') + d(v, v') + d(u', f(u, v))}, \frac{d(u', f(u, v))d(v, v')}{1 + d(u, u') + d(v, v') + d(u', f(u, v))}, \max\{d(u', f(u, v)), d(f(u, v), g(u', v'))\}\right\} \\ \leq \max\left\{\frac{d(u, u') + d(v, v')}{2s}, d(u, u')\right\}.$$

If  $M(u, v, u', v') = d(u, u')$  then we have

$$\zeta(s^3 d(u, u'), M(u, v, u', v')) = d(u, u') - s^3 d(u, u') \geq 0,$$

which is a contradiction. Therefore

$$d(u, u') \leq \frac{d(u, u') + d(v, v')}{2s}. \quad (4.8)$$

Similarly, we can prove that

$$d(v, v') \leq \frac{d(u, u') + d(v, v')}{2s}. \quad (4.9)$$

Adding the inequalities (4.8) and (4.9), we get that

$$d(u, u') + d(v, v') \leq \frac{d(u, u') + d(v, v')}{2s} < d(u, u') + d(v, v'),$$

it is a contradiction.

Therefore  $(u, v) = (u', v')$  is the unique coupled fixed point of  $f$  and  $g$  in  $X$ .  $\square$

**Theorem 4.3.** Let  $(X, d)$  be a complete  $b$ -metric space with coefficient  $s \geq 1$  and the pair  $(f, g)$  be a generalized rational type  $\mathcal{Z}$ -contraction maps. Then  $f$  and  $g$  have a unique coupled fixed point in  $X$ .

**Proof .** Let  $x_0$  and  $y_0$  be arbitrary points in  $X$ . We define  $x_{2i+1} = f(x_{2i}, y_{2i}), y_{2i+1} = f(y_{2i}, x_{2i})$  and  $x_{2i+2} = g(x_{2i+1}, y_{2i+1}), y_{2i+2} = g(y_{2i+1}, x_{2i+1})$  for  $i = 0, 1, 2, \dots$ . We consider

$$\zeta(s^3 d(x_{2n+1}, x_{2n+2}), M(x_{2n}, y_{2n}, x_{2n+1}, y_{2n+1})) = \zeta(s^3 d(f(x_{2n}, y_{2n}), g(x_{2n+1}, y_{2n+1})), M(x_{2n}, y_{2n}, x_{2n+1}, y_{2n+1})) \geq 0, \quad (4.10)$$

where

$$M(x_{2n}, y_{2n}, x_{2n+1}, y_{2n+1}) = \max\left\{\frac{d(x_{2n}, x_{2n+1}) + d(y_{2n}, y_{2n+1})}{2s}, \frac{d(x_{2n}, f(x_{2n}, y_{2n}))d(x_{2n+1}, g(x_{2n+1}, y_{2n+1}))}{1 + d(x_{2n}, x_{2n+1}) + d(y_{2n}, y_{2n+1}) + d(x_{2n+1}, f(x_{2n}, y_{2n}))}, \frac{d(x_{2n+1}, f(x_{2n}, y_{2n}))d(x_{2n}, g(x_{2n+1}, y_{2n+1}))}{1 + d(x_{2n}, x_{2n+1}) + d(y_{2n}, y_{2n+1}) + d(x_{2n+1}, f(x_{2n}, y_{2n}))}, \frac{d(f(x_{2n}, y_{2n}), g(x_{2n+1}, y_{2n+1}))d(x_{2n}, x_{2n+1})}{1 + d(x_{2n}, x_{2n+1}) + d(y_{2n}, y_{2n+1}) + d(x_{2n+1}, f(x_{2n}, y_{2n}))}, \frac{d(f(x_{2n}, y_{2n}), g(x_{2n+1}, y_{2n+1}))d(y_{2n}, y_{2n+1})}{1 + d(x_{2n}, x_{2n+1}) + d(y_{2n}, y_{2n+1}) + d(x_{2n+1}, f(x_{2n}, y_{2n}))}, \frac{d(x_{2n}, g(x_{2n+1}, y_{2n+1}))d(y_{2n}, y_{2n+1})}{1 + d(x_{2n}, x_{2n+1}) + d(y_{2n}, y_{2n+1}) + d(x_{2n+1}, f(x_{2n}, y_{2n}))}, \frac{d(x_{2n+1}, g(x_{2n+1}, y_{2n+1}))d(x_{2n}, x_{2n+1})}{1 + d(x_{2n}, x_{2n+1}) + d(y_{2n}, y_{2n+1}) + d(x_{2n+1}, f(x_{2n}, y_{2n}))}, \frac{d(x_{2n}, f(x_{2n}, y_{2n}))d(x_{2n+1}, g(x_{2n+1}, y_{2n+1}))}{1 + d(x_{2n}, x_{2n+1}) + d(y_{2n}, y_{2n+1}) + d(x_{2n+1}, f(x_{2n}, y_{2n}))}, \frac{d(x_{2n+1}, f(x_{2n}, y_{2n}))d(x_{2n}, g(x_{2n+1}, y_{2n+1}))}{1 + d(x_{2n}, x_{2n+1}) + d(y_{2n}, y_{2n+1}) + d(x_{2n+1}, f(x_{2n}, y_{2n}))}, \max\{d(x_{2n}, f(x_{2n}, y_{2n})), d(f(x_{2n}, y_{2n}), g(x_{2n+1}, y_{2n+1}))\}\right\}$$



$$\begin{aligned}
& \frac{d(x_{2n+1}, g(x_{2n+1}, y_{2n+1}))d(y_{2n}, y_{2n+1})}{1+d(x_{2n}, x_{2n+1})+d(y_{2n}, y_{2n+1})+d(x_{2n+1}, f(x_{2n}, y_{2n}))}, \\
& \frac{d(x_{2n+1}, f(x_{2n}, y_{2n}))d(x_{2n}, x_{2n+1})}{1+d(x_{2n}, x_{2n+1})+d(y_{2n}, y_{2n+1})+d(x_{2n+1}, f(x_{2n}, y_{2n}))}, \\
& \frac{d(x_{2n+1}, f(x_{2n}, y_{2n}))d(y_{2n}, y_{2n+1})}{1+d(x_{2n}, x_{2n+1})+d(y_{2n}, y_{2n+1})+d(x_{2n+1}, f(x_{2n}, y_{2n}))}, \\
& \max\{d(x_{2n+1}, f(x_{2n}, y_{2n})), d(f(x_{2n}, y_{2n}), g(x_{2n+1}, y_{2n+1}))\} \\
= & \max\left\{\frac{d(x_{2n}, x_{2n+1})+d(y_{2n}, y_{2n+1})}{2s}, \right. \\
& \frac{d(x_{2n}, x_{2n+1})d(x_{2n+1}, x_{2n+2})+d(x_{2n+1}, x_{2n+1})}{1+d(x_{2n}, x_{2n+1})+d(y_{2n}, y_{2n+1})+d(x_{2n+1}, x_{2n+1})}, \\
& \frac{d(x_{2n+1}, x_{2n+1})d(x_{2n}, x_{2n+2})}{1+d(x_{2n}, x_{2n+1})+d(y_{2n}, y_{2n+1})+d(x_{2n+1}, x_{2n+1})}, \\
& \frac{d(x_{2n+1}, x_{2n+2})d(x_{2n}, x_{2n+1})}{1+d(x_{2n}, x_{2n+1})+d(y_{2n}, y_{2n+1})+d(x_{2n+1}, x_{2n+1})}, \\
& \frac{d(x_{2n+1}, x_{2n+2})d(y_{2n}, y_{2n+1})}{1+d(x_{2n}, x_{2n+1})+d(y_{2n}, y_{2n+1})+d(x_{2n+1}, x_{2n+1})}, \\
& \frac{d(x_{2n+1}, x_{2n+2})d(y_{2n}, y_{2n+1})}{1+d(x_{2n}, x_{2n+1})+d(y_{2n}, y_{2n+1})+d(x_{2n+1}, x_{2n+1})}, \\
& \frac{d(x_{2n+1}, x_{2n+2})d(y_{2n}, y_{2n+1})}{1+d(x_{2n}, x_{2n+1})+d(y_{2n}, y_{2n+1})+d(x_{2n+1}, x_{2n+1})}, \\
& \frac{d(x_{2n+1}, x_{2n+2})d(y_{2n}, y_{2n+1})}{1+d(x_{2n}, x_{2n+1})+d(y_{2n}, y_{2n+1})+d(x_{2n+1}, x_{2n+1})}, \\
& \left. \max\{d(x_{2n+1}, x_{2n+1}), d(x_{2n+1}, x_{2n+2})\}\right\} \\
\leq & \max\left\{\frac{d(x_{2n}, x_{2n+1})+d(y_{2n}, y_{2n+1})}{2s}, d(x_{2n+1}, x_{2n+2})\right\}.
\end{aligned}$$

If  $M(x_{2n}, y_{2n}, x_{2n+1}, y_{2n+1}) = d(x_{2n+1}, x_{2n+2})$  then from (4.10), we have

$$\begin{aligned}
0 \leq \zeta(s^3 d(x_{2n+1}, x_{2n+2}), M(x_{2n}, y_{2n}, x_{2n+1}, y_{2n+1})) &= \zeta(s^3 d(x_{2n+1}, x_{2n+2}), d(x_{2n+1}, x_{2n+2})) \\
&< d(x_{2n+1}, x_{2n+2}) - s^3 d(x_{2n+1}, x_{2n+2}),
\end{aligned}$$

which is a contradiction. Therefore

$$d(x_{2n+1}, x_{2n+2}) \leq \frac{d(x_{2n}, x_{2n+1}) + d(y_{2n}, y_{2n+1})}{2s} \quad (4.11)$$

for all  $n = 0, 1, 2, \dots$

Similarly, we can prove that

$$d(y_{2n+1}, y_{2n+2}) \leq \frac{d(y_{2n}, y_{2n+1}) + d(x_{2n}, x_{2n+1})}{2s} \quad (4.12)$$

for all  $n = 0, 1, 2, \dots$ . Adding the inequalities (4.11) and (4.12), we have

$$d(x_{2n+1}, x_{2n+2}) + d(y_{2n+1}, y_{2n+2}) \leq h[d(x_{2n}, x_{2n+1}) + d(y_{2n}, y_{2n+1})],$$

where  $h = \frac{1}{2s} < 1$ . Also, it is easy to see that

$$d(x_{2n+2}, x_{2n+3}) + d(y_{2n+2}, y_{2n+3}) \leq h[d(x_{2n+1}, x_{2n+2}) + d(y_{2n+1}, y_{2n+2})].$$

Therefore

$$d(x_n, x_{n+1}) + d(y_n, y_{n+1}) \leq h[d(x_{n-1}, x_n) + d(y_{n-1}, y_n)],$$

for all  $n = 1, 2, 3, \dots$ . Continuing in the same way, we get that

$$d(x_n, x_{n+1}) + d(y_n, y_{n+1}) \leq h^n[d(x_0, x_1) + d(y_0, y_1)].$$

For  $m > n, m, n \in \mathbb{N}$ , we have

$$\begin{aligned}
d(x_n, x_m) + d(y_n, y_m) &\leq s[d(x_n, x_{n+1}) + d(x_{n+1}, x_m)] + s[d(y_n, y_{n+1}) + d(y_{n+1}, y_m)] \\
&\leq s[d(x_n, x_{n+1}) + d(y_n, y_{n+1})] + s^2[d(x_{n+1}, x_{n+2}) + d(x_{n+2}, x_m)] \\
&\quad + s^2[d(y_{n+1}, y_{n+2}) + d(y_{n+2}, y_m)] \\
&= s[d(x_n, x_{n+1}) + d(y_n, y_{n+1})] + s^2[d(x_{n+1}, x_{n+2}) + d(y_{n+1}, y_{n+2})] \\
&\quad + s^2[d(x_{n+2}, x_m) + d(y_{n+2}, y_m)] \dots + s^{m-n}[d(x_{m-1}, x_m) + d(y_{m-1}, y_m)] \\
&\leq [sh^n + s^2h^{n+1} + \dots + s^{m-n}h^{m-1}][d(x_0, x_1) + d(y_0, y_1)] \\
&\leq sh^n[1 + sh + (sh)^2 \dots + (sh)^{m-1} + \dots][d(x_0, x_1) + d(y_0, y_1)] \\
&= sh^n\left(\frac{1}{1-sh}\right)[d(x_0, x_1) + d(y_0, y_1)] \rightarrow 0 \text{ as } n \rightarrow \infty.
\end{aligned}$$

Therefore  $\{x_n\}$  and  $\{y_n\}$  are  $b$ -Cauchy sequences in  $X$ . Since  $X$  is  $b$ -complete, there exist  $x, y \in X$  such that  $x_n \rightarrow x$  and  $y_n \rightarrow y$  as  $n \rightarrow \infty$ . We now prove that  $x = f(x, y)$  and  $y = f(y, x)$ . On the contrary suppose that  $x \neq f(x, y)$  and  $y \neq f(y, x)$ . We now consider

$$\begin{aligned}
\zeta(s^3 d(f(x, y), x_{2n+2}), M(x, y, x_{2n+1}, y_{2n+1})) &= \zeta(s^3 d(f(x, y), g(x_{2n+1}, y_{2n+1})), \\
M(x, y, x_{2n+1}, y_{2n+1})) &\geq 0,
\end{aligned} \quad (4.13)$$

where

$$\begin{aligned}
M(x, y, x_{2n+1}, y_{2n+1}) &= \max\left\{\frac{d(x, x_{2n+1})+d(y, y_{2n+1})}{2s}, \frac{d(x, f(x, y))d(x_{2n+1}, g(x_{2n+1}, y_{2n+1}))}{1+d(x, x_{2n+1})+d(y, y_{2n+1})+d(x_{2n+1}, f(x, y))}, \right. \\
&\frac{d(x_{2n+1}, f(x, y))d(x, g(x_{2n+1}, y_{2n+1}))}{1+d(x, x_{2n+1})+d(y, y_{2n+1})+d(x_{2n+1}, f(x, y))}, \frac{d(f(x, y), g(x_{2n+1}, y_{2n+1}))d(x, x_{2n+1})}{1+d(x, x_{2n+1})+d(y, y_{2n+1})+d(x_{2n+1}, f(x, y))}, \\
&\frac{d(f(x, y), g(x_{2n+1}, y_{2n+1}))d(y, y_{2n+1})}{1+d(x, x_{2n+1})+d(y, y_{2n+1})+d(x_{2n+1}, f(x, y))}, \frac{d(x_{2n+1}, g(x_{2n+1}, y_{2n+1}))d(y, y_{2n+1})}{1+d(x, x_{2n+1})+d(y, y_{2n+1})+d(x_{2n+1}, f(x, y))}, \\
&\frac{d(x_{2n+1}, f(x, y))d(x, x_{2n+1})}{1+d(x, x_{2n+1})+d(y, y_{2n+1})+d(x_{2n+1}, f(x, y))}, \frac{d(x_{2n+1}, f(x, y))d(y, y_{2n+1})}{1+d(x, x_{2n+1})+d(y, y_{2n+1})+d(x_{2n+1}, f(x, y))}, \\
&\left. \max\{d(x_{2n+1}, f(x, y)), d(f(x, y), g(x_{2n+1}, y_{2n+1}))\}\right\} \\
&= \max\left\{\frac{d(x, x_{2n+1})+d(y, y_{2n+1})}{2s}, \frac{d(x, f(x, y))d(x_{2n+1}, x_{2n+2})}{1+d(x, x_{2n+1})+d(y, y_{2n+1})+d(x_{2n+1}, f(x, y))}, \right. \\
&\frac{d(x_{2n+1}, f(x, y))d(x, x_{2n+2})}{1+d(x, x_{2n+1})+d(y, y_{2n+1})+d(x_{2n+1}, f(x, y))}, \frac{d(f(x, y), x_{2n+2})d(x, x_{2n+1})}{1+d(x, x_{2n+1})+d(y, y_{2n+1})+d(x_{2n+1}, f(x, y))}, \\
&\frac{d(f(x, y), x_{2n+2})d(y, y_{2n+1})}{1+d(x, x_{2n+1})+d(y, y_{2n+1})+d(x_{2n+1}, f(x, y))}, \frac{d(x_{2n+1}, x_{2n+2})d(y, y_{2n+1})}{1+d(x, x_{2n+1})+d(y, y_{2n+1})+d(x_{2n+1}, f(x, y))}, \\
&\frac{d(x_{2n+1}, f(x, y))d(x, x_{2n+1})}{1+d(x, x_{2n+1})+d(y, y_{2n+1})+d(x_{2n+1}, f(x, y))}, \frac{d(x_{2n+1}, f(x, y))d(y, y_{2n+1})}{1+d(x, x_{2n+1})+d(y, y_{2n+1})+d(x_{2n+1}, f(x, y))}, \\
&\left. \max\{d(x_{2n+1}, f(x, y)), d(f(x, y), x_{2n+2})\}\right\}.
\end{aligned}$$

On taking limit superior as  $n \rightarrow \infty$  in  $M(x, y, x_n, y_n)$  and using Lemma 2.7, we have

$$\limsup_{n \rightarrow \infty} M(x, y, x_n, y_n) \leq sd(x, f(x, y)).$$

On letting limit superior as  $n \rightarrow \infty$  in (4.13) and using the Lemma 2.7, we have

$$\begin{aligned}
0 &\leq \limsup_{n \rightarrow \infty} \zeta(s^3 d(f(x, y), x_{2n+2}), M(x, y, x_{2n+1}, y_{2n+1})) \\
&= \limsup_{n \rightarrow \infty} M(x, y, x_{2n+1}, y_{2n+1}) - \liminf_{n \rightarrow \infty} s^3 d(f(x, y), x_{2n+2}) \\
&\leq sd(x, f(x, y)) - s^3 \frac{d(x, f(x, y))}{s},
\end{aligned}$$

a contradiction. Therefore  $x = f(x, y)$ . Similarly we can prove that  $y = f(y, x)$ . Therefore  $(x, y)$  is a coupled fixed point of  $f$ . By Proposition 4.2, we have  $(x, y)$  is a unique common coupled fixed point of  $f$  and  $g$  in  $X$ .  $\square$

## 5 Corollaries and examples

**Corollary 5.1.** Let  $(X, d)$  be a complete  $b$ -metric space with coefficient  $s \geq 1$ .  $f : X \times X \rightarrow X$  be two maps. Assume that there exist two continuous functions  $\varphi, \psi : [0, \infty) \rightarrow [0, \infty)$  with  $\varphi(t) < t \leq \psi(t)$  for all  $t > 0$  and  $\varphi(t) = \psi(t) = 0$  if and only if  $t = 0$  such that

$$\psi(s^d(f(x, y), f(u, v))) \leq \varphi(M(x, y, u, v))$$

where

$$\begin{aligned}
M(x, y, u, v) &= \max\left\{\frac{d(x, u)+d(y, v)}{2s}, \frac{d(x, f(x, y))d(u, f(u, v))}{1+d(x, u)+d(y, v)+d(u, f(x, y))}, \frac{d(u, f(x, y))d(x, f(u, v))}{1+d(x, u)+d(y, v)+d(u, f(x, y))}, \right. \\
&\frac{d(f(x, y), f(u, v))d(x, u)}{1+d(x, u)+d(y, v)+d(u, f(x, y))}, \frac{d(f(x, y), f(u, v))d(y, v)}{1+d(x, u)+d(y, v)+d(u, f(x, y))}, \frac{d(u, f(u, v))d(y, v)}{1+d(x, u)+d(y, v)+d(u, f(x, y))}, \\
&\frac{d(u, f(x, y))d(x, u)}{1+d(x, u)+d(y, v)+d(u, f(x, y))}, \frac{d(u, f(x, y))d(y, v)}{1+d(x, u)+d(y, v)+d(u, f(x, y))}, \\
&\left. \max\{d(u, f(x, y)), d(f(x, y), f(u, v))\}\right\}, \text{ for all } x, y, u, v \in X.
\end{aligned}$$

Then  $f$  has a unique common coupled fixed point in  $X$ .

**Proof .** Follows from Theorem 4.1 by choosing  $\zeta(s, t) = \varphi(t) - \psi(t)$  for all  $t, s \in [0, \infty)$ .  $\square$

**Corollary 5.2.** Let  $(X, d)$  be a complete  $b$ -metric space with coefficient  $s \geq 1$ .  $f, g : X \times X \rightarrow X$  be two maps. Assume that there exist two continuous functions  $\varphi, \psi : [0, \infty) \rightarrow [0, \infty)$  with  $\varphi(t) < t \leq \psi(t)$ , for all  $t > 0$  and  $\varphi(t) = \psi(t) = 0$  if and only if  $t = 0$  such that

$$\psi(s^d(f(x, y), g(u, v))) \leq \varphi(M(x, y, u, v))$$

where

$$\begin{aligned}
M(x, y, u, v) &= \max\left\{\frac{d(x, u)+d(y, v)}{2s}, \frac{d(x, f(x, y))d(u, g(u, v))}{1+d(x, u)+d(y, v)+d(u, f(x, y))}, \frac{d(u, f(x, y))d(x, g(u, v))}{1+d(x, u)+d(y, v)+d(u, f(x, y))}, \right. \\
&\frac{d(f(x, y), g(u, v))d(x, u)}{1+d(x, u)+d(y, v)+d(u, f(x, y))}, \frac{d(f(x, y), g(u, v))d(y, v)}{1+d(x, u)+d(y, v)+d(u, f(x, y))}, \frac{d(u, g(u, v))d(y, v)}{1+d(x, u)+d(y, v)+d(u, f(x, y))}, \\
&\frac{d(u, f(x, y))d(x, u)}{1+d(x, u)+d(y, v)+d(u, f(x, y))}, \frac{d(u, f(x, y))d(y, v)}{1+d(x, u)+d(y, v)+d(u, f(x, y))}, \\
&\left. \max\{d(u, f(x, y)), d(f(x, y), g(u, v))\}\right\}, \text{ for all } x, y, u, v \in X.
\end{aligned}$$

Then  $f$  and  $g$  have a unique common coupled fixed point in  $X$ .

**Proof .** Follows by taking  $g = f$  in Corollary 5.1.  $\square$

The following is an example in support of Theorem 4.1.

**Example 5.3.** Let  $X = [0, 1]$  and let  $d : X \times X \rightarrow \mathbb{R}^+$  defined by

$$d(x, y) = \begin{cases} 0 & \text{if } x = y \\ (x + y)^2 & \text{if } x \neq y. \end{cases}$$

Then clearly  $(X, d)$  is a  $b$ -metric space with coefficient  $s = 2$ . We define  $f, g : X \times X \rightarrow X$  by

$$f(x, y) = \begin{cases} \frac{x^2+y^2}{16} & \text{if } x, y \in [0, \frac{1}{2}) \\ \frac{1}{32} & \text{if } x, y \in [\frac{1}{2}, 1] \\ 0 & \text{otherwise} \end{cases}$$

$\zeta : \mathbb{R}^+ \times \mathbb{R}^+ \rightarrow (-\infty, \infty)$  by  $\zeta(t, s) = \frac{99}{100}s - t, t \geq 0, s \geq 0$ .

**Case (i).**  $x, y, u, v \in [0, \frac{1}{2})$ .

$$\begin{aligned} s^3 d(f(x, y), g(u, v)) &= 8 \left[ \frac{x^2+y^2}{16} + \frac{u^2+v^2}{16} \right]^2 \\ &\leq \frac{99}{400} [(x+u)^2 + (y+v)^2] \\ &= \frac{99}{100} \left( \frac{d(x,u)+d(y,v)}{2s} \right) \\ &\leq \frac{99}{100} \left( \max \left\{ \frac{d(x,u)+d(y,v)}{2s}, \frac{d(x,f(x,y))d(u,f(u,v))}{1+d(x,u)+d(y,v)+d(u,f(x,y))}, \frac{d(u,f(x,y))d(x,f(u,v))}{1+d(x,u)+d(y,v)+d(u,f(x,y))}, \right. \right. \\ &\quad \frac{d(f(x,y),f(u,v))d(x,u)}{1+d(x,u)+d(y,v)+d(u,f(x,y))}, \frac{d(f(x,y),f(u,v))d(y,v)}{1+d(x,u)+d(y,v)+d(u,f(x,y))}, \frac{d(u,f(u,v))d(y,v)}{1+d(x,u)+d(y,v)+d(u,f(x,y))}, \\ &\quad \frac{d(u,f(x,y))d(x,u)}{1+d(x,u)+d(y,v)+d(u,f(x,y))}, \frac{d(u,f(x,y))d(y,v)}{1+d(x,u)+d(y,v)+d(u,f(x,y))}, \\ &\quad \left. \max \{ d(u, f(x, y)), d(f(x, y), f(u, v)) \} \right\} \right). \end{aligned}$$

**Case (ii).**  $x, y, u, v \in [\frac{1}{2}, 1]$ .

$$\begin{aligned} s^3 d(f(x, y), g(u, v)) &= 8 \left[ \frac{1}{32} + \frac{1}{32} \right]^2 \\ &\leq \frac{99}{400} [(x+u)^2 + (y+v)^2] \\ &= \frac{99}{100} \left( \frac{d(x,u)+d(y,v)}{2s} \right) \\ &\leq \frac{99}{100} \left( \max \left\{ \frac{d(x,u)+d(y,v)}{2s}, \frac{d(x,f(x,y))d(u,f(u,v))}{1+d(x,u)+d(y,v)+d(u,f(x,y))}, \frac{d(u,f(x,y))d(x,f(u,v))}{1+d(x,u)+d(y,v)+d(u,f(x,y))}, \right. \right. \\ &\quad \frac{d(f(x,y),f(u,v))d(x,u)}{1+d(x,u)+d(y,v)+d(u,f(x,y))}, \frac{d(f(x,y),f(u,v))d(y,v)}{1+d(x,u)+d(y,v)+d(u,f(x,y))}, \frac{d(u,f(u,v))d(y,v)}{1+d(x,u)+d(y,v)+d(u,f(x,y))}, \\ &\quad \frac{d(u,f(x,y))d(x,u)}{1+d(x,u)+d(y,v)+d(u,f(x,y))}, \frac{d(u,f(x,y))d(y,v)}{1+d(x,u)+d(y,v)+d(u,f(x,y))}, \\ &\quad \left. \max \{ d(u, f(x, y)), d(f(x, y), f(u, v)) \} \right\} \right). \end{aligned}$$

**Case (iii).**  $x, y \in [\frac{1}{2}, 1], u, v \in [0, \frac{1}{2})$ .

$$\begin{aligned} s^3 d(f(x, y), g(u, v)) &= 8 \left[ \frac{1}{32} + \frac{u^2+v^2}{16} \right]^2 \\ &\leq \frac{99}{400} [(x+u)^2 + (y+v)^2] \\ &= \frac{99}{100} \left( \frac{d(x,u)+d(y,v)}{2s} \right) \\ &\leq \frac{99}{100} \left( \max \left\{ \frac{d(x,u)+d(y,v)}{2s}, \frac{d(x,f(x,y))d(u,f(u,v))}{1+d(x,u)+d(y,v)+d(u,f(x,y))}, \frac{d(u,f(x,y))d(x,f(u,v))}{1+d(x,u)+d(y,v)+d(u,f(x,y))}, \right. \right. \\ &\quad \frac{d(f(x,y),f(u,v))d(x,u)}{1+d(x,u)+d(y,v)+d(u,f(x,y))}, \frac{d(f(x,y),f(u,v))d(y,v)}{1+d(x,u)+d(y,v)+d(u,f(x,y))}, \frac{d(u,f(u,v))d(y,v)}{1+d(x,u)+d(y,v)+d(u,f(x,y))}, \\ &\quad \frac{d(u,f(x,y))d(x,u)}{1+d(x,u)+d(y,v)+d(u,f(x,y))}, \frac{d(u,f(x,y))d(y,v)}{1+d(x,u)+d(y,v)+d(u,f(x,y))}, \\ &\quad \left. \max \{ d(u, f(x, y)), d(f(x, y), f(u, v)) \} \right\} \right). \end{aligned}$$

**Case (iv).**  $x, y \in [0, \frac{1}{2}), u, v \in [\frac{1}{2}, 1]$ .

$$\begin{aligned} s^3 d(f(x, y), g(u, v)) &= 8 \left[ \frac{x^2+y^2}{16} + \frac{1}{32} \right]^2 \\ &\leq \frac{99}{400} [(x+u)^2 + (y+v)^2] \\ &= \frac{99}{100} \left( \frac{d(x,u)+d(y,v)}{2s} \right) \\ &\leq \frac{99}{100} \left( \max \left\{ \frac{d(x,u)+d(y,v)}{2s}, \frac{d(x,f(x,y))d(u,f(u,v))}{1+d(x,u)+d(y,v)+d(u,f(x,y))}, \frac{d(u,f(x,y))d(x,f(u,v))}{1+d(x,u)+d(y,v)+d(u,f(x,y))}, \right. \right. \\ &\quad \frac{d(f(x,y),f(u,v))d(x,u)}{1+d(x,u)+d(y,v)+d(u,f(x,y))}, \frac{d(f(x,y),f(u,v))d(y,v)}{1+d(x,u)+d(y,v)+d(u,f(x,y))}, \frac{d(u,f(u,v))d(y,v)}{1+d(x,u)+d(y,v)+d(u,f(x,y))}, \\ &\quad \frac{d(u,f(x,y))d(x,u)}{1+d(x,u)+d(y,v)+d(u,f(x,y))}, \frac{d(u,f(x,y))d(y,v)}{1+d(x,u)+d(y,v)+d(u,f(x,y))}, \\ &\quad \left. \max \{ d(u, f(x, y)), d(f(x, y), f(u, v)) \} \right\} \right). \end{aligned}$$

Therefore  $f$  satisfy all the hypothesis of Theorem 4.1 and  $(0, 0)$  is a unique coupled fixed point of  $f$ .

The following is an example in support of Theorem 4.3.

**Example 5.4.** Let  $X = [0, 1]$  and let  $d : X \times X \rightarrow \mathbb{R}^+$  defined by

$$d(x, y) = \begin{cases} 0 & \text{if } x = y \\ (x + y)^2 & \text{if } x \neq y. \end{cases}$$

Then clearly  $(X, d)$  is a  $b$ -metric space with coefficient  $s = 2$ . We define  $f, g : X \times X \rightarrow X$  by

$$f(x, y) = \begin{cases} \frac{\log(1+x+y)}{16} & \text{if } x, y \in [0, \frac{1}{2}) \\ \frac{1}{32} & \text{if } x, y \in [\frac{1}{2}, 1] \end{cases}$$

and

$$g(x, y) = \begin{cases} \frac{xye^{xy}}{8} & \text{if } x, y \in [0, \frac{1}{2}) \\ \log(x + y) & \text{if } x, y \in [\frac{1}{2}, 1]. \end{cases}$$

$\zeta : \mathbb{R}^+ \times \mathbb{R}^+ \rightarrow (-\infty, \infty)$  by  $\zeta(t, s) = \frac{99}{100}s - t, t \geq 0, s \geq 0$ .

**Case (i).**  $x, y, u, v \in [0, \frac{1}{2})$ .

$$\begin{aligned} s^3 d(f(x, y), g(u, v)) &= 8 \left[ \frac{\log(1+x+y)}{16} + \frac{uve^{uv}}{8} \right]^2 \\ &\leq \frac{99}{400} [(x+u)^2 + (y+v)^2] \\ &= \frac{99}{100} \left( \frac{d(x,u)+d(y,v)}{2s} \right) \\ &\leq \frac{99}{100} \left( \max \left\{ \frac{d(x,u)+d(y,v)}{2s}, \frac{d(x,f(x,y))d(u,g(u,v))}{1+d(x,u)+d(y,v)+d(u,f(x,y))}, \frac{d(u,f(x,y))d(x,g(u,v))}{1+d(x,u)+d(y,v)+d(u,f(x,y))}, \right. \right. \\ &\quad \frac{d(f(x,y),g(u,v))d(x,u)}{1+d(x,u)+d(y,v)+d(u,f(x,y))}, \frac{d(f(x,y),g(u,v))d(y,v)}{1+d(x,u)+d(y,v)+d(u,f(x,y))}, \frac{d(u,g(u,v))d(y,v)}{1+d(x,u)+d(y,v)+d(u,f(x,y))}, \\ &\quad \frac{d(u,f(x,y))d(x,u)}{1+d(x,u)+d(y,v)+d(u,f(x,y))}, \frac{d(u,f(x,y))d(y,v)}{1+d(x,u)+d(y,v)+d(u,f(x,y))}, \\ &\quad \left. \left. \max \{ d(u, f(x, y)), d(f(x, y), g(u, v)) \} \right\} \right). \end{aligned}$$

**Case (ii).**  $x, y, u, v \in [\frac{1}{2}, 1]$ .

$$\begin{aligned} s^3 d(f(x, y), g(u, v)) &= 8 \left[ \frac{1}{32} + \log(u+v) \right]^2 \\ &\leq \frac{99}{400} [(x+u)^2 + (y+v)^2] \\ &= \frac{99}{100} \left( \frac{d(x,u)+d(y,v)}{2s} \right) \\ &\leq \frac{99}{100} \left( \max \left\{ \frac{d(x,u)+d(y,v)}{2s}, \frac{d(x,f(x,y))d(u,g(u,v))}{1+d(x,u)+d(y,v)+d(u,f(x,y))}, \frac{d(u,f(x,y))d(x,g(u,v))}{1+d(x,u)+d(y,v)+d(u,f(x,y))}, \right. \right. \\ &\quad \frac{d(f(x,y),g(u,v))d(x,u)}{1+d(x,u)+d(y,v)+d(u,f(x,y))}, \frac{d(f(x,y),g(u,v))d(y,v)}{1+d(x,u)+d(y,v)+d(u,f(x,y))}, \frac{d(u,g(u,v))d(y,v)}{1+d(x,u)+d(y,v)+d(u,f(x,y))}, \\ &\quad \frac{d(u,f(x,y))d(x,u)}{1+d(x,u)+d(y,v)+d(u,f(x,y))}, \frac{d(u,f(x,y))d(y,v)}{1+d(x,u)+d(y,v)+d(u,f(x,y))}, \\ &\quad \left. \left. \max \{ d(u, f(x, y)), d(f(x, y), g(u, v)) \} \right\} \right). \end{aligned}$$

**Case (iii).**  $x, y \in [\frac{1}{2}, 1], u, v \in [0, \frac{1}{2})$ .

$$\begin{aligned} s^3 d(f(x, y), g(u, v)) &= 8 \left[ \frac{1}{16} + \frac{uve^{uv}}{8} \right]^2 \\ &\leq \frac{99}{400} [(x+u)^2 + (y+v)^2] \\ &= \frac{99}{100} \left( \frac{d(x,u)+d(y,v)}{2s} \right) \\ &\leq \frac{99}{100} \left( \max \left\{ \frac{d(x,u)+d(y,v)}{2s}, \frac{d(x,f(x,y))d(u,g(u,v))}{1+d(x,u)+d(y,v)+d(u,f(x,y))}, \frac{d(u,f(x,y))d(x,g(u,v))}{1+d(x,u)+d(y,v)+d(u,f(x,y))}, \right. \right. \\ &\quad \frac{d(f(x,y),g(u,v))d(x,u)}{1+d(x,u)+d(y,v)+d(u,f(x,y))}, \frac{d(f(x,y),g(u,v))d(y,v)}{1+d(x,u)+d(y,v)+d(u,f(x,y))}, \frac{d(u,g(u,v))d(y,v)}{1+d(x,u)+d(y,v)+d(u,f(x,y))}, \\ &\quad \frac{d(u,f(x,y))d(x,u)}{1+d(x,u)+d(y,v)+d(u,f(x,y))}, \frac{d(u,f(x,y))d(y,v)}{1+d(x,u)+d(y,v)+d(u,f(x,y))}, \\ &\quad \left. \left. \max \{ d(u, f(x, y)), d(f(x, y), g(u, v)) \} \right\} \right). \end{aligned}$$

**Case (iv).**  $x, y \in [0, \frac{1}{2}), u, v \in [\frac{1}{2}, 1]$ .

$$\begin{aligned} s^3 d(f(x, y), g(u, v)) &= 8 \left[ \frac{\log(1+x+y)}{8} + \log(x+y) \right]^2 \\ &\leq \frac{99}{400} [(x+u)^2 + (y+v)^2] \\ &= \frac{99}{100} \left( \frac{d(x,u)+d(y,v)}{2s} \right) \\ &\leq \frac{99}{100} \left( \max \left\{ \frac{d(x,u)+d(y,v)}{2s}, \frac{d(x,f(x,y))d(u,g(u,v))}{1+d(x,u)+d(y,v)+d(u,f(x,y))}, \frac{d(u,f(x,y))d(x,g(u,v))}{1+d(x,u)+d(y,v)+d(u,f(x,y))}, \right. \right. \\ &\quad \frac{d(f(x,y),g(u,v))d(x,u)}{1+d(x,u)+d(y,v)+d(u,f(x,y))}, \frac{d(f(x,y),g(u,v))d(y,v)}{1+d(x,u)+d(y,v)+d(u,f(x,y))}, \frac{d(u,g(u,v))d(y,v)}{1+d(x,u)+d(y,v)+d(u,f(x,y))}, \\ &\quad \frac{d(u,f(x,y))d(x,u)}{1+d(x,u)+d(y,v)+d(u,f(x,y))}, \frac{d(u,f(x,y))d(y,v)}{1+d(x,u)+d(y,v)+d(u,f(x,y))}, \\ &\quad \left. \left. \max \{ d(u, f(x, y)), d(f(x, y), g(u, v)) \} \right\} \right). \end{aligned}$$

Therefore the pair  $(f, g)$  satisfy all the hypotheses of Theorem 4.3 and  $(0, 0)$  is a unique common coupled fixed point of  $f$  and  $g$ .

## References

- [1] A. Aghajani, M. Abbas and J. R. Roshan, *Common fixed point of generalized weak contractive mappings in partially ordered  $b$ -metric spaces*, Math. Slovaca **64** (2014), no. 4, 941–960.
- [2] H. Aydi, M-F. Bota, E. Karapinar and S. Mitrović, *A fixed point theorem for set-valued quasi contractions in  $b$ -metric spaces*, Fixed Point Theory Appl. **88** (2012), 8 pages.
- [3] H. Aydi, M-F. Bota, E. Karapinar and S. Moradi, *A common fixed point for weak  $\phi$ -contractions on  $b$ -metric spaces*, Fixed Point Theory **13** (2012), no. 2, 337–346.
- [4] G.V.R. Babu, T.M. Dula and P.S. Kumar, *A common fixed point theorem in  $b$ -metric spaces via simulation function*, J. Fixed Point Theory **12** (2018), 15 pages.
- [5] I.A. Bakhtin, *The contraction mapping principle in almost metric spaces*, Funct. Anal. Gos. Ped. Inst. Unianowsk **30** (1989), 26–37.
- [6] T.G. Bhaskar and V. Lakshmikantham, *Fixed point theorems in partially ordered metric spaces and applications*, Nonlinear Anal. **65** (2006), 1379–1393.
- [7] B. Bindu and N. Malhotra, *Common coupled fixed point for generalized rational type contractions in  $b$ -metric spaces*, J. Nonlinear Anal. Appl. **2018** (2018), no. 2, 201–211.
- [8] M. Boriceanu, *Strict fixed point theorems for multivalued operators in  $b$ -metric spaces*, Int. J. Mod. Math. **4** (2009), no. 3, 285–301.
- [9] M. Boriceanu, M.-F. Bota and A. Petrusel, *Multivalued fractals in  $b$ -metric spaces*, Cent. Eur. J. Math. **8** (2010), no. 2, 367–377.
- [10] N. Bourbaki, *Topologie generale*, Herman: Paris, France, 1974.
- [11] S. Czerwik, *Contraction mappings in  $b$ -metric spaces*, Acta Math. Inform. Univ. Ostraviensis **1** (1993), 5–11.
- [12] S. Czerwik, *Nonlinear set-valued contraction mappings in  $b$ -metric spaces*, Atti Sem. Mat. Fis. Univ. Modena **46** (1998), 263–276.
- [13] B.K. Dass and S. Gupta, *An extension of Banach contraction principle through rational expressions*, Indian J. Pure Appl. Math. **6** (1975), 1455–1458.
- [14] H. Huang, L. Paunović and S. Radenović, *On some fixed point results for rational Geraghty contractive mappings in ordered  $b$ -metric spaces*, J. Nonlinear Sci. Appl. **8** (2015), 800–807.
- [15] N. Hussain, V. Paraneh, J.R. Roshan and Z. Kadelburg, *Fixed points of cycle weakly  $(\psi, \varphi, L, A, B)$ -contractive mappings in ordered  $b$ -metric spaces with applications*, Fixed Point Theory Appl. **2013** (2013), 256, 18 pages.
- [16] N. Hussain, J.R. Roshan, V. Parvaneh and M. Abbas, *Common fixed point results for weak contractive mappings in ordered  $b$ -dislocated metric spaces with applications*, J. Inequal. Appl. **2013** (2013), 486, 21 pages.
- [17] F. Khojasteh, S. Shukla and S. Redenović, *A new approach to the study fixed point theorems via simulation functions*, Filomat **29** (2015), no. 6, 1189–1194.
- [18] P. Kumam and W. Sintunavarat, *The existence of fixed point theorems for partial  $q$ -set valued quasi-contractions in  $b$ -metric spaces and related results*, Fixed Point Theory Appl. **2014** (2014), 226, 20 pages.
- [19] V. Lakshmikantham and L. Ćirić, *Coupled fixed point theorems for nonlinear contractions in partially ordered metric spaces*, Nonlinear Anal., **70** (2009), 4341–4349.
- [20] N. Malhotra and B. Bansal, *Some common coupled fixed point theorems for generalized contraction in  $b$ -metric spaces*, J. Nonlinear Sci. Appl. **8** (2015), 8–16.
- [21] M. Olgun, O. Bicer and T. Alyildiz, *A new aspect to Picard operators with simulation functions*, Turk. J. Math. **40** (2016), 832–837.
- [22] N.S. Prasad, D.R. Babu and V.A. Babu, *Common coupled fixed points of generalized contraction maps in  $b$ -metric spaces*, Electron. J. Math. Anal. Appl. **9** (2021), no. 1, 131–150.
- [23] R.J. Shahkoobi and A. Razani, *Some fixed point theorems for rational Geraghty contractive mappings in ordered*

- b*-metric spaces, J. Inequal. Appl. **2014** (2014), no. 1, 1–23.
- [24] W. Shatanawi, *Fixed and common fixed point for mappings satisfying some nonlinear contractions in b-metric spaces*, J. Math. Anal. **7** (2016), no. 4, 1–12.
- [25] W. Shatanawi and M.B. Hani, *A coupled fixed point theorem in b-metric spaces*, Int. J. Pure Appl. Math. **109** (2016), no. 4, 889–897.
- [26] W. Shatanawi, B. Samet and M. Abbas, *Coupled fixed point theorems for mixed monotone mappings in ordered partial metric spaces*, Math. Comp. Model. **55** (2012), 680–687.